Developing a gene therapy for Stargardt Disease

A thesis submitted for the degree of Doctor of Philosophy

Elena Piotter

St. Cross College
Nuffield Department of Clinical Neurosciences
University of Oxford

Supervisors:
Professor Robert E MacLaren
Dr. Michelle McClements

Michaelmas term 2024

Abstract

Stargardt disease was first described by Stargardt in Bonn in 1909 and is the most common recessively inherited macular degeneration, affecting 1:8,000-10,000. It results in progressive vision loss and legal blindness by the fourth to seventh decade of life, therefore, it is highly clinically relevant. Stargardt disease is caused by mutations in the *ABCA4* gene, which encodes the ATP-binding Cassette protein -4 (ABCA4), a transport protein essential to the visual cycle which is expressed in photoreceptor outer segments.

Gene therapy has shown promise in treating autosomal recessive or X-linked inherited retinal degenerations, where genes can be packaged into the adeno-associated viral vector (AAV) capsid and delivered to target cells. However, the packaging capacity of AAV is ~4.7kb and thus, at 6.8kb, *ABCA4* is too large for AAV gene supplementation therapy. Novel CRISPR technologies, such as DNA and RNA base editing, enable correction of pathogenic transition mutations (A-G, C-T). *ABCA4* has ~1200 known pathogenic mutations of which 63% are editable transition mutations. In this thesis, I explore and compare the therapeutic potential of CRISPR-Cas mediated DNA and RNA base editing of *ABCA4.*

First, the experiments reported in this thesis investigated the relevance of DNA and RNA base editors in targeting *ABCA4* by analysing multiple online databases and clinical cohorts. In particular, the PAM-site requirement of DNA base editors was investigated and determined to not be a limiting factor due to the high degree of heterogeneity observed in *ABCA4.* Following the screen, a clinically relevant nonsense mutation, c.206 G>A (W69*) in *ABCA4* was targeted by both an SaKKHABE8e DNA base editor and dPspCas13b-ADAR$_{DD}$ RNA base editor *in vitro,* and analysed at the DNA, RNA, and protein level. I demonstrated robust and targeted editing by both DNA and RNA base editors that resulted in production of full-length ABCA4 protein.

This work went on to evaluate the AAV-delivered SaKKHABE8e DNA base editor and dPspCas13b-ADAR$_{DD}$ RNA base editor in complex pre-clinical models, including in a mouse model and in retinal organoids, to establish the translational capabilities of the editors in the retina targeting *ABCA4*. Initially, both models were to contain the patient c.93 G>A nonsense mutation, however, production of both models is still ongoing and was thus not possible to target

within this thesis. Instead, after *in vitro* screens, the base editors were used to knockdown *ABCA4 in vivo* and target a mutation near c.93 in retinal organoids to evaluate base editor efficacy across models and across target sites. I demonstrated that for dCas13b-ADAR$_{DD}$ there is a large discrepancy in editing efficiencies between *in vitro* data and the complex models. Further, I successfully used SaKKHABE8e *in vivo* by AAV delivery to specifically and robustly target the *ABCA4* start codon. This represents the first use of the single AAV all-in-one SaKKHABE8e in photoreceptors.

Acknowledgements

I am sincerely grateful to my supervisor Prof Robert MacLaren for his mentorship, steadfast encouragement, and positivity throughout this PhD, and for fostering such an amazing lab community. I am also sincerely grateful to my second supervisor Dr. Michelle McClements for her kindness, optimism, support, and time, and for always seeing the silver-lining and going from there. I feel truly fortunate to have had this opportunity and for their supervision.

I want to express my deep gratitude to both RetinaUK and the Macula Society for jointly funding this research (GR599) and for their continued support throughout the project. Both are incredible oranisations that I feel lucky to have worked with. I am also thankful to the Nuffield Department of Clinical Neurosciences and St Cross College for the financial support to travel to conferences. At St Cross College, I would like to thank and extend gratitude to the library for many cozy days, filled with wonderful goodies provided by the St Cross librarian, Philippa Taney, and for the fabulous lunches.

I would like to thank the selfless individuals who volunteer themselves and their time to be participants in research, and to the clinical teams that make this happen. Without them, biomedical research and progress would not be possible.

The lab was an immensely supportive and fun community of wonderful individuals who I feel extremely lucky to have met and have adventures with at conferences, the legendary lab dinners, and around Oxford. Thank you to everyone in the lab for their time, humour, discussion, and for teaching me so much. A special thank you goes to a few people. First, to Dr. Ahmed Salman for his generosity with his time and conversations, for helping me tackle the many subretinal injections, for patiently teaching me many procedures, and for his kindness. To Dr. Imran Yusuf for also helping me tackle the many subretinal injections and for the fun chats. To Dr. Lewis Fry and Dr. Caroline Peddle for helping me get started in the lab and getting me stoked on CRISPR. To Dr. Sophia Bellingrath, Dr. Connie Han, Dr. Lauren Major, and Dr. Monica Hu for being the best partners-in-crime in Oxford/conference adventuring and in discussing all the important things ranging from data to the best carb, recipes, restaurants, and cooking.

Thank you to the whole lab crew for such wonderful times – Joel Quinn, Molly John, Dr. Kanmin Xue, Dr. Jasmina Kapetanovic, Dr. Maria Kaukonen, Dr. Celia Sourd, Dr. Cristina Martinez-Fernandez de la Camara, Dr. Qingyun Zheng, Dr. Silja Haldrup, Dr. Hoda Shamsnajafabadi, Dr. Aman Josan, Dr. Ariel Kantor, Dr. Tien Tan, Dr. Vasil Kostin, Sylvia Franklin, Dr. Federica Staurenghi, Dr. Marta Stevanovic, Dr. Maram Abdalla, Dr. Tom Buckley, Dr. Jasleen Jolly, Dr. Ben Ng, Laura Taylor, Lauren Collins, Dr. Lucy McDermott, Dr. Grace Borchert, Dr. Ellie Rhodes, Dorothea Stark, Leah Fogarty, and Dr. Marco Bellini.

I would like to thank the animal technicians at the John Radcliffe BMS for their work and dedication to caring for the animals.

Lastly, I would like to express my gratitude and thanks to my family and friends for their unconditional love, support, and friendship. To my parents and brother (BP, DP, HP): thank you for your love, confidence, guidance, support, and for always making me laugh. You guys are the best. To Martha (MM, KM, MV): I am so grateful – I couldn't have done it without your love, encouragement, and our fun adventures together. To my grandparents: thank you for instilling a love of learning and curiosity, for your love, and for supporting me throughout this process until the very end. Prost! To the wild swimmers: thank you for the relaxed summer swims and the frigid January swims at Hinksey lake and around Oxfordshire – the swims were exhilarating and the swimmers a wonderful community of ducklings. To 51 St Mary's: living there made even the pandemic a fun and cozy time filled with cook-offs, swimming, BBQs, picnics, and dancing. To the power puffin girls + big I: thank you for the best bike rides, games, adventures, endless Covid walks, and wild swimming in all seasons – it made this time wonderful and made Oxford home. To Olive, the gOrLs, CBM, schpui, vb_everlight, and schmegan: thank you for your friendship and love over many years, for letting me always practice my presentations (no matter how long and boring), and for the best times.

Declaration

The work presented in this thesis was undertaken in Professor Robert MacLaren's laboratory in the Nuffield Department of Clinical Neurosciences at the University of Oxford between 2020 and 2024. I, Elena Piotter, hereby declare that this is all my own work except where otherwise stated.

Where chapters contain published content, this has been clearly stated and co-author permission granted. At the time of submission, data from Chapter 3 had been published in *Frontiers.* In Chapter 5, Michelle McClements and Lauren Major assisted in maintaining the organoids whenever I was absent. In Chapter 6, Ahmed Salman and Imran Yusuf performed the mouse subretinal injections that contributed to data. Ahmed Salman and Michelle McClements taught and assisted in animal procedures that contributed to data in this chapter as well. One virus in Chapter 6 was made by Ahmed Salman and is acknowledged. DNA sequencing was commercially outsourced to Genewiz (UK) and Eurofins (Germany). One of the plasmids commercially underwent site-directed mutagenesis by Genewiz (UK). Sources for all materials kindly provided as gifts by other researchers or from commercial manufacturers are acknowledged throughout and listed in the Appendix.

All figures are original, and it has been clearly attributed if adapted from another source. Diagrams were produced in Biorender.com and graphs in Prism 10 or Microsoft Excel. The word count excluding the Table of Contents, the Table of Figures/Tables, Abbreviations, figure legends, the Appendix, and References, is ~49,900 words.

No material presented here has been previously submitted to the University of Oxford, or to any other academic institution, for another degree or qualification.

- Elena Piotter, 2025

Contents

Figures

Tables

Abbreviations

AAV	Adeno-Associated Virus
ABCA4	ATP binding cassette protein subfamily A, member 4
ABE	Adenine Base Editor
AD	Autosomal dominant
$ADAR_{DD}$	Adenine deaminase acting on RNA deaminase domain
AMD	Age-related macular degeneration
ANOVA	Analysis of Variance
APOBEC1	Apolipoprotein B mRNA Editing Enzyme Catalytic subunit 1
AR	Autosomal recessive
ART	Automated real time
ASO/AON	Antisense oligonucleotide
ATP	Adenosine triphosphate
ATR	All-trans retinal
BAF	Blue autofluorescence
BEST1	Bestrophin 1
BER	Base excision repair
bGH	Bovine growth hormone polyA
BSA	Bovine serum albumin
cadRNA	Circular ADAR recruiting guide RNAs
Cas	CRISPR-associated
CBE	Cytosine Base Editor
cDNA	Complementary DNA
CDS	Coding Sequence
CEP290	Centrosomal protein, 290-KD
CjCas	*Campylobacter jejuni* Cas9
CMV	Cytomegalovirus
CNGA/B3	Cyclic nucleotide gated channel subunit alpha/beta 3
CRB1	Crumbs cell polarity complex component 1
CRISPR	Clustered regularly interspaced short palindromic repeats
CRISPR a/i	CRISPR activation/interference
crRNA	CRISPR RNA
cSLO	Confocal scanning laser ophthalmoscope
Ct	Cycle threshold
DAPI	4’6,-diamidino-2-phenylindole
dCas	Dead Cas

DMEM	Dulbecco's modified Eagle medium
DNA	Deoxyribonucleic acid
DR	Direct repeat
DSB	Double-strand break
dsDNA/RNA	Double-stranded DNA/RNA
ECD	Exocytoplasmic domain
EditR	Edit deconvolution by interference of traces in R
EFS	Elongation factor 1-alpha core
EIAV	Equine infectious anemia virus
ELM	External limiting membrane
ELOVL4	Elongation of very long chain fatty acids
ESC	Embryonic stem cell
EYS	Eyes shut homologue
FECD	Fuchs' endothelial corneal dystrophy
GAF	Green autofluorescence
GCL	Ganglion cell layer
GFAP	Glial fibrillary acidic protein
GFP	Green fluorescent protein
gRNA	Guide RNA
GRK1	Human rhodopsin kinase promoter
HDR	Homology-directed repair
HEK293T	Human embryonic kidney 293 cells expressing mutant sv40 T antigen
HEPN	Higher eukaryotes and prokaryotes nucleotide binding domain
HI-FBS	Heat inactivated FBS
IHC	Immunohistochemistry
ILM	Inner limiting membrane
INL	Inner nuclear layer
IPL	Inner plexiform layer
iPSC	Induced- pluripotent stem cells
IRD	Inherited retinal degnerations
IS	Inner segment
ITR	Inverted terminal repeats
LB	Luria broth
LCA	Leber's congenital amaurosis
LEAPER	Leveraging Endogenous ADAR for Programmable Editing of RNA
LNP	Lipid nanoparticle
LOVD	Leiden Open variation database
LV	Lentiviral vector
mABCA4	Mouse *ABCA4*
NBD	Nucleotide binding domain

nCas9	Cas9 nickase
NGS	Next generation sequencing
NHEJ	Non-homologous end joining
NHP	Non-human primate
NIR	Near infrared reflectance
NmeCas	*Neisseria meningitidis* Cas
N-ret-PE	N-retinylidene-phosphatidylethanolamine
ns	Not significant
NTC	Non-target control
OCT	Optical coherence tomography
OCT	Optimal cutting temperature compound
ONL	Outer nuclear layer
OPL	Outer plexiform layer
ORF	Open reading frame
OS	Outer segment
PACE	Phage assisted continuous evolution
PAGE	Polyacrylamide gel electrophoresis
PAM	Protospacer adjacent motif
PBS	Phosphate buffered saline
PCR	Polymerase chain reaction
PE	Phosphatidylethanolamine
PE2/3	Prime editor 2/3
pegRNA	Prime editor guide RNA
PFA	Paraformaldehyde
PFS	Protospacer flanking site
PNK	Polynucleotide kinase
PR	Photoreceptor
PRL	Photoreceptor layer
PRPH2	Peripherin 2
PTC	Premature termination codon
PVFD	Polyvinylidene difluoride
rAAV	Recombinant adeno-associated virus
RDH8	Retinol dehydrogenase 8
REPAIR	RNA editing for Programmable A to I Replacement
RFP	Red fluorescent protein
RGC	Retinal ganglion cell
RGR	Retinal G-protein coupled receptor
RIPA	Radioimmunoprecipitation
RK	Rhodopsin kinase
RNA	Ribonucleic acid

RNP	Ribonucleoprotein
RO	Retinal organoid
RP	Retinitis pigmentosa
RPE	Retinal pigment epithelium
RT-qPCR	Real time quantitative PCR
SaCas	*Staphylococcus aureus* Cas
SauriCas	*Staphylococcus auricularis* Cas
SD	Standard deviation
SD	Stargardt disease
SEM	Standard error of the mean
SNP	Single nucleotide polymorphism
SOC	Super optimal broth with catabolite repression
SpCas	*Streptococcus pyogenes* Cas
ssRNA/DNA	Single stranded RNA/DNA
TadA	tRNA-specific adenosine deaminase
TAE	Tris/acetate/Ethylenediaminetetraacetic acid
TBS	Tris-buffered saline
TBS-T	Tris-buffered saline with 0.01% Tween®-20
TIDE	Tracking of Indels by Decomposition
TMD	Transmembrane domain
tracrRNA	Trans-activating RNA
VEGF	Vascular endothelial growth factor
vg	Vector genomes
WT	Wildtype
ZFN	Zinc finger nucleases

1 Introduction

1.1 The Retina

The retina is a complex neural tissue composed of multiple cell types that forms a specialized laminated structure, lining the inside surface of the eye (Figure 1-1). Light that is focused on the retina is transduced from light energy into electrical impulses and transmitted to the brain via the optic nerve. Much of the light is focused on the fovea, a cone-dense area at the centre of the macula that enables high acuity vision.[1,2] The macula is implicated in many inherited retinal degenerations (IRDs), such as Stargardt disease, age-related macular degeneration (AMD), and Best disease.[3]

The retina consists of five main classes of cells which form three nuclear layers separated by two plexiform layers (Figure 1-1). Collectively, the five cell types (photoreceptors, bipolar, amacrine, horizontal, and ganglion) allow for image processing that results in information such as shade, motion, colour, and depth, alongside determination of eye movement and pupil size. The retina is oriented such that the inner layer borders the vitreous and the outer layer borders the choroid (Figure 1-1). The outer nuclear layer (ONL) consists of the photoreceptor nuclei and the inner nuclear layer (INL) consists of the nuclei of bipolar, amacrine, horizontal, and Müller glial cells. These are connected by the outer plexiform layer (OPL) which contains the synaptic terminals and processes allowing for cellular crosstalk. Lastly, the ganglion cell layer (GCL) consists of the nuclei of ganglion cells. The inner plexiform layer (IPL) connects the INL and the GCL, consisting of terminals and processes of amacrine, horizontal, bipolar, and ganglion cells. The retinal pigment epithelium (RPE) is in between the photoceptors and the choroid and is critical for photoreceptor survival (Figure 1-1).[1,4-6]

1.2 Photoreceptor cells

The light sensing cells, the rod and cone photoreceptors, are located farthest from incoming light in the outer part of the retina. Counterintuitively, the light passes through the

transparent inner layers to reach the light-sensitive photoreceptors. However, this allows the retinal pigment epithelium (RPE) to absorb scattered light.[1]

Photoreceptors comprise of the outer segment (OS), inner segment (IS), cell body, and the synaptic compartment (Figure 1-1). The synaptic terminals connect with the INL allowing for relay of information between cells and to the brain.[1,7] The nucleus is located in the cell body and the inner segment is responsible for all metabolism, biosynthesis, and endocytosis. Much of the protein produced in the inner segment is transported to the outer segment, where phototransduction occurs.[1,8]

The outer segment (OS) contains densely packed outer discs, allowing for high opsin protein density and increased probability of photon capture.[1] For example, in rods, ~95% of the total disc protein consists of rhodopsin.[1,9] A key aspect of outer segment physiology is renewal, whereby discs are generated at the base of the outer segment and move distally toward the RPE. The aged discs are then phagocytosed by the RPE, with ~10% of outer segment discs phagocytosed each day. Complete outer segment renewal takes ~10-11 days in humans and exists in a steady state of outer segment phagocytosis and renewal.[7,10,11] Photoreceptors, however, do not divide or regenerate because they are post-mitotic.[7]

Humans have ~130 million photoreceptors, where rods and cones exist at a ratio of 20:1.[1] Cones are concentrated in the fovea and macula, outside of which is predominantly rods.[2,9] Rods and cones exhibit key differences that result in specialised roles for vision. Broadly, rods are specialised for night-time vision due to high light sensitivity and low spatial resolution, whereas cones are specialised for day-time vision with limited light sensitivity and high spatial resolution.[9] Other critical factors including outer segment morphology, photopigment, and metabolic needs, further affect differing function. Notably, rod outer segment discs are fully separated discs in a cylindrical outer segment, whereas cone outer discs are invaginations and form a conical structure. The continuous membrane structure of cone outer discs increases surface area, likely enabling a rapid substance exchange and perhaps explains the metabolic differences observed in rods and cones.[9,12] Specifically, cones demonstrate greater metabolic needs per cell, at roughly 1.5E+8 ATP/s versus the 8E+7 ATP/s seen in rods cells.[13] Further, a cone-specific visual cycle has been hypothesised to enable the rapid chromophore recycling observed in cones, which functions via a subpopulation of Müller glial cells containing retinal G-protein coupled receptor (RGR).[12,14] These factors may potentially affect the differing rates of

degeneration in rod and cone cells typically seen in Stargardt disease, where cones typically degenerate first, but this is still to be determined.

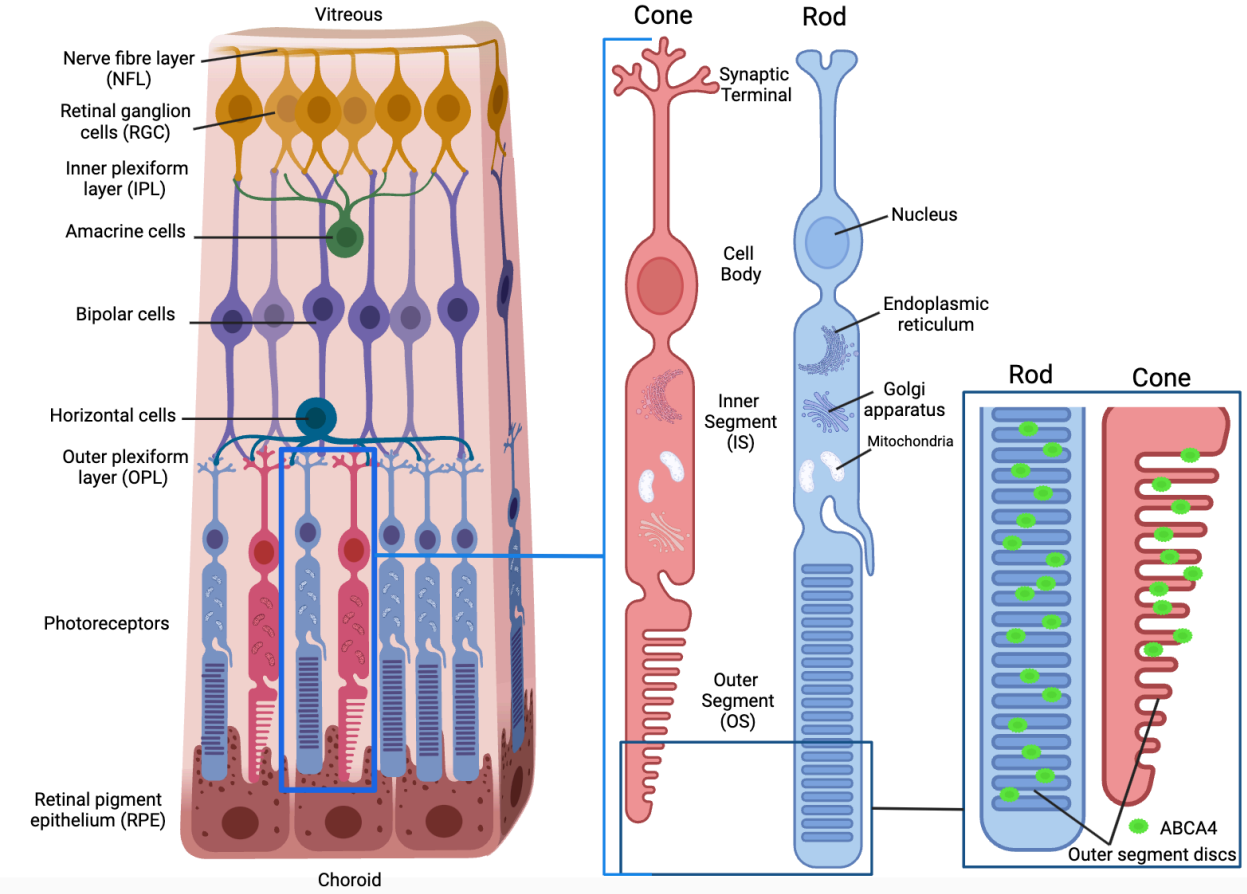

Figure 1-1: Structure of the retina and *ABCA4* localisation.
Diagram of retinal cell organisation. The choroid and vitreous labels are for orientation, where the choroid is 'outer' and vitreous is 'inner.' The amplified blue box indicates a rod and cone photoreceptor, labelled in the centre. Further amplification of the outer segments reveals the outer segment discs and indicates where ABCA4 localises.

1.3 Inherited retinal degenerations

Considering the complexity of the retina, it is unsurprising that dysfunction at any stage can affect cell health and interfere with the visual pathway. Inherited retinal degenerations (IRDs) are complex, where genetic mutations can result in retinal malfunction which can progress to cell death and loss of vision. IRDs are highly heterogenous and are caused by mutations in over 300 genes (Figure 1-2).[15,16] Individually, the diseases are rare, but collectively

IRDs have become the leading cause of vision loss in high-income countries in people aged 15-45, with an incidence of 1:2,000[17] (due to improved diagnostics).

IRDs are extremely varied and complex. Inheritance patterns typically occur by either autosomal recessive (AR), autosomal dominant (AD), or X-linked patterns, however, more complex or multimodal patterns have been reported.[18] Further, IRDs can have one causative gene or multiple causative genes, such as retinitis pigmentosa which can be caused by mutations in 84 different genes.[17,19] In addition, modifying variants can affect the penetrance and expressivity of other variants, seen with a common *ABCA4* variant.[20] Lastly, many IRDs are isolated to the eye, however, more than 80 syndromes with effects beyond the eye and associated with 200 genes have been described.[21]

This genetic complexity is reflected in the disease presentation, where age-of-onset, progression, severity, and phenotype vary significantly. Leber's congenital amaurosis (LCA) is the most severe, where patients suffer vision loss at birth or in the first few years of life.[22] Even within the same disease, severity and progression can vary substantially. For example, Stargardt disease has an age of onset ranging from childhood/ early-teens to the fourth to seventh decade of life. Severity corresponds with this, where more severe variants have an earlier age of onset.[23]

Diagnostics have vastly improved in the last twenty years, with a diagnostic yield of 52-74%.[15,24] This reflects the percentage of genes causing retinal degenerations that have been identified, at 50-70%.[25] Few IRDs have therapy or treatment options.

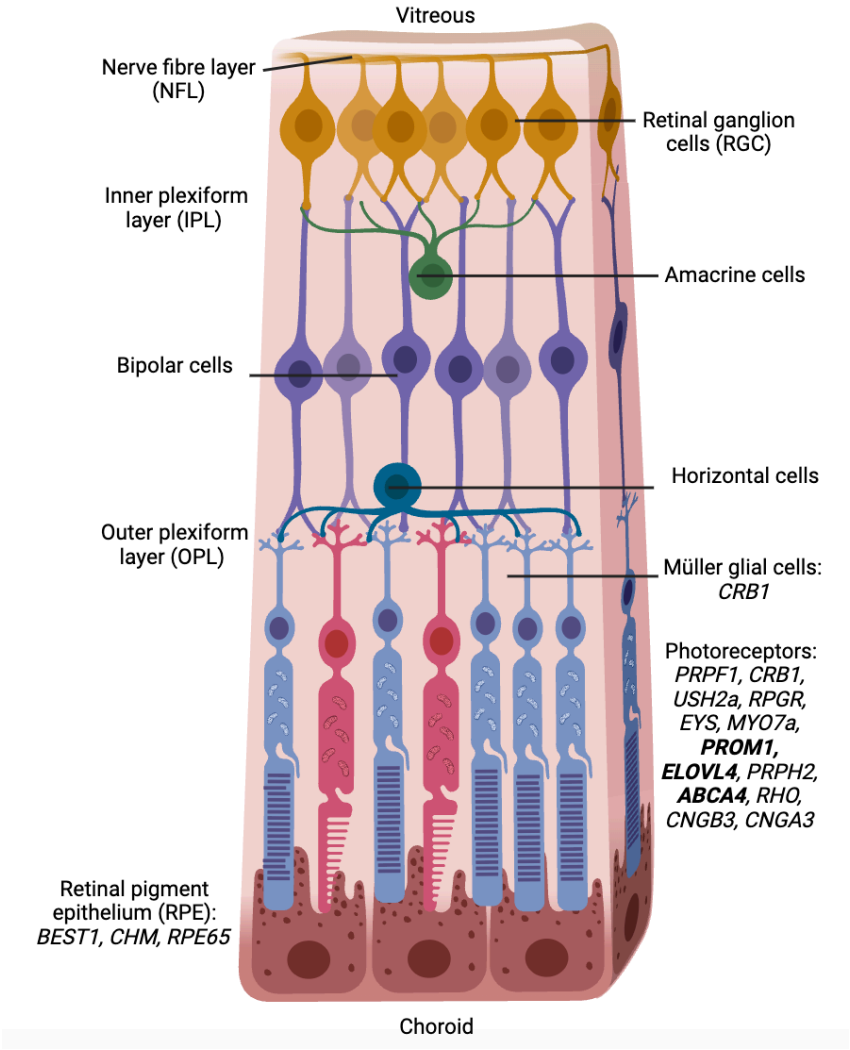

Figure 1-2: Diagram of the retina indicating inherited retinal degenerations.
Retinal layers and cell types with associated inherited retinal degenerations. The photoreceptors and RPE are most implicated. Müller glial cells are indicated in the space between since they extend across multiple retinal layers. Causative genes for Stargardt are *ABCA4, PROM1, ELOVL4,* highlighted in bold.

1.4 Existing therapeutic strategies for IRDs

1.4.1 Gene supplementation via AAV

As the understanding of IRD genetics has progressed, so has the possibility of treating the genetic cause. In principle, supplying a functional gene or correcting the implicated gene would allow for slowed disease progression or restored visual function.[26] Indeed, the first FDA approved AAV gene supplementation therapy was for the treatment of *RPE65*-associated Leber's congenital amaurosis (LCA), which has shown long-term safety and efficacy in the four-year follow-up data.[27] This paved the way for many other gene supplementation therapies in the eye,

such as X-linked retinitis pigmentosa (*RPGR),* Bietti's crystalline dystrophy (*CyP4V2),* and achromatopsia (*CNGA3, CNGAB3),* among many others.[28] None of these have achieved FDA approval, to date.[29]

The retina presents many advantages as a target given the proportion of monogenic diseases, surgical access, and the relative immune privilege due to the blood-brain barrier.[30,31] This has resulted in a "boom" in gene therapy development targeting the retina, initially with the aim of delivering a correct copy of the implicated gene and progressing to a variety of gene editing methods. There have been ~130 recent retinal gene therapy clinical trials.[32]

To date, multiple viral vectors have been tested, including recombinant lentiviruses (LV), adenoviruses (AV), and adeno-associated viruses (AAV). Although lentiviruses have been tested due to the large packaging capacity, transduction is limited to the RPE and there is a risk of insertional mutagenesis, reducing its application to photoreceptor diseases. LVs have shown minimal reported efficacy in clinical trials, including for Stargardt disease.[33-35] Adenoviruses tend to be rapidly cleared due to preexisting immunity, limiting their application. AAV has emerged as the vector of choice due to the low risk of insertional mutagenesis, mild inflammatory response, efficient RPE and photoreceptor transduction, multiple retina-specific serotypes, and long transgene expression.[29] Many pre-clinical projects and clinical trials targeting the retina are underway using AAV to deliver the transgene.[36]

AAV is a single-stranded DNA parvovirus that is thought to be non-pathogenic. Its lifecycle requires a helper virus genes for replication. In wtAAV, inverted terminal repeats (ITRs) flank the AAV genome and contain the required *cis* elements for replication and packaging of the necessary *rep/cap* genes for formation of a viral particle. Critically, the AAV genome consisting of the *rep* and *cap* genes can be delivered in *trans* alongside the helper genes for virus production. For gene therapy, this has been exploited and enables replacement of the *rep/cap* genes with a transgene of choice flanked by the AAV ITRs, resulting in expression of the transgene. The transgene packaging capacity is ~4.7kb. Moreover, removal of the *rep/cap* genes lowers the toxicity and immunogenicity of the vector and reduces rates of viral integration. Lastly, ITR circularisation and concatemerisation yields episomal DNA, enabling persistent expression in post-mitotic cells, such as photoreceptors, and ensures long-term transduction.[37,38]

Twelve natural serotypes and many other variants provide tissue-specific tropism. The directed evolution and rational design of novel variants enable the potential to minimise immune response and improve transduction efficiencies.[39,40]

1.4.2 Other therapeutic approaches

Many causative genes of IRDs exceed the packaging capacity of AAV. Although methods have been developed to circumvent this, such as a dual vector,[41,42] lentiviral vector,[34,35] or lipid nanoparticles,[43] they have yet to demonstrate efficacy in clinical trial. Pre-clinical data for dual vector and lipid nanoparticle delivery show promising results, however, these methods are typically less efficient in the retina.[32] These are discussed in greater detail in section 1.7.

Alternative approaches to modulate genes are also being applied, including anti-sense oligonucleotides (ASO) to modify splicing in mutant transcripts. For example, QR-1101 successfully corrected splicing of multiple non-canonical splice sites in *ABCA4,* including a prevalent disease-causing variant, c.5461-10 C>T, in retinal organoids.[44] ASOs can also be applied to silence mutant transcripts which can be applied in cases of autosomal dominant disease.[45,46]

Finally, small molecules to treat IRDs can alter cellular pathways in the eye and are discussed further in 1.7.3.[47-49]

1.4.3 Current limitations

Unfortunately, gene supplementation is limited in its application for several reasons. As described, the limited packaging capacity means a large proportion of IRDs cannot be targeted by single AAV gene supplementation, with limited efficacy found in adapted approaches.[50]

Gene supplementation is also not applicable for autosomal dominant diseases, given the continued expression of the pathogenic mutant allele.[51,52] To overcome this, approaches have been tested that simultaneously knockdown the mutant allele and deliver a wildtype copy.[53]

For diseases in which gene supplementation is not possible, correcting the underlying mutation is a possible therapeutic strategy with novel gene editing methods. These are discussed further in 1.8.

Lastly, although AAV is non-pathogenic and the estimated integration rate minimal (>0.1%),[54,55] immune response and viral integration remain key considerations. Clinical trial

results are split, with some trials demonstrating tolerance of the vector and others showing dose-dependent immune responses.[56] Further, recent *in vivo* data of split-intein AAV delivery demonstrated integration at the target site, corroborating initial EDIT-101 data demonstrating AAV insertion in 25 treated human retinal explant punches.[57,58] This highlights the importance of pre-clinical dose-escalation studies and the continued investigation of the host response and alternative delivery methods.

1.5 ABCA4

1.5.1 Function, structure, and localisation

The discs in the outer segment contain a multitude of proteins that enable reactions to process light stimuli. This begins with isomerisation of 11-cis-retinal within the opsin protein which results in the production of all-trans retinal (ATR). Most of the ATR is reduced by retinol dehydrogenase 8 (RDH8) to all-trans retinol for downstream processing in the visual cycle. However, a significant portion of ATR produced is not reduced by RDH8 and reacts with excess 11-cis-retinal and phosphatidylethanolamine (PE) to form N-retinylidene-phosphatidylethanolamine (N-ret-PE). This can lead to the build-up of toxic bisretinoid compounds if it is not cleared.[59,60]

ATP-binding cassette family member 4 (ABCA4) is a large, complex protein essential in clearing the 11-cis and all-trans isomers of N-ret-PE from the outer disc lumen to the cytoplasm via a flippase mechanism, and thus prevents the build-up of toxic compounds. The transport activity allows for subsequent processing of dissociated products, 11-cis and all-trans retinal, in the visual cycle.[60,61]

ABCA4 is predominantly localised to the photoreceptor outer segment discs (Figure 1-1and Figure 1-4), although it has been reported in the RPE with a hypothesised function in lipid metabolism. The exact mechanism in the RPE is yet to be determined.[62-65] Further reports have suggested expression in hair follicle cells and keratinocytes, however this has not shown clinical implications thus far, but rather provides cell-model possibilities.[66]

The ABCA4 protein consists of 2273 amino acids which are organised in nonidentical halves. Each half contains a transmembrane domain, nucleotide-binding domain, and exocytoplasmic domain (Figure 1-3).[60]

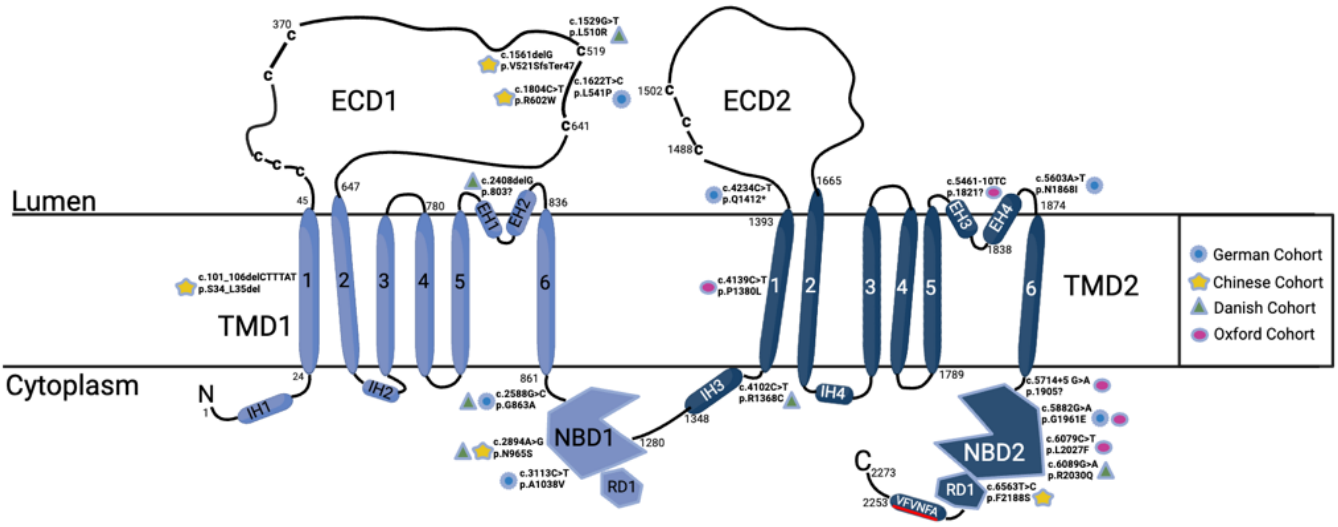

Figure 1-3: ABCA4 protein structure.
The structure of ABCA4 in the outer disc. Each half includes a transmembrane domains (TMD) consisting of six membrane-spanning segments, a nucleotide binding domain (NBD), and an exocytoplasmic domain (ECD1). Key mutations from patient cohorts are indicated throughout the protein structure. Figure from: *Piotter, E., McClements, M. E. & MacLaren, R. E. The Scope of Pathogenic ABCA4 Mutations Targetable by CRISPR DNA Base Editing Systems-A Systematic Review. Front Genet* ***12*** *(2022). https://doi.org/ARTN 81413110.3389/fgene.2021.814131*[67]

1.5.2 Stargardt disease

Text, figures, and tables in this chapter sections 1.5.2-1.7.4 have been adapted from: *Piotter, E., McClements, M. E. & MacLaren, R. E. Therapy Approaches for Stargardt Disease. Biomolecules* ***11*** *(2021). https://doi.org/ARTN 117910.3390/biom11081179* [50] and *Piotter, E., McClements, M. E. & MacLaren, R. E. The Scope of Pathogenic ABCA4 Mutations Targetable by CRISPR DNA Base Editing Systems-A Systematic Review. Front Genet* ***12*** *(2022). https://doi.org/ARTN 81413110.3389/fgene.2021.814131*[67]

Stargardt disease is a monogenic, recessively inherited condition resulting from mutations in the *ABCA4* gene that reduce or abolish protein function.[68] The importance of the structure of ABCA4 and transport by ABCA4, described above, is evidenced by the ~1200 known pathogenic mutations that can result in disease.[23,60] It is the most common macular dystrophy, with an incidence of 1:8,000-10,000[23,69] and a carrier frequency reported to be as high as 1:20, depending on the population.[70,71] As with many IRDs, severity, progression, and age of onset of Stargardt disease vary significantly, with variable and inconsistent genotype-phenotype correlation. Individuals typically first experience symptoms in the first two decades of life, with most suffering severe visual impairment or legal blindness by the 4th to 7th decade of life.[23]

Reduced or lack of function of ABCA4 results in the build-up of bisretinoids, such as insoluble *N*-retinylidene-*N*-retinylethanolamine (A2E), in the photoreceptor outer segments.[72]

As the RPE cells phagocytose the outer discs, bisretinoids aggregate in the RPE and eventually cause RPE cell damage and degeneration. (Figure 1-4) Subsequently, since photoreceptor health and visual cycle function is dependent on the health of the RPE, photoreceptors also undergo damage and degeneration. This results in the loss of the macula and thus central vision (Figure 1-4).[73,74]

Due to the slow disease progression, there exists an ample treatment window, however, no proven therapies or treatments exist. Many methods have been tested or are under investigation and are described in detail below.

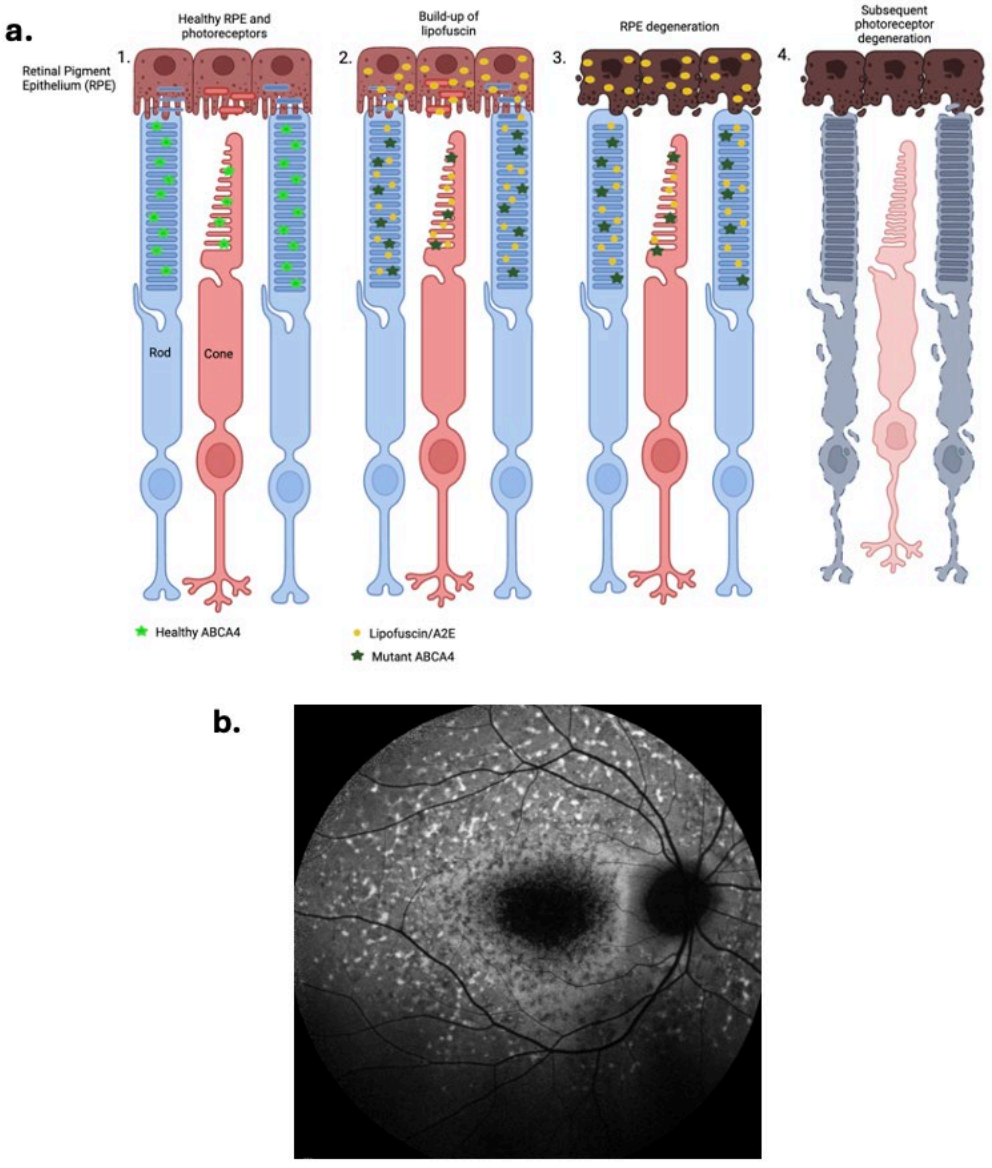

Figure 1-4: Retinal degeneration in Stargardt disease.

Stargardt disease progression (a) from 1-4. 1. Functional ABCA4 allows for phagocytosis of healthy outer segment discs. Healthy ABCA4 indicated by the light green star. 2. Mutant ABCA4 (dark green) does not enable transport of N-ret-PE isomers leading to the subsequent build-up of A2E and bisretinoids (yellow dots). As the RPE phagocytoses the A2E/bisretinoids it accumulates in the RPE. 3. Continued accumulation of A2E and bisretinoids leads to the formation of lipofuscin and eventual degeneration of the RPE. 4. The photoreceptors subsequently degenerate. b. Image of a Stargardt-affected eye, showing degeneration at the dark central spot and peripheral flecks. Kindly provided by Saoud Al-Khuzaei.

1.5.3 Genetic landscape and genotype-phenotype correlations

Stargardt disease has a notoriously complex genetic and phenotypic landscape, given the ~1200 known pathogenic mutations coupled with minimal genotype-phenotype correlation.[23,62,75] Indeed, it has been shown that some missense variants result in a more severe phenotype than variants that cause protein truncations.[76] Despite the phenotypic heterogeneity, three features tend to remain in patients with Stargardt disease – macular affectation, fundus flecks, and peripapillary sparing.[23] Since these are found in other macular degenerations, such as age-related macular degeneration (AMD), genetic confirmation is necessary.[23,77]

Further, there are contradictory reports of the pathogenicity of variants.[23,78-80] For example, c.5882 G>A, one of the most common variants in Europe, is listed as ‘conflicting classifications of pathogenicity’ in ClinVar. A contributing factor to this may be due to the effect of cis-acting modifiers on the penetrance of variants.[20] Moreover, complex alleles are observed in 10-16% of alleles, with high heterogeneity.[23,69]

Interestingly, monoallelic Stargardt cases have been reported at rates of up to 20-25% in some studies.[81] However, these likely have a second variant that is yet to be determined.[82,83] For example, determination of the pathogenicity of p.(Asn1868Ile) in *trans* resolved ~50% of the cases thought to be monoallelic cases in a cohort.[81] One explanation and alternative source of a second variants is deep-intronic variants, which can affect splicing.[84] Studies investigating monoallelic cases found 35 deep-intronic variants to be causal and often occurred in more than one patient.[23] Lastly, variants in regulatory regions can affect *ABCA4* expression and require further investigation.[23,85,86]

Common *ABCA4* variants tend to be location-dependent due to founder mutations arising in particular geographic populations, such that most nations in Europe each have a distinct high-prevalence variant.[23] For example, c.768 G>T is very frequent in the Netherlands but minimally present in Germany.[23,87] Interestingly, c.5882 G>A is the most common variant in Europe but is

an East African founder mutation found in ~10% of Somalis.[23,88,89] With changing geopolitical events and an increased globalisation, the founder alleles will likely spread across the world.

1.6 Models of ABCA4

1.6.1 Cellular models

Immortalised cell lines, such as Human Embryonic Kidney 293 cells (HEK293), are commonly used for *in vitro* assays to overexpress mutant proteins and explore subsequent effects, allowing for analysis of the expression profile, cellular localisation, and function of a given mutant relative to the wildtype prior to testing and evaluating treatments. Thus, they provide an easy and cost-effective method of screening potential therapeutics. However, in the context of *ABCA4*, which is not expressed in standard cell lines, development of cell lines expressing *ABCA4* or exogenously delivered DNA is required. Analysis of expression in cells can be coupled with ATP-ase functional assays to develop a holistic understanding of the effects of a mutation.[90] However, while *in vitro* assays are a good starting point for screening and initial analysis, they have their limitations. For example, determining the effects of splice-site mutations through splice assays is particularly difficult to achieve due to retina-specific splicing mechanisms that are not recapitulated in standard cell lines, including HEK293 cells.[23,84,91] This has led to investigation of alternative cell lines, such as hair follicles and keratinocytes, which natively express *ABCA4*.[66]

Alternative models such as induced pluripotent stem cells (iPSCs) and 3D retinal organoids provide an opportunity to study *ABCA4* in a model that more accurately recapitulates retinal genetics and physiology. Specifically, this would enable study of variant-specific disease progression and mechanisms, development, and efficacy of potential therapeutics.[92] Although extremely promising as a model, retinal organoids lack an RPE monolayer, immune response, and vascularisation which can affect the study of age-related retinal degenerations such as Stargardt disease.[93]

1.6.2 Animal models

1.6.2.1 Differences in mouse retina

Mice are widely accepted as a pre-clinical animal model to investigate novel therapeutics, including for retinal degenerations. The human and mouse retina have many similarities, such as

stratified retinal layers, however, there are critical differences between the two which affect disease progression and phenotype.[94,95] Most notably, mice do not have a cone-dense macula for high acuity vision, a key consideration in studying a macular dystrophy such as Stargardt Disease (Figure 1-5).[95,96] This is coupled with a much higher rod density distributed throughout the retina for nocturnal vision, with fewer cones overall and without a region of higher cone density.[94,96] In addition, the photoreceptor to RPE cell ratio in the central and peripheral retina is ~7-fold higher than in humans.[94] Interestingly, despite relatively fewer RPE cells, the Stargardt phenotype in mice is very mild.[74] Mice are dichromats with gradient distributions of L/M-cones and S-cones throughout the retina, likely adapted for mouse habitat and behaviour (Figure 1-5).[97] Specifically, L/M-cones are mostly found in the superior retina, whereas S-cones are distributed in the inferior retina, however, most cones co-express both opsins.[97,98] Lastly, the drusen-like deposits produced by rodents are not deposited at the base of the RPE as in humans, suggesting a potentially different waste transport process.[96]

Other animal models (mentioned below) more closely resemble human retinas or have higher cone densities thereby enabling improved study of novel therapeutics for macular dystrophies, however these typically come at much higher costs.

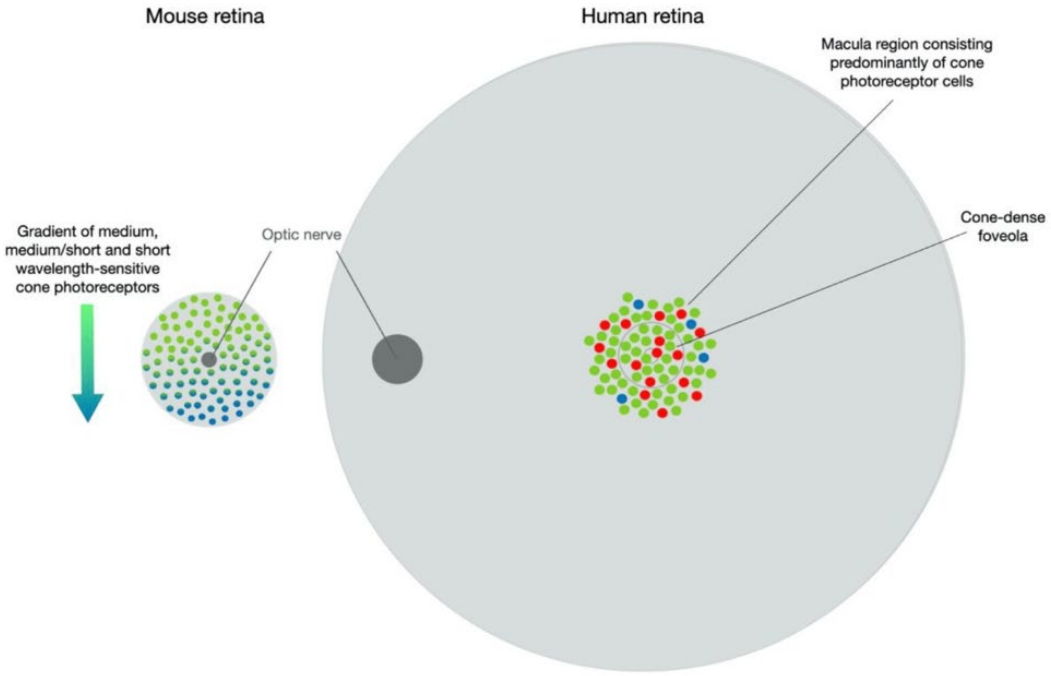

Figure 1-5: Comparison of the human and mouse retina.

Diagram indicating the key differences between the human and the mouse retina. Critically, the human has a cone-dense region of the retina called the fovea, surrounded by the cone-rich macula. Mice do not possess a macula, rather they exhibit various cone gradients depending on the wavelength sensitivity. Figure from *Piotter, E., McClements, M. E. & MacLaren, R. E. Therapy Approaches for Stargardt Disease. Biomolecules* ***11*** *(2021). https://doi.org/ARTN 117910.3390/biom11081179* [50]

1.6.2.2 *ABCA4* models

The favoured murine *in vivo* model presents a general issue in studying macular degenerations and potential treatments for safety and efficacy in that they lack a macula. The mouse retina is composed of 95% rods with various cone gradients throughout, whereas the human macula is cone dense and contains a macula/fovea to enable high acuity vision. While mouse models of inherited retinal disease readily recapitulate humans, a phenotype is rarely generated by mutant genes affecting the macula. For Stargardt disease, while *ABCA4* knockout mice do not exhibit obvious Stargardt attributes, they do experience a build-up of lipofuscin over time, which can be detected by scanning laser ophthalmoscopy (SLO), high-performance liquid chromatography (HPLC), and electron microscopy.[99,100]

Novel mouse models with human mutations were developed to better reflect the human genotype. The *ABCA4* homozygous p.Leu541Pro; Ala1038Val (PV/PV) model demonstrated reduction in ABCA4 protein relative to the wildtype and developed A2E and lipofuscin accumulation over time.[76] Similarly, a homozygous *ABCA4* Asn965Ser model demonstrated reduced ABCA4 protein overall and showed mislocalisation of ABCA4 to the inner segment. This was coupled with accumulation of lipofuscin and A2E.[101] More recently, a heterozygous mouse model containing one knockout allele and one allele containing the common variant c.5882 G>A (p.G1961E) variant was developed for testing of gene therapies. This model did not develop an increase in autofluorescence observable by SLO relative to the wildtype mice.[102] Although age-related structural changes can occur in mutant models, lipofuscin and A2E build-up are an effective measure to establish functional effect in severe variants and determine a treatment effect. Critically, murine models enable investigation of toxic and immune response in the context of screening novel therapeutics.

To enable improved study of gene therapies for Stargardt, alternative animal models with greater resemblance to the human eye are used. This includes rats,[103] pigs,[104] dogs,[105,106] NHPs,[107] and, more recently, zebrafish[108-110] and fat sand rats,[111] which provide the advantage of a cone-rich retina (Table 1-1).

Model type	Details	Structural features	Functional features	Strengths/ limitations
Non-mouse animals				
	Pig *ABCA4 KO*[104]	Absence of *ABCA4.* Lipofuscin accumulation reflecting patients.	KO models demonstrate lipofuscin accumulation in RPE and absence of ABCA4 protein by WB.	Pig eye more closely resembles human eye: rod/cone ratio, cone-rich region, eye size. Detection of ABCA4 and functional assessments following gene supplementation. However, pigs age slowly and are large, increasing cost.
	Dog *ABCA4* loss-of-function mutant (InsC)[105,106]	Morphological changes: abnormal fovea-like centre, outer retinal thinning, abnormal segmentation outer retina, focal loss of RPE.	Slow visual deterioration and morphological changes observed via imaging. Some vision retained throughout life.	Dog eye more closely resembles human eye: eye size, cone-rich area. However, slow aging/life-span and large size increase cost.
	Zebrafish *ABCA4* KO[108-110]	Cone-rich retina with structural similarity to human. However, they are tetrachromats.	Elongated cone outer segments, dysmorphology, reduced RPE phagocytosis, absence of ABCA4 protein.	Zebrafish are diurnal with cone-rich retina. Easy to edit embryos and develop models, and relatively short lifespan, decreasing costs. However, have two *ABCA4* paralogs with only 63-70% similarity to human *ABCA4.*
	Rat G1961E (hom) or -/KO Het[103]	All genotypes – normal retinal layers. G1961E hom/het – wt	Bisretinoid accumulation only in KO and compound het. All three mutant	Larger eyes than mice – improved reproducibility of subretinal injections. Low proportion of cones

		ABCA4 localisation. KO- absence of ABCA4.	models showed increased fundus autofluorescence over time.	(0.9%).[112,113] Gene supplement allows for detection of ABCA4.
	Fat sand rat (*Psammomys obesus)*[111]	Knockdown of *ABCA4* by Cas9 – reduced ABCA4 expression.	Lipid inclusions, disrupted cell integrity, cell loss, no bisretinoid differences.	Naturally diurnal and cone-rich (33%) – more readily recapitulates human phenotype. Atypical animal model – costly.
	Non-human primates *ABCA4* KO (exon2, exon 6 disrupted)[107]	Phenotype early stage STGD - progressive retinal thinning.	Photoreceptor dysfunction (ffERG).	'Gold standard' due to physiological and anatomical similarity to human. Generating mutant models and maintaining NHPs very costly and time-consuming
Mouse				
	ABCA4 KO[114,115]	Absence of *ABCA4* expression. Lipofuscin granule accumulation in the RPE.	*ABCA4* KO models exhibit accumulation of bisretinoids/ A2E/ lipofuscin.	Gene supplementation allows for detection of ABCA4. Assessment of therapy efficacy achievable by reduction in associated build-up of bisretinoids/A2E/lipofuscin. However, the KO genotype does not reflect typical human disease.
	Leu451Pro and Ala1038Val (PV/PV) Hom[76]	Mislocalised and reduced ABCA4.	*ABCA4* KO models exhibit accumulation of bisretinoids/ A2E/ lipofuscin.	Efficacy evident in these models would be more relevant to human disease. Good for testing gene editing technologies.
	Asn965Ser Hom[101]	Mislocalised and reduced ABCA4.	*ABCA4* KO models exhibit accumulation of bisretinoids/ A2E/ lipofuscin.	Efficacy evident in these models would be more relevant to human disease. Good for testing gene editing technologies.

	G1961E/KO Het[102]	Resembles WT phenotype.	No change in autofluorescence due to A2E/lipofuscin accumulation.	Good for testing gene editing technology but lacks any functional/protein outcome measure.

In vitro

Immortalised cell lines	Wild type	Lack of native retinal gene expression and absence of specialised retinal structures.	Enables expression and localisation assessments; downstream isolation and functional assays	Exogenous delivery of retinal genes of interest is required but basic assessments of vectors and downstream functional assays are achievable.
iPSCs	Patient-specific genotype	Cells can be differentiated to better reflect photoreceptor cell morphology and gene expression profiles	Functional outputs achievable by expression profile analysis and downstream protein isolation and functional assays	Particularly useful for gene-editing techniques in assessing mutation-specific therapies. Editing efficiencies and protein outputs could be compared to cells from control donors.
Fibroblasts	Patient-specific genotype	Some retinal gene expression may be evident, as for *ABCA4*	Functional outputs could be achieved by expression profile analysis and downstream protein isolation and functional assays	Supplementary to preliminary pre-clinical assessments of new therapies as expression of retinal genes will be limited. Patient-derived - added benefit of being useful for gene-editing strategies.
Hair follicles	Patient-specific genotype	Some retinal gene expression may be evident, as for *ABCA4*	As for fibroblast samples, functional outputs could be achieved by expression profile analysis and downstream protein isolation and functional assays	As for fibroblast samples, the use of these will likely be supplementary to other preliminary pre-clinical assessments but being patient-derived they will have the added benefit of being useful for gene-editing therapies.

Retinal organoids	Patient-specific genotype	Represent laminar retinal structure but missing key features such as the RPE. Better reflect gene expression profile.	As for other patient-derived samples, functional outputs could be achieved by expression profile analysis and downstream protein isolation and functional assays	Changes in expression profiles and protein localisation plus cell morphology could be assessed following treatment application. Retinal organoids will provide an ideal model for mutation-specific treatments.

Table 1-1: Models and their applications for *ABCA4.*
Summary of *in vitro* and *in vivo* models by which *ABCA4* therapeutic screens are possible. The advent of CRISPR will enable much easier generation of mutation-specific models in mice and cell-models. From: *Piotter, E., McClements, M. E. & MacLaren, R. E. Therapy Approaches for Stargardt Disease. Biomolecules* ***11*** *(2021). https://doi.org/ARTN 117910.3390/biom11081179* and updated.

1.7 Existing pre-clinical work and clinical trials

Stargardt disease is the most common inherited macular degeneration in patients under 50.[116] *ABCA4* is thus a key target of interest for gene therapy. However, due to its 6.8kb coding sequence, it exceeds the packaging capacity of AAV (~4.7kb).[117] Many approaches have been investigated with no treatment to date.

1.7.1 Viral delivery

Early attempts of packaging *ABCA4* in AAV involved "oversized" packaging of the whole 6.8kb transgene, which did enable production of full-length protein *in vitro* and *in vivo.* However, the unpredictable nature of truncated gene packaging led it to be referred to as a fragmented dual vector approach, where coincidental recombination of overlapping regions resulted in the full-length transcript.[118,119] Due to the unpredictability of this, the approach was not deemed feasible.

Subsequent dual vector approaches were developed whereby the transgene was split between two vectors for delivery to enable formation of the full-length transcript. To facilitate this, multiple methods enabling joining of the fragments were tested, such as overlapping regions, *trans*-splicing, and a hybrid version. Given the multitude of steps required for full-length *ABCA4* formation, the efficiency is likely decreased. Nonetheless, all three methods successfully

led to full-length ABCA4 expression in knockout mice.[41,42,120] Two companies, Splice Bio and AAVantgarde, have launched Phase I/II clinical trials using a dual vector strategy.[121]

To circumvent the packaging capacity of AAV, lentiviral delivery was deemed an attractive option for large genes, including *ABCA4,* due to its large packaging capacity of ~8kb. Initial mouse *in vivo* data using this approach showed promising results with full-length protein expression and reductions in lipofuscin.[122] The vector was well-tolerated in macaque and rabbit follow-up studies.[123] However, the subsequent clinical trial resulted in adverse events and no efficacy.[35] Despite the large packaging capacity, transduction appears to be limited due to viral size and structure.[124]

A novel method of mRNA *trans*-splicing allows for the delivery of the wildtype 5' or 3' half of *ABCA4* by AAV for subsequent splicing to the natively expressed transcript. This ensures wildtype expression levels while enabling treatment using either vector regardless of mutation. A Phase I/II clinical trial by Ascidian Therapeutics is currently underway.[125]

1.7.2 Non-viral delivery

Non-viral delivery offers a larger carrying capacity and likely a reduced immune response.[126,127] Lipid nanoparticles (LNP) are cationic compounds that get wrapped in negatively charged plasmid DNA, minimising the risk of nuclease-mediated degradation while enabling endocytosis or receptor-mediated uptake. Initial attempts of *ABCA4* delivery by lipid nanoparticles did not achieve transduction of photoreceptors. However, more recent attempts using an ECO/*pRHO-ABCA4* nanoparticle in *ABCA4* knockout mice demonstrated robust *ABCA4* expression in the outer segment 8-months post-injection, with subsequent improvement with the addition of an RK-promoter.[43,128]

A novel delivery method by SalioGen uses a proprietary LNP to deliver *ABCA4* alongside a proprietary enzyme that enables gene insertion by transposition. *In vivo* mouse and non-human primate experiments showed robust *ABCA4* expression in outer segments and ~30% transduction when analysing retinal whole mounts.[129,130] It has not been reported how many times the gene of interest inserts into the genome, which could be a point of concern in the future. However, it does not induce double-strand breaks upon insertion, vastly improving the safety profile.[129,130] The clinical trial, SGT-1001, was intended to begin in 2025, but the company has since shut down (https://saliogen.com/).

An alternative method to LNPs are virus-like particles (VLPs), which are protein complexes that resemble a virus but are non-infectious. Although these have not yet been used to deliver *ABCA4,* they have been used *in vivo* to deliver Cas-based (discussed in 1.8) ribonucleoproteins to the retina for gene editing.[131]

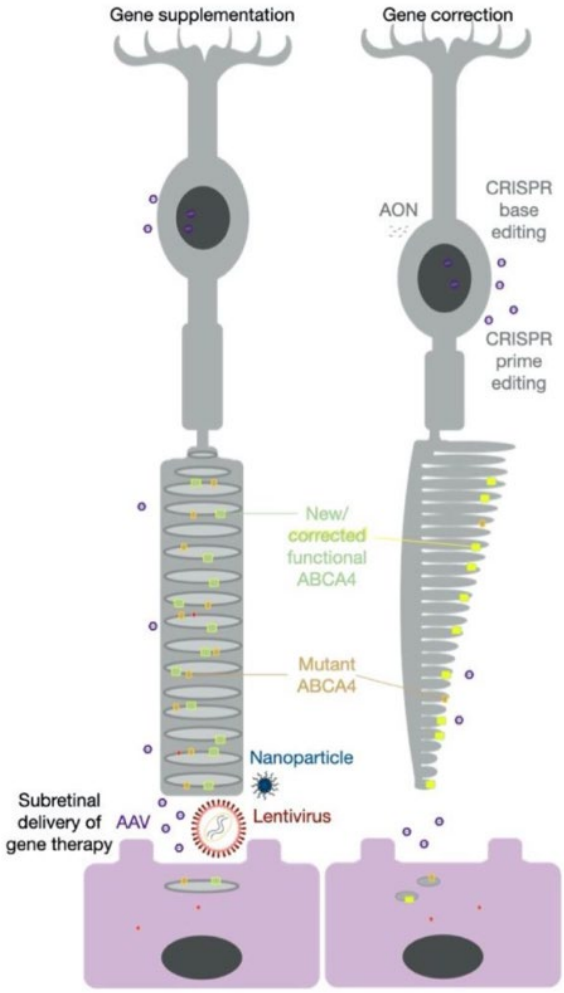

Figure 1-6: Viral and non-viral gene therapy active sites in the retina.
Diagram showing where several gene therapy delivery methods would act. Subretinal injection would insert the gene therapy between the photoreceptors and the RPE. Gene supplementation would enable wildtype expression of *ABCA4*; however, this would be alongside mutant *ABCA4.* Targeting by CRISPR-Cas therapies would correct the genomic or transcriptomic mutation, leading to corrected *ABCA4* expressed in the cell. Either would hopefully mitigate the build-up of bisretinoids. From: *Piotter, E., McClements, M. E. & MacLaren, R. E. Therapy Approaches for Stargardt Disease. Biomolecules* ***11*** *(2021). https://doi.org/ARTN 117910.3390/biom11081179.*

1.7.3 Small molecule and cell therapy treatments

An alternative approach to gene therapies are small molecule therapies where points in the visual cycle or retinal function that are affected by Stargardt disease are targeted. These are unlikely to be curative but may alleviate symptoms and/or inhibit progression of the disease. Finding candidates is difficult and usually requires large-scale screening processes. Several clinical trials have been undertaken or are currently underway, with some yielding promising results (Table 1-2 and Figure 1-7).

It is hypothesised that levels of all-*trans*-retinal/PE and subsequently A2E could be reduced by reducing levels of Vitamin A, a precursor to 11-*cis*-retinol. Administration of deuterated vitamin A, gildeuretinol, which is unable to dimerise and thus form bisretinoids, showed prevention of a disease phenotype in *ABCA4* knockout mice.[74] The Phase I and II clinical trial (ALK-001) results have been promising, demonstrating a favourable safety profile and showing 28% slower growth rate of atrophic lesions in the treated arm.[132] ALK-001 has very recently been granted Breakthrough Therapy Designation and Orphan Drug Designation in the treatment of Stargardt, with negotiations ongoing (Alkeuspharma.com; accessed 9-12-24). Another vitamin A-related treatment, fenretinide, is a synthetic vitamin A derivative that binds retinol-binding protein (IRBP), reducing circulating levels of vitamin A and thus A2E. While *in vivo* preclinical work showed promising results, a Phase II clinical trial of age-related macular degeneration showed adverse events in the high dose and no significant efficacy at the lower doses. Another promising clinical trial, the DRAGON Phase III trial by Belite Bio, reduces the transport of retinol to the retina by inhibiting retinol binding protein 4 (RBP4). This has shown promising results of slowed disease progression and a favourable safety profile.[133,134] Long-term effects of altered vitamin A levels by novel small molecule therapies remain unknown. Emixustat hydrochloride reduces retinaldehyde by inhibiting RPE65 and thus slows the regeneration of 11-*cis*-retinal.[135] Results of the Phase IIa clinical trial confirmed biological activity and a 24-month Phase III trial is currently in progress.[136] Several other dietary supplements and small molecule therapies have been tested and are shown in Table 1-2.

Lastly, cell replacement of the RPE has been tested with human embryonic stem cell derived RPE monolayers. No adverse events were reported, however, no improvements in retinal function or visual acuity were apparent. A key consideration with RPE cell replacement is that it

does not target the cause of the disease and is likely a shorter-term solution but potentially has a greater treatment window.[137]

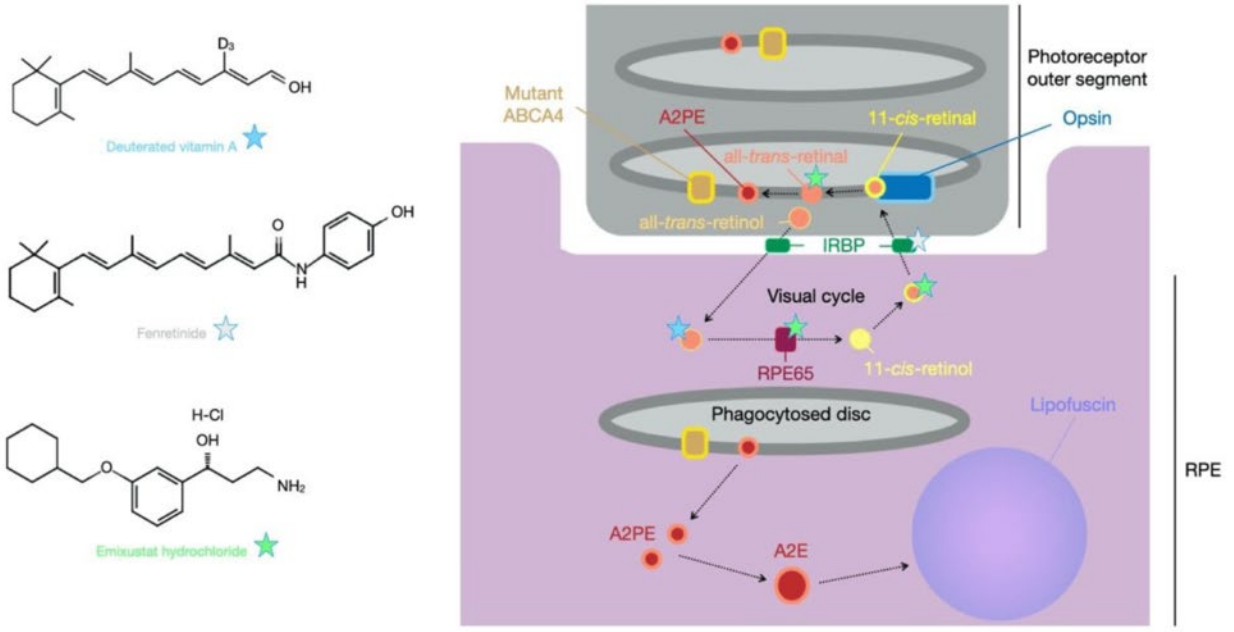

Figure 1-7: Sites of activity of representative small molecule therapies for Stargardt disease. Representative small molecule therapies that act at various points throughout the visual cycle to minimise the effects of nonfunctional ABCA4 and slow disease progression. Deuterated vitamin A/ALK-001 (blue star) cannot dimerise and is thus cannot form toxic bisretinoids. Fenretidine binds to retinol-binding protein (IRBP) reducing retinol transport, thus reducing vitamin A and subsequent A2E build-up (Grey/light blue star). Emixustat hydrochloride inhibits *RPE65,* slowing the visual cycle and reducing regeneration of 11-*cis*-retinal. This reduces all-*trans*-retinal decreasing build-up of A2E. *Piotter, E., McClements, M. E. & MacLaren, R. E. Therapy Approaches for Stargardt Disease. Biomolecules* ***11*** *(2021). https://doi.org/ARTN 117910.3390/biom11081179*

1.7.4 Unmet need for treatments

Multiple clinical trials for small molecules have shown promising results in reducing symptoms and demonstrate favourable safety profiles.[132,133] However, the long-term efficacy and systemic effects of these is unknown. Gene therapies for Stargardt disease have shown limited success *in vivo* with little translation to success in clinical trials, thus far. Nonetheless, many clinical trials using novel methods are underway, providing an exciting outlook for potential therapeutics.

Strategy	Therapy	Trial	Phase	Data
Gene based				

Gene supplementation	Lentivirus	NCT01367444 NCT01736592	Phase I/IIa	Adverse events and no visual improvements.[35]
	Dual AAV	Splice Bio*	Phase I/II 2024-2025	
	Dual AAV	AAVantgarde*	Phase I/II 2024-2025	
	Lipid nanoparticle delivery	SalioGen	Phase I/II 2024-2025	SalioGen has shut down
	mRNA- trans splicing	NA	Pre-clinical	
Gene modulation	Pre-mRNA *trans*-splicing (ACDN-01)	NCT06467344	Phase I/II	
Optogenetics	MCO AAV delivery and light activation	NCT05417126	Phase IIa	3dB gain, no adverse events[138,139]
Gene modulation	AON	NA	Pre-clinical	
Gene editing	CRISPR base editing G1961E	NA	Pre-clinical	

Pharmaceutical

Deuterated Vit. A	ALK-001	NCT02402660 NCT04239625	Phase II Open-label extension	28% reduction of atrophic lesions.[132]
Visual cycle modulater	Emixustat hydrochloride	NCT03772665	Phase III completed	No change in macular atrophy growth; subgroup with small atrophic lesions showed 40.8% reduction after 2 years.[139]
IRBP inhibitor	Fenretidine	No STGD trial		
	A1120	None reported		
	STG-001	NCT04489511	Phase II completed	
RBP4 inhibitor	Tinlarebant	NCT05244304	Phase III	Safety and tolerability in completed Phase II. Breakthrough Therapy designation granted.[134]
C5 inhibition	Avacincaptad pegol	NCT03364153	Phase IIb (initiated 2017)	No data for STGD1 patients published.
	Eculzimab	No STGD trial		

				Well tolerated in AMD patients but no signs of efficacy
Dietary				
	DHA	NCT00060749	Phase I (completed 2017)	No effect on visual function.[140]
	Omega-3 Fatty Acids	NCT03297515	Prospective trial completed 2020	6 ETDRS letter improvement. [141]
	Saffron	NCT01278277	Phase I/II completed	No adverse effects, no visual improvements.[142]

Table 1-2: Clinical trials for Stargardt disease.
Table summarising completed or ongoing clinical trials for Stargardt disease organised by therapy type. Entries with a * are aiming to launch clinical trials in 2024-2025. Several pre-clinical studies are reviewed further in Wang et al, 2023.[139] Adapted from: *Piotter, E., McClements, M. E. & MacLaren, R. E. Therapy Approaches for Stargardt Disease. Biomolecules **11** (2021). https://doi.org/ARTN 117910.3390/biom11081179* and updated.

1.8 Gene editing systems

1.8.1 Discovery and evolution – CRISPR-Cas

Initially, genome editing research was centred on zinc-finger nucleases (ZFN)[143,144] and Transcription Activator-Like Effector Nucleases (TALENs).[145-147] Although editing was achievable, the design was complex, requiring engineering of new enzymes for each target. [148,149] Simultaneously, research was undertaken to understand the role of Clustered Interspaced Short Palindromic Repeats (CRISPR) discovered in *E.coli* and their role in bacterial immunity.[150,151] The cumulative acquired knowledge from developing and researching gene editors and understanding the innate CRISPR system enabled the subsequent application of CRISPR-Cas as a simple yet powerful gene editor.[152-155]

The Cas (CRISPR-associated) family is complex but maintains the same guide-directed mechanism, whereby the Cas enzyme complexes with a target-specific guide enabling editing at a specific site. For this, all of the Cas systems require a CRISPR RNA (crRNA) to target a specific region. The Cas9 variants that target DNA also require a trans-activating CRISPR RNA (tracrRNA) that forms a scaffold to which the Cas enzyme can bind.[156] Fortunately, the system of two CRISPR RNAs was simplified into one small guide RNA (sgRNA) consisting of the protospacer to bind the target site and a scaffold to complex the Cas. For cleavage to occur, the

protospacer requires an adjacent short sequence motif of ~2-7bp, called the protospacer adjacent motif (PAM), which differs between Cas species/orthologues. Taken together, the Cas9:sgRNA complex randomly interrogates the cell genome for appropriate PAM sites, where, upon PAM recognition, the Cas9 protein unwinds the target region. If the sequence is complementary, the Cas9 creates a double-strand break through cleavage by the RuvC and HNH domains.[152,157] If not, the Cas9 continues interrogating the genome.

Streptococcus pyogenes Cas9 was the initial variant used.[152] Several variants from a variety of bacterial species have since been discovered, with continued investigation into novel variants. For example, *Staphylococcus aureus,*[158] *Campylobacter jejuni,*[159,160] and *Staphylococcus auricularis*[161] are smaller Cas9 proteins with diverse PAM sites, enabling a broader range of gene targeting strategies. These variants have been engineered further by Phage-Assisted (non-)Continuous Evolution (PA(N)CE) to improve PAM-site flexibility.[162]

1.8.2 DNA editing with CRISPR-Cas

1.8.2.1 Non-homologous end joining (NHEJ) and Homology-directed repair (HDR)

Double-strand breaks can be repaired by non-homologous end joining (NHEJ)[163,164] or homology-directed repair (HDR)[165] in eukaryotic cells. These cell repair mechanisms determine the sequence alteration, rather than the Cas9. NHEJ is an error prone repair that can occur throughout the cell cycle, including in post-mitotic cells such as photoreceptors.[166] It results in random insertions and deletions (indels) that disrupt the target sequence, which renders it useful in gene knockdown. This approach has been translated to a clinical trial by Editas Medicine (EDIT-101), using two gRNAs to target a cryptic splice site mutation in *CEP-290*.[57] Despite initial data indicating a promising safety profile and encouraging data, where 64% of patients demonstrated meaningful improvement from baseline, the trial was paused in 2022.[57,167]

The homology-directed repair (HDR) pathway uses DNA templates for relatively error-free repair, which enables gene editing through administration of a donor template with long homology arms.[165] Unfortunately, HDR is inefficient in post-mitotic cells given its activity during the S/G2 phases of the cell cycle.[166] It has therefore also demonstrated minimal efficacy in photoreceptors. However, in iPSC models targeting *ABCA4* by HDR, successful editing was achieved in 70% of clones, albeit alongside administration of HDR activators and NHEJ

inhibitors.[168] This remains a viable possible strategy in instances of personalised cell-replacement therapy.

Since the development and application of Cas9 to gene editing, many iterations have been created by modifying the Cas or fusing effectors to the Cas enzyme to further editing capabilities.

1.8.2.2 Epigenetic editing

Initial modifications to Cas9 enabled gene expression modulation of a target gene through up- or down- regulation. CRISPR inhibition (CRISPRi)[169,170] and CRISPR activation (CRISPRa)[170] retain a guide-directed DNA targeting mechanism but have a catalytically inactive, or 'dead,' Cas enzyme (dCas). The binding of dCas to the target site can result in gene repression, however, regulatory function is improved through fusion to a repressor. Conversely, fusion to an activator protein domain can enable gene expression.[171] Although not as efficient as active Cas9, this is of particular translational interest due to the decreased risk of off-target activity, given the lack of double-strand breaks.[170,172,173] Epigenetic editing has continued to evolve to enable changes to gene expression such as DNA methylation, histone modifications, chromatin accessibility, and interactions with RNA through the addition of effectors, RNA aptamer systems, protein-recruitment systems, or chemical ligation strategies to dCas9.[174]

1.8.2.3 DNA base editing

The development of two DNA base editors, Cytosine Base Editors (CBE) and Adenine Base Editors (ABE), has allowed for precise editing of mutations in non-dividing cells, independent of HDR and double-strand breaks.[175] Base editors consist of a modifying effector enzyme, a deaminase, that acts on ssDNA fused to a catalytically impaired Cas9, enabling implementation of all four transition mutations (C-T, A-G) (Figure 1-8). Specifically, the gRNA:Cas complex binds the target region, exposing the target to the deaminase domain for modification. To promote repair of the non-edited strand, the Cas9 'nickase' makes a cut (ie 'nick') in the non-edited strand, directing cellular repair processes to the site.[176,177] The deaminase domains of both CBEs and ABEs act within a specific "editing window" within the spacer. A restricted editing window improves target specificity by reducing the chances of bystander editing, however, this further limits the targetable bases beyond the PAM site

requirement. Conversely, a larger editing window increases targetable bases, but also increases the likelihood of bystander editing at non-target bases within the editing window.

Adenine base editors (ABEs) were developed since they are highly translationally relevant, with ~48% of pathogenic point mutations amenable to A>G correction. Since no adenosine deaminase enzymes that act on ssDNA naturally occur, the first generations of ABEs used a modified *E. coli* tRNA adenosine deaminase (ecTadA). The modified TadA catalytic site enabled effective targeting of ssDNA and converted adenosine to inosine, which is functionally read as guanosine and thus enables A>G editing.[176] To improve editing rates, the first-generation ABE underwent significant directed evolution and iterative testing to develop ABE8e. The catalytic rate of the TadA domain was improved 590-fold, an efficiency reflecting the DNA association time of size minimised Cas variants. However, this simultaneously increased off-target editing. The introduction of a point mutation, V106W, substantially reduced the observed off-target editing.[178] Interestingly, off-target editing *in vivo* is further reduced.[177,179,180]

Cytosine base editors initially used a rat-derived cytosine deaminase Apolipoprotein B MRNA Editing Enzyme Catalytic Subunit 1 (APOBEC1) fused to an impaired Cas9 enzyme, facilitating cytosine to uracil conversions. Uracil is functionally read as a thymine, thus making C>T edits. The first-generation CBE was highly efficient *in vitro* but lacked activity in human cells due to the base excision repair (BER) pathway, which resulted in reversion to the mutant base. The addition of uracil DNA glycosylase inhibitor (UGI) inhibited BER activity and thereby mitigated reversion to the mutant base.[176,177] Interestingly, recently developed CBEs use an evolved TadA deaminase domain (TadCBEs) instead of an APOBEC domain and exhibit on-target editing levels of the best-performing APOBEC CBE (BE4max).[181] Further flexibility to the TadA catalytic site has enabled deamination of both cytosines and adenines with one base editor, the CABE-T.[182]

Both ABEs and CBEs have undergone significant directed evolution to improve on-target editing, reduce off-target editing, and improve PAM flexibility.[183,184] These improvements are ongoing, with the recent release of ABE9e.[185] Further, to create size-minimised versions, SpCas was replaced by smaller Cas variants. The size-minimised ABEs initially demonstrated substantially reduced editing due to an insufficient binding time by non-SpCas9 variants. The evolved TadA with improved catalytic activity (590-fold improvement) enabled the production of size-minimised ABEs as editing could occur within the time the Cas was target bound.[179] Since,

Staphylococcus aureus Cas9 and other small Cas9 variants have shown promising editing rates as base editors,[179] and have been size minimised further through iterative design to enable packaging in single AAVs. *In vivo* testing of the single AAVs exhibited editing at or above the rate of the dual vector approach, with *in vivo* editing rates of 66% (liver), 33% (heart), and 22% (muscle).[180] Retinal DNA editing using the SaCas size-minimised ABEs is a significant theme of this thesis.

For retinal disease, base editors have demonstrated efficient editing in both the RPE and photoreceptors. Dual AAV delivery of a PAMless SpCas9 ABE orthologue, SpRYABE8e, to photoreceptors achieved mean editing of 9.6% targeting *Pde6b*, resulting in restored PDE6B protein expression in the outer segments and demonstrated functional rescue.[186] Another study used a lentivirus delivered ABE to target a mutation in *RPE65* (expressed in the RPE and thus readily targetable by lentivirus) and showed mean editing rates of 27% and achieved up to 40% *in vivo.*[187] Most recently, an AAV delivered split-intein SpABE targeting the G1961E mutation in *ABCA4* demonstrated editing of 31% in mice and 10% in NHP cones at a clinically relevant dose.[102] Base editors have been expanded to include glycosylase base editors and transversion base editors, enabling greater flexibility in precision base editing.[188,189]

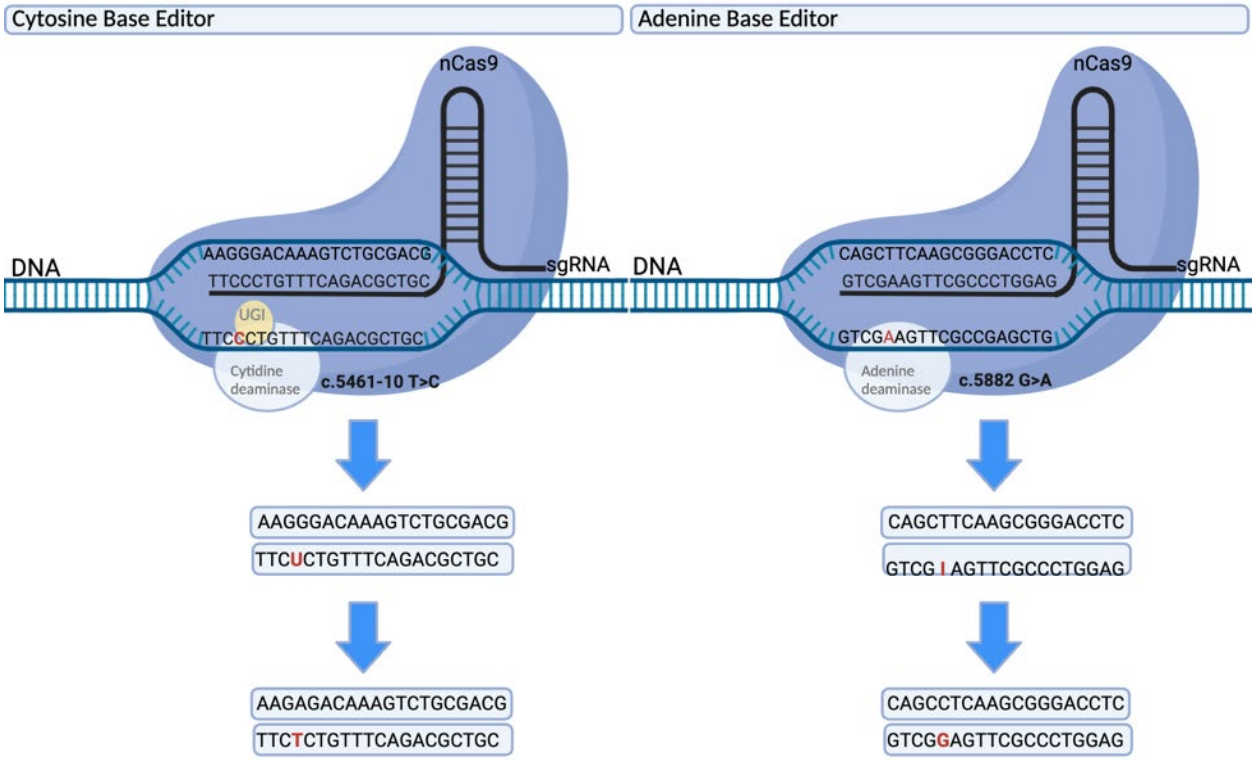

Figure 1-8: Cytosine and adenine base editing.

Diagram of cytosine (left) and adenine (right) base editing. The gRNA:nCas9-deaminase complex interrogates the genome for PAM-sites, unwinds the DNA, and attempts to hybridise the guide. When sequence complementarity is found, the guide binds and freeing up the target strand. This allows the deaminase domain to act on the editing window and deaminate the target cytosine (CBEs) or adenine (ABEs) to a uracil or inosine. Uracil is functionally read as thymine and inosine is functionally read as guanosine, thereby mediating C>T (CBE) or A>G (ABE) editing in DNA. *Piotter, E., McClements, M. E. & MacLaren, R. E. The Scope of Pathogenic ABCA4 Mutations Targetable by CRISPR DNA Base Editing Systems-A Systematic Review. Front Genet* ***12*** *(2022). https://doi.org/ARTN 81413110.3389/fgene.2021.814131*[67]

1.8.2.4 Prime editing

Prime editing is a relatively recent method to overcome the limitations of base editing by enabling precise editing of all 12 transition and transversion mutations, alongside small insertions and deletions. Prime editors consist of a Cas9 nickase fused to an engineered reverse transcriptase and are delivered with a complex prime editing guide RNA (pegRNA). Contrary to prior Cas systems, the pegRNA contains a segment of the guide to bind the target-site, as well as a segment of the guide containing the correct sequence. This enables modification of the target region in a programmable manner.[190] However, prime editing is notoriously site-dependent, likely given the complexity of the mechanism. Due to the increased points of required complementarity, the relative risk of off-target editing is decreased.[190] Prime editing is highly versatile, though, with novel methods, such as twin prime editing, enabling targeted integration of >5,000bp.[191]

In the retina, prime editing has yielded exciting results. AAV split-intein delivery of a prime editor targeting *RPE65* c.130 C>T in *rd12* mice resulted in 16% on-target editing with no detectible off-target edits, restored RPE65 expression, rescued function, and preserved photoreceptors.[192] This was investigated further using an RNP prime editor delivered by virus-like particle, achieving 7.2% editing.[131] Another study targeting *Pde6a* c.2009 A>G achieved editing rates of 9.7% *in vivo* with no off-target editing in photoreceptors.[193]

One of the main limitations of prime editing is hypothesised to be the extreme site-specificity due to the relative complexity of the system.[194]

A novel Bridge RNA editing system allows for many of the advantages of prime editing by enabling insertion, excision, and inversion editing at target sites through an RNA-guided recombinase. This system overcomes the size limitation of prime editing, at ~1700bp.[195]

1.8.3 RNA base editing

RNA has been an attractive target for gene editing due to its transient nature and reduced implications of off-target editing. Although off-target editing remains a point of concern, no irreversible changes are made to the genome. Cas13 RNA base editing is a main theme of this thesis.

Although no adenosine deaminase acting on ssDNA exists, two adenosine deaminase acting on RNA (ADAR) mediate A-to-I editing of dsRNA in human cells.[196] A third ADAR exists that is hypothesised to regulate mRNA stability and inhibits translation in neuronal development and is thus not discussed throughout the thesis.[197] As with the ABEs, the adenosine deaminated to inosine is functionally read as guanosine, and thus mediates A>G editing.[196] The edit-site is indicated within the guide by an A-C mismatch, which is preferred by ADARs. ADAR1 is expressed ubiquitously, has two isoforms, and mainly targets repetitive regions. ADAR2 is most highly expressed in the brain, lung, and bladder, and targets non-repetitive coding regions.[196,198,199] Expression of ADAR2 has been observed in retinal ganglion cells,[200] but has not been thoroughly examined in other retinal cell types.[198] Given the natural A>G mechanism of ADARs, these have been harnessed and modified to allow for precision base editing of RNA by multiple modalities.

ADAR1 and ADAR2 have known sequence preferences. Both ADAR1 and ADAR2 show a preference following U > A > C > G at the 5' site. At the 3' site, ADAR1 has a G > C ≈ A > U preference and ADAR2 exhibits a G > C > U ≈ A preference.[198]

1.8.3.1 Cas13b-ADAR base editing

Cas13 is an RNA-guided endonuclease that mediates cleavage of ssRNA with the higher eukaryotes and prokaryotes nucleotide-binding (HEPN) domains.[201,202] Multiple Cas13 orthologues exist, including Cas13a[201,202] Cas13b,[203] Cas13c,[204] Cas13d,[205] Cas13X, and Cas13Y.[206] Similar to Cas9, the Cas13 orthologues have a protospacer flanking site (PFS) in bacteria, however, this is a sequence preference that affects efficacy rather than a cleavage necessity.[202] Interestingly, in mammalian cells, all PFS combinations resulted in activity suggesting a PFS constraint does not exist.[199] This provides a significant advantage over PAM-restricted Cas9 editing. Cas13-mediated transcript knockdown using the size-minimised Cas13bt has shown success *in vivo* and in retinal organoid models targeting *VEGFA,* where significant

knockdown of ~50% was achieved and disease progression was impeded.[207] As with DNA base editors, the guide-directed Cas13 is conducive to precision RNA editing by fusion to effectors.

A Cas13-ADAR fusion has allowed for guide-directed base editing of RNA. In Cox et al the *Prevotella* species Cas13b showed the most consistent and site-specific knockdown of mRNA targets. A deactivated PspCas13b was thus fused to the deaminase domain of ADAR1(E1008Q)[208] and ADAR2(E488Q).[209] These previously determined hyperactive ADAR variants[209] were used to increase the likelihood of on-target activity, despite the increased likelihood of off-target editing.[199] The dCas13b-ADAR$_{DD}$ is directed to the target site by the C-mismatch containing guide, where the bound guide forms a double-stranded RNA region. This allows for ADAR activity at the target A-C mismatch site, where the target A is deaminated. The dCas13b-ADAR$_{DD}$(E488Q) became known as REPAIRv1 and demonstrated *in vitro* editing rates between 15-40%. However, there was substantial off-target editing due to the hyperactive variant. Subsequent rational design with the addition of a second mutant, T375G, significantly reduced off-target editing, which corresponded with significantly less on-target editing. The dCas13b-ADAR$_{DD}$(E488Q/T375G) orthologue was called REPAIRv2. Both REPAIR systems demonstrated targeting of a broad range of sequence contexts, despite the known ADAR motif preferences mentioned earlier.[199] Throughout this thesis, REPAIRv1 was used given the increased editing efficiency.

REPAIRv1 has recently been applied in the retina, achieving ~2% editing and demonstrating detectable protein by IHC.[210] Two *in vivo* studies targeting the inner hair cells of the ear with a size-minimised Cas13-ADAR (mxABE) have demonstrated on-target editing, although at varying efficiencies. One study targeting *MYO6 in vivo* achieved editing of ~4%.[211] In contrast, the study targeting the *OTOF* gene reported on-target editing of 80%.[212]

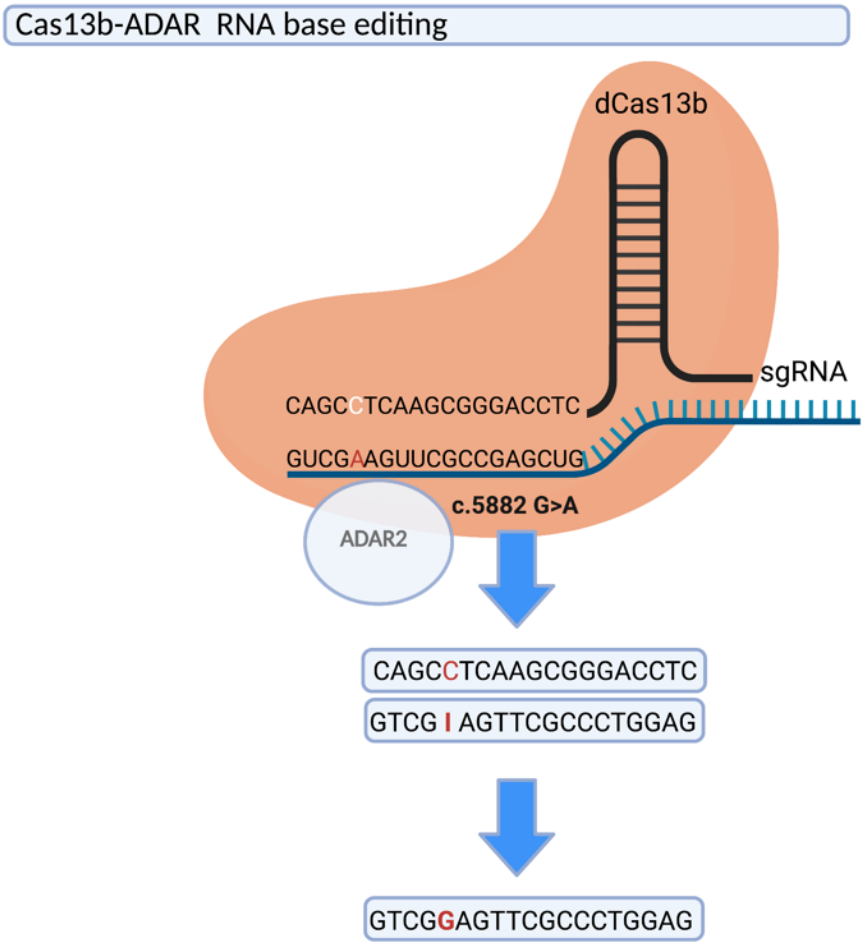

Figure 1-9: dCas13b-ADAR$_{DD}$(E488Q) RNA base editing.
The dCas13b-ADAR$_{DD}$ binds to the target site, creating a double stranded RNA target region. An A-C mismatch indicates the target site. The ADAR2 deaminase domain fused to the dCas13b deaminates the target A to inosine, which is functionally read as guanosine, enabling A>G editing of RNA. *Piotter, E., McClements, M. E. & MacLaren, R. E. The Scope of Pathogenic ABCA4 Mutations Targetable by CRISPR DNA Base Editing Systems-A Systematic Review. Front Genet* ***12*** *(2022). https://doi.org/ARTN 81413110.3389/fgene.2021.814131*[67]

1.8.3.2 Exogenous and endogenous ADAR

Alternative methods focus on ADAR recruitment to a target site via specially designed guides, coupled with either exogenous ADAR delivery or harnessing endogenously expressed ADAR. Many variations of ADAR and guide design have been tested, such as the MS2 stem-loop, GluR2 hairpin motif, and other chemically modified guides.[213,214] Novel circularised ADAR recruiting guide (cadRNA) designs have yielded promising results *in vitro* and *in vivo* using both exogenously delivered and endogenous ADAR. The circular design prevents guide degradation by exonucleases, thus enabling sufficient time for editing of the target site. Further

guide modification with the creation of bulges has improved on-target editing and reduced off-target and bystander editing, a particularly important feature given the 100-200nt length of the guide.[215]

In vivo AAV delivery of a cadRNA harnessing endogenous ADAR targeting a mutation in *PCSK9* achieved editing efficiencies of 53%. Further editing of a common stop mutation in the *IDUA* gene implicated in Hurler syndrome yielded editing of 7-17%.[215,216] Critically, it was confirmed that editing occurred due to ADAR1 recruitment, which is ubiquitously expressed. This would allow for application in the retina, where it is yet to be tested and it is currently unknown if ADAR2 is expressed.[198] While exogenously delivered ADAR can be utilised, regulation of expression is critical given that ADAR overexpression can possibly alter cell-physiology due to high levels off-target activity.[215]

1.8.4 Off-target editing

Although DNA and RNA base editing have revolutionised gene editing and its clinical potential, careful consideration of the limitations is required. Off-target editing due to mismatch tolerance within the guide poses the risk of unwanted, detrimental edits throughout the genome or transcriptome. Continued evolution of base editors has created multiple high-fidelity orthologues that have substantially reduced or show no detectable levels off-target editing.[179,217] Further, off-target editing by SaCas9 base editors *in vivo* had not been reported.[158,218] However, low-levels have been reported with the single AAV deliverable orthologue.[180] When targeting the transcriptome, the potential side-effects are in principle lower given the transient nature of RNA, but truncated transcripts, altered protein interactions, and subsequent altered cell physiology remain risks.[215]

In silico tools allow for prediction of potential off-target sites but this is limited as prediction tools are typically designed for SpCas, rather than other Cas variants such as SaCas or Cas13. Further, many predictive algorithms exist, which present varied accuracy.[219] *In silico* predictive tools can be coupled with sensitive assays, that enable screening of off-target sites for DNA editing.[220] To thoroughly examine off-target editing, whole-genome/transcriptome sequencing provides the most accurate look at off-target sites however, this is costly.

Cas-independent off-targets also pose a risk, where local bystander editing by the deaminase domain occurs within the editing window.[178] Fortunately, these are easy to predict and

determine the outcome of. Given the rapidly increasing number of Cas9 orthologues, site specificity can be optimised.[180,221] In the case of Cas13-ADAR, promiscuous ADAR activity can result in Cas-independent off-target sites, particularly at preferred ADAR motifs.[198,199] For RNA base editors, creating bulges via G- mismatches reduces bystander editing within the guide.[198,215]

Fortunately, the plethora of pre-clinical work and exciting novel clinical trials will continue to shed light on off-target editing.

1.9 Thesis aims and outline

ABCA4 is the most common inherited macular degeneration with no treatment available. DNA and RNA base editing have revolutionised the potential of gene editing and provide site-specific amelioration of pathogenic mutations. This thesis aimed to compare different base editing approaches in targeting *ABCA4* across multiple models to determine an effective gene editing strategy. Based on this, specific aims were examined:

1. **To characterise the genetic landscape of ABCA4 and establish the relevance of base editing for ABCA4.**
   DNA and RNA base editing have become promising therapeutic approaches in correcting pathogenic genetic variants for genes not amenable to gene augmentation therapy. Due to limitations such as PAM sites and editing windows, variant databases and published patient cohorts were analysed to determine the applicability of common base editors as an editing strategy for *ABCA4.*

2. **Develop a pipeline to compare DNA and RNA base editing in targeting the same *ABCA4* mutation.**
   Based on the analysis in aim 1, a nonsense mutation (c.206 G>A) with multiple PAM sites was selected for targeting. A size-minimised SaKKHABE8e DNA base editor and dCas13b-ADAR$_{DD}$ RNA base editor were selected to target the mutation and determine which is more suitable for targeting *ABCA4,* hypothesising that the DNA base editors enable the required editing rate for outer segment renewal. *In vitro* screens were conducted, and analysis performed at the DNA, RNA and protein level to provide a well-rounded comparison.

3. **Test AAV-delivered DNA and RNA base editors in targeting *ABCA4 in vivo.***
   Since the clinically relevant mouse model could not be developed within a sufficient timeframe (still in production), SaKKHABE8e and dCas13b-ADAR$_{DD}$ were compared by targeting the *ABCA4* start codon to knockdown expression in a heterozygous *ABCA4*$^{wt/ko}$ mouse. During the time of this project, a novel all-in-one SaKKHABE8e deliverable in a single AAV was published and added to the comparison, as it was hypothesised to perform best *in vivo* given the all-in-one delivery. The three base editors were first screened *in vitro* using the pipeline developed in aim 2 and then tested at a range of doses *in vivo* to determine which base editor most effectively targets *ABCA4* in a complex model.
4. **Screen a clinically relevant mutation and transduce retinal organoids to target *ABCA4***
   Initially, a patient-derived retinal organoid was to be developed and targeted by the three base editors. For this, *in vitro* screens targeting the patient mutation were conducted further comparing the DNA and RNA base editors. Unfortunately, the organoids did not differentiate and thus were not available. Instead, a base near the patient mutation was targeted in wildtype organoids to determine if the exon 2 region is targetable and determine if AAV-delivered base editing is achievable in retinal organoids.

2 Methods and Materials

Experiments were conducted using calibrated instruments. Nucleotide sequences such as primers, oligos, plasmid maps, and cell-lines for the general methods are detailed in the Appendix.

2.1 Base editing plasmids

The key base editing constructs used are in Table 2-1. Figure 2-1 shows plasmid maps of these constructs.

Plasmid components	Name/Referenced as	Source	Target	Further details
pC0053-CMV(or RK).IE-dPspCas13b-GS-ADAR2DD(E488Q)-delta-984-1090 [199]	dPspCas13-ADAR$_{DD}$ (Cas13-ADAR)	Kind gift of Lewis Fry; Addgene 103869	RNA	Guide delivered separately
pCMV (or RK)-ecTadA(8e)-nSaCas9(KKH)[179]	SaKKH – ABE8e (Dual vector SaKKH)	Kind gift of Maria Kaukonnen; Addgene138502	DNA	Guide delivered separately
AAV-EFS (or RK)-SaKKHABE8e-bGH-U6-sgRNA-BsmBI[180]	AiO SaKKH	Kind gift of Ahmed Salman; Addgene 189923	DNA	All-in-one

Table 2-1: Key DNA and RNA base editing plasmids.
CMV promoter used *in vitro* and RK promoter used *in vivo.*

The dPspCas13b-ADAR$_{DD}$ (Figure 2-1) was used for RNA editing throughout this project. This Cas13b variant is deactivated and derived from the *Prevotella* species. Two mutations, H133A and H1058A, inactivate the HEPN RNase domains of Cas13b, thereby deactivating it. The dPspCas13b has an HIV nuclear export signal (NES$_{HIV}$) which is fused via a linker to the human ADAR2 deaminase domain (hADAR2$_{DD}$), enabling A>G editing. The hADAR2$_{DD}$ contains the E488Q mutation which drastically increases editing efficiencies, including off-target editing. This construct was delivered separately to the guide-containing plasmid in a dual vector delivery system.

An evolved *Staphylococcus aureus* Cas9 base editor, SaKKH-ABE8e (Figure 2-1) was used for DNA base editing. This variant contains three mutations that relax the PAM site – E782K, N968K, and R1015H (KKH). To allow for nicking of the non-target strand, only the HNH domain is mutated with the H840A substitution.[222] To enable A>G editing, a hyper evolved e coli TadA domain is fused to the nSaKKH by an XTEN linker. For the 8e version, the TadA domain was further evolved to contain the V106W mutant to reduce off-target editing. SaKKH-ABE8e has a biparticle nuclear localisation signal (NLS). This construct was delivered separately to the guide-containing plasmid via a dual vector delivery system.

An all-in-one SaKKH-ABE8e (Figure 2-1) was also used in Chapter 6, where the base editor is identical but the W3 gamma region of the woodchuck hepatitis post-transcriptional regulatory element (WPRE) was removed, leaving only the bGH polyadenylation signal. This provided enough space between ITRs for the U6 promoter, gRNA, and scaffold region in reverse orientation, thus enabling single AAV packaging and delivery.

All three constructs were under a CMV promoter for *in vitro* experiments and a rhodopsin-kinase (GRK1) promoter for *in vivo* and organoid experiments.

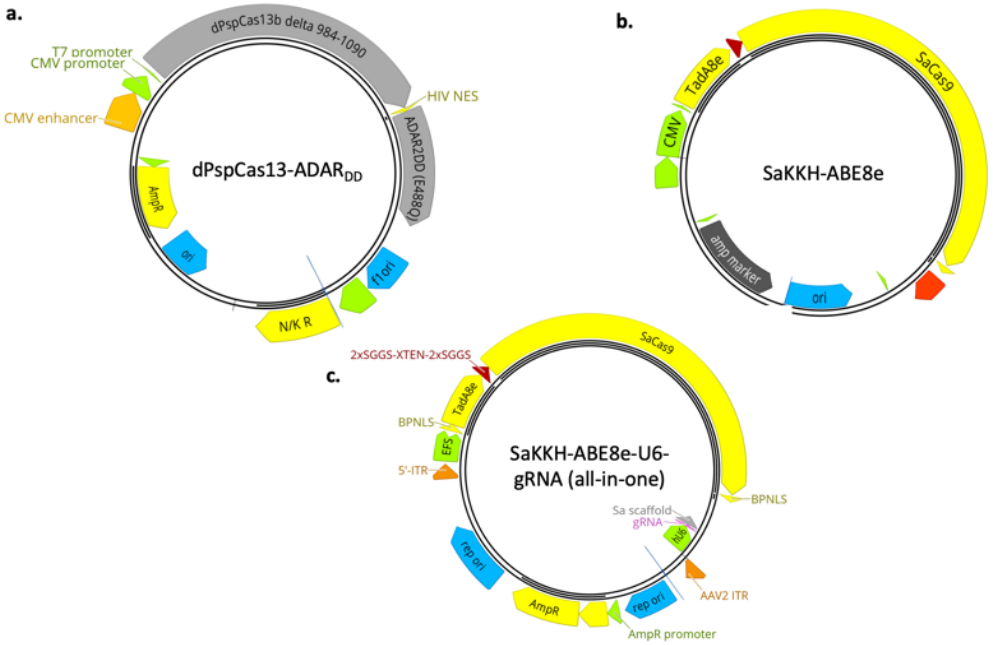

Figure 2-1: Base editing plasmid constructs.
The dPspCas13b-ADAR$_{DD}$ (a) and SaKKH-ABE8e (b) are delivered alongside a guide-containing plasmid. c. Guide plasmids are referenced in specific chapters where used. c. all-in-one delivered SaKKHABE8e with gRNA in reverse.

2.2 Molecular biology

2.2.1 *In silico* Design and Analysis

Geneious Prime software was used for all cloning experiments, primer design, variant and PAM-site analysis, and interpretation of chromatogram (.ab1) and NGS raw read sequencing results (.fasta; .fastq). To determine the effects of mutations on RNA secondary structure, 50-100bp sequences were analysed in MXfold2,[223] Vienna RNAfold,[224,225] and mFold.[226] MXfold2 uses a combination of Tuner's nearest-neighbour free energy, a deep neural network, a Zuker-style dynamic programming, and structured support vector machine to determine optimal folding. Mfold uses the Zuker algorithm and Vienna RNAfold uses the Turner 2004 parameters.

2.2.2 Polymerase Chain Reaction

Polymerase chain reactions (PCR) were performed in a Bio-Rad T1000 or SimpliAmp™ thermocycler (Bio-Rad; Thermo Fisher Scientific). Primer design followed the criteria in Table 2-2 and were commercially synthesised (Sigma-Aldrich, UK; Integrated DNA Technologies).

Property	Parameters
Length	15-25
Melting temperature	50°C - 69°C
GC content	40-60%
GC clamp	Minimum one GC nucleotide at both the 5' and 3' end
Predicted hairpin	None
Predicted self-dimerisation	None

Table 2-2: General guidelines for PCR primer design.
All parameters could not always be fulfilled.

KOD Hotstart master mix (Sigma-Aldrich), Phusion® High-Fidelity PCR Master Mix (New England Biolabs), and Platinum™ SuperFi™ II PCR Master Mix (Thermo Fisher Scientific) were used for cloning and target amplification per the manufacturer instructions. Reactions had a total volume of 50μL with components detailed in Table 2-3. Typical reactions contained 1-10ng plasmid DNA, 40ng cell-extracted plasmid DNA, 100ng genomic DNA, or 2μL reverse transcription reaction (qPCR). Cycling conditions for KOD, Phusion, and SuperFi are in Table 2-4, Table 2-5, Table 2-6 respectively.

When required, gradient PCR was performed to optimise annealing temperature and minimise non-specific amplification by running identical reactions simultaneously at different annealing temperatures. If needed, 1% DMSO was added to reactions to further minimise non-specific amplification and primer-dimer. To check PCR outcomes including band size, non-specific amplification, and contamination, products were run on a 0.8-1% agarose gel.

Component	Polymerase		
	KOD	Phusion	SuperFi
PCR Grade Water	X μL	X μL	X μL
Sense (5') Primer (10uM)	1.5 μL	1.5 μL	2.5 μL
Anti-Sense (3') Primer (10uM)	1.5 μL	1.5 μL	2.5μL
Template DNA	Y μL	Y μL	Y μL
2x Polymerase Master Mix	25 μL	25 μL	25μL
Total reaction volume	50 μL	50 μL	50 μL

Table 2-3: Components added to respective PCR reactions
For difficult PCR reactions, 1% DMSO was added to minimise non-specific amplification.

Cycles	Step	Target size			
		<500bp	500-1000bp	1000-3000bp	>3000bp
1	**Polymerase Activation**	95°C 2 min	95°C 2 min	95°C 2 min	95°C 2 min
25-35	**Denature**	95°C 20 sec	95°C 20 sec	95°C 20 sec	95°C 20 sec
	Annealing	Lowest primer T_M for 10 sec			
	Extension	70°C 10 sec/kbp	70°C 15 sec/kbp	70°C 20 sec/kbp	70°C 25 sec/kbp
1	**Hold**	4°C for ∞			

Table 2-4: PCR Cycle Conditions for KOD Hotstart Mastermix.

Step	Temperature	Time	Cycles
Initial denaturation	98°C	30 sec	1
Denature	98°C	10 sec	25-35
Annealing	Variable	20-30 sec	
Extension	72°C	15-30 sec/kbp	
Final Extension	72°C	5 min	1
Hold	4°C for ∞		

Table 2-5: PCR Cycle Conditions Phusion® High-Fidelity Master Mix.

Step	Temperature	Time	Cycles
Initial denaturation	98°C	30 sec	1
Denaturation	98°C	10 sec	25-35
Annealing	60°C	10 sec	
Extension	72°C	15-30 sec/kbp	
Final Extension	72°C	5 min	1
Hold		4°C for ∞	

Table 2-6: PCR Cycle Conditions Platinum™ SuperFi™ II PCR Master Mix.

2.2.3 Nucleic Acid Quantification

DNA and RNA concentrations were quantified using a NanoDrop spectrophotometer (Thermo Fisher Scientific). Purity was determined by the ratio of absorbance at 280nm/260nm where a ratio of 1.8-1.9 and 2.0-2.1 were accepted for DNA and RNA, respectively. Sample contamination was assessed at 230nm/260nm, with an acceptable ratio from 2.0-2.3. Some purification or extraction kits resulted in 230nm/260nm ratios <1.0.

2.2.4 Cloning Techniques

Where outsourcing was more cost-effective, particularly for difficult-to-clone plasmids, cloning was completed by Genewiz. This is indicated where relevant when listing plasmids.

2.2.4.1 Gel Extraction

0.8-1% agarose gels with ethidium bromide or GelRed (Sigma-Aldrich, UK) were visualised on an ultraviolet transilluminator. Required DNA bands were excised from the gel and extracted using the QIAquick Gel Extraction kit (Qiagen, Germany) according to manufacturer instruction.

2.2.4.2 Restriction Digestion

Restriction digestion was performed according to manufacturer instructions, typically NEB, USA or Thermo Fisher, UK. Typically, reactions were run at a ratio of 1unit restriction enzyme to 1μg DNA and 1x buffer at 37°C for 60-90 minutes unless otherwise specified. If required, shrimp alkaline phosphatase (rSAP) from NEB, USA was used for dephosphorylation.

2.2.4.3 Oligonucleotide annealing and phosphorylation

Complementary oligonucleotide pairs with restriction overhangs at the 5’ or 3’ ends were obtained from Merck. Oligos were annealed and phosphorylated in a 20μL reaction containing a

final concentration of 1.25μM forward and reverse oligos, 1μL T4 polynucelotide kinase (PNK) (Thermo Fisher Scientific), 1X reaction buffer A for T4 PNK, and 1mM adenosine triphosphate (ATP). Phosphorylation was performed at 37°C for 20 mins, followed by incubating at 95°C for 4 min and annealing via a step-wise incubation from 95°C to room temperature over 45 min.

2.2.4.4 Ligation

Ligations were performed in 10-20μL reactions with 1μL T4 DNA ligase (NEB, USA) and 1X T4 DNA ligase buffer. Backbone and oligo quantity and ratio varied depending on the ligation reaction. Reactions were incubated at room temperature (~20°C) for 2-24hrs and heat inactivated at 65°C for 10 mins. A backbone only control was run to show background re-ligation.

2.2.4.5 NEBuilder HiFi DNA Assembly™

The NEBuilder HiFi DNA Assembly™ kit was used for difficult cloning or multiple-fragment cloning per the manufacturer instructions. A molar ratio of 1:1 or 2:1 of insert:backbone was used depending on the fragment number. Reaction volume depended on fragment concentration and would be scaled accordingly to ensure 1X NEBuilder HiFi Mastermix. Samples were incubated at 50°C for 50-60 minutes and then stored on ice or at 4°C.

2.2.4.6 Site-directed mutagenesis

The QuikChange II XL Site-Directed Mutagenesis Kit was used per the manufacturer instructions. Primers were designed as described in Table 2-2, except the length was between 25-40 bases and included the desired base change. The reaction contained 10ng plasmid, QuikSolution reagent, dNTP mix, 1X reaction buffer, 1.25μM of each primer, and 1U *PfuUltra* HF DNA polymerase. Samples were cycled according to Table 2-7 and digested with *DpnI* at 37°C for 1 hour prior to transformation.

Step	Temperature	Time	Cycles
Initial denaturation	95°C	1 min	1
Denature	95°C	50 sec	18
Annealing	60°C	50 sec	
Extension	68°C	1min/kb	
Final Extension	68°C	7 min	1
Hold		4°C for ∞	

Table 2-7: Cycling conditions for QuikChange II XL Site-Directed Mutagenesis.

2.2.5 Bacterial Transformation

The various cloning protocols required a range of *E.coli* competent cells. XL-10 Gold Ultracompetent *E. coli* Cells (Agilent Technologies) were primarily used during site-directed mutagenesis, for difficult to clone plasmids, and for AAV inverted terminal repeat (ITR) containing plasmids. NEB® 5-Alpha and NEB® Stable Competent cells were used for all other transformations. All cells followed a general transformation protocol. Cells were pre-treated for 10 minutes on ice with 1-2μL of 1.43M β-mercaptoethanol per 25-50μL of cells, respectively. 2-5μL of ligation product or 1-10ng of plasmid were added to cells and incubated on ice for a further 30 minutes. Cells were heat-shocked at 42°C for 30 seconds and incubated for 2-5 minutes on ice. 225-450μL super optimal broth with catabolite repression (SOC) outgrowth medium was added to cells and then placed in an incubator-shaker at 37°C at 225rpm for 45-60 minutes. Cells were plated on LB-Agar containing Kanamycin (25-50μg/mL) or Ampicillin (100μg/mL) and were incubated at 37°C overnight. A positive control plasmid and no-plasmid negative control were included to ensure a successful transformation and no contamination.

2.2.6 Colony selection, plasmid isolation and amplification

Colonies were individually selected and cultured in 3mL LB with ampicillin (100μg/mL) or kanamycin (25-50μg/mL) in a shaker at 37°C at 225rpm for ~15-16hrs. Glycerol stocks were made by mixing the culture broth and 50% glycerol at a 1:1 ratio and stored at -80°C. Cells were then pelleted by centrifugation at 4600xg for 15 mins in a Megafuge™ (Thermo Fisher Scientific). Plasmids were isolated by Zyppy™ miniprep kit (Zymo Research) according to manufacturer protocol. Minipreps were sent for sanger sequencing to screen for correct ligation. Confirmation of ITRs was done by *Xma*I digest.

For larger, endotoxin-free preps, plasmids were expanded using either the EndoFree® Plasmid Maxi Kit (Qiagen) or NucleoBond Xtra EF Midi Kit (Macherey-Nagel). Starter cultures were LB-antibiotic inoculated from glycerol stocks or individual colonies and incubated at 37°C and 200-220 rpm for 8 hours. Larger 250-300mL LB-antibiotic overnight cultures were inoculated with 500-1000μL of the starter culture. Cultures were pelleted in 500mL Nalgene flasks at 4600xg in a Megafuge™ (Thermo Fisher Scientific) for 15 minutes at 4°C. Manufacture

protocol was then followed for the remaining prep. Plasmid expansion was occasionally outsourced to Genewiz if more time and cost-effective.

2.2.7 Cloning of sgRNAs for DNA and RNA base editing

Single guide RNAs (sgRNAs) were cloned using the same general method for both DNA and RNA base editors (Figure 2-2). Cloning specifics are described in chapter-based materials and methods. Guide oligos were designed using GeneiousPrime and commercially synthesised (Merck). Complementary oligos with desired 5' and 3' overhangs were annealed and phosphorylated (2.2.4.3) and target plasmids were digested and dephosphorylated as in 2.2.4.3. Successful digestion was confirmed by gel electrophoresis after which samples were purified using the QIAquick™ PCR purification kit (Qiagen). Annealed and phosphorylated guides were diluted 1:25 and ligated according to 2.2.4.4 with 30ng digested backbone. 2 μL ligation reaction were used for bacterial transformation. Colony selection and plasmid isolation were done as described in 2.2.6, where the best-performing guides were amplified further for downstream use. Sequences were confirmed by Sanger sequencing. Typically, for RNA editing, 15 guides would be cloned simultaneously and for DNA editing 5 guides would be cloned simultaneously.

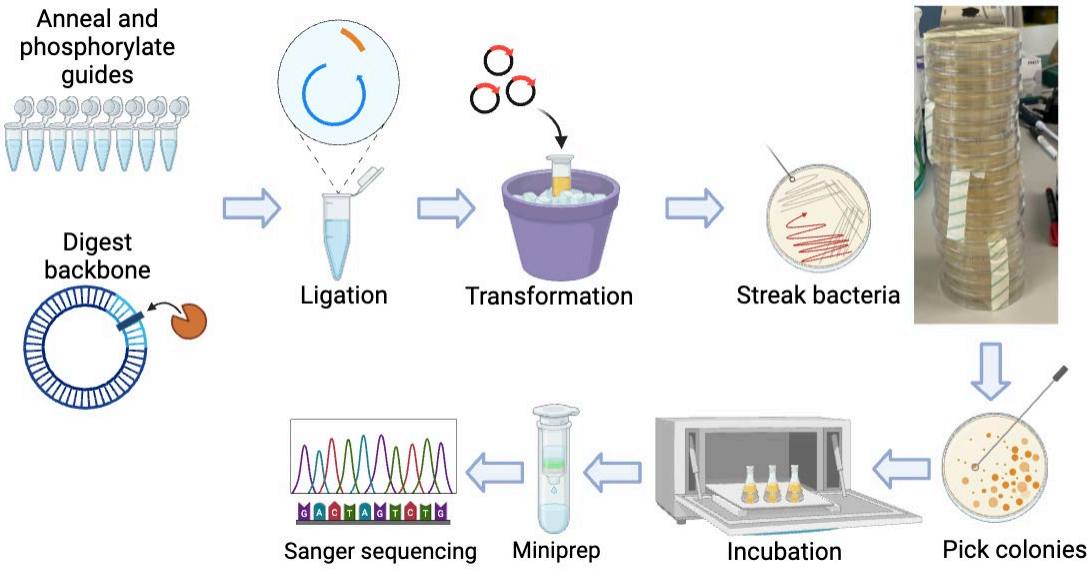

Figure 2-2: sgRNA cloning workflow.

2.2.8 DNA extraction

Cell pellets were defrosted and resuspended in PBS, RNAse A and proteinase K. The QIAamp DNA mini kit was used to extract DNA (plasmid and genomic) according to manufacturer instruction and eluted in molecular grade water. Initially, DNA extraction from neural retina samples included an extra step of homogenising for 30-60 seconds to lyse the samples before adding to RNAse A and proteinase K. For the majority of *in vivo* experiments, DNA extraction was done with the AllPrep DNA/RNA/Protein Mini Kit (Qiagen), described further in Chapter 6.

2.2.9 RNA extraction

Prior to extraction, the lab bench and instruments were bleached for 10 minutes and subsequently wiped down with RNaseZAP wipes (Thermo Fisher Scientific). Instruments would also be placed in a UV hood for 2 minutes.

RNA extraction from cells to obtain mRNA was done with the Monarch® Total RNA Miniprep Kit (NEB) according to manufacturer protocol and included the optional DNA removal step by DNAse digestion. Samples were eluted with molecular grade water.

2.2.10 cDNA synthesis

RNA was reverse transcribed to complementary DNA (cDNA) using the EvoScript Universal cDNA Master (Roche) or Transcriptor Universal cDNA Master Kit (Roche) according to manufacturer protocol. A standard 1μg RNA was combined with reverse transcription primer buffer and molecular grade water and incubated on ice for at least 5 minutes. The reverse transcriptase was added and incubated in the thermocycler according to Table 2-8.

	Evoscript		**Transcriptor**	
Step	**Temp (**°C)	**Time**	**Temp (**°C)	**Time**
Primer annealing	42	15 min	25	5 min
Reverse transcription	85	5 min	55	10 min
Denaturation	65	15 min	85	5 min
Hold	4	∞	4	∞

Table 2-8: Incubation protocols for cDNA synthesis

2.2.11 Real Time Quantitative PCR

Real time quantitative PCR (RT-qPCR) was used to measure levels of gene expression and to titre virus. For both, triplicates of each sample were run in opaque white 96 well plates (BioRad) with clear film covers (BioRad) on a CFX Connect Optics Module real time PCR machine (BioRad). The qPCR plate was centrifuged prior to the run. Cycling conditions are in Table 2-10.

For viral titre, primers were designed as in Table 2-2 and amplified regions between 60-110bp apart in iTaq Universal SYBR Green Supermix according to manufacturer protocol. The AAV titration by RT-qPCR protocol is in section 2.4.8

For gene expression, TaqMan™ probes (Thermo Fisher Scientific) targeting *abca4* and two housekeeping genes, beta-actin (actb) and glyceraldehyde 3-phosphate dehydrogenase (gapdh), were used. To test for photoreceptor health and viability in injected neural retina, a rhodopsin probe was used given the photoreceptor specific expression. Depending on the samples, custom TaqMan™ probes (20x) targeting SaCas9 and the SaCas9 guide scaffold were also used. 1μL cell cDNA sample and 1μL neural retina cDNA sample were loaded/well and the probes were used according to manufacturer protocol with the TaqMan™ Fast Universal PCR Master Mix (2x), no AmpErase™ UNG. Probes are listed in Table 2-9.

TaqMan™ Probe	Reference number
Mouse abca4	Mm00492035_m1
Human abca4	Hs00979570_m1
Mouse beta-actin	Mm02619580_g1
Human beta-actin	Hs01060665_g1
Mouse GAPDH	Mm99999915_g1
SaCas9	Custom: APKA4TC
SaCas9 Scaffold (gRNA)	Custom: APH6A7E
Mouse Rhodopsin	Mm01184405_m1

Table 2-9: TaqMan™ probes for gene expression.

Step	SYBR		Taqman™		Cycles
	Temp (°C)	Time (s)	Temp (°C)	Time (s)	
Initial denaturation	95	180	95	20	1

Denaturation	95	10	95	3	40
Annealing + extension	55	30	60	30	

Table 2-10: qPCR cycling conditions for gene expression (Taqman™) and viral titration (SYBR).

To calculate relative gene expression, the double delta CT analysis ($2^{-\Delta\Delta CT}$) was conducted. Ct and Cq values were determined in regression mode in the CFX Maestro™ Software. The geomean of the housekeeping genes was calculated for experimental and control samples (typically PBS injected samples) and used to determine the ΔCT for each sample. Given the large number of samples, an averaged PBS value was used for downstream calculations per 'batch' of qPCRs (each batch of plates was run as mouse eyes were harvested and processed). The ΔCT of the control was subtracted from the ΔCT of the experimental samples to calculate the $\Delta\Delta CT$. Statistical analysis compared the ΔCT between groups of interest depending on how the data was presented. In graphs depicting dCt values (rather than relative expression), if no transcripts were detected, the highest value of 41 was used to calculate dCt to enable graphing.

2.2.12 Protein Extraction and Quantification by bicinchoninic acid (BCA) assay

Cell pellets or retinal tissue were thawed on ice and resuspended in lysis buffer consisting of radio-immunoprecipitation assay (RIPA) buffer (Sigma Aldrich) mixed with cOmplete™ mini protease inhibitor cocktail (Roche Diagnostics). A handheld homogeniser was used for 30-60sec per sample to disrupt cells. Samples were left on ice for 30 minutes and then centrifuged for 10 minutes at 10,000xg at 4°C. The supernatant was saved for downstream use or stored at -80°C and the pellet was discarded.

A Pierce bicinchoninic acid protein assay kit (Thermo Fisher Scientific) was used according to manufacturer instruction to quantify lysate total protein. Samples were diluted 1 in 10 and incubated in darkness at 37°C for 30 minutes. Absorbance readings were measured using an iMark™ (BioRad) plate reader at 562nm with medium shaking for 3 seconds. A standard curve was derived from diluted bovine serum albumin (BSA) standards (25-2000μg/mL) from which protein concentrations were determined.

2.2.13 Western Blot

Protein lysates were prepared to equal masses and made up to equal volumes with molecular grade water. Samples were combined with 5x protein loading dye (National Diagnostics) and loaded onto a pre-cast 7.50% tris-glycine Criterion™ TGX™ gel (BioRad) alongside a BLUeye protein ladder (GeneFlow). The gel was submerged in Tris-Glycine Sodium-Dodecyl-Sulfate PAGE (SDS-PAGE) running buffer (National Diagnostics) and run at 115V.

Low fluorescence polyvinylidene difluoride (PVDF) membranes were activated in methanol and then soaked in 1X Transblot Turbo transfer buffer (BioRad). Transfer stackers were also soaked in transfer buffer. The membrane and gel were gently placed between the transfer stacks in a cassette. Proteins were transferred in the semi-dry Trans-Blot Turbo transfer system (BioRad) using the 'Mixed Weight' 2.5A/25V, 7-minute program. The PVFD membranes were briefly washed in Tris-Buffered Saline (TBS) and rocked in 5% skim milk diluted in TBS with 0.0 1% Tween®-20 (TBS-T) blocking buffer for at least one hour. Membranes were incubated in primary antibody solution at 4°C overnight and washed with TBS-T. Membranes were incubated in secondary antibody solution for 1.5 hours at room temperature protected from light and washed with TBS-T. Prior to imaging, membranes were air-dried for 10 minutes. The Odyssey Fc imaging system (Li-COR Biosciences) was used to image the membranes using 600nm, 700nm, and 800nm detection channels with exposure times of 30 seconds or 2 minutes. Image Studio Lite software was used for quantification of protein expression by outlining bands of interest. Expression was normalised to a stably expressed housekeeping protein by calculating a lane normalisation factor. Antibodies are listed in Table 2-11.

Antibody	Host	Dilution	Source
ABCA4 (C-term)	Rabbit	1:1000	Abcam; ab72955
ABCA4 clone 5B4 (N-term)	Mouse	1:1000	Sigma; MABN2440
alpha-tubulin	Mouse	1:1000	Abcam; ab7291
Beta-actin	Rabbit	1:1000	Abcam; ab8227
RED1 (ADAR2)	Rabbit	1:500	Abcam; ab64830
CRISPR-Cas9	Rabbit	1:1000	Abcam; ab203933
PspCas13b	Mouse	1:500	Diagenode; C15200250-10
IRDye 680 RD Donkey anti-Mouse	Donkey	1:10,000	Licor; 926-68072
IRDye 680 RD Donkey anti-Rabbit	Donkey	1:10,000	Licor; 926-68073

IRDye 800CW Donkey anti-Mouse	Donkey	1:10,000	Licor; 926-32212
IRDye 800CW Donkey anti-Rabbit	Donkey	1:10,000	Licor; 926-32213

Table 2-11: List of primary and secondary antibodies for western blot.

2.2.14 Sequencing and chromatogram analysis

Sequencing was commercially performed for both Sanger sequencing and Next-Generation Sequencing (NGS) by Genewiz and Eurofins Genomics. Custom designed primers were typically used for Sanger sequencing. A nanopore NGS service, PlasmidEZ (Genewiz) became available in ~ late-2022 and was used for full-length plasmid sequencing. No primers are required.

For *in vitro* work, the sequencing chromatograms were analysed in two programs to measure indel formation and/or rates of base editing. Tracking of Indels by Decomposition (TIDE) is an algorithm that measures the rate of indels by comparison of the target sequence to a wild-type sequence. EditR is an algorithm that predicts base editing in a chromatogram. It is worth noting that both algorithms require clean reads to ensure accurate output.

2.3 Cell Culture

2.3.1 Cell culture

All cell culture work was done in a designated tissue culture laboratory within class II biological safety cabinets with vertical laminar flow and aseptic technique. Testing for mycoplasma was not undertaken.

Immortalised cell lines were stored in liquid nitrogen for long-term storage. When needed, cells were thawed at 37°C, added to 9mL pre-warmed media, and centrifuged at 300xg for 5 minutes. The supernatant was discarded and the cells were resuspended in 5mL media. The full volume was transferred to a T75 flask and topped up with 5mL media and placed in a humidified incubator at 37°C and 5% CO2. After 24 hours, the media was removed and replaced with fresh media. After 48hrs further incubation, cells were ready for passage and were passaged at least two times before experimental application.

2.3.2 Cell lines and maintenance

Human embryonic kidney 293 cells expressing mutant simian virus-40 (SV40) T antigen (HEK293T) were cultured in complete high glucose (25mM) Dulbecco's Modified Eagle

Medium (DMEM). The DMEM contained 4mM L-glutamine, 1mM sodium pyruvate and phenol red, and was supplemented with 1% penicillin-streptomycin (100units/mL-0.1mg/mL) and 10% heat-inactivated or filtered fetal bovine serum (FBS). Cells were maintained in a humidified incubator at 37°C and 5% CO2 in adherent, sterile T75 flasks. Every 3-5 days, or at 70-90% confluency, cells were passaged. For passage, old media was removed, and the cells were gently washed with pre-warmed phosphate buffered saline (PBS). Cells were dissociated with 2.5mL TrypLE Express dissociation reagent (Thermo Fisher Scientific) and incubated at 37°C for 5 minutes. In the meantime, a new T75 flask was prepared with 10mL pre-warmed DMEM. Cells were resuspended in 7.5mL pre-warmed DMEM, of which 1-2mL of the cell suspension was added to the freshly prepared flask.

2.3.3 *In vitro* Plasmid Transfection

2.3.3.1 Cell Seeding

Confluent cells (>90%) underwent steps for passage as described in section 2.2.2. The remaining cell suspension was used for seeding. 100μL cell suspension was mixed with 100μL undiluted Trypan Blue Solution and placed in a Biorad TC20™ automated cell counter to count cells and assess cell viability. Cells were diluted as needed using supplemented DMEM and seeded into adherent tissue culture plates (Corning) according to Table 2-12. These values were adapted depending on growth rates of different cells batches.

Plate	Well size (cm^2)	Seeding Density (cells/well)	OptiMEM reduced serum μL/well
12 well	3.65	4.5×10^5	100
24 well	1.82	2.25×10^5	50
96 well	0.32	4.5×10^4	~9.5

Table 2-12: Cell Seeding Density and OptiMEM volumes for plasmid transfection.

2.3.3.2 Plasmid transfection

Cells were transfected 24-hours after seeding or at 60-80% confluence. TransIT-LT1 transfection reagent (Mirus Bio) and OptiMEM reduced serum media (Thermo Fisher Scientific) were brought to room temperature while plasmids were diluted and mixed according to experimental plan. TransIT-LT1, OptiMEM, and DNA were mixed and allowed to complex for

15-20 minutes at room temperature. TransIT-LT1 was used at a ratio of 3μL per 1μg DNA and OptiMEM volumes are listed in Table 2-12. The total volume of DNA, LT1 and OptiMEM was added to the corresponding well on the plate. Cells were harvested 48-72 hours post-transfection.

2.3.3.3 Cell Harvesting

Cells were washed, dissociated, and resuspended with ice cold PBS, and transferred to pre-cooled microcentrifuge tubes on ice. If the cells were required for various downstream protocols (ie DNA, RNA and/or protein extraction), the suspension volume was split across multiple tubes. The cells were centrifuged at 1100xg for 10 minutes. The supernatant was discarded and cell pellets were either stored at -80°C or immediately used in downstream protocols.

2.4 AAV Production

2.4.1 Plasmids for AAV production

AAV vectors were produced by transient transfection of HEK293T cells with plasmids encoding elements[37] for AAV formation:

- *Rep/cap* plasmid: essential for capsid proteins and replication.
- Helper plasmid: contains essential replication genes, VA, E2A, and E4.
- Transgene plasmid (pTransgene): contains the gene of interest flanked by ITRs, which are essential for replication, packaging and vector persistence.

For AAV8 production, the *rep/cap* genes and the helper genes were provided on a single plasmid, pDB8.ape (PlasmidFactory) and used in a dual transfection with the relevant pTransgene. A triple transfection was used for AAV2 where plasmids encoding the helper genes (pAdDeltaF6) and the *rep/cap* genes (pRep2Cap2 quad mutant Y272F, Y444F, Y500F, Y730F) were on separate plasmids and transfected together with pTransgene.

AAV plasmids other than pDB8.ape were expanded and purified as described in Section 2.2.6 (pHelper produced by Genewiz). Prior to use, plasmids were sequence confirmed and digested with XmaI to confirm presence of both ITRs. A summary of AAV production is outlined in Figure 2-3 and described further in the following sections.

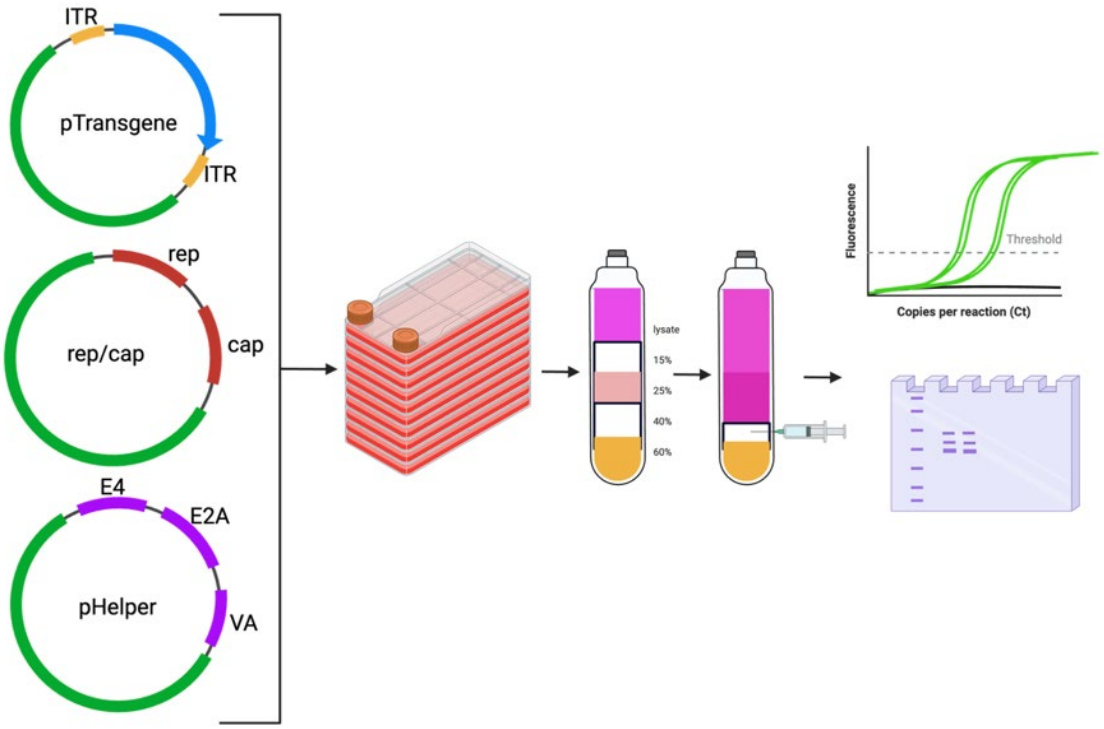

Figure 2-3: AAV production workflow.
Two or three plasmids were transfected in hyperflasks. Cells were harvested and purified by iodixanol gradient, where the 40% fraction containing viral particles were removed. Virus was quantified by qPCR and assessed for purity by SDS-PAGE.

2.4.2 Expanding Cells

HEK293T cells were cultured in pyruvate-free complete DMEM supplemented with 10% FBS and 1% pencillin-streptomycin (100U/mL; 100 μg). Cells were passaged as previously described and seeded in T175 flasks (Sarstedt), where two T175s were used per virus. At 90% confluence, cells were seeded into CellBIND Surface HYPERflasks (Corning), where the full cell suspension volume of the T175 was used in a corresponding hyperflask. Bubbles were carefully removed, and flasks were incubated at 37°C 5%CO2 for 72 hours.

2.4.3 Transfection of HEK293T cells

Transfection was done using the TransIT-virusGEN® protocol. Hyperflasks were transfected with 500 μg plasmid DNA in equimolar ratios as described in Table 2-13. The plasmids were well mixed and made up to 40mL with PBS in a 50mL Falcon tube. 1mL of TransIT-virusGEN was added to each tube, mixed well, and incubated at room temperature to

allow for complexing. The total volume was added to pre-warmed pyruvate-free complete DMEM supplemented with 2% FBS and 1% penicillin-streptomycin. The hyperflasks were gently emptied to ensure minimal disruption to the monolayer and slowly filled with the transfection media until full. Bubbles were gently removed and hyperflasks were incubated again at 37°C 5%CO2 for 72 hours.

AAV8			AAV2		
Plasmid	**Size (kb)**	**Mass (μg)**	**Plasmid**	**Size (kb)**	**Mass (μg)**
pTransgene	T	T x R	**pTransgene**	T	T x R
pDP8.ape	21.9	21.9 x R	**phelper**	15.424	15.424 x R
			prepcap	7.4	7.4 x R
Total	K	500 μg	**Total**	K	500 μg
Ratio (R) mass/kb	500/K		**Ratio (R) mass/kb**	500/K	

Table 2-13: Transfection calculations to determine plasmid concentrations for AAV production.
The ratio (R) of the total mass to the combined total plasmid size (K) was used to achieve equimolar ratios by multiplying R by individual plasmid length. T refers to the size of the whole transgene plasmid.

2.4.4 Harvesting and Lysis

Post-incubation, 200mL media were removed from each hyperflask and discarded. Flasks were shaken vigorously to dissociate cells into suspension. Light microscopy was used to confirm all cells were loosened. The cell suspension was poured into 500mL Nalgene autoclave bottles and centrifuged at 1200xg for 10 minutes at room temperature to pellet cells. ~300mL media were carefully removed from the bottle and discarded. The cell pellet was resuspended in the remaining ~50mL, placed in 50mL Falcon tubes, and centrifuged at 1200xg for 10 minutes at room temperature for a more secure pellet. This allowed for removal of the remaining media.

Lysis buffer containing 1M tris (hydroxymethyl aminomethane) and 150mM NaCL was pre-autoclaved and filtered. A protease inhibitor solution containing 1 tablet of cOmplete mini protease inhibitor (Roche Diagnostics) was dissolved in 1mL lysis buffer while spinning down the cells. For lysis, 15mL lysis buffer was added to each pellet and mixed well by pipetting up and down. 500 μL of the protease inhibitor solution were added to each tube and mixed. The lysates were immediately placed at -80°C, and subject to three freeze-thaw cycles of -80°C for at least 45 minutes and thawing at 37°C for 15 minutes. Lysates were shaken vigorously every 5-7 minutes whilst thawing. Lysates were stored at -80°C until AAV isolation.

2.4.5 Isolation of AAV particles

Frozen lysates were thawed at 37°C for 15-20 minutes with vigorous shaking every 5 minutes. Benzonase was added at a final concentration of 50 units/mL to digest unpackaged DNA and incubated for a further 45-60 minutes at 37°C with vigorous shaking at regular intervals. The lysate was centrifuged at 3700xg for 20 minutes at room temperature to remove debris. AAV was isolated by iodixanol gradients, where the fractions were prepared according to Table 2-14.[227-229] The gradients were made by adding fractions from lowest to highest density. First, 7.2mL of the 15% fraction was added at the bottom of an OptiSeal™ ultracentrifuge tube. Subsequent fractions were added by Pasteur pipette at the bottom of the prior fraction. The lysate was gently dropped on top of the gradient by Pasteur pipette. The total gradient is shown in Figure 2-4. Tubes were sealed with caps upon completion.

Fraction	Iodixanol	5M NaCl	5X PBS-MK	H2O	Phenol Red
15%	4mL	3.2mL	3.2mL	5.6mL	-
25%	5mL	-	2.4mL	4.6mL	20 μL
40%	6.7mL	-	2mL	1.3mL	-
60%	10mL	-	-	-	20 μL

Table 2-14: Components of Iodixanol Gradient.
Volumes listed are to prepare two gradients. Three gradients are needed/virus. Iodixanol: OptiPrep™ density gradient medium; 5x PBS-MK: PBS with 5mM $MgCl_2$ (Sigma-Aldrich), 12.5mM KCl (Sigma-Aldrich), autoclaved and filtered; 5M NaCl (Sigma-Aldrich); H_2O: sterile, DEPC-treated molecular grade water; 0.5% phenol red (Sigma-Aldrich).

Gradients were centrifuged at 59000 rpm in a 70Ti rotor in an Optima XE-90 ultracentrifuge for 90 minutes at 20°C. AAV was isolated from the 40% fraction as shown in Figure 2-4. An 18G needle attached to a 5mL syringe was used to pierce the Optiseal tube at the 60-40% fraction interface. Facing the needle bevel up, 1.5-2mL of the 40% fraction were drawn up and placed in a 15mL Falcon tube. Since three Optiseal tubes were used per virus, collected fractions for the same virus but from different Optiseal tubes were pooled in the 15mL tubes at this stage. The total collected fraction volume per virus typically totalled at 4.5-6mL. Collected fractions were stored overnight at 4°C.

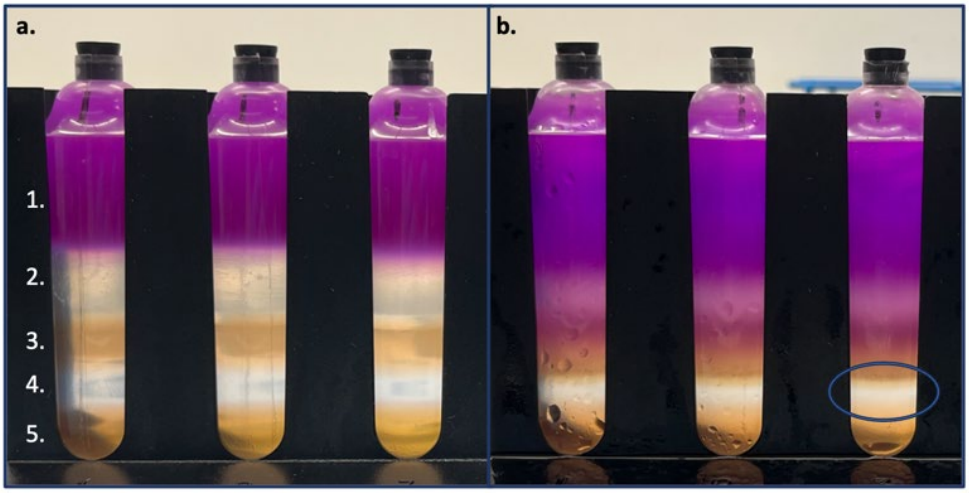

Figure 2-4: Viral Particle Isolation by Iodixanol Gradient.
a. Complete gradient prior to centrifugation. 1: virus-containing lysate; 2: 15% fraction; 3: 25% fraction; 4.: 40% fraction; 5: 60% fraction. b. post-centrifugation. The viral particles are in the 40% fraction, indicated by a circle on the right-most tube.

2.4.6 Purification and concentration of AAV

Amicon®Ultra 100K filters used for virus purification were prepared by adding 5mL PBS and centrifuging at 3000xg for 10 minutes. Collected iodixanol fractions were made up to 15mL with sterile PBS and mixed well. The total volume was transferred to the pre-wet filter and centrifuged at 3500xg at 20°C for 90-120 minutes. The flow-through was discarded and 5mL PBS were added to the filter and mixed well. Samples were spun down for a further 60 minutes or until the samples reached the 500μL marker. The filter was washed three more times with 15mL PBS and centrifugation until concentrated to <500μL each time. The final wash was concentrated to <200μL to ensure a higher viral titre. Samples were divided into 10μL aliquots. The filter was washed by running 500 μL across each side of filter 20 times to collect remaining viral particles. The 'wash' suspensions were divided into 100 μL aliquots. All aliquots were stored at -80°C.

Viruses produced	Application
AAV8-RK-SaKKHABE8e	Mouse
AAV8-U6-gRNA-CAG-mCherry-targeting	Mouse
AAV8-U6-gRNA-CAG-mCherry-non-targeting	Mouse
AAV8-AiO-SaKKHABE8e-U6-gRNA-targeting	Mouse
AAV8-AiO-SaKKHABE8e-U6-gRNA-non-targeting	Mouse

AAV8-U6-gRNA-CAG-GFP-targeting	Mouse
AAV8-U6-gRNA-CAG-GFP-non-targeting	Mouse
AAV2QM-RK-dCas13b-ADAR$_{DD}$(E488Q)	Organoids
AAV2QM-U6-gRNA-CAG-GFP-targeting	Organoids

Table 2-15: AAVs produced.
Note: AAV8-RK-dCas13b-ADAR$_{DD}$(E488Q) was produced by Ahmed Salman to demonstrate the virus production protocol.

2.4.7 AAV Capsid Analysis with SDS-PAGE

To determine capsid yield and purity, AAV preps were analysed by SDS-PAGE. 10μL pure AAV were added to 14μL PBS and 5uL 5X protein loading dye (National Diagnostics) and denatured at 95°C for 10 minutes. Samples were loaded onto a 10% pre-cast Criterion™ TGX™ gel alongside a protein size ladder (BLUeye, GeneFlow), submerged in Tris-Glycine SDS-PAGE running buffer (National Diagnostics) and run at 115V. Following electrophoresis, the gel was washed 3 times for 10 minutes with distilled water under gentle agitation. The gel was stained by submersion in Bio-Safe Coomassie G-250 Stain (BioRad) for 2-4 hours with gentle shaking. Gels were washed a further three times and imaged on the ChemiDocMP Imaging System (BioRad) using the Coomassie Blue protocol.

2.4.8 AAV Titration

RT-qPCR was used to determine the concentration of DNase-resistant viral genomes in each purified sample. AAV samples were DNase treated in a reaction containing 1 μL AAV sample, 1μL DNAse 10X buffer, 1μL DNAse, and 7μL molecular grade water, and incubated at 37°C for 30 minutes.

RT-qPCR was performed as described in 2.2.11 using promoter, transgene, or BgH specific primers, listed in Table 2-16. A four-fold $\log_{10}$ dilution series of linearised plasmid containing the amplification region was used to generate a standard curve. DNAse digested AAV samples were diluted 1:10 and 1:100. The standard curve was used to determine viral genome copy number. Cycling conditions are in Table 2-10.

Primer name	Sequence	Target
U6-F5	CGATACAAGGCTGTTAGAGAGATA	U6
U6-R5	AAACTGCAAACTACCCAAGAAA	U6

Cas13-F4	AGAACAGAGCGGTACAGAAAG	Cas13
Cas13-R4	CCAGGATTGTCTCGATCTCTTC	Cas13
GRK1-F	GTACCGGGCCCCAGAAGCCTG	GRK1
GRK1-R	GGCTGACACAGCACCAGGCTA	GRK1

Table 2-16: RT-qPCR primers for AAV titration.

2.5 Immunohistochemistry

Tissue embedding is described on a chapter specific basis. Eyes were sectioned at 14μm and organoids at 10μm thickness. Frozen sections were cut on a -20°C pre-chilled cryostat (Leica Biosystems), mounted on Superfrost Plus slides (VWR International), dried for 20-30 minutes, and stored at -20°C until further use.

Slides were thawed for at least 1 hour before IHC. A hydrophobic barrier pen was used to encircle all sections on the slide. One slide was used for antibody staining and one used as the secondary-only control for each condition. Slides were washed by immersion in 0.01M PBS and 0.1% Triton X (0.1% PBS-T) for 10 minutes and subsequently permeabilised in 0.02M PBS and 0.2% Triton X at room temperature. Slides were washed with 0.1% PBS-T two times for five minutes and blocked with 0.1% PBS-T with 10% donkey serum and 10% bovine serum albumin (BSA) for one hour at room temperature. Samples were washed in 0.1% PBS-T for five minutes. The primary antibody solution was diluted by the factors shown in Table 2-17 in 1% serum, 1% BSA, and 0.1% PBS-T. Primary antibody solution (~200μL) was added to the main sections of the slides and incubated at 4°C overnight in the dark. Samples were washed two times for ten minutes with 0.1% PBS-T and one time with 0.01M PBS for ten minutes. Secondary antibodies were diluted 1:400 in 1% serum, 1% BSA, and 0.1% PBS-T and added to the main sections of the slides. Samples were incubated at room temperature for two hours in the dark and then washed two times for five minutes with 0.01% PBS-T. Slides were mounted in ProLong® Diamond Antifade with DAPI mounting media, cured overnight at room temperature in the dark, and stored at 4°C until imaging. All primary and secondary antibodies are shown in Table 2-17.

Antibody	Host	Dilution	Source
Mouse abca4	Goat	1:200	Antibodies online; ABIN343052
Mouse l-opsin red/green	Rabbit	1:200	abcam; ab5405
Mouse abca4	Rabbit	1:200	Abcam; ab72955
Mouse abca4	Rabbit	1:100	Invitrogen; PA5-104099

Mouse l-opsin red/green	Chicken	1:200	Chemicon®; ab5745
Alexa Fluor™ 488 Donkey anti-Rabbit	Donkey	1:400	Invitrogen;
Alexa Fluor™ 555 Donkey anti-Rabbit	Donkey	1:400	Invitrogen; A31572
Alexa Fluor™ 647 Donkey anti-Goat	Donkey	1:400	Invitrogen; A32849
IRDye 800CW Donkey anti-Rabbit	Donkey	1:400	Licor; 926-32213

Table 2-17: IHC primary and secondary antibodies.

2.6 Microscopy

2.6.1 EVOS LED Microscopy

For imaging of cells and retinal organoids, the EVOS FL Auto 2 Cell Imaging systems (ThermoFisher Scientific) was used with a neutral density filter cover to reduce incident light. To avoid saturation, LED light intensity and gain were adjusted.

2.6.2 Confocal Microscopy

A FLUOVIEW FV3000 laser scanning confocal microscope (Olympus) with FV31S-SW software was used for most confocal microscopy. The areas of interest were imaged on 10x, 20x, and 40x. Image optimisation was performed on secondary-only samples with adjustments to laser power, gain, and offset. Image acquisition was done with XY resolution of 1024 x 1024 pixels and optimal thickness determined by the software. Subsequent experimental samples were run using the same settings. For analysis, samples were exported and analysed in Fiji ImageJ (National Institutes of Health).

2.7 Statistical Analysis

Statistical analysis and graph production was performed using GraphPad Prism 10. All data were analysed for normality by visually examining the QQ plots and performing the Shapiro-Wilk test or the Kolmogorov-Smirnov test depending on data set size. For comparison of two independent non-parametric groups, a Mann-Whitney test (unpaired) or Wilcoxon matched pairs signed rank test (paired) was performed. For three or more independent groups, the majority of this thesis used a one-way ANOVA (parametric) or Kruskal-Wallis test (non-parametric) alongside *post hoc* Dunnett's, Tukey's, or Dunn's (non-parametric) multiple comparisons tests. In instances of non-parametric analysis, significance on the graphs is always denoted with one asterisk by Prism 10. A two-way ANOVA was used to examine the effects of multiple factors.

Descriptive statistics were run for all data sets and presented as mean $\pm$SEM. A p-value of less than 0.05 was considered significant.

3 *In Silico* analysis of *ABCA4* variants and the relevance of CRISPR

3.1 Introduction

All data and discussion in this chapter were published as a review[67]: Piotter, E., M.E. McClements, and R.E. MacLaren, *The Scope of Pathogenic ABCA4 Mutations Targetable by CRISPR DNA Base Editing Systems-A Systematic Review.* Frontiers in Genetics, 2022. **12**

AAV vectors have been a popular method for gene supplementation in the realm of IRDs since the success of Luxturna in treating LCA. However, as discussed in the general introduction, *ABCA4* is too large to fit in an AAV at 6.8kb. To overcome this, research has focussed on small molecules and alternative delivery methods such as nanoparticles, dual vector delivery, and lentiviruses. Further to this, the long-term efficacy of gene augmentation is unknown, with several reports raising concerns of declining vision after 1-3 years post-treatment.[230-233] Recent advances in CRISPR technologies have led to the development of adenine and cytosine DNA base editors, which allow for the correction of all four transition mutations through deamination.[176]

While base editing provides flexibility and new gene editing approaches, a key limitation in achieving successful editing is the PAM site requirement, which must place the mutation within a specific editing window. The most common, effective, and verified Cas systems are SpCas, SaCas, and SaKKH, which also exist as DNA base editors. These three Cas species offer PAM and editing window diversity.

ABCA4 has an estimated 1200 pathogenic mutations of which 63% are transition mutations amenable to DNA base editing.[234] Given the high number of pathogenic mutations and the high degree of heterogeneity, base editing may provide a treatment solution. It is therefore important to shed light on which pathogenic variants within *ABCA4* should be prioritised due to prevalence, which have multiple editing strategies, and to determine the frequency of mutations with available PAM-sites.

Here, to better understand the relevance of DNA base editing in targeting mutations in *ABCA4,* variants from three databases and three previously published patient datasets were screened.

3.1.1 Chapter aims

The work described in this chapter seeks to guide the direction of base editing strategies in targeting pathogenic *ABCA4* variants. Three datasets – Leiden Open Variation Database (LOVD), genome aggregation database v2.1.1 (gnomAD), and ClinVar – and three patient datasets from Germany, China and Denmark were screened and analysed. The aims include:

1. Establish the genetic landscape of *ABCA4* by mutation type.
2. Identify the most common pathogenic transition variants that are potentially targetable by DNA base editing.
3. Screen for PAM-sites to estimate the relevance/applicability of DNA base editing in the listed variants and in a patient-specific context.

3.2 Methods

3.2.1 Databases analysed

Three variant databases and three patient data sets were analysed for mutation type, nearby PAM-sites, and editability. Figure 3-1 shows the workflow used. To analyse for PAM-sites, the human *ABCA4* gene sequence (*ABCA4-24)* was downloaded from the National Center for Biotechnology Information (NCBI) to GeneiousPrime® and all sorted variants manually annotated on the reference file. Parameters and PAM site screening are described in 3.2.2.

ABCA4 variants were downloaded from three databases: Genome Aggregation Database (gnomAD) v2.1.1 (3,979), ClinVar (1,072 Stargardt; 698 *ABCA4*), and Leiden Open Variation Database v3.0 (6,540). Variants were first sorted and analysed by mutation-type (transition,

frameshift, etc). The three data sets were individually sorted and screened for "pathogenic" and "likely pathogenic" variants, excluding all "VUS," "Conflicting interpretations of pathogenicity," "uncertain significance," "benign," and "likely benign" entries. The LOVD entries were analysed both including and excluding repeat entries to account for variant prevalence. Sorted variants were analysed for PAM sites, described in more detail below.

Anonymised patient data were downloaded from three previously published inherited retinal degenerative disease study cohorts from Germany, Denmark, and China. As with the databases, variants were first analysed by mutation type. Variants were analysed for nearby PAM sites and patients with an 'editable' allele indicated. Complex alleles were deemed 'non-editable.' Patients with at least one targetable allele were defined as 'editable' patients.

3.2.2 Parameters of analysis and workflow

Variants were screened for PAM sites of three different Cas: *Streptococcus pyogenes* Cas9 (SpCas), *Staphylococcus aureus* Cas9 (SaCas), and the KKH variant of *Staphylococcus aureus* Cas9 (SaKKH). The canonical PAM sites for these Cas were used for screening and analysis – 5' NGG (SpCas), 5'-NNGRRT (SaCas), and 5'-NNNRRT (SaKKH). Guide lengths up to 24bp have shown efficacy, however, for consistency, a guide length of 20 base pairs from the 5' end of the PAM site was used for all three Cas variants. Editing windows within the 20bp guide were based on previously published and defined windows: positions 4-8 (SpCas), positions 4-12 (SaCas) and positions 2-15 (SaKKH) where position 1 starts at the 5' end of the guide. Since different editing windows are described for SaCas and SaKKH across different reviews, an 'average' editing window was used for this analysis. Given that the SaKKH PAM site includes the SaCas PAM site, an SaCas PAM with a mutation at positions 2-3 and 14-15 was described as SaKKH. An "SaCas + SaKKH" column was also shown in the analysis due to the similarities. The described parameters were considered the 'ideal' targeting windows but are seen as guidelines given the target site variability and success of non-canonical PAM sites. Variants with a nearby PAM that put the target site outside of the editing window but within the 20bp guide were accounted for separately in the analysis as 'any.' This analysis also excluded targeting neighbouring bases for alternative amino acid correction. Lastly, bystander editing potential was not included in analysis although this is a major consideration when targeting a mutation. Patient data were analysed in the context of only targetable transition mutations and of total variants to provide insight into the

relevance within base editing technology and as a therapeutic approach overall. Data were analysed in Microsoft Excel. Note: multiple python scripts and algorithms now exist that enable large-scale screening for PAM prevalence, bystander editing, and targetable neighbouring bases.[235]

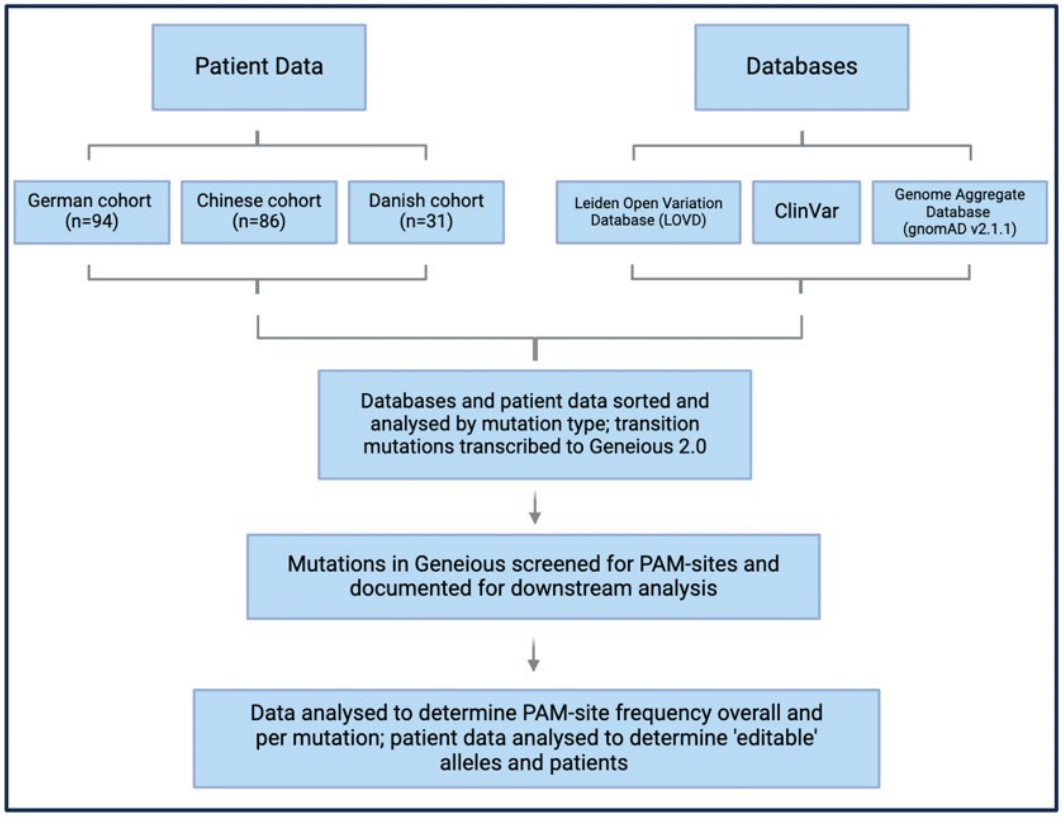

Figure 3-1: Flowchart of in silico analysis of *ABCA4* variants.

3.3 Results

3.3.1 Analysis of open-source data bases

3.3.1.1 Variant analysis in gnomAD v2.1.1 and ClinVar

The Genome Aggregation Database (gnomAD) v2.1.1 consists of aggregate sequencing data of 125,748 exomes and 15,708 whole genome sequences from unrelated individuals. *ABCA4* has 3,979 variants reported in gnomAD, of which 62% are transition mutations (T/A-C/G) (Figure 3-2). The distribution of mutation type was similar between Clinvar and gnomAD, with 59% of the 690 *ABCA4* Stargardt disease Clinvar entries being transition mutations (Figure

3-2b). Variants were spread evenly across the gene, rather than in "hotspot" locations (Figure 3-2a).

The filtered pathogenic, transition mutations were analysed in Geneious Prime for nearby PAM sites to determine base editing potential. Depending on the mutation, either the forward or reverse strand was searched for a relevant PAM site – NGG (SpCas), NNGRRT (SaCas), and NNNRRT (SaKKH) – to enable mutation correction. In gnomAD and Clinvar, 64% and 66% of transition mutations had PAM sites within the parameters described in section 3.2.2. In the context of total pathogenic mutations, this made up 46% and 36% of mutations. Further, 28% and 30% of mutations had multiple PAM sites, respectively (Figure 3-2c).When suboptimal PAM sites were included in the analysis ('any' ie the target mutation occurred anywhere within the 20bp guide) the total editable mutations increased to 88% and 89% of transition mutations and 62% and 46% of total mutations.

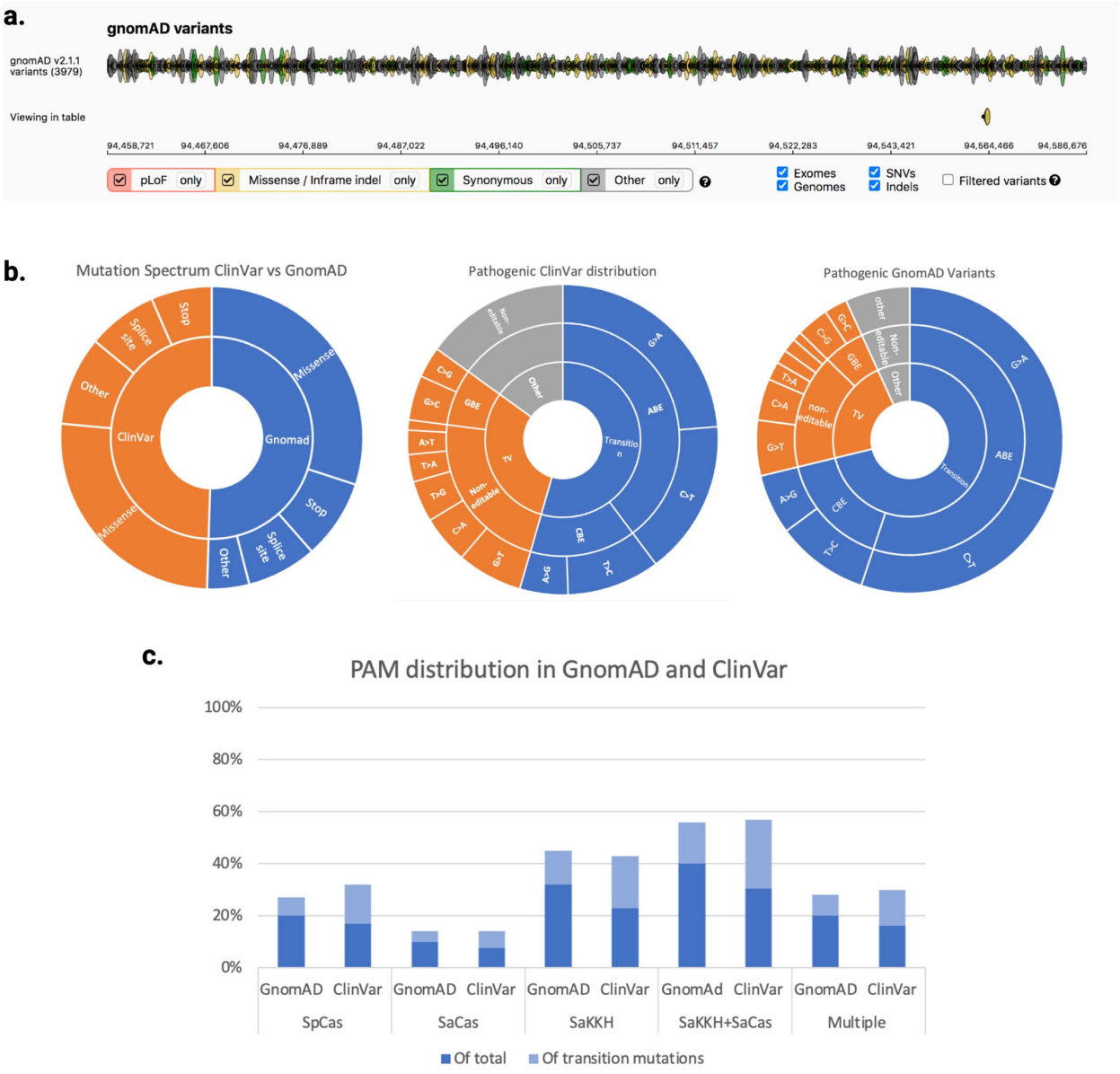

Figure 3-2: Mutation and PAM-site distribution in gnomAD v2.1.1 and ClinVar.
a) All variants in gnomAD v2.1.1 spatially distributed across *abca4.* No mutation "hotspots" observed. b) Mutation spectrum compared in ClinVar and gnomAD (left). Point mutation distribution in ClinVar (middle) and gnomAD (right). c) PAM-site prevalence by Cas species for gnomAD and ClinVar pathogenic *abca4* mutations. This was analysed in the context of total mutations and from the transition mutations. Mutations with more than one PAM site are indicated on the right.

Interestingly, in gnomAD and Clinvar, "ideal" SaKKH had the highest prevalence with ~44% of transition mutations, likely due to having the largest editing window. Inversely, despite having a more flexible PAM site, SpCas only had a prevalence of ~30% because of the smaller editing window. Lastly, SaCas had the lowest prevalence, at 14% of transition mutations, given both the stricter PAM site and smaller editing window. When combined, however, SaCas and

SaKKH cover ~56% of transition mutations, or 40% (gnomAD) and 30.5% (Clinvar) of total pathogenic mutations (Figure 3-2c).

3.3.1.2 Variant analysis in LOVD

Since LOVD consists of individual entries, with multiple entries for the same variant, it was analysed separately. Repeat entries were not removed to account for mutation prevalence and the potential effect on the data output. Notably, the five most common mutations made up 29% of the entries (Figure 3-3). However, the percentage of transition mutations remained consistent when including or excluding the most common variants at 77-78%. The distribution of targetable transition mutations remained consistent with gnomAD and Clinvar, where 66% of transition or 47% of total entries had an "ideal" PAM. (Figure 3-3c)

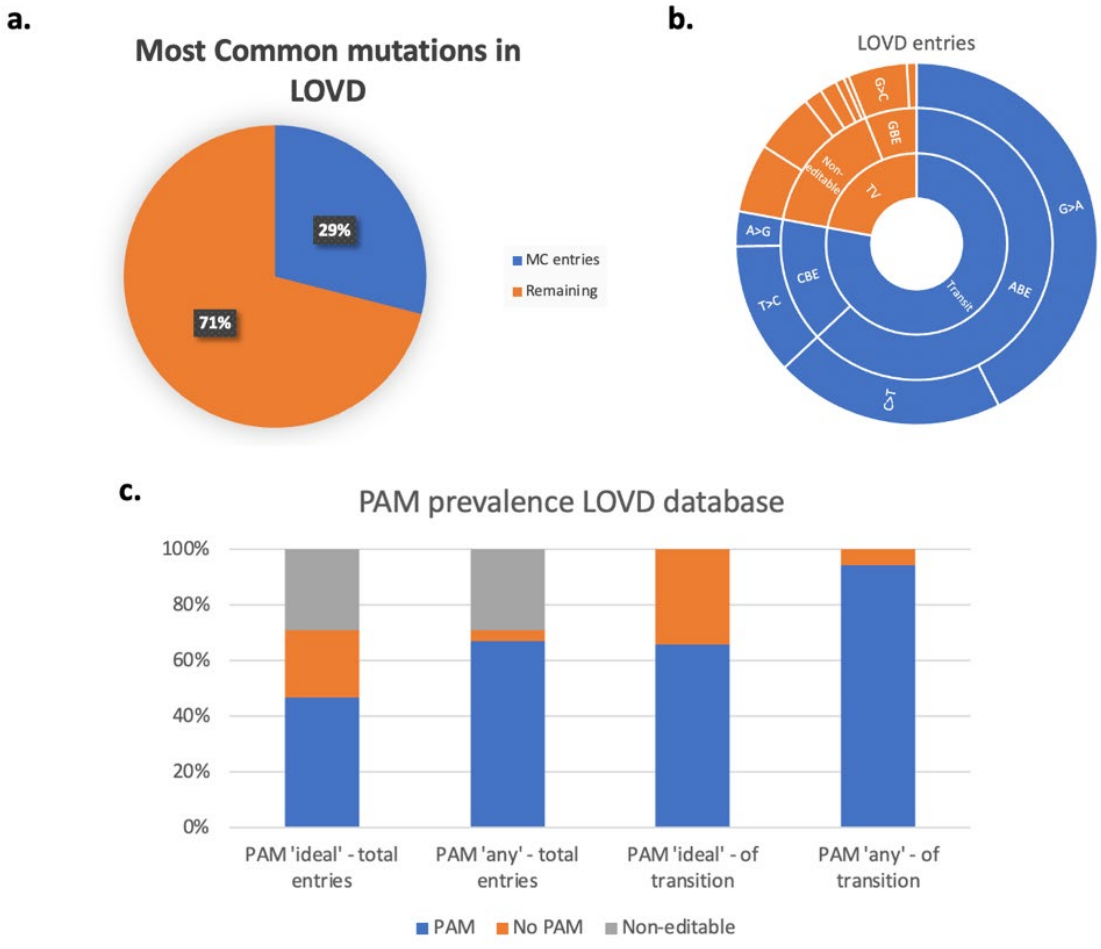

Figure 3-3: Mutation and PAM distribution in LOVD.
a) 29% of LOVD entries consisted of the 5 most common (MC) variants. b) Mutation distribution of all LOVD entries. When the five most common entries were removed, the distribution remained the same, with 77-78% being transition mutations. c) PAM prevalence in the LOVD database in the context of total entries versus of transition

mutations. ‘Ideal’ refers to parameters defined in the methods; ‘any’ refers to the target site falls within the 20bp guide sequence.

3.3.2 Analysis of published patient data

Three patient data sets from published cohorts were analysed for PAM site prevalence to shed light on translational relevance. The cohorts were from Germany, China, and Denmark, and contained different degrees of information, affecting the possible analyses. Since most patients were compound heterozygous, there was a higher chance of at least one targetable variant. Indeed, 84% of the German cohort, 84% of the Chinese cohort, and 90.3% of the Danish cohort had an allele with an editable transition variant. This reflected the findings in Fry et al. and Stone et al. where 88.8% and 92.7% of *ABCA4* patients had editable transition variants.[234,236] Complex alleles were deemed non-editable and excluded from patient data pools because alleles were not specified. In instances where all variants for a given patients were editable, the allele was noted as having multiplexing potential but was not counted as “editable.”

Figure 3-4: Mutation and PAM-site distribution across the three patient cohorts.
Mutation distribution (left) and PAM-site distribution (right) by patient cohort. PAM-site prevalence was greatly weighted by common mutations and heterogeneity. In all three cohorts, most patients with editable transition mutations had multiple PAM options due to heterogeneity. Further, SpCas and SaKKH showed roughly equal prevalence due to the increased editing window of SaKKH.

3.3.2.1 Patient Data – German cohort

A published study consisting of 251 patients with cone-rod dystrophies was extracted, where only patients with *ABCA4* mutations were analysed. This totalled to 94 patients and 229 variants. The dataset had broad mutation distribution, where 38% of patients had at least one complex allele and only 4.2% were homozygous for a single mutation. 75.5% of variants were missense changes with 96.8% of patients carrying at least one missense change. The remaining variants were split evenly between stop (9.8%), splice (7.7%), and "other" (6.8%), with stop, splice, and other mutations occurring in 23.4%, 19.1%, and 17% of patients, respectively. Overall, 84% of patients had at least one targetable allele, likely weighted by the 5 most common mutations, which made up 43% of the mutations. (Table 3-1)

After excluding patients with complex alleles, 44% of all patients carried editable transition mutations. SaKKH had the highest prevalence, with 73% being 'ideal' editable mutations. SaCas had a much higher prevalence of 56% in this cohort compared to the 14% in gnomAD and ClinVar likely due to weighting by common variants with multiple potential PAM sites. In this case, c.5882 G>A was present in 19.8% of the "editable" patients and has both an SaKKH and SaCas PAM site. This is expected given the high population frequency of c.5882 G>A in Europe at 0.4%.[23] Interestingly, c.5882 G>A was not seen in the Danish cohort. Lastly, 78% of patients with targetable mutations had SpCas PAM sites. Overall, 91% of editable transition mutations had an "ideal" PAM, or 44% of the total *ABCA4* cohort. Further, 76% had more than one PAM site, which would enable testing multiple editing strategies and provide increased chances of success. (Figure 3-4)

The high rate of complex alleles (38%) in the German cohort and in *ABCA4* overall (~10% overall)[23] is particularly compelling in applying multiplex editing, where multiple guides are provided alongside one base editor. This enables correction of multiple mutations simultaneously. This would require specific mutation pairings where ABEs target G>A/G>A, G>A/C>T, or C>T/C>T mutations and CBEs target A>G/A>G, A>G/T>C, or T>C/T>C. Of the patients with complex alleles, 52% had a combination conducive to multiplexing. Alleles were not specified, however, and would likely affect the possibility of a multiplexed approach. PAM sites were therefore not investigated but would further affect targetability. However, the novel CABE-T editor can edit all four transition mutations, omitting the need for mutation pairing, but it requires further investigation *in vivo* and optimisation.[182] Lastly, the high rate of complex

alleles is observable in Figure 3-4, where the PAM prevalence of total patients drops substantially relative to patients with editable mutations due to the number of excluded patients.

3.3.2.2 Patient Data – Chinese cohort

A published Chinese cohort of patient data consisting of 86 *ABCA4* Stargardt disease patients was analysed. 9.3% of patients were homozygous, significantly higher than the German cohort, and 81% of patients had at least one allele with a transition mutation. Three patients (3.5%) had complex alleles and were excluded from analysis. Of total mutations in the cohort, 70% were transition mutations. Mutation distribution is detailed in Figure 3-4. The five most common mutations in the cohort consisted of 19% of mutations overall (Table 3-1), less than half of the 43% seen in the German cohort. One of these, c.2894 A>G, is a founder mutation in the Chinese population, and interestingly also in the Danish population.[23,161,237,238] The overall PAM prevalence was likely weighted by c.2894 A>G given it has all three PAM sites nearby.

76% of the total patients had at least one PAM-site on one allele, but of patients with editable transition mutations, 90% had at least one PAM-site. Of patients with transition mutations, the PAM prevalence was 57%, 54%, and 29% for SpCas, SaKKH, and SaCas, respectively. The greater mutation diversity of this cohort likely affected the PAM distribution, where the most common variants carried less weight than in the German cohort. Further, given the low number of patients with complex alleles in the Chinese cohort, the PAM prevalence between ‘of transition mutations’ and ‘of the total patients’ does not vary as much as in the German cohort.

3.3.2.3 Patient Data – Danish cohort

The Danish patient data were taken from a published cohort that included 31 *ABCA4*-related retinopathy patients. Of these, 9.7% had complex alleles, none were homozygous, and 88% of total patients had at least one transition mutation, with the mutation distribution shown in Figure 3-4. The five most common mutations in the cohort accounted for 34% of mutations present (Table 3-1). The most common, c.2588 G>C, shows conflicting pathogenicity dependent on other mutations in *cis* or *trans.*[23,81] C.2894 G>A is the second most common and a known founder mutation, and has multiple PAM options.[23]

Of the patients with transition mutations, 77% had at least one PAM-site, half (52%) of which had multiple PAM-sites, enabling multiple potential editing strategies. This equated to 68% of total patients having at least one PAM-site. Specifically, SpCas and SaKKH were equally

represented, each with a prevalence of 45% of the total cohort. SaCas was present in 35% of patients (Figure 3-4). Because only three patients did not have at least one transition mutation, the PAM-site percentages only marginally changed. Lastly, as with the Chinese cohort, given the low number of patients with complex alleles, the PAM prevalence between 'of transition mutations' and 'of the total patients' does not vary as much as in the German cohort.

German cohort Birtel et al. (2018)		Chinese cohort Hu et al. (2019)		Danish cohort Duno et al. (2012)		Oxford cohort Fry et al. (2021)	
c.5603A > T	14%	c.101_106 delCTTTAT	7.2%	c.2588G > C	11%	c.5882G > A	9.3%
c.5882G > A	10%	c.2894A > G	4.2%	c.2894A > G	6.5%	c.5461-10T > C	6.5%
c.1622T > C c.3113C > T	6%	c.1804C > T	2.4%	c.1529G > T	6.5%	c.6079C > T	6.5%
c.2588 G > C	5%	c.1561delG	2.4%	c.6089G > A	5%	c.4139C > T	5.1%
c.4234 C > T	2.6%	c.6563T > C	2.4%	c.4102C > T/c.2408delG	5%	c.5714+5G > A	4.7%
Total	43%	Total	18.6%	Total	34%	Total	32.2%

Table 3-1: Most common mutations in each patient cohort.
The five most common mutations in the three selected patient cohorts from Germany,[239] China,[240] and Denmark.[241] An additional, previously published cohort from Oxford is included (right)[234]. The total shows combined prevalence within a cohort out of all mutations, not patients. The underlined entries indicate mutations in multiple cohorts.

3.4 Discussion

With ~1200 known pathogenic mutations, this chapter aimed to show the complexity of the *ABCA4* genetic landscape and create a roadmap for base editing applications in *ABCA4*. Although complex, the mutation frequency of 63% of transition mutations in *ABCA4* observed in LOVD reflected the frequency reported for the human genome at 62% of pathogenic SNVs.[23,176,234,235] Another study looking at 53,469 human pathogenic mutations found 42.8% were potentially targetable transition mutations.[242] When looking at other available *ABCA4* databases, 62% of gnomAD entries and 59% of ClinVar entries were transition mutations. Despite these slight reporting variabilities in both the *ABCA4* and overall human genetic landscape, DNA base editors provide an exciting opportunity to target a large portion of pathogenic mutations in *ABCA4*.

To date, base editors have shown exciting activity *in vivo* in photoreceptors[243] and the RPE,[175] with reported photoreceptor editing rates of 31% targeting c.5882 G>A using a split-intein SpCas base editor.[175,242,244,245] While SpCas is too large for a single AAV, efforts have been

ongoing to broaden delivery and editing methods for large transgenes, such as dual AAV vectors, [42,218,243,245,246] lentiviral vectors, [175] and nanoparticle delivery. [247-249] Further, DNA base editing constructs have been evolved to improve PAM flexibility and decrease construct size to increase targeting capabilities. [177,250] For example, SaKKH has been size minimised to fit in a single AAV, showing editing rates of 54-61% *in vivo* targeting *Pcsk9* and *Angptl3*.[180] Here, the most verified and therapeutically relevant Cas species – SpCas, SaCas, and SaKKH – were analysed in the context of "pathogenic" and "likely pathogenic" *ABCA4* variants across three databases and three patient datasets.

Previous papers looking at base editing applicability targeting pathogenic mutations across the whole human genome, found that 72.4% of mutations were *not* amenable to SpCas base editing due to the 5'-NGG PAM limitation.[242] Similarly, when looking at the *ABCA4* variant databases, ~70% of did not have an SpCas PAM site nearby. However, when including SaCas and SaKKH in the analysis, ~65% of transition variants had a PAM site which accounted for 36% and 46% of overall *ABCA4* mutations in gnomAD and ClinVar, respectively (only a slight increase). Further, in the context of patient data, given the high heterogeneity, 44%, 76% and 68% (German, Chinese, and Danish) of total cohort patients had an allele targetable by base editor. Of total transition mutations, this increased to 91%, 90%, and 75%, respectively.

Correcting one pathogenic allele would likely provide a therapeutic benefit in a recessive condition such as Stargardt disease. Targeting common mutations and prominent founder mutations would address a large portion of patients - the five most common *ABCA4* variants accounted for ~30% of entries in LOVD. One specific example, c.5882 G>A, accounts for roughly 10% of all mutations in the German and Oxford cohorts, reflecting the Europe-wide frequency, and has multiple PAM options.[23,234] Interestingly, this variant originates in East Africa and has a high population frequency in Somalia, Kenya, and Ethiopia.[23,251] A dual AAV delivery of an SpCas ABE has been tested targeting c.5882 G>A and c.5883 A in a murine model and non-human primates, showing 31% and 18 % editing, respectively.[252] However, other common or founder mutations, such as many seen in the Chinese cohort, are not amenable to base editing due to mutation type but may be targetable using different gene editing tools or alternative strategies.

Prime editing (PE) enables editing of all point mutations and small insertions and deletions with reported editing rates of up to 15% *in vivo* in neonatal mouse liver. [190,253] More

recent generations of prime editing, such as twin prime editing, allow for the replacement of DNA fragments >5kb at 6.8% efficiency and smaller fragments of 108bp at ~16% efficiency. [191] Delivery issues have been circumvented using a dual AAV split-intein approach, which has shown efficient editing of up to 16% in the RPE.[192,243,254] While prime editing shows immense potential in targeting nearly all mutations in *ABCA4*, efficiency is heavily affected by the target site and requires much optimisation.[190]

Complex alleles provide another challenge in the realm of gene editing and in this study were not typically analysed for PAM sites given that alleles were not specified in the patient data. Nonetheless, base editing has multiplexing potential in targeting complex alleles, but it greatly depends on the variants. Overall rates of complex alleles are ~10-16%,[23,69] but can be skewed by founder effects. For example, in the German cohort, 38% of patients had at least one complex allele due to a deleterious founder mutation, c[1622 T>C; 3113C>T], p[Leu541Pro; Ala1038Val], which made up 36% of all complex alleles in the German cohort. This aligns with the 34% observed broadly in Germany.[23] Neither of the mutations have nearby canonical PAM sites that would put the mutation in the appropriate editing window. For targetable mutations though, multiplexing has been shown to work, where Cas9-knockdown with ten gRNAs targeting ten different loci effectively edited some of the targets. Specifically, the first three guides showed the highest rates of knockdown with waning efficacy thereafter.[255] Despite the difficulty of targeting complex alleles, given the high rate in European populations and an overall rate of ~10%, multiplexing may provide a solution to enable more widespread treatment potential.

Many Cas are also being used with non-canonical PAM sites and evolved to improve PAM flexibility. Suh et al demonstrated that higher editing rates of 29% were observed using NAG and NGA PAM sites instead of the canonical NGG in a proof-of-principle *in vivo* study targeting *RPE65* by SpCas ABE delivered by lentivirus.[175] More recently, a nearly PAMless ABE, SpRY-ABE, successfully edited target sites at a mean rate of 34.7%.[184] This greatly increases the targetable transition mutations and potential editing strategies to improve editing rates and/or specificity.

Fortunately, in this study, most transition variants had at least one desired nearby PAM site, particularly in the patient data due to the extreme heterogeneity. In the German cohort, 91% of patients with compound heterozygous alleles had a relevant nearby PAM site, 76% of which

had more than one. Of total Danish and Chinese cohort patients, 68% and 76%, respectively, had nearby PAM sites, with 52% having multiple PAM sites. Having multiple PAM sites per mutation and/or two possible alleles to target would allow for flexibility and optimisation of editing strategy. This analysis demonstrates that existing methods are broadly applicable to known pathogenic transition mutations throughout *ABCA4* with potential translational applications.

The data presented showed the exciting potential of targeting transition mutations by DNA base editors for the treatment of Stargardt disease, but with some limitations. First, 92.6% of gnomAD entries were unclassified and thus excluded from analysis. Screening these would provide further insight and a more robust understanding of base editor relevance. Second, common mutations such as c.5882 G>A were excluded from some database analyses due to the classification as 'conflicting interpretations of pathogenicity.' However, these were partially accounted for in the patient data. Additionally, the patient data from different countries aimed to provide some diversity and reflect different founder/common mutations seen across populations. Including more datasets from around the world would greatly improve the output of this study. Lastly, an average editing window and only the canonical PAM sites were used in the screening process, thus the percentage of potentially targetable mutations is likely higher.

Although the improved PAM flexibility improves variant targetability, in the current regulatory context, base and prime editing are not optimised for translation provided each variant requires a different guide.[256]

In regard to safety, one of the main limitations faced by CRISPR DNA editing systems is the possibility of bystander and off-target editing, yielding potentially detrimental, long-term effects.[257,258] As the systems have evolved, efficient on-target editing has been maintained or improved, alongside a notable decline of off-target editing.[250] In *ABCA4*, bystander editing is of particular concern given the vast number of pathogenic variants. Narrowing the editing window while increasing PAM flexibility may provide a solution, as seen with SpRY-ABE.[184]

Alternatively, editing RNA provides a more clinically safe alternative, as no permanent change is introduced in the genome. Indeed, various RNA base editing systems using Cas13, endogenous adenosine deaminase acting on RNA (ADARs) recruitment or exogenous ADAR delivery have found successful *in vivo* editing.[215,259] In the context of *ABCA4,* depending on the database analysed, 23-42.4% of pathogenic mutations were the G>A variant required for RNA

base editing. Overcoming this barrier, a notable novel therapy in Phase I clinical trials targeting RNA facilitates mRNA trans-splicing of the N-terminal half of *ABCA4.*[260] Despite the limitations faced by gene editing technologies, new delivery methods, size-minimised variants, new species, and new editing methods are rapidly evolving to overcome them.

3.5 Conclusion

Finding a functional therapy for Stargardt disease has been a long journey ranging from small molecule therapies to gene supplementation and editing. This study investigated multiple databases to establish an understanding of *ABCA4* mutation distribution and to determine the potential of DNA base editing, a CRISPR-Cas derivative, in targeting mutations in *ABCA4.* The results were highly encouraging with the majority of *ABCA4* mutations in both the databases and patient cohorts being targetable transition mutations with nearby PAM sites, thereby providing an opportunity for correction. Here, a roadmap for editing the complex, mutation-rich *ABCA4* was highlighted, demonstrating the relevance of existing base editing tools in correcting relevant pathogenic mutations.

4 *In vitro* proof-of-principle – targeting *ABCA4* c.206 G>A (p.W69*) by DNA and RNA base editors

4.1 Introduction

The previous chapter described the relevance of base editors in targeting pathogenic mutations in *ABCA4.* Two methods enable site-specific deamination and thus allow A>G editing: 1) CRISPR-Cas9 adenine base editors enable correction of DNA and 2) CRISPR-Cas13 RNA editors enable correction of mRNA.[176,199]

The work described in this chapter aims to compare these approaches in targeting the same pathogenic *ABCA4* mutation *in vitro.* As described in Chapter 1, adenine base editors consist of nickase Cas9 (nCas9) fused to an evolved *E. coli* deamination domain (ecTadA) to enable ssDNA editing and can be directed to a mutation using a guide RNA (gRNA). Depending on the target-region, the TadA domain deaminates adenosines within the editing window to inosine. This is functionally read as a guanine, thus mediating efficient A>G editing. Since the non-target strand is nicked, DNA repair machinery replaces the complementary thymine with a cytosine.[176,250,261] Similarly, the RNA base editor consists of a deactivated Cas13b (dCas13b) fused to an adenosine deaminase acting on RNA ($ADAR_{DD}$). This is directed to mRNA once

complexed with a gRNA. The bound gRNA creates a double-stranded RNA target region on which the ADAR can act, where the target adenine is indicated within a bulged A-C mismatch. The target adenine is deaminated to inosine and functionally read as guanine.[62,199,250,262-265]

Both DNA and RNA base editors were first described in 2017 by Cox et al and Gaudelli et al and have since been evolved for greater efficiency with reduced off-target and bystander editing. In addition, size-minimised versions have been developed for easier delivery by AAV using smaller Cas9 orthologues, such as an *S. aureus* Cas9 nickase. This underwent multiple iterations of phage-assisted continuous evolution (PACE) to improve PAM flexibility and editing efficiencies, creating SaKKH ABE8e.[179,266] Within the time of this PhD, this was size minimised further to enable delivery by a single AAV – described further in Chapter 6.

The dCas13b-ADAR underwent mutagenesis to include an E488Q mutation, resulting in a hyperactive ADAR that introduced high rates of both on- and off-target editing. The off-target editing has since been reduced with the introduction of a further variant (T375G), however, this was not used in this thesis given the substantially lower editing rates.[199] Similarly, the size-minimised Cas13-ADAR editors were not used in this thesis given the reduced reported editing rates.[199,204]

Following the screen of *ABCA4* variants in Chapter 3, c.206 G>A was chosen to compare SaKKHABE8e and Cas13-ADAR rates of correction at the same target. The c. 206 G>A (p.W69X) results in a premature stop codon in exon 3. Although this is a rare variant, it fulfilled essential criteria in the screening process. First, to compare DNA and RNA base editing, a G>A mutation was necessary to allow for A>G deamination. Although targeting a cytosine would have been possible, RNA cytosine base editors are highly site-specific and were thus excluded as an option.[267,268] Second, a stop mutation was chosen to allow for detecting editing through restoration of protein expression. Third, a mutation with multiple PAM sites was selected to allow for strategy optimisation. Developing an editing strategy targeting this mutation would allow for proof-of-principle editing comparison of *ABCA4* using an SaKKH DNA base editor and the dCas13b-ADAR RNA base editor, aiding in the determination of a suitable therapeutic path for *ABCA4* gene therapy development. Targeting *ABCA4* by SaKKHABE8e and dCas13b-ADAR has yet to be demonstrated.

ABCA4 expression is restricted to photoreceptors, the RPE, and keratinocytes, limiting the screening strategies for testing novel therapeutics.[65,66,269] Although a patient-derived keratinocyte

cell-line could have been developed, this would have been time consuming and costly, and thus screening guides via mutant cell lines was not possible. Instead, a more flexible, moderately high throughput guide screening process targeting mutant plasmids in widely available cell lines was used.

4.2 Chapter aims

This chapter aims to compare dCas13b-ADAR$_{DD}$ (E488Q) and SaKKHABE8e *in vitro* targeting the same patient mutation, *ABCA4* c. 206 G>A, and establish a workflow to allow for downstream *in vivo* comparison.

1. Identify efficient gRNAs targeting *ABCA4* c.206 G>A using dCas13b-ADAR$_{DD}$ (E488Q)
2. Identify efficient gRNAs targeting *ABCA4* c.206 G>A using SaKKHABE8e
3. Compare on-target editing efficiencies of best performing guides for DNA and RNA base editors targeting the c.206 G>A mutant plasmid *in vitro* at the DNA, RNA, and protein levels
4. Assess bystander and local off-target editing of base editors
5. Explore dCas13b-ADAR$_{DD}$ (E488Q) targeting a clinically relevant mutation, c.5882 G>A *in vitro*

4.3 Materials and methods

4.3.1 Design and cloning of dual-glo luciferase reporter assay

4.3.1.1 Design

The pSGDlucV3.0 plasmid (kind gift of Lewis Fry, Addgene plasmid #119760) was used to clone dual-luciferase constructs for DNA and RNA editing reporting when targeting stop mutations. The plasmid consists of *Renilla* and Firefly luciferase, with a ‘target cassette’ in between (Figure 4-1). An SV40 promoter drives *Renilla* production, which is ubiquitously expressed and thus the normalisaiton control, while Firefly reports editing activity. The ‘target cassette’ contains either the wild-type sequence or the stop mutation of interest and is flanked by two F2A sequences, which enable independent encoding of *Renilla* and Firefly through co-translational excision of the target cassette. At baseline, the stop mutation prevents read-through of the cassette, so Firefly is not expressed (‘Off’). Upon correction of the stop mutation or in the wild-type control, read-through of the cassette results in Firefly production (Figure 4-1). The

ratio of Firefly:*Renilla* read-out estimates the editing efficiency and was used as a guide screening process for RNA base editing. The full calculation method is described in 4.3.1.3.

4.3.1.2 Cloning dual-glo luciferase reporter assay

Target cassettes for the c.206 G>A region were cloned using the 5' PSpXi and 2' BglIII flanking restriction sites as per the general methods. Oligos 112bp in length of mutant sequence with corresponding restriction overhangs were ordered and commercially synthesised (Merck). Complementary oligos were annealed and phosphorylated as in the general methods. To create the wild-type control, site-directed mutagenesis was performed as described in the general methods. Cloning sites are shown in Figure 4-1.

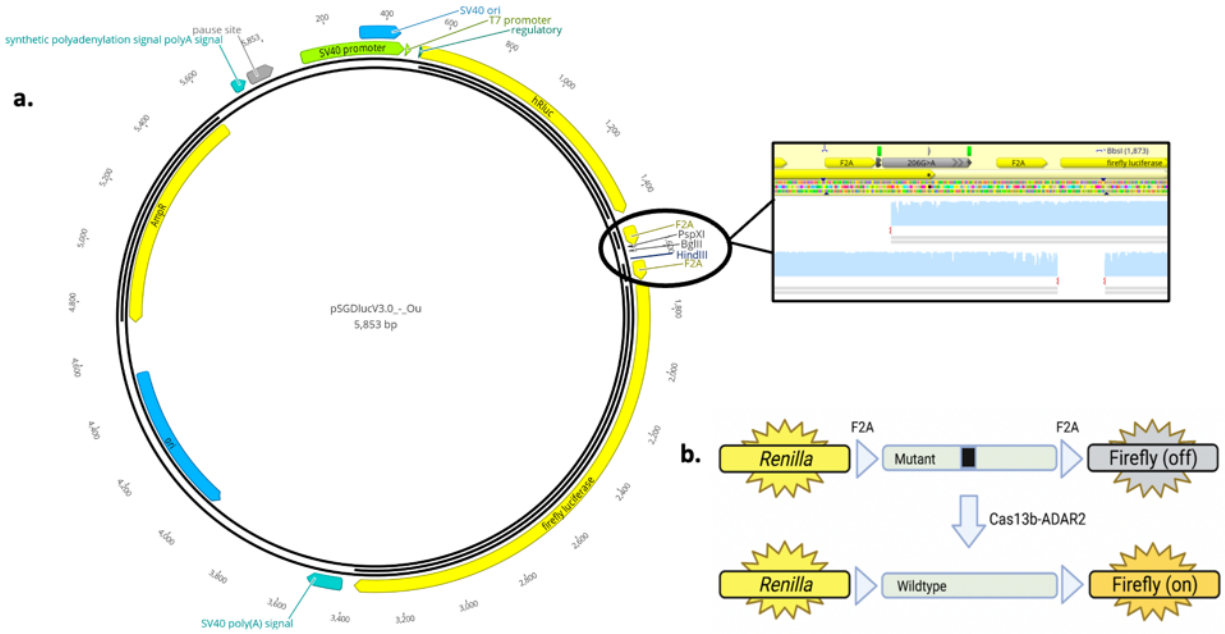

Figure 4-1: Cloning strategy and Dual-Glo® luciferase assay mechanism.
a) The cloning sites PspXI and BglII or HindIII for target cassette insertion between *Renilla* and Firefly luciferase. **b)** *Renilla* is constitutively expressed to allow for normalisation. The mutant cassette containing the stop codon does not allow read-through and thus does not allow for Firefly expression. Upon correction to the wildtype sequence, firefly is expressed. Positive controls included a wildtype target cassette and an in-frame pSGDlucV3.0 plasmid where firefly was expressed. Negative controls included the mutant fragment and the out-of-frame pSGDlucV3.0 plasmid where firefly was not expressed.

For DNA base editing reporting, a positive control plasmid was created that enabled the use of a previously validated guide (kind gift of Ariel Kantor) as an additional positive control (Figure 4-2). The target cassette contained a GFP coding sequence with either a stop mutation or the wild-type sequence. This cassette was generated by HindIII digestion of pSGDlucV3.0 and

using the NEBuilder® HiFi DNA Assembly kit to insert double stranded DNA fragments with flanking 25bp overhangs complementary to the insertion site as described in the general methods. Primers for PCR amplifying the cassette are listed in the Appendix. The target cassettes were annealed at 60-66°C temp with an extension time of 10s for a ~300bp long fragment. Double stranded DNA fragments were ordered and commercially synthesised by Twist bioscience and are listed in the appendix.

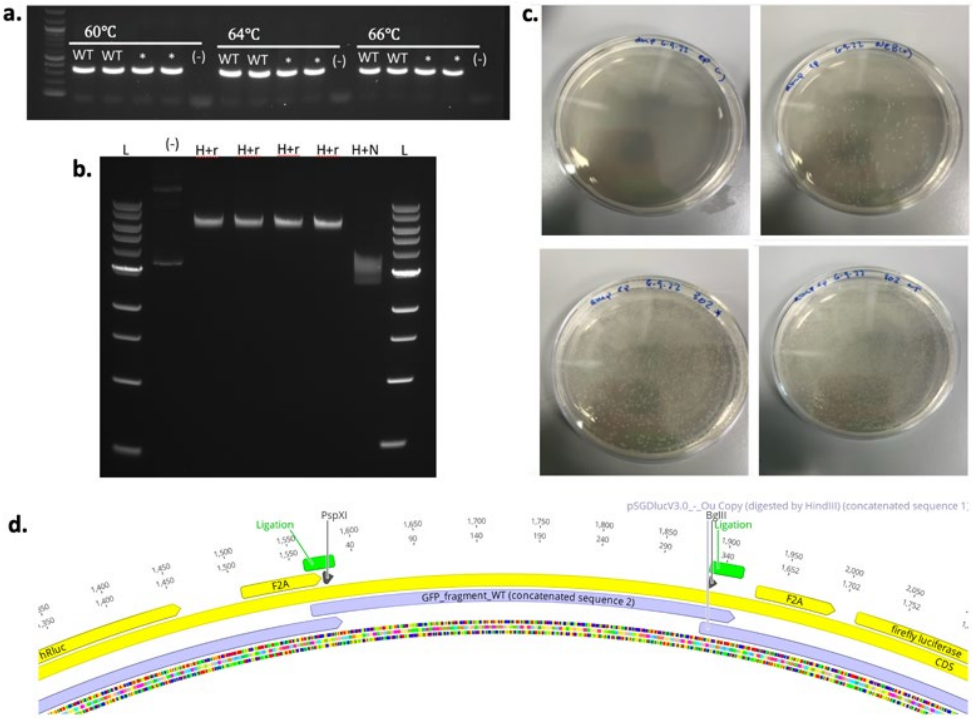

Figure 4-2: Examples of target cassette cloning for the dual-glo luciferase assay by NEBuilder HiFi DNA Assembly.
a) Gel of a successful gradient PCR of wildtype (WT) and mutant (*) inserts to clone into the pSGDlucV3.0 using the HindIII restriction site. **b)** Gel of the digested pSGDlucV3.0 backbone. (-) is the undigested backbone, 'H+r' refers to HindIII + rSAP for dephosphorylation, and 'H+N' was a control using HindIII and NotI resulting in 2 bands of 3.1kb and 2.8kb. **c)** Plates with colonies where the top two panels are controls and the bottom panels are the WT and * insert. 302 refers to the insert length. **d)** *in silico* cloning of the WT target cassette for the GFP positive control.

4.3.1.3 Dual-Glo® luciferase assay cell culture and assay

All cell culture was conducted as described in the general methods. For the luciferase assay, a Corning® white-walled 96-well adherent plate was seeded with 100μL HEK293T cells at 4.5x10^4 cells/well in phenol-free complete DMEM (Thermo Fisher) supplemented with 10% HI-FBS (Thermo Fisher) and 1% penicillin-streptomycin (SigmaAldrich). After 24 hours

incubation, cells were transfected with endotoxin-free plasmid (50ng dual luciferase reporter, 75ng dCas13b-ADAR$_{DD}$ or SaKKHABE8e, and 150ng gRNA) using TransIT-LT1 (Mirus Bio). Positive and negative control wells were included using the same total plasmid and conditions. All samples were run in duplicate or triplicate depending on the plate layout and the outer row and column were not transfected to decrease variability. Kits described in the general methods were used for endotoxin free plasmid: mini- (Zymo) or maxi- preps (Qiagen; Macherey-Nagel).

48-hours post-transfection, cells were imaged to check for viability and transfection-control RFP expression. For *Renilla* and Firefly detection, the Dual-Glo® luciferase assay kit (Promega) was used according to manufacturer instruction. The plate was brought to room-temperature and ~50-55 μL media was removed so Dual-Glo® reagents would have a final 1:1:1 ratio. For firefly detection, 60 μL of the Dual-Glo® luciferase reagent was added to each well to lyse cells and provide the firefly luciferase substrate. The plate was incubated at room-temperature for 15 minutes and luminescence was measured on the FLUOstar®Omega microplate reader (BMG Labtech). For *Renilla* detection, 60μL of Stop&Glo® reagent were added, providing the Renilla luciferase substrate and halting firefly activity. The plate was incubated for 15 minutes at room temperature and luminescence measured.

An 'editing efficiency' was determined from the Firefly:*Renilla* ratio output of this assay. Untransfected wells (transfection-reagent only) were used to determine a mean background luminescence for both Firefly and *Renilla* and subtracted from all respective raw values. To determine the Firefly:*Renilla* ratio, the mean of each sample duplicate or triplicate was taken for both Firefly and *Renilla* and then used to calculate the ratio for each condition. To determine an editing rate, the ratio was normalised to the positive and negative control, where the positive control was set to 100% and the negative control to 0%. This was done for each condition to calculate an estimated editing efficiency:

$$Editing\ efficiency\ (\%) = \frac{(Experimental\ sample\ ratio) - (negative\ control\ ratio)}{(Positive\ control\ ratio) - (Negative\ control\ ratio)}$$

4.3.2 Cloning of DNA and RNA base editing gRNA plasmids and target *ABCA4* plasmids

4.3.2.1 sgRNA cloning

Fifteen RNA editing guides and five DNA editing guides were cloned as described in the general methods including commercial synthesising by Merck. The 15 guides for dCas13-ADAR$_{DD}$ had the required 'C' mismatch every second base between positions 17-39, and at every base between positions 30-35. These guides were cloned into pC0043-PspCas13b crRNA backbone (Addgene #103854) using the BbsI restriction enzyme (New England Bio) (Figure 4-3). For DNA base editing, guides ranging in length between 20-22 bases from the PAM site were cloned in the pAK212 plasmid (kind gift of Ariel Kantor) using the SapI restriction enzyme (Figure 4-3). Sequences were confirmed using sanger sequencing. All guide sequences are in the appendix.

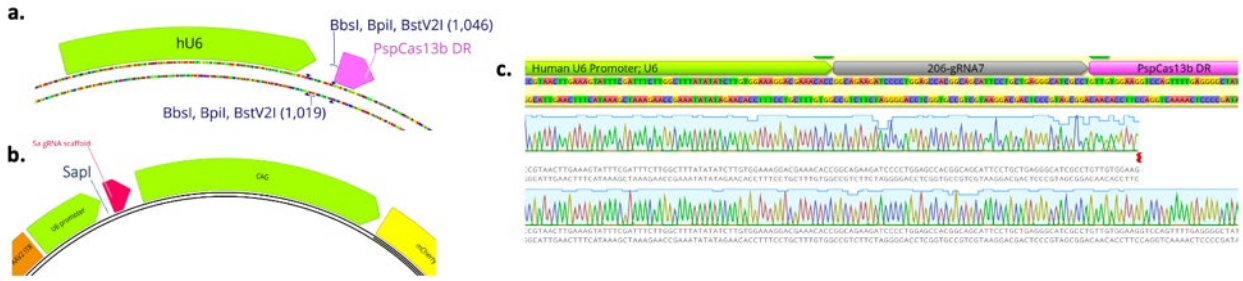

Figure 4-3: sgRNA cloning sites for DNA and RNA base editors.
a) the BbsI cloning site for the 50bp dPspC13b-ADAR guides between the U6 promoter and the Direct Repeat**. b)** the SapI restriction site between the U6 promoter and SaCas9 scaffold for the SaKKH guides. This plasmid also contained an mCherry reporter on the CAG promoter to indicate successful transfection/transduction. **c)** Sanger sequencing output of a cloned guide targeting c.206G>A for dPspC13b-ADAR.

4.3.2.2 Cloning of mutant *ABCA4* plasmid, c. 206 G>A

A myc-tagged *ABCA4* plasmid was ordered from Origene (NM_00350; RC213827) and used to make all mutant plasmids. In this chapter, the c.206 G>A (p. W69*) mutation was introduced according to the site-directed mutagenesis in the general methods. The primers used for site-directed mutagenesis are in Table 4-1. After screening guides using the previously described dual-glo luciferase assay, the best performing guides were tested on this mutant *ABCA4* plasmid to test for transcript level editing rates and protein effects.

Primer	Sequence
ABCA4-206-F	GCAGGAATGCTGCCGTAGCTCCAGGGGATCTTCTGC
ABCA4-206-R	GCAGAAGATCCCCTGGAGCTACGGCAGCATTCCTGC

Table 4-1: Site-directed mutagenesis primers to introduce c. 206G>A

4.3.3 Transfections targeting mutant *ABCA4* plasmid, c. 206 G>A

HEK293T cells were maintained as described in the general methods and seeded in 12-well plates at 4.5 x 10^5 cells/well. After ~24 hrs or 70-80% confluence, cells underwent a triple transfection with 1100ng total plasmid – 200ng target plasmid (WT or mutant *ABCA4*), the guide plasmid, and a base editor. For RNA editors, a 1:2 ratio of editor:guide was used ie 300ng of dPspCas13b-ADAR and 600ng guide. For DNA editors, a variety of ratios were tested but totalling 1000ng for both the guide and the base editor. In control wells, a filler plasmid was included to ensure an equal amount of plasmid per well. Plasmids were diluted, aliquoted by condition into a PCR plate, incubated at a 3:1 TransIT-LT1(Mirus Bio):DNA ratio for 15-20 minutes and added to the corresponding well on the plate. Plates were left to incubate for 48hrs at 37°C.

4.3.4 Detection of DNA and RNA editing via EditR

Cells were harvested 48 hours post-transfection and cell pellets were split into three Eppendorf tubes for separate analysis of DNA, RNA, and protein (Figure 4-4). RNA was extracted from cells and reverse transcribed according to the general methods using the Monarch® Total RNA Miniprep Kit (NEB) and the Evoscript Universal cDNA Master Kit (Roche). For cDNA synthesis, 1ug total RNA was used. DNA was extracted using the QIAamp® DNA mini kit (Qiagen) as described in the general methods.

To amplify the region of interest, 2μL cDNA or 40ng DNA were used in a PCR reaction using KOD Hotstart Polymerase Master Mix and the primers in Table 4-2. The reaction was run using the cycling conditions in the general methods, with an annealing temperature of 53°C and an extension time of 15 seconds for an 862bp amplicon. A gel was run using 5μL of the PCR reaction to confirm successful amplification. The remaining PCR product was purified using the

QIAquick® PCR purification kit (Qiagen) and sent for Sanger sequencing using the same primers as for PCR.

Primer	Sequence
206-TIDE-F1	CGACTCACTATAGGGCG
TIDE-206-R	GGCTGTCTAGGAGTGTGG

Table 4-2: PCR and sequencing primers for c.206 G>A target amplification

Sequencing chromatograms were first manually trimmed and analysed in Geneious Prime. The .ab1 files were then analysed using EditR, an algorithm that predicts base editing from Sanger sequencing outputs by quantifying the proportion of bases at each position.[270] Overall, for detecting base editing, the relevant guide sequence was input for the corresponding data file. For RNA base editing, the reverse complement of the guide was input for easier analysis as this corresponds with the target region (the guide is the complement of the target).

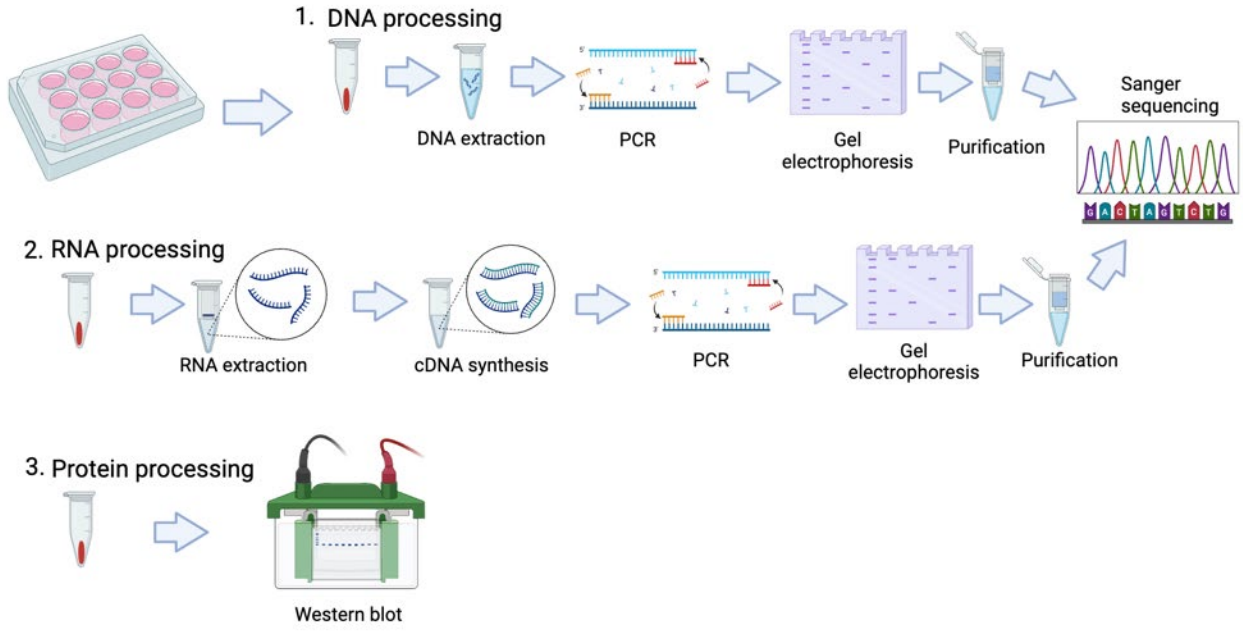

Figure 4-4: Workflow for detecting editing at the DNA, RNA, and protein level *in vitro*.
Cells from each well were split into three pellets when harvesting to allow for high-quality extractions and downstream processing.

4.3.5 Western blot

Western blots were run according to the general methods. Cells were lysed and protein denatured in RIPA lysis buffer. 40μg protein were loaded and run on 7.5% Tris-glycine gels (Criterion TGX, Biorad) in Tris-Glycine SDS-PAGE running buffer (National Diagnostics). Following transfer, membranes were blocked in 5% skimmed milk TBS-T blocking buffer and incubated in primary antibody solution. Antibodies are listed in Table 2-11. The membrane was washed and incubated in secondary antibody solution using IRDye® Donkey anti-rabbit and IRDye® Donkey anti-mouse (Li-Cor) at 680RD or 800CW at 1:10,000.

4.3.6 Statistical analysis

Statistical tests applied are explained in the general methods. Data were first tested for normality, after which a parametric or non-parametric test was applied.

4.4 Results

4.4.1 Screening Cas13-ADAR RNA editing guides

4.4.1.1 Dual-Glo® luciferase reporter assay

To target c.206 G>A with dPspCas13b-ADAR$_{DD}$, guides were screened for maximum on-target editing and minimum off-target editing. The optimised guide length for dPspCas13b-ADAR$_{DD}$ has been reported as 50bp in length with a C-mismatch at the target site to enable ADAR deamination (Figure 4-5).[199] Fifteen guides were screened placing the mismatch between positions 17-39 (Figure 4-5) and using a 2:1 guide:Cas13 ratio. Initial luciferase assay screens resulted in significant editing in five of fifteen guides (G6, G7, G10, G11, G12), with the highest mean editing rates of 33.2 $\pm$ 6.45% and 41.8 $\pm$ 7.6% in guides 6 and 7, respectively ($p<0.05$). These were selected for continued downstream testing. For further downstream comparison, a third guide with a greater mismatch distance, G12, was also selected. G12 achieved 29.8 $\pm$ 5.1% editing (Figure 4-5).

To determine if the luciferase assay output corresponded to transcript analysis, cells transfected with the luciferase target plasmid were processed and sent for Sanger sequencing. Analysis in EditR for guides 6, 7, and 12 revealed 38.5 $\pm$ 9.3%, 47.7 $\pm$ 1.5 %, and 38.84 $\pm$ 3.5% editing above background at the target site (Figure 4-5). This revealed that the luciferase assay mildly underestimated editing efficiencies. Further, this emphasised the need for high quality

PCR and sequencing for accurate output and analysis, which were improved in downstream experiments.

4.4.1.2 Targeting c.206 G>A mutant *ABCA4* plasmid

To confirm editing in the native *ABCA4* environment and determine if this leads to protein restoration, G6, 7, and 12 were tested targeting a c.206 G>A mutant plasmid. Editing rates remained consistent at 44.67 ± 2.8% (p=0.0003), 46 ± 1.5% (p<0.0001), and 45.67 ± 1.5% (p=0.0019), with no background in the non-targeting controls (Figure 4-5). Guide-only controls indicated no endogenous or exogenous ADAR activity and confirmed that observed editing is due to Cas13-ADAR.

Samples were next analysed for restoration of ABCA4 protein. Mutant plasmids were first run on a western blot to confirm a lack of ABCA4 protein (Figure 4-5) using a C-terminal anti-ABCA4 antibody and an anti-Myc-tag antibody (Appendix A). The C-terminal antibody indicated a potentially truncated protein. However, this is likely overexposure since this was not observed with the anti-Myc antibody (C-terminal) or in downstream control wells.

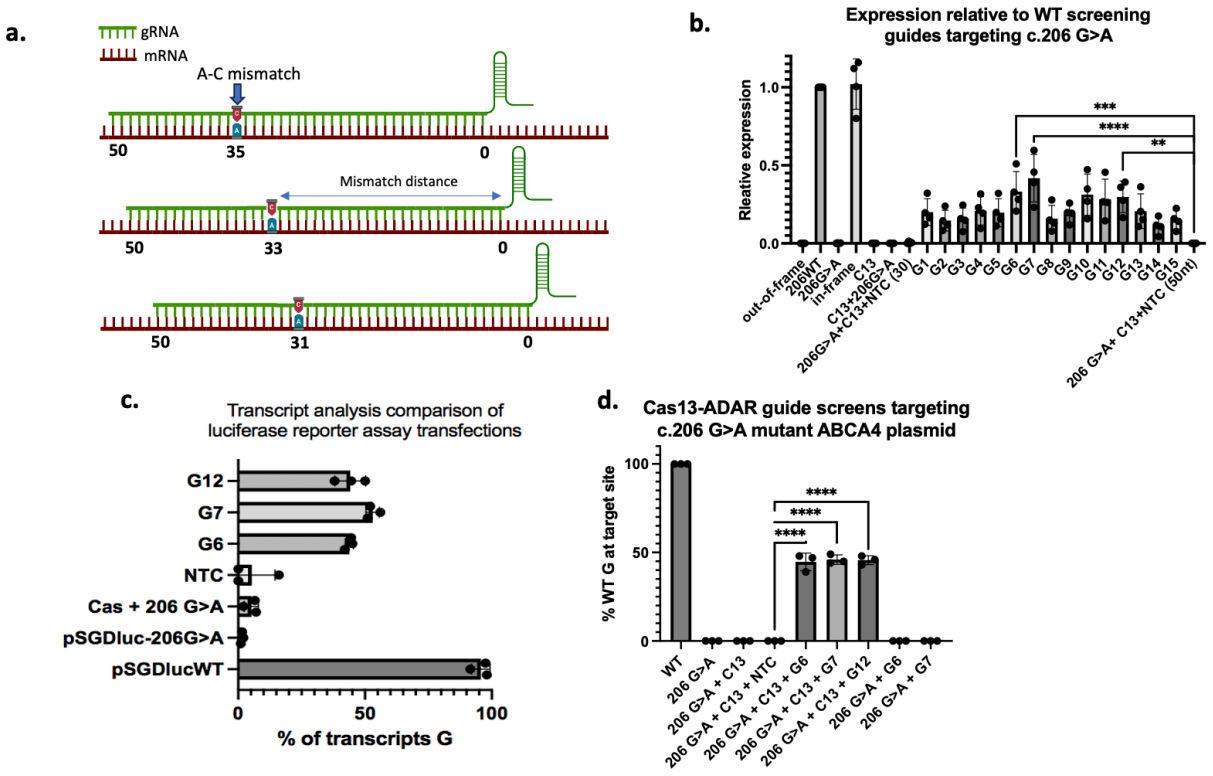

Figure 4-5: Guide screening dCas13b-ADARdd targeting c.206 G>A.
a. gRNA binding and 'C' mismatch location in the 50nt Cas13-ADAR guide. Fifteen guides were screened, shifting the 'C' mismatch between positions 17-39. No PAM site is required for Cas13-ADAR RNA base editing. **b.** Luciferase assay guide screen targeting the c.206 G>A stop mutation as a proportion of wildtype (206WT)

expression. Guides 6, 7, 10, and 12 showed the highest editing rates ranging from 30-41% ($p<0.05$; N=3). Guides 6, 7, and 12 were taken forward into downstream experiments. **c.** Transcript analysis by EditR targeting the luciferase reporter assay with guides 6, 7, and 12 to determine the accuracy of the luminescence assay output. Editing rates were similar (38-47%) and reflected the relative editing observed in the luciferase assay. The negative controls showed background noise. **d.** Screens targeting the c.206 G>A mutant *ABCA4* plasmid by Cas13-ADAR with the pre-screened guides. Significant editing of 44-46% was observed ($p<0.05$).

4.4.2 Screening and optimising guides targeting c.206 G>A by SaKKHABE8e dual vector

Guides for SaKKHABE8e were initially screened using the Dual-Glo® reporter assay. However, given the PAM site and optimal guide lengths, the number of guides screened was much lower (Figure 4-6). Of the three guides screened, only guide 2 (G2) showed significant editing at 28% of wildtype expression ($p=0.0334$), and was thus used in downstream experiments.

To further optimise editing rates with G2, six ratios of guide:ABE were tested – 2:1, 3:1, 5:1, 1:2, 1:3, 2:3. The 1:3 ratio was hypothesised to work most efficiently given previously published reports.[176] Further, these samples were incubated for 96 hours with a media change after 48 hours to improve editing outcomes.[176] Interestingly, across all ratios tested, editing rates remained consistent with the outcome of the luciferase assay mean editing rates ranging from 25.5%-29.5%. The greatest editing rate of 29.5% was observed when using a 2:3 ratio (Figure 4-6).

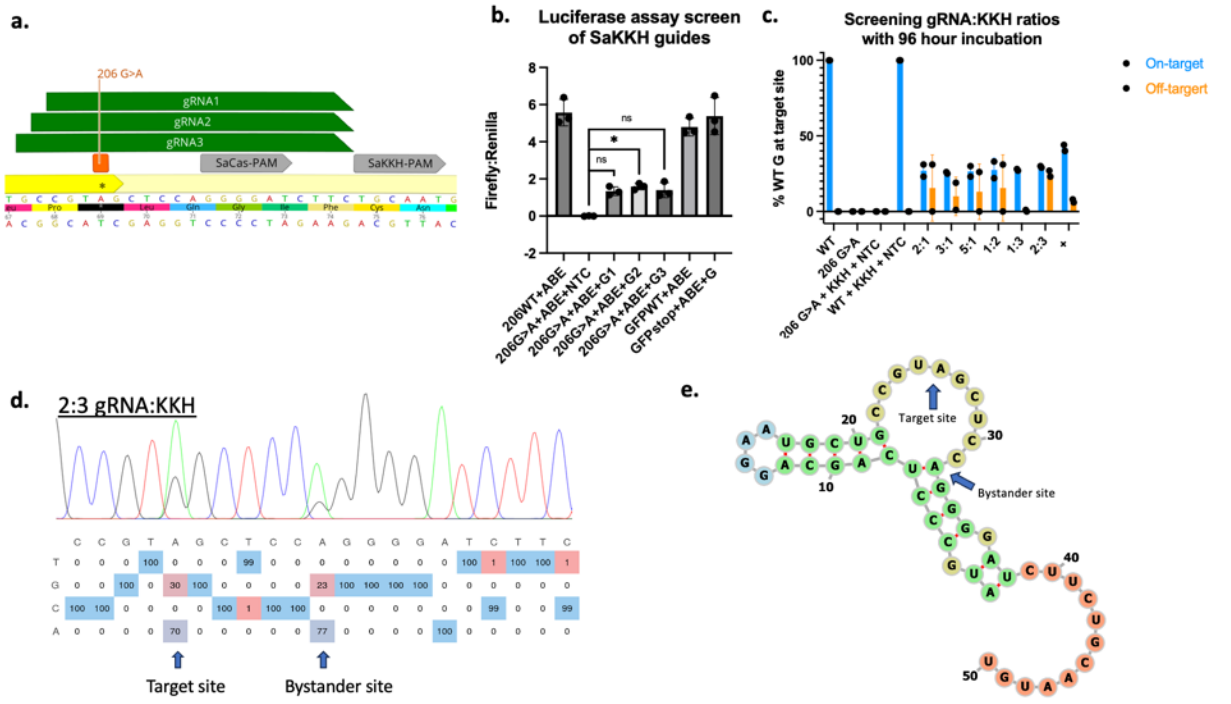

Figure 4-6: Guide screen of SaKKHABE8e targeting c.206 G>A *in vitro*.
a. The guides screened using the downstream SaKKH PAM site. Guides ranged in length from 20-22nt. The SaKKH PAM was used instead of the SaCas given the improved placement within the editing window at positions 4-6 (5' end is position 1). **b.** The luciferase assay guide screen revealed significant editing for guide 2 (G2) (p=0.033). This was used in downstream experiments. GFPWT and GFP-stop are positive controls. **c.** Guides were screened further at different ratios with a 96-hour incubation – substantial bystander editing was observed and minimal difference in on-target editing between the ratios. Bystander editing was variable across all ratios and the positive control. The 1:3 ratio had no observed bystander editing. N=2. **d.** EditR output showing both the on-target edit and the off-target edit. **e.** RNA secondary structure by Mxfold2 showing the c.206 G>A mutant (target site) and the c.212 A bystander site.

However, substantial bystander editing was observed at nearly the rate of on-target editing (Figure 4-6) at all ratios except 1:3. Bystander editing could not be observed with the luciferase assay, so it was unknown if this was a new development. The c.212 A>G bystander edit, although not a reported variant, caused a CAG – CGG missense edit, resulting in a glutamine to arginine amino acid change. When analysed in MutationTaster[271] c.212A>G was predicted to be pathogenic. Further analysis of the effect of the bystander edit on mRNA secondary structure in MXfold2 showed the formation of one large stem-loop, instead of the two stem-loops seen in the wild-type sequence. Interestingly, the bystander containing sequence more closely resembles the mutant c.206 G>A sequence, which also shows one longer stem-loop interrupted by a large bulge (Figure 4-8). This may affect translation, but the effects of the variant are unknown.

Given the likely downstream comparison of the dual vector to an all-in-one SaKKHABE8e *in vivo* due to the publication of the single AAV SaKKHABE8e[180] and the consistency across the

guide:ABE ratios tested, a 1:1 ratio was chosen for downstream testing. Further, due to the high rates of off-target editing with a 96hr incubation and that Cas13-ADAR RNA editing transfections used a 48hr incubation, downstream tests only used a 48hr incubation. Lastly, protein levels were investigated during the side-by-side comparison below.

4.4.3 Side-by-side comparison of DNA and RNA base editing targeting *ABCA4* c.206 G>A plasmid *in vitro*

4.4.3.1 Sequencing analysis

To reduce experimental variation, a side-by-side comparison was performed of the best performing Cas13-ADAR and SaKKHABE8e guides targeting the same mutant *ABCA4* plasmid containing c.206 G>A. EditR analysis of SaKKHABE8e DNA-level editing revealed slightly lower editing than prior screens at 24.3 ± 1.76 % with no observed off-target editing (Figure 4-7). This was likely due to the reduced incubation time of 48hrs. At the RNA level, however, this resulted in 48 ± 9.45% of transcripts containing the edit (Figure 4-7). In Cas13-ADAR targeted samples, G7 demonstrated the highest editing efficiencies of 46.67 ± 0.88%, similar to the downstream RNA-level effect of the SaKKHABE8e. G6 and G12 showed editing consistent with the luciferase assay data but lower than the initial screens targeting the mutant c.206 G>A plasmid, with 38.33 ± 1.86% and 38 ± 1% editing, respectively.

No editing was observed in non-target control samples or in samples transfected with a guide but without Cas13-ADAR. This suggests editing due to Cas13-ADAR rather than endogenous recruitment. However, it is unknown if ADAR recruitment to the target site was due to the gRNA-dPspCas13b complex or only the gRNA and requires further testing.[272]

Representative expression analysis by qPCR of pooled samples showed transcript levels ranging from 30-50% of wildtype levels in the c.206 G>A mutant plasmid. The observed toxicity due to base editors was observed by qPCR, as well, with a notable reduction in *ABCA4* expression relative to ABCA4 WT samples, particularly with the addition of the SaKKHABE8e. However, this experiment was representative and run with pooled (N=3) samples due to limited cDNA. Future work would increase the experimental sample size of the qPCRs run and include the targeting guides (Figure 4-7). This was not done due to time constraints.

4.4.3.2 Protein analysis

To compare the ability of editing by Cas13-ADAR and SaKKH to restore full-length ABCA4 protein, extracted protein was run on a western blot and quantified. Both Cas13-ADAR and SaKKHABE8e wells transfected with targeting guides resulted in restoration of full-length ABCA4 protein (Figure 4-7). Cas13-ADAR samples demonstrated stronger signal than the SaKKHABE8e samples. Signal quantitation revealed 15-25% of wildtype signal above background for Cas13-ADAR edited samples with G6, 7, and 12. SaKKHABE8e showed similar levels, with 26.7 $\pm$ 3.3% of wildtype expression. Non-targeting Cas13-ADAR guide-only wells indicated 1-2% expression above background, whereas the SaKKHABE8e non-target control showed no protein (Figure 4-7).

Samples transfected with a targeting guide but without Cas13-ADAR remained consistent with transcript level analysis and showed no observed restoration of protein. This indicates that editing is due to guide directed Cas13-ADAR editing, not endogenous ADAR1 activity.

Wildtype *ABCA4* samples treated with a base editor and a non-targeting guide showed reduced signal for both Cas13-ADAR and SaKKHABE8e samples relative to untreated *ABCA4* wild-type samples. This likely indicates toxicity due to base editor presence and requires further investigation for safety. SaKKHABE8e treated samples showed a greater reduction in signal relative to wild-type than Cas13-ADAR samples.

Lastly, the faint band above the ABCA4 band is an artefact seen in HEK cells and is seen in other publications blotting for ABCA4.[273,274] This is not seen in neural retinal extracts.

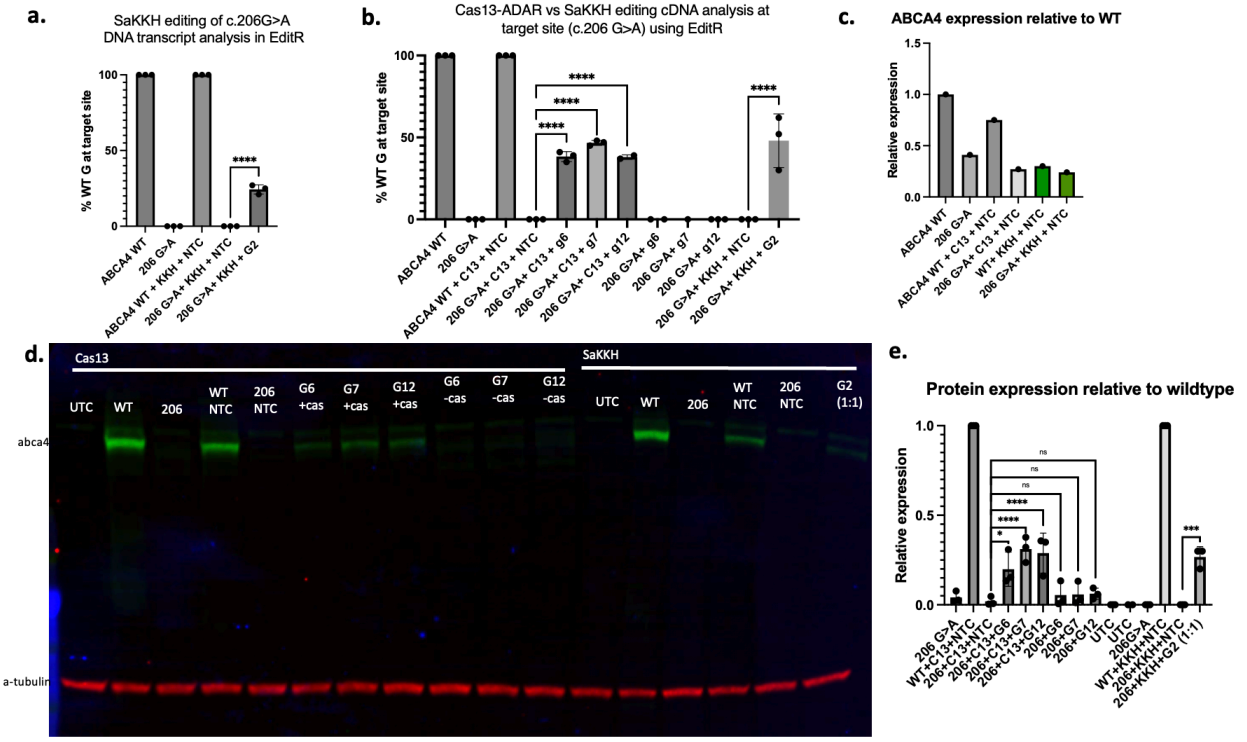

Figure 4-7: Side-by-side comparison of SaKKHABE8e and dCas13b-ADARdd targeting c.206 G>A. **a.** SaKKHABE8e targeting a c.206 G>A mutant *ABCA4* plasmid. Sanger sequencing revealed 24.3 ± 1.76 % ($p<0.0001$) editing. **b.** Comparison of Cas13-ADAR and SaKKHABE8e RNA level analysis showing similar mean percentages of the desired wildtype G. Cas13-ADAR G6, 7, ad 12 achieved 38.33 ± 1.86%, 46.67 ± 0.88%, and 38 ± 1%, respectively, and SaKKHABE8e G2 resulted in 48 ± 9.45% ($p<0.0001$). **c.** Representative qPCR of pooled samples (N=3) showing transcript levels of the wildtype vs mutant *ABCA4* plasmids. Greater sample size required to draw conclusions. **d.** Representative western blot showing restored full-length protein in base editor and targeting guide containing samples. The addition of Cas13-ADAR and SaKKH with wildtype ABCA4 (WT NTC wells) showed a reduction in protein signal perhaps due to toxicity. Alpha-tubulin was used for housekeeping. The band seen above ABCA4 is an artefact consistently observed in HEK cell lysates with this protocol. e. Protein quantitation relative to wildtype levels. These were taken relative to the wildtype + base editor (C13 or KKH) + non-targeting control (NTC) samples. Significant full-length protein restoration of 15-26% was observed by both Cas13-ADAR and SaKKH base editors ($p<0.05$). Data presented as mean ± SEM. Statistics: One-way ANOVA and Kruskal-Wallis.

4.4.4 Assessing bystander editing with Sanger sequencing

Interestingly, SaKKHABE8e showed high bystander activity compared to Cas13-ADAR (Figure 4-6). Bystander editing occurred at the downstream adenosine (c.212 A>G) within the editing window of SaKKHABE8e, but only after a 96-hour incubation. The bystander edit resulted in a glutamine to arginine amino acid change (CAG-CGG), which was predicted to be pathogenic, as described in greater detail in 4.4.4.

Samples undergoing 48-hour incubation, resulted in no bystander editing in both SaKKHABE8e and Cas13-ADAR samples. No local off-target edits were observed by visual

examination within the amplicon by Sanger sequencing. Deep sequencing results would likely indicate off-target editing given the overexpression of ADAR.[199,213,215]

Analysis of RNA secondary structure in MXfold2 revealed a differing structure between the wildtype sequence and the c.206G>A-containing sequence. The c.206 G>A results in a larger bulge, likely improving accessibility/recruitment by ADAR.[275,276] However, the bystander edit resulted in one elongated stem-loop (Figure 4-8). Free energy scores of gRNAs and the target regions may affect the on-target efficiency and the likelihood of off-target editing.[277]

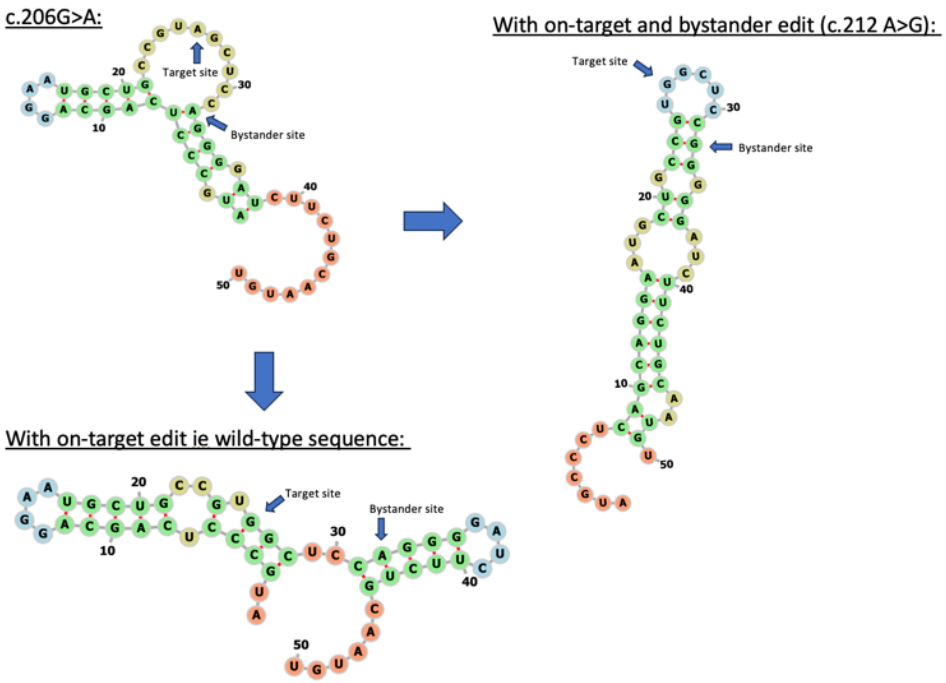

Figure 4-8: RNA secondary structure of c.206 region.
Predictions of mRNA folding using Mxfold2.[223] The c.206 G>A mutation substantially changes RNA secondary structure, creating a bulge at the target site and likely improving gRNA binding. Further, the 5' UAG 3' sequence is the preferred sequence to which ADAR is recruited.[198] The c.212 A>G bystander edit results in a decreased bulge and increased stem-loop length.

4.4.5 Targeting the common missense mutation, *ABCA4* c.5882 G>A

To establish clinical relevance of base editing, the most common *ABCA4* mutation, c.5882 G>A, was targeted. Initially, guides for both DNA and RNA base editors were to be screened. However, during this project, c.5882 G>A was successfully targeted by the SpCas DNA base

editor across a variety of models ranging from organoids to non-human primates.[102] Thus, only RNA base editing guides were screened targeting this mutation.

Since c.5882 G>A is a missense mutation rather than a nonsense mutation, a luciferase assay could not be performed. Three guides with mismatches in the most typically 'active' region (positions 31-33)[199] were chosen to target a c.5882 G>A mutant *ABCA4* plasmid. Transcript analysis revealed activity for all three guides, achieving 7.5 ± 3.5%, 29.5 ± 0.5%, and 21 ± 7% editing for G5, G6, and G7, respectively. In the absence of Cas13-ADAR but in the presence of the guide and the target, no activity was detected, suggesting a lack of endogenous ADAR1 activity and editing due to Cas13-ADAR.

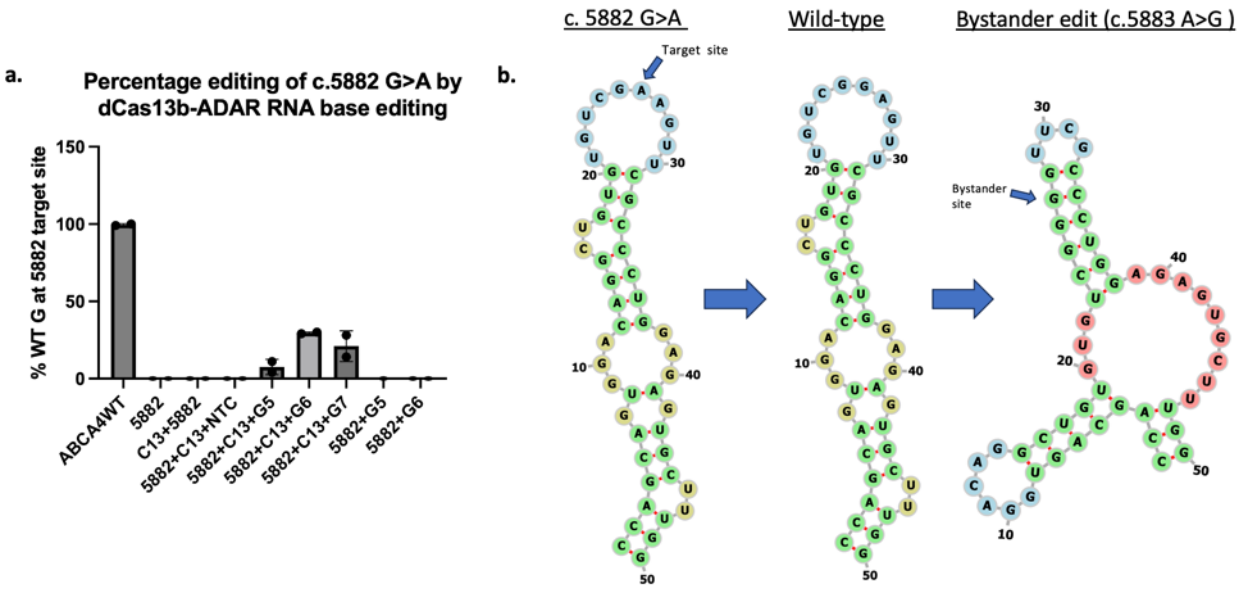

Figure 4-9: Editing at clinically relevant site c.5882 G>A.
a. Testing three Cas13-ADAR guides targeting c.5882 G>A. Transcript analysis showed up to 29% editing with G6. **b.** RNA secondary structures of the c.5882 region. The structure remained the same when comparing the wildtype to the mutant c.5882 G>A structure. Interestingly, the bystander edit c.5883 A>G resulted in the formation of a second stem-loop with a large central bulge. However, the mutation results in a silent amino acid change and is not a reported variant, likely having no clinical significance.

Analysis of the effect of the c.5882 G>A mutation on RNA secondary structure demonstrated no change when compared to the wildtype. Further, the location of the mutation at the bulged end of the stem-loop potentially enables greater access to the gRNA.

Bystander editing at this site was likely, given the neighbouring adenosine, which was observed with an SpCas adenine base editor *in vivo*.[102] Bystander editing of up to 10% was observed by dCas13b-ADAR editing. However, this resulted in a silent Gly-Gly amino acid

change which is not a reported variant in LOVD, but could nonetheless affect splicing. Interestingly, introduction of the bystander edit c.5883 A>G results in a drastic RNA secondary structure change, forming a second hairpin and a large bulge (Figure 4-9). Mutation taster predicted this site to be pathogenic. This requires further investigation including greater sequence context and protein folding analysis.

The c.5882 G>A mutant plasmid showed full-length ABCA4 production using two different antibodies (Appendix). Due to this, analysis of the edited samples at the protein level was not possible.

4.5 Discussion

CRISPR base editing technologies have emerged as an effective approach to targeting pathogenic mutations and have translational potential. Base editing can be applied to DNA or RNA, each offering advantages and disadvantages. Editing DNA provides the opportunity to target nucleotides on both the plus or minus DNA strand, has reduced off-target activity and promiscuity compared to ADAR, and genomic DNA has a much lower copy number than mRNA transcripts. Further, the edits are permanent and thus provide the potential for a life-long correction in the context of treatment. While this has remarkable therapeutic potential, this comes with the risk of accumulating off-target edits with potentially detrimental outcomes.[278,279] Inversely, RNA editing offers an inherent and essential safety feature since mRNA is transient and off-target edits are thus not permanent. Due to this, RNA editing is more easily reversible and enables greater control of editing outcomes.[199] However, given the large likely number of mRNA transcripts that would require targeting in *ABCA4* due to continued outer segment renewal,[10,11,280] high editing efficiencies may be essential.[281,282]

This chapter aimed to compare DNA and RNA base editors *in vitro* by targeting a clinically relevant stop mutation, c.206 G>A. Outcomes were measured at the DNA, RNA, and protein level, as well as functional analysis by luciferase assay.

Analysis and reflection of the *in vitro* assays is discussed in the General Discussion since they were across all lab data chapters.

4.5.1 Further optimisation of DNA and RNA base editing

An efficient, straightforward dual luciferase assay system containing the target region was used to screen the high number of guides. Efficient guide designs ranging the length of the 50nt

spacer based on previous publications were determined, enabling up to 40% editing.[62,199] The 'C' mismatches at positions 31 and 32 (G7, G6) reflected the activity across a multitude of target sites reported in Cox et al. and Abudeyyeh et al.[62,199] Interestingly, roughly equal levels of editing activity were observed at positions 23-27 (G12, G11, and G10). A greater number of Cas13-ADAR guide designs could have been tested applying new design innovations, such as increasing the length[62,199] and creating A-G mismatch bulges[215,216] to increase editing efficiency and decrease bystander activity.

Continued optimisation of the DNA base editing system at this site may have improved editing rates or decreased off-target editing. As seen when testing various 'gRNA: base editor' ratios, the previously published 1:3 showed high on-target editing with no off-target editing, even after 96-hours.[250] However, given the likely downstream *in vivo* testing, a 1:1 ratio was used to best compare to an all-in-one vector in initial testing. Continued investigation *in vivo* would test the 1:3 ratio with the dual vector SaKKHABE8e to observe changes in on target, off target, and bystander editing, and test for a possible advantage the ratio alterations may provide. Testing of other DNA editors such as split-intein SpCas base editors or prime editors may have led to further improvements as well. An SaABE8e (NNGRRT) was tested using an upstream PAM site (Appendix) and showed restored protein by western blot. This was not investigated in greater detail given the restrictive nature of the SaABE8e PAM site.

4.5.2 Editing comparison of dCas13b-ADAR$_{DD}$(E488Q) and SaKKHABE8e

DCas13b-ADAR2$_{DD}$ and SaKKHABE8e results confirmed published data showing effective *in vitro* editing.[62,199,250,283,284] Comparison of the two editing systems targeting the same site revealed roughly equal effects at the transcript and protein levels. For SaKKHABE8e, it was surprising to observe such a substantial increase from DNA level editing to downstream transcript-level change, where DNA editing levels of 24% resulted in 48% correction at the RNA level. In addition, equivalent editing efficiencies by both base editors was an unexpected outcome in targeting this site given known target specificity of guides and deaminases.[285-287]

The exception to this was the qPCR output looking at *ABCA4* expression. Interestingly, the c.206 G>A mutant plasmid showed relatively high transcript levels, despite the absence of ABCA4 protein, suggesting a reduced nonsense-mediated decay (NMD) efficiency. Indeed, rates

of NMD can vary significantly between transcripts, cell lines, and tissues, with a reported reduced efficiency in HEK293T cells.[288,289] Further to this, transfecting a plasmid of a mutant *ABCA4* coding sequence does not allow for the typical deposit of exon junction complexes (EJCs) upstream of splice sites, since the CDS is already spliced, suggesting an EJC-independent mechanism.[290,291] Although plasmid overexpression may overload the NMD pathway and reduce its efficiency, previous reports showed that the amount of transfected DNA did not affect NMD efficiency.[288] However, this requires further investigation including repeating expression studies and testing in other cell-lines or patient-derived cell models.

One factor potentially leading to the consistently high on-target editing rates by Cas13-ADAR was the likely effect of the preferred ADAR2 recruitment sequence 5'-TAG-3.'[198] Editing due to endogenous ADAR was ruled out given that non-targeting guides and that samples without Cas13-ADAR resulted in no editing at the target sites. Moreover, only low levels of ADAR1 are expressed in HEK cells, further reducing the likelihood of endogenous activity.[292] Continued experiments are required to determine if recruitment to the target site is due to dPspCas13b or ADAR2. Previous publications have shown that 20-60% of editing is possible without the Direct Repeat (DR) scaffold, suggesting exogenous ADAR recruitment to the target may occur independently of dPspCas13b.[272] Lastly, alternative novel base editing by exogenous and endogenous ADAR recruitment have shown great promise and are an exciting area of further research for RNA base editing.[215,216]

New and exciting DNA base editing orthologues have been developed that improve on-target editing and decrease off-target editing, such as ABE9e.[185] Further, size-minimised versions of SaKKHABE8e were developed that can be packaged in a single AAV. This is tested in Chapter 6.

4.5.3 Targeting a common *ABCA4* variant, c.5882 G>A

The c.5882 G>A missense variant is the most common variant in *ABCA4* in European populations.[23] Disease severity varies substantially depending on which other variants are in *cis* or *trans*.[20] The target site motif 5'-GAA-3' is a less-preferred motif than at the c.206 site.[198] Editing rates reflected this, with notably lower editing rates with the best-performing guide targeting c.5882 G>A than c.206 G>A. It is possible that a guide placing the mismatch in a different part of the spacer would increase editing rates, which would be investigated in the future. Interestingly, when analysing the secondary structure of the c.5882 G>A mutant in

MXfold2, the structure remained the same. This aligns with publications and clinical data that show a milder disease expression and later mean age-of-onset in patients with c.5882 G>A.[23,81,88,293]

The bystander edit, c.5883 A>G, was observed at a rate of ~10% and resulted in the formation of another stem-loop using predictive tools. This is a silent mutation (Gly-Gly) that is not reported as pathogenic in Gnomad4.0 (Gnomad.broadinstitute.org; accessed 11-12-24), or as a variant in LOVD (accessed 11-12-24) or ClinVar (accessed 11-12-24). Despite the lack of reporting, silent mutations can affect splicing, mRNA secondary structure, and affect translational efficiency due to altered tRNA anti-codon availability, potentially resulting in pathogenic outcomes.[294,295] Work at the Institute of molecular and clinical ophthalmology Basel (IOB) is ongoing to target c.5882 G>A by a split-intein SpABE.[102]

4.5.4 Toxicity and off-targets

The off-target editing profile was surprising, as greater bystander editing was observed with DNA base editing than Cas13-ADAR. While bystander editing is expected with DNA base editors,[176,177,250,258,261] Cas13-ADAR is notoriously promiscuous in its base editing activity within the spacer region and throughout the transcriptome.[215,216] Furthermore, the overexpression of the Cas13-ADAR would be expected to increase bystander and off-target activity,[199] however, this was not observed.

The observed bystander editing with SaKKHABE8e was likely due to the increased incubation time of 96-hours. When the incubation was reduced to 48-hours to match the Cas13-ADAR samples, no bystander editing was observed. This confirms previous publications that hypothesised increased likelihood of off-target editing following increased expression time, as in a therapeutic setting.[296,297]

SaKKHABE8e gRNA efficiency is difficult to predict, but in reports correlating it to free energy scores, gRNAs with a weak free energy resulted in the highest editing. If the free energy of the target region was also weak, this resulted in higher rates of off-target editing.[277] In addition, GC rich regions are shown to increase off-target activity in Cas9 editing.[277,298] This was reflected in the bystander editing where the target adenosine was surrounded by Gs and Cs (Figure 4-6a).

Next-generation sequencing of RNA and DNA could have been conducted to determine genome and transcriptome-wide off-target editing. Alternatively, future work could include CIRCLE-seq screening *in vitro* to determine off-target editing by DNA base editors.[220] While many tools have been developed to predict off-target sites *in silico*, these have significant shortcomings and are not accurate enough for translational tests.[299]

Lastly, a toxic effect was observable in base editor transfected conditions. This can be seen by western blot and qPCR, where wildtype *ABCA4* without a base editor, but with an empty guide plasmid to maintain consistent transfection conditions, showed greater expression than when transfected with a base editor. A notable difference was seen between SaKKHABE8e and Cas13-ADAR transfected cells, were SaKKHABE8e reduced expression more than Cas13-ADAR.

4.5.5 *In vivo* considerations

Downstream testing in more complex models targeting c.206 G>A would have provided greater insight into which base editing system can best affect functional and/or phenotypic changes. While this mutation is rare, targeting a nonsense mutation *in vivo* or in other pre-clinical models such as organoids allows for clear output measures, including production of full-length protein, protein localisation, and transcript output, and the subsequent functional and phenotypic effects. A recent publication targeted the most common *ABCA4* mutation, c.5882 G>A, across most pre-clinical models ranging from retinal explants to non-human primates. Where possible, the mutation was corrected in a disease-model, however, in many instances the bystander site was targeted. Since this is a missense variant, transcript analysis was the only proof-of-editing.[102] Future work would aim to investigate a stop mutation in retinal organoids and/or *in vivo* to establish editing and downstream functional effects in complex systems.

4.6 Conclusion

This chapter established a pipeline to compare editing of *ABCA4* by both DNA and RNA base editing. Analysis included DNA, RNA, and protein level outputs to allow for holistic comparison of the two editing systems. Next steps include further evaluation in pre-clinical models at different target mutations to determine editing in a native environment.

5 Targeting a clinically relevant region in retinal organoids

5.1 Introduction

ABCA4 is known for the high number of pathogenic variants, of which 62% are transition variants targetable by DNA base editors and ~23% are specifically G>A variants also targetable by RNA base editors.[67] Chapter 3 further established the relevance of DNA and RNA base editing in targeting pathogenic mutations in Stargardt disease. While the results are promising, base editing efficiencies are extremely site specific and affected by the target sequences.[286] Efficiencies can be influenced by deaminase preferences for consensus sequence[285] and sgRNA binding efficiencies, which are difficult to predict with existing computational tools.[287] Thus far in this thesis, *in vitro* screens have been conducted targeting several sites throughout *ABCA4*, enabling a holistic comparison of DNA and RNA base editors across sites.

However, in the laboratory-to-clinic-pathway, one of the major translational obstacles is the limited availability of diverse, clinically relevant preclinical models, particularly for Stargardt disease.[50] Mouse models have been invaluable in providing insight into the pathobiology of retinal disease and testing of novel therapeutics. In the context of gene therapies, mouse models provide functional insight, shed light on immune responses, uncover potential toxic effects from vectors, and enable dose response testing. Nonetheless, given species differences and extensive inbreeding, these models may not reliably recapitulate human disease or functional effects of treatment.[50,94,300]

Retinal organoid models have recently emerged to partially bridge that gap by emulating the human retina. Patient-derived organoids from induced pluripotent stem cells (iPSCs) or

embryonic stem cells (ESCs) offer the additional benefit of a native genetic environment in which to study the effects of pathogenic variants and evaluate novel therapeutics *in vitro*.[301-304] Initially, the c.93 G>A clinically relevant stop mutation was to be targeted in patient-derived organoids and *in vivo* in a humanised mouse model (Chapter 6). Unfortunately, neither the organoid nor the mouse model production were completed within the time of this project. As a result, alternative targets near the c.93 site were assessed to establish site targetability and the application of base editors targeting *ABCA4* in retinal organoids for downstream use.

This chapter continues comparing SaKKHABE8e DNA base editing and dCas13b-ADAR$_{DD}$(E488Q) RNA base editing at a clinically relevant stop mutation *in vitro.* Further testing of AAV-delivered dCas13b-ADAR$_{DD}$(E488Q) is undertaken in wildtype 3D retinal organoids.

5.1.1 Chapter aims

1. Screen guides *in vitro* for DNA and RNA base editors targeting a clinically relevant stop mutation, c.93 G>A, and evaluate the best guides by transcript analysis and full-length protein production.
2. Since development of patient-derived organoids was not possible, establish editing of a base near c.93 *in vitro* to provide proof-of-principle editing of the c.93 target region.
3. Test the screened guides in a wildtype organoid model to determine whether dCas13b-ADAR editing is possible in organoids.
4. Determine the safety of the vector by analysing off-target effects and observe signs of toxicity.

5.2 Materials and methods

5.2.1 Organoid model design and production

Initially, a DNA versus RNA base editing comparison was to be tested in a patient-derived organoid model. Like prior *in vitro* work, the organoid model required a null G>A mutation with a nearby SaKKH PAM site. For this, the Oxford and Moorfields Stargardt patient databases were screened for homozygous null mutations, which yielded 25 patients. Of these patients, two patients with the same mutation (c.93 G>A) met the remaining criteria, however, one of these patients could not participate. The other patient kindly agreed to participate. All sample isolation and handling were conducted under IRAS 301603 ethics approval. Samples

were taken and PBMCs isolated by a member of the lab in accordance with the Human Tissue Act and under appropriate ethics approval. PBMC samples were sent to Newcells Biotech for retinal organoid production. After three attempts at production, patient-derived organoid production was deemed unsuccessful.

An alternative approach was undertaken in a wild-type retinal organoid model also produced by Newcells Biotech (Figure 5-1). All organoid maintenance is described in Section 5.2.7.

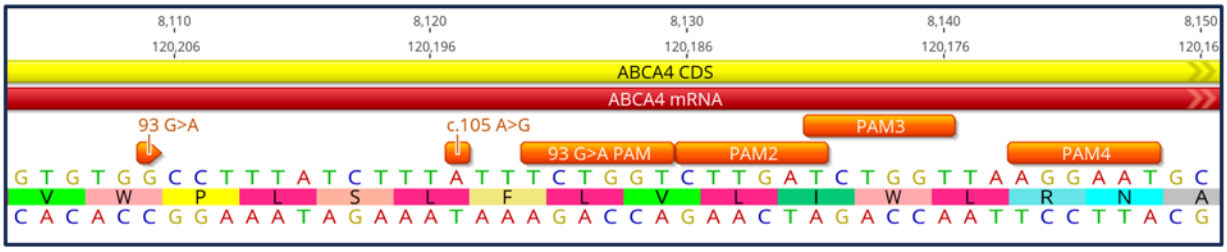

Figure 5-1: Retinal organoid target sites and corresponding PAM sites.
The original patient mutation, C.93 G>A, with the corresponding PAM site, 93 G>A PAM. C.105A was chosen as an alternative target to introduce c.105 A>G by base editing. Alternative PAM sites are indicated by PAM2-4.

5.2.2 Cloning

5.2.2.1 Cloning of target plasmids: luciferase assay plasmids for *in vitro* screening and c.93G>A mutant *ABCA4* plasmid

All dPspCas13b-ADAR$_{DD}$ guides were screened by Dual-Glo® luciferase assay for nonsense mutations as described in Chapter 4. The pSGDlucV3.0 plasmid was digested with HindIII. Target cassettes were commercially synthesised (IDT, Merck), amplified by PCR using KOD Hot Start Polymerase Mix (Sigma-Aldrich), and annealed at 65°C with primers listed in Table 5-1. Cassettes were cloned into the pSGDlucV3.0 backbone using the NEBuilder HiFi DNA Assembly™ with 25bp overhangs. Various cassette lengths were tested ranging from 125-308bp (Figure 5-2) all containing the patient mutation c.93 G>A or the wild-type sequence. Cassette sequences are listed in the Appendix.

The *ABCA4* target plasmid (Origene) was sent for commercial cloning and maxiprep (Genewiz) for addition of the c.93 G>A mutation. The plasmid was Sanger sequence confirmed.

Primer	Sequence

93_Fw_Primer	CAACCCCGGGCCCTACTCGAGCAGAATGGGCTTC GTGAGACAGATACAGC
93_Rv_Primer	TTGCTTATGCCGTGCCTCAGATCTAGCCAAGAT GGAGTTGTTATAGTTTG
93_short_NEBFwdp	CAACCCCGGGCCCTACTCGAGCAGAAACTGGA CCCTGCGGAAAAGGCAAA
93_short_NEBRvp	TTTTGCTTATGCCGTGCCTCAGATCTACCTGGGG TGGGGCTTTGAAAACAGG
93 shortest rv	TTTTGCTTATGCCGTGCCTCAGATCTATGGCATT CATGATGGCTGTAGAGC

Table 5-1: Primers for pSGDlucV3.0 93 G>A luciferase assay screen cloning.

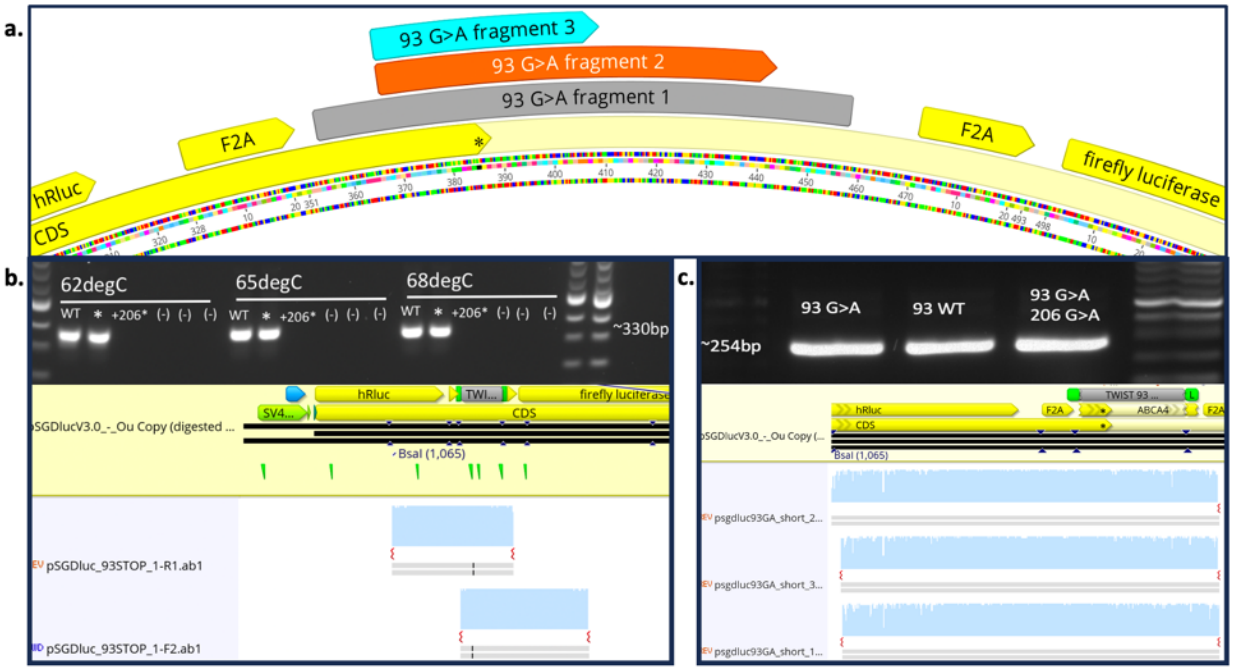

Figure 5-2: Cloning of pSGDlucV3.0 93 G>A luciferase plasmid.
a) Three fragments of different lengths were tested ranging from 308bp (fragment 1) to 125bp (fragment 3). **b)** Top: gradient PCR of fragment 1 cassette. WT = wild-type sequence and *= stop codon containing sequence. +206* had an additional nonsense mutation. Bottom: Sanger sequence confirmation of successfully cloned cassette, with the black line indicating the c.93G>A mutation. **c)** Top: PCR amplification of the 224bp fragment (additional length from insertion site overhangs). Bottom: Sanger sequence confirmation of successfully clones cassettes.

5.2.2.2 DNA and RNA base editing guide RNAs

All guides were cloned as described in the general methods and Chapter 4 methods. Guide sequences are listed in the appendix. Oligonucleotides were commercially synthesised (Merck) and annealed and phosphorylated with complementary overhangs to the insertion site. Ligations were transformed, incubated overnight, and two colonies picked per plate. Colonies were grown overnight, miniprepped and confirmed by Sanger sequencing.

5.2.3 Detection of DNA and RNA editing

Cells were processed as described in the general methods. Protocol specifics for PCR amplification of the c.93 G>A region were the same as described in Chapter 4 given the proximity of the mutation. Samples were sent for Sanger sequencing (Genewiz) and analysed in EditR.[270] For confirmation of indel formation in instances of using Cas9, Tracking of Indels by DEcomposition (TIDE) was used.[305]

Organoids were removed from -80°C and lysis buffer immediately added for thawing. Once thawed, samples were homogenised for 10 seconds. RNA extraction was conducted using the Monarch® Total RNA miniprep kit according to manufacturer protocol including the optional DNase incubation step. Two batches of organoids were processed with slightly different specifications to improve downstream samples sent for sequencing. 103.5ng (first batch) or 129ng (second batch) total RNA were used for cDNA synthesis with the Transcriptor Universal cDNA master mix kit (Roche) as described in the general methods. The target region was amplified by PCR using Platinum SuperFi II PCR master mix with 3μL (first batch) or 5μL (second batch) cDNA using the primers in Table 5-2 with an annealing temperature of 60°C and a 10 second extension time. Samples were run on a gel to confirm amplification and purified by Qiaquick PCR purification kit. PCR purified concentrations remained low given organoid yields. In batch 1, the PCR product was amplified again and run on a gel, where the correct band was excised and processed using the Qiaquick Gel Extraction kit. The correct band was amplified by PCR a third time and confirmed by gel electrophoresis. With the second batch of organoids, to minimise total PCRs run, 5μL cDNA were used in the PCR and the correct band was excised from the gel and purified. The samples were sequenced using the amplicon-EZ NGS service (Genewiz) and analysed in Crispresso2.0. Sequencing results were analysed in EditR.

Primer	Sequence
1.5F abca4	GAAGAACTGGACCCTGC
RO-93-rnaR3	CTGTCCAAATACGGCCAAGG

Table 5-2: Primers for amplification of target region.

5.2.4 Sequencing and analysis

Both Sanger sequencing and NGS were completed using Genewiz services. Samples were prepped according to Genewiz instructions and analysed in EditR and Crispresso2 as described in the general methods. For analysis of Cas9 editing, Tracking of Indels by DEcomposition (TIDE) was used to quantify editing efficiency using sequence trace data from two capillary sequencing reactions ie Sanger.ab1 files. Specifically, TIDE compares targeting and wildtype chromatograms to measure small indels. Sanger sequencing outputs were additionally manually reviewed in GeneiousPrime.

5.2.5 Retinal organoid culture and processing

Retinal organoids made by Newcells Biotech were sent at day 150 or day 180, and were maintained at 37°C, 5% CO_2 in 96-well plates with one organoid per well in 200μL proprietary media provided by Newcells Biotech. 100 μL of room-temperature media was removed and replaced with fresh media every 3-4 days in designated tissue culture hoods. Organoids were transduced with virus at day ~180. The virus was mixed with an aliquot of media to the desired dose of 2E+10vg/organoid, ie 1E+10vg of each virus (batch 1), and 5E+10vg/organoid, or 2.5E+10vg of each virus (batch 2). 100 μL media was removed from each well and replaced with 100 μL of the virus-media mix. Organoids were maintained for 4-8 weeks and imaged weekly for fluorescence expression with an EVOS FL Auto2.

Organoids were harvested at 42-days (batch 1) or 30-days post-transduction (batch 2). Media was removed and organoids washed with 500 μL ice-cold PBS three times. Organoids were snap frozen with dry ice and stored at -80°C for downstream use. For IHC, organoids of the same experimental conditions were placed in one 1.5mL Eppendorf tube with 1mL ice-cold PBS and were allowed to sink to the bottom of the tube. After three PBS washes, organoids were incubated in 4% PFA (Sigma-Aldrich) for 20 minutes and washed in PBS 3 more times. Organoids were incubated in 30% sucrose for 2 hours and transferred by Pasteur pipette into a

base mould. The mould was filled with optimal cutting temperature (OCT) mounting media (VWR), frozen on dry ice, and transferred to -80°C for long-term storage.

5.2.6 Immunohistochemistry

Embedded, frozen samples were removed from the mounting mould and excess OCT cut away in the cryostat pre-cooled to -20°C. Samples were sectioned at 10μm and placed on Superfrost Plus™ slides, dried, and stored at -20°C. For IHC, slides were processed as described in the general methods using antibodies shown in the table of IHC antibodies (Chapter 2). The rabbit anti-ABCA4 (ab72955) worked most reliably.

5.2.7 AAV production and titration

All AAV was produced and titred as described in the general methods. Since retinal organoids do not seem to have receptors for AAV8, an AAV2 quad mutant (Y272F, Y444F, Y500F, Y730F) was used to achieve maximum transduction.[306,307] Plasmids for AAV2qm production are in Table 5-3. Virus was made of RK-dPspCas13b-ADAR$_{DD}$ and a targeting guide (5.2.9). The viruses were checked for purity by SDS-PAGE and titred by qPCR using SYBR Green Universal master mix (BioRad) and the primers in the general methods.

Plasmid purpose	Plasmid name
pHelper	pAdDeltaF6
pRep/cap	pRep2Cap2 quad mutant Y272F, Y444F, Y500F, Y730F
pTransgene	AAV-ITR-GRK1-dPspCas13b-ADAR$_{DD}$ and AAV-ITR-U6-gRNAC13-CAG-GFP

Table 5-3: Plasmids used for production of AAV2 quad mutant for retinal organoid transduction.

5.2.8 Confocal and EVOS LED microscopy

All microscopy was performed as described in the general methods. During maintenance of organoids, the EVOS was used to track organoid health and GFP expression over time. The confocal FV3000 was used for imaging of organoid sections. Z-stacks were processed in ImageJ Fiji.[308]

5.2.9 Statistical analysis

Statistics were performed as described in the general methods. Samples were tested for normality using the Shapiro-Wilkes or Kolmogorov-Smirnov test depending on sample size and followed up with visual examination of the QQ plot. Subsequent analysis was performed parametrically or non-parametrically.

5.2.10 Mutation screen and model design

As described in 5.2.1 and in Chapter 6, a clinically relevant stop mutation, c.93 G>A, was screened for from available patient databases with the aim of developing a humanised exon 2 c.93 G>A mouse model and a patient-derived retinal organoid model. This mutation was chosen as it fulfils three key criteria. First, it is a G>A mutation, allowing for screening of both DNA and RNA base editors. Second, it is a stop mutation, so upon mutation correction, protein production and localisation are measurable outputs. Third, there were multiple SaKKHABE8e PAM sites to enable strategy optimisation.

These two models would allow for *in vivo* testing with greater translational application given further examination in the organoid model. While the patient kindly agreed to participate, organoid production was halted by NewCells Biotech after three failed differentiation attempts. An alternative path to introduce the mutation was pursued but, as with the mouse model (Chapter 6), this is still in production.

Since the patient-derived organoid model was no longer a possibility, wildtype organoids were targeted near c.93 to induce a missense mutation. This was to test whether this region is targetable in a translational model and establish AAV-SaKKHABE8e and AAV-Cas13-ADAR editing in retinal organoids.

5.3 Results

5.3.1 Base editing *in vitro* targeting patient mutation, c.93 G>A

5.3.1.1 Dual-Glo® Luciferase reporter assay to detect RNA base editing

To screen c.93 G>A guides for dCas13-ADAR, the same approach to Chapter 4 was used. Fifteen guides 50nt in length were designed with a ‘C’ mismatch every other base from position 17-39. Since positions 31-34 have shown greater reported activity,[199] a C-mismatch was tested at

each of these positions (instead of every other base). Guides were first screened using the Dual-Glo® luciferase assay described in Chapter 4, containing cassettes with the wild-type or mutant sequence between *Renilla* and Firefly. *Renilla* was constitutively expressed and subsequent readthrough of the cassette upon mutation correction allowed for Firefly expression (Figure 4-1).

Initially, a longer cassette ~330bp in length was cloned to provide greater wildtype sequence context around the mutation site. In addition, this cassette included the c.206 site so downstream testing of multiplexed guides could be tested, but this was omitted in initial experiments.

An initial guide screen exhibited substantially decreased Firefly expression in the wildtype c.93 when compared to the c.206 wildtype positive control (from Chapter 4). Interestingly, the *Renilla* expression was consistent, suggesting the Firefly reduction was due to the cassette. Further, in wells containing Cas13, there was almost no Firefly or *Renilla* expression. Discerning any information about guide performance was not possible (Figure 5-3). Secondary structure analysis of the cassette revealed a large hairpin, perhaps affecting translational efficiency.

To interrupt the hairpin, smaller cassettes were tested for Firefly output and compared to the in-frame psiCheck2 control plasmid and the 206-wildtype plasmid. First, the cassette was truncated to 224bp, which still demonstrated greatly reduced Firefly expression relative to the 206-wildtype control. As with the longer cassette, *Renilla* expression remained roughly consistent (Figure 5-3). Finally, a cassette of 125bp was tested which was the same size as the 206-wildtype positive control. Firefly expression improved slightly and *Renilla* expression remained consistent. Based on the predicted RNA secondary structure, this cassette length relaxed the hairpin, perhaps enabling improved translation (Figure 5-3).

Future experiments would investigate repeating luciferase assays with codon optimisation of the c.93 cassette to determine if an altered sequence would enable improved translation and luciferase activity. Additionally, disruption of the numerous PAM sites may shed light on the role of steric hinderance on the lack of DNA base editing.

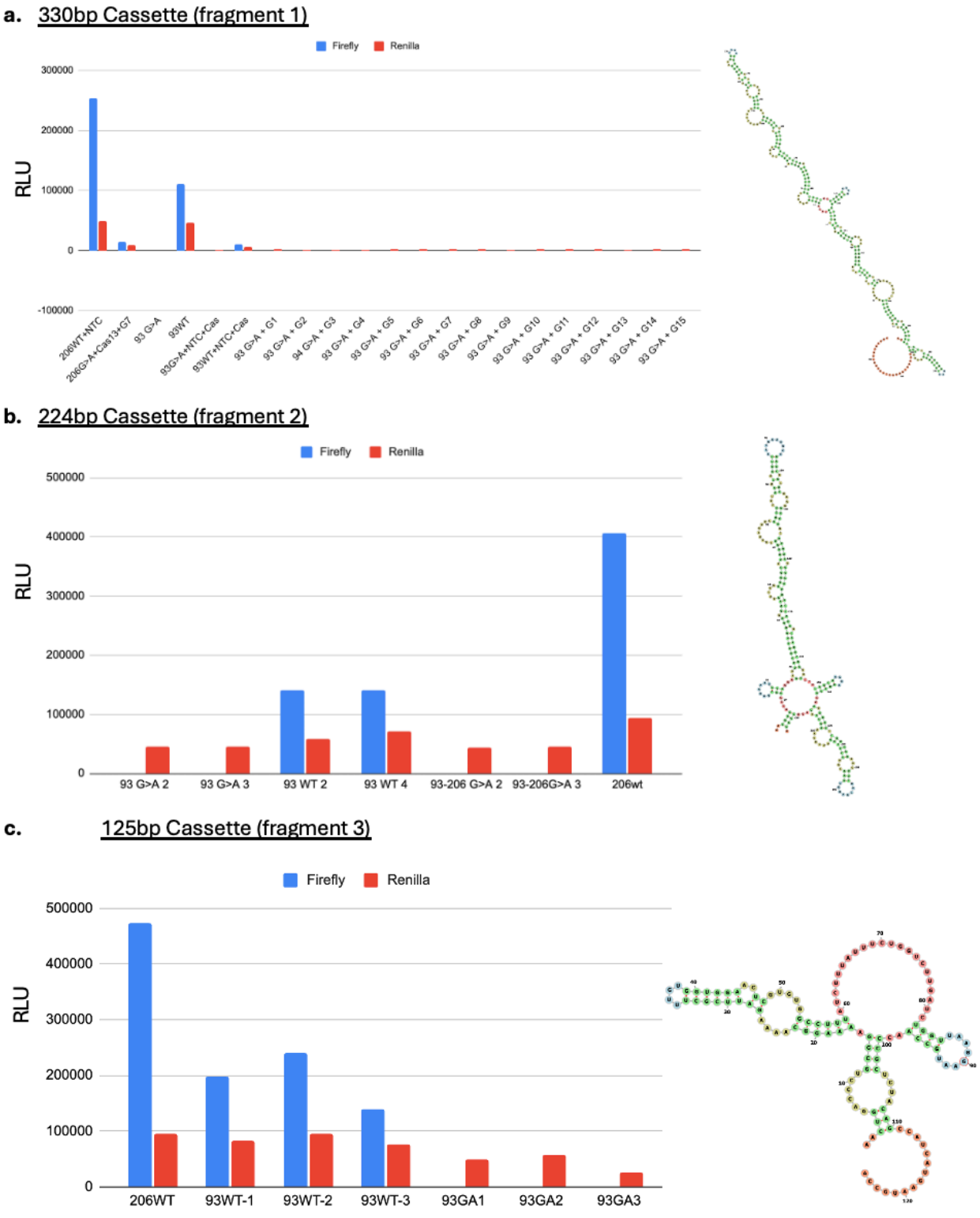

Figure 5-3: Screen of c.93 cassettes for luciferase assay.
a. An initial guide screen using the Dual-Glo® luciferase assay. Renilla is constitutively expressed which is indicated by the consistency across the red bars between the two wildtype samples (206WT and 93WT). Firefly is substantially reduced in the 93WT sample. This could be due to the hairpin structure as seen on the right. Addition

of Cas13-ADAR to samples reduced overall expression. **b**. A shorter cassette was tested to try and interrupt the hairpin structure. This was unsuccessful and only continued to show consistent Renilla expression. The predicted structure indicated a sustained hairpin. c. A cassette equalling the 206WT positive control in length (124bp) was tested last. As with the other two cassettes, Renilla expression remained consistent with a slight improvement in Firefly expression. The secondary structure indicated smaller stem-loops with larger bulges, potentially improving translational efficiency. The numbers (ie 93 WT 2) refer to the miniprep number.

5.3.1.2 Guide screen targeting c.93 G>A and bystander sites in HEK293T cells

Given the issue of Firefly expression with the c.93 cassette, the luciferase assay was abandoned, and guides were screened by targeting a c.93 G>A mutant *ABCA4* plasmid. The screens proved variable, with editing ranging significantly between replicates (Figure 5-4). In addition, there was substantial editing at two bystander sites, c.99 and c.105. As with the on-target editing, this varied significantly (Figure 5-4).

Despite the variability and bystander editing, guides 2 and 7 showed the greatest on-target mean editing activity with 16.2 ± 3.9% and 15 ± 6.2%, respectively. However, this was not significant likely due to the variation. Bystander editing at site c.99 was observed for Guide 7 at 5 ± 3.82% and Guide 2 at 1.2 ± 0.58%. Neither showed bystander activity at site c.105 (Figure 5-4). Inversely, guides with low on-target activity showed high rates of bystander activity, such as guides 10, 11, and 13, which had editing rates of 33 ± 5.79% ($p=0.0029$), 26.6 ± 9.6% ($p=0.0055$), and 27.4 ± 5.2% ($p=0.0037$) at either c.99 or c.105 (Figure 5-4).

Two guides (G6 and G10) were selected to target the luciferase assay target plasmid with the shortest c.93 G>A cassette (Figure 5-3c) for transcript analysis of editing. Interestingly, both guides showed higher mean on-target and bystander editing than when targeting the c.93 G>A mutant plasmid, suggesting a structural difference affecting editing activity. The c.206 G>A was used as a positive control and showed consistent high on-target activity with no bystander editing.

To establish if G2 and G7 were efficient enough to restore ABCA4 protein, a western blot was run. Each was transfected with the target plasmid and Cas13-ADAR in two wells to account for the observed variability in editing activity. No ABCA4 signal was detected beyond the background in the c.93 G>A mutant plasmid lane, except for ’93 +G2’ which showed faint signal. This would indicate endogenous ADAR1 activity given that no Cas13-ADAR was transfected in that sample. However, this is more likely due to blot smearing as observed in neighbouring wells or contamination. Further, it would indicate either no editing or insufficient editing rates in Cas13-ADAR transfected samples (Figure 5-5).

a.

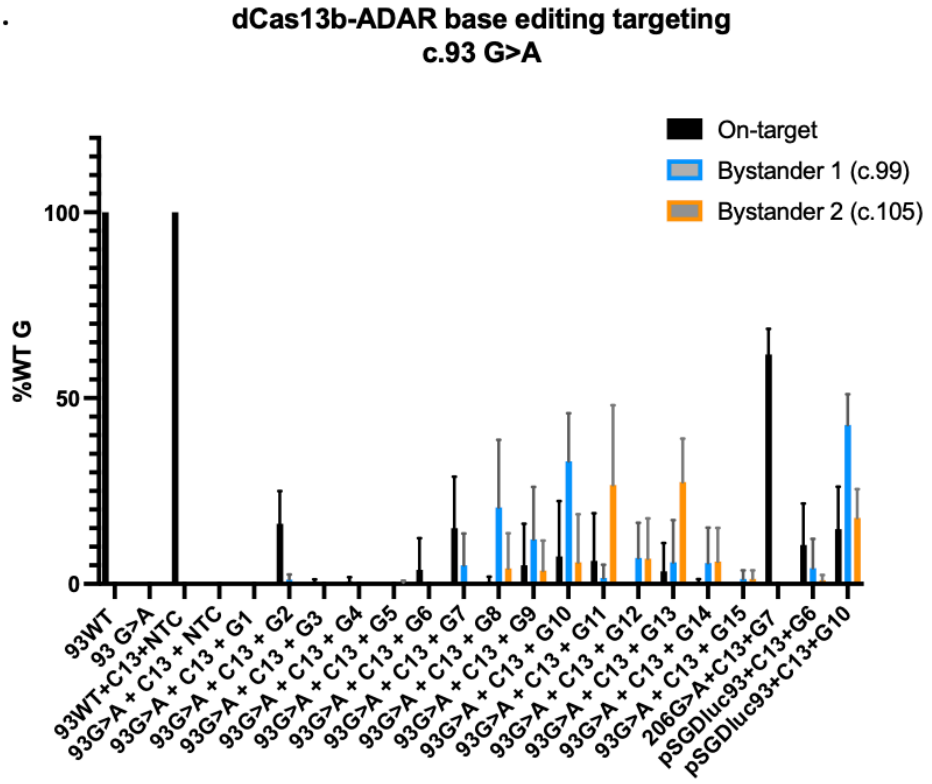

b.

Table format: Grouped		Group A					Group B				
		On-target					Bystander 1 (c.99)				
		A:Y1	A:Y2	A:Y3	A:Y4	A:Y5	B:Y1	B:Y2	B:Y3	B:Y4	B:Y5
1	93WT	100	100	100	100	100	0	0	0	0	0
2	93 G>A	0	0	0	0	0	0	0	0	0	0
3	93WT+C13+NTC	100	100	100	100	100	0	0	0	0	0
4	93G>A + C13 + NTC	0	0	0	0	0	0	0	0	0	0
5	93G>A + C13 + G1	0	0	0			0	0	0	0	
6	93G>A + C13 + G2	18	23	21	1	18	2	0	1	0	3
7	93G>A + C13 + G3		0	1				0	0		
8	93G>A + C13 + G4	2	0	0			0	0	0		
9	93G>A + C13 + G5	0	0	0			0	0	0		
10	93G>A + C13 + G6	19	0	0	0	0	0	0	0	0	0
11	93G>A + C13 + G7	34	20	3	18	0	20	1	0	4	0
12	93G>A + C13 + G8	3	0	0	0	0	50	20	2	21	10
13	93G>A + C13 + G9	25	0	0	0	0	33	3	0	4	20
14	93G>A + C13 + G10	34	2	0	1	0	56	29	27	28	25
15	93G>A + C13 + G11	29	0	0	2	0	8	0	0	0	0
16	93G>A + C13 + G12	0	0	0	0	0	23	5	0	7	0
17	93G>A + C13 + G13	17	0	0	0	0	26	0	0	3	0
18	93G>A + C13 + G14	2	0	0	0	0	22	0	0	6	0
19	93G>A + C13 + G15	0	0	0			4	0	0		
20	206G>A+C13+G7	70	64	54		59					
21	pSGDluc93+C13+G6		26	0	10	6		16	0	1	0
22	pSGDluc93+C13+G10		30	17	6	6		55	37	40	39

Figure 5-4: dCas13b-ADARdd guide screen targeting c.93 G>A mutant *ABCA4* plasmid analysed with EditR. **a.** Guide screen of fifteen guides targeting c.93 G>A (black) by dCas13b-ADARdd and the corresponding raw values (N=5) (**b.**) to demonstrate the editing variability. Sites c.99 (blue) and c.105 (orange) were prominent off-target sites. Examples with notable editing efficiency variability at on- or off- target sites are highlighted. Guides 2 and 7 exhibited the highest mean on-target editing with minimal bystander editing, at 16.2 ± 3.9% and 15 ± 6.2%. Guides 10, 11, and 13 showed significant rates of bystander editing at either c.99 or c.105, with 33 ± 5.79% (p=0.0029), 26.6 ± 9.6% (p=0.0055), and 27.4 ± 5.2% (p=0.0037), respectively. '206 +C13+G7' is used as the

positive control. pSGDluc93 is the luciferase assay target plasmid with the 125bp 93 G>A target cassette (N=4) to further examine the role of sequence context in editing efficiency outcomes. Editing was more consistently high when targeting the cassette rather than the c.93 G>A mutant ABCA4 plasmid. Data = mean ± SEM.

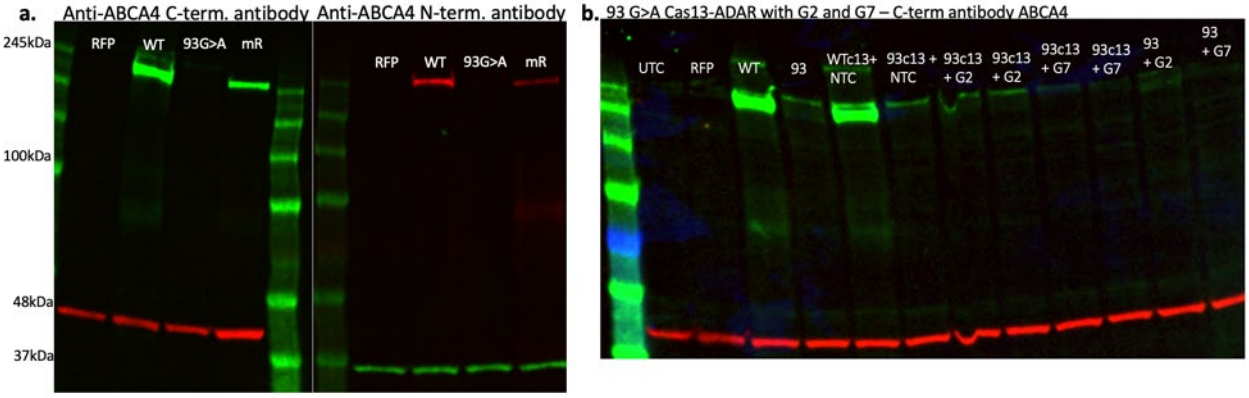

Figure 5-5: Western blot of dCas13b-ADARdd targeting of c.93 G>A.
a. Confirmation of no ABCA4 protein with the c.93 G>A mutation using C- (left) and N- (right) terminal antibodies for detecting ABCA4. RFP= negative control, WT= wildtype, mR= mouse retina. Note the lack of the artefact band as seen in the HEK293T WT (WT) sample. **b.** Test of the best performing dCas13b-ADAR guides targeting c.93 G>A to determine protein restoration. Overall, only '93 +G2' demonstrated signal detection beyond the faint background signal detected in the '93' lane, likely due to blot smearing or contamination. No wells with Cas13-ADAR exhibited any full-length protein restoration. Two replicates of each targeting guide were transfected and run on the blot given the observed editing variability at this site. All wells show the artefact band found above ABCA4 since these are HEK samples.

5.3.1.3 DNA editing *in vitro* targeting c.93 G>A region

Since it was established that the luciferase assay containing the c.93 cassette would not be effective for screening guides, SaKKHABE8e guides were screened targeting the c.93 G>A mutant *ABCA4* plasmid. Three guides ranging in length from 20-22bp were tested and the Sanger sequencing analysed in EditR. None of the guides demonstrated any on-target or bystander editing (Figure 5-6a).

To determine if the lack of editing was site specific, four guides were designed using the four different PAM sites available in the c.93 region (Figure 5-6b) to induce a missense mutation in the HEK293T genome. Three SaKKH PAM sites and one SaCas PAM site (NNGRRT) were tested and spanned a 40nt region with targetable adenosines. The SaCas PAM site was used with an SaABE8e as well as an SaCas9 to establish if the issue arose from guide binding or inhibited deamination.

None of the base editors demonstrated activity targeting the adenosines within the sgRNA editing windows (Figure 5-6b and c). Interestingly, the SaCas9 was able to target the region. Samples were first analysed in EditR for consistency with the base editors, revealing ~9%

"editing" (Figure 5-6b). However, analysis in TIDE indicated true cleavage efficiencies of 4.2-4.5% (Figure 5-6d). Decomposition downstream of the cut-site was observable in the Sanger sequencing output (Figure 5-6e).

Although the cleavage efficiency is low, this suggests that the Cas can bind the region downstream of c.93 but cannot deaminate in the case of the SaABE8e base editor in HEK293T cells. It is unclear what inhibited the deamination. One possibility is that the only editable adenosine is at the 3' end of the editing window at position 12. While technically within the editing window, efficiency may be decreased. In addition, it is unknown whether the activity is specific to this region, ~30 bases downstream of c.93. Further testing using SaKKHCas9 at the other PAM sites would provide clarity on the targetability of c.93 specifically.

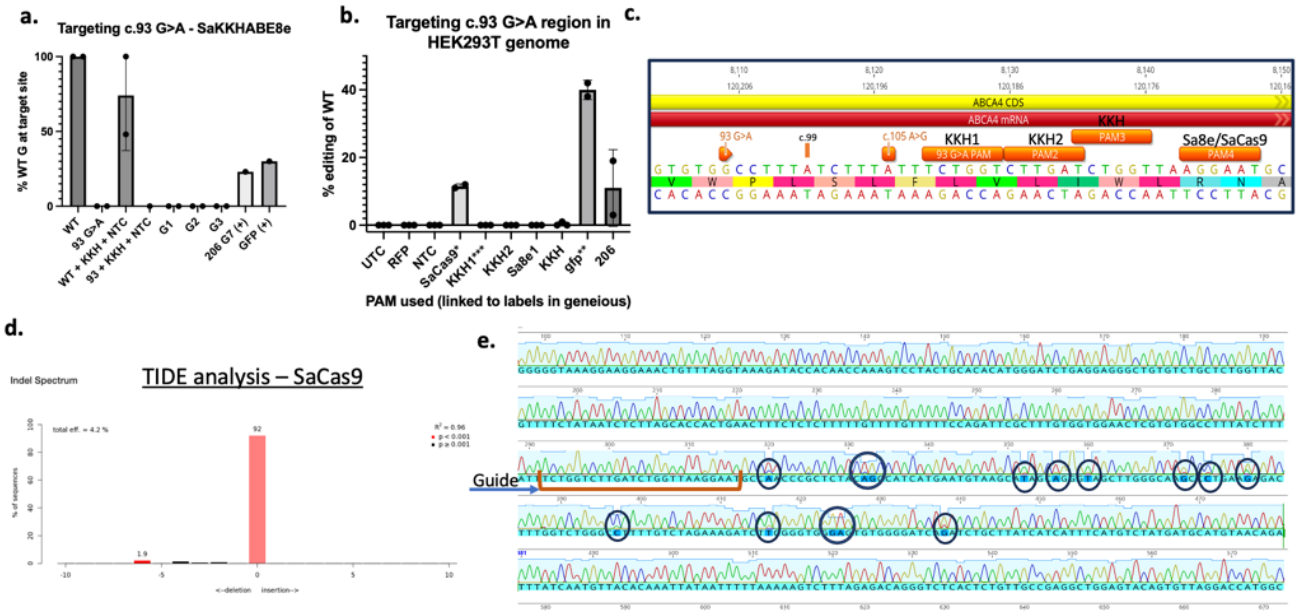

Figure 5-6: Targeting the c.93 region by DNA editors.
a. Targeting the c.93 G>A mutant *ABCA4* plasmid with SaKKHBAE8e. No editing was observed with any of the three guides screened. **b.** Four PAM sites in the c.93 region (**c.**) were tested with SaKKHABE8e, SaABE8e (Sa8e) and SaCas9 to induce missense mutations in genomic HEK293 cells. Analysis was completed in EditR with Sanger sequencing output. No editing by base editors was observed, however, SaCas9 showed activity. In EditR (b.) observed editing was estimated at 9%. When using TIDE analysis (designed for SaCas9) (**d.**), editing was ~4%. GFP and 206 were positive controls (b.). **e.** Example of observable decomposition after the target site in the SaCas9 samples.

5.3.2 dPspCas13b-ADAR$_{DD}$ editing in wildtype retinal organoid model to induce c.105 A>G

5.3.2.1 *In vitro* screens to induce a mutation in wildtype organoids

Given that the patient-derived retinal organoid was unable to be produced, in order to gain preliminary data comparing DNA and RNA base editors in retinal organoids, an alternative approach of directly targeting the bystander sites c.99 and c.105 was tested to induce a missense mutation in wildtype organoids. This was only tested by Cas13-ADAR RNA editing since the SaKKHABE8e did not successfully deaminate any bases in the target region of c.93 in the *ABCA4* c.93 G>A mutant plasmid or in the HEK293T genome.

Two of the guides with high activity at the bystander site in the initial guide screen, G8 and G11, were selected to induce the bystander edit (Figure 5-4 and Figure 5-7). Editing of both c.99 and c.105 results in a silent Leu-Leu amino acid change.

The ‘C’ mismatch was shifted to the new target site - c.99 for G8 and c.105 for G11 (Figure 5-7) - to improve on-target editing. The screens yielded more consistent results than when targeting c.93 G>A, achieving 28.3 $\pm$ 6.4% (p=0.01) and 34.7 $\pm$ 6.23% (p=0.0037) for G8(c.99) and G11(c.105), respectively. Due to the higher editing rate, G11(c.105) was chosen for virus production and downstream attempts to induce c.105 A>G by dCas13b-ADARdd in wildtype retinal organoids.

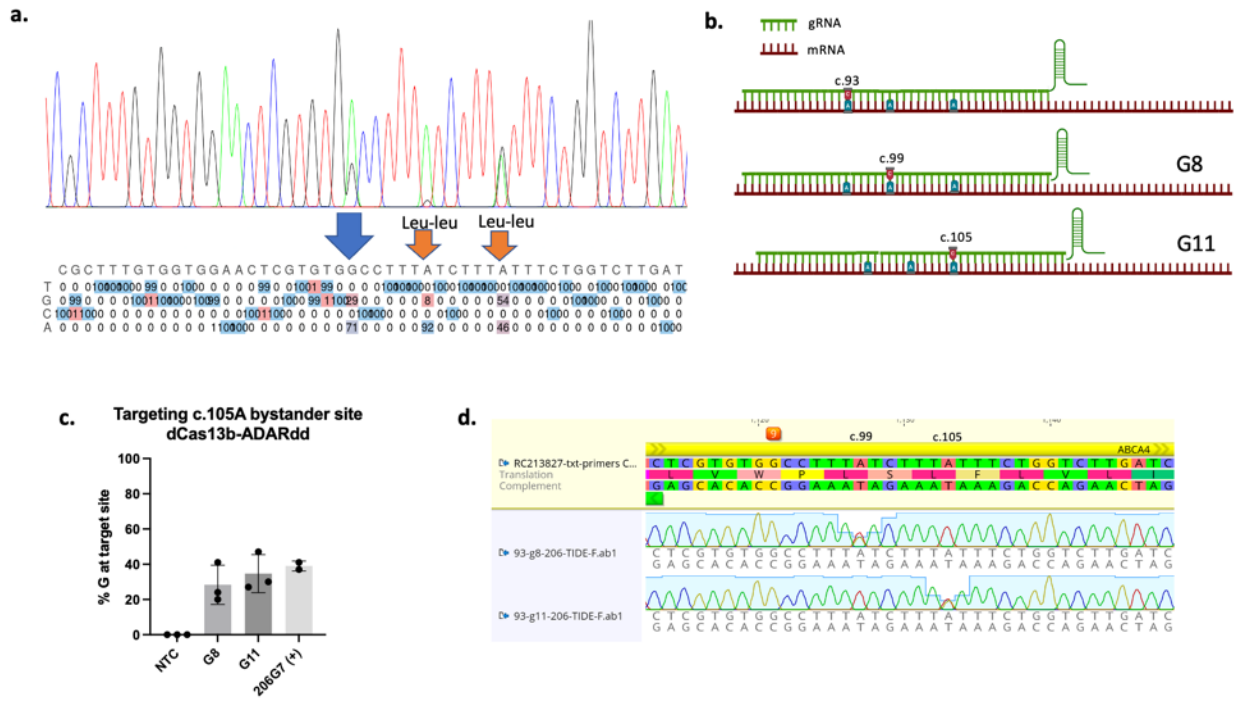

Figure 5-7: Targeting bystander site of c.93 by dCas13b-ADARdd.
a. Example of chromatogram in EditR showing the on-target editing (blue arrow) alongside the bystander edits (orange). Leu-leu indicates the amino acid change the bystander edit would induce. **b.** The guide design for introducing either the c.99 A>G or c.105 A>G edit by dCas13b-ADARdd. The C mismatch was shifted to the new target base within G8 and G11. **c.** The *in vitro* results yielded 28.3 ± 6.4% (p=0.01) and 34.7 ± 6.23% (p=0.0037) for G8(c.99) and G11(c.105) which can be seen in the Sanger sequencing chromatograms (**d.**).

5.3.2.2 AAV2 quad mutant production

To effectively transduce retinal organoids, the AAV2 quad mutant (Y272F, Y444F, Y500F, Y730F) was used given its reported tropism.[306,307] Viruses were produced as described in the general methods and in 5.2.9. Virus production successfully yielded a high titre virus, as seen in Figure 5-8. Two doses were tested for organoid transduction. The low dose was 1E+10vg of each Cas13-ADAR and U6-gRNA for a total dose of 2E+10vg/organoid. The high dose was 2.5E+10vg of each Cas13-ADAR and U6-gRNA with a total dose of 5E+10vg/organoid. Both doses have been reported to work, with observed increased GFP expression corresponding to dose escalation.[306,307] Higher doses have been reported, but not with this serotype.[309]

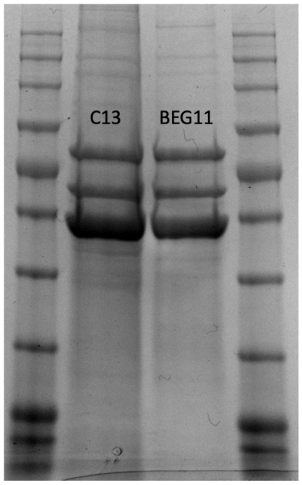

Figure 5-8: AAV2QM production for transducing retinal organoids.
SDS-PAGE of both viruses showing strong bands for desired capsid proteins, VP1, VP2, VP3. Minimal impurity is observed. C13= RK-dCas13b-ADARdd(E488Q), BEG11= U6-gRNA-CAG-GFP using guide 11 (G11) sequence targeting the c.105 site.

5.3.2.3 Inducing a nearby mutation, c.105 A>G via dual vector dPspCas13b-ADAR$_{DD}$ - 2E+10vg/organoid

Wildtype retinal organoids were transduced on day 180 as described in the Chapter 5 methods with 1E+10vg of each the AAV2QM-RK-dCas13b-ADAR$_{DD}$(E488Q) and AAV2QM-U6-gRNA-CAG-GFP. GFP expression from the guide vector observably increased over time (Figure 5-9). By 42 days post-transduction, in the organoids with the highest expression, GFP expression extended the entirety of the organoid (Figure 5-9). Variability between samples was substantial, where samples receiving the same dose displayed vastly different GFP expression levels (Figure 5-10). A large sample size is needed to address this.

Organoids were harvested and processed to determine editing at the target site, c.105. Deep sequencing revealed no editing at the target site despite high transduction indicated by observable GFP expression (Figure 5-9). In addition, no low-level bystander or off-target editing was observed. This was surprising given the promiscuous ADAR activity *in vivo* (Chapter 6) despite the lack of on-target editing. However, no experiment to confirm dCas13-ADAR transduction or expression was performed due to time constraints, perhaps contributing to the lack of editing.

IHC of the organoids reflected the fluorescence microscopy and revealed GFP expression in the treated sample. It was difficult to compare fluorescence microscopy images of the organoids to the sectioned organoids imaged by confocal microscopy (Figure 5-12Figure 5-13).

GFP expression appeared significantly reduced in IHC samples than in the same samples imaged by fluorescence microscopy, and it is unclear why. Further imaging and continued investigation are required.

Imaging of the whole organoid and sections revealed sparsely present outer segments by day 42 (day ~222), which is in line with some organoid development protocols that see more complete outer segments by day ~240-245.[310] Areas with what looks like the outer segment are present on some organoids. This likely affected the lack of specific *ABCA4* staining in the sections and may be an indicator of vector toxicity. However, this does not explain the high levels of observed background.

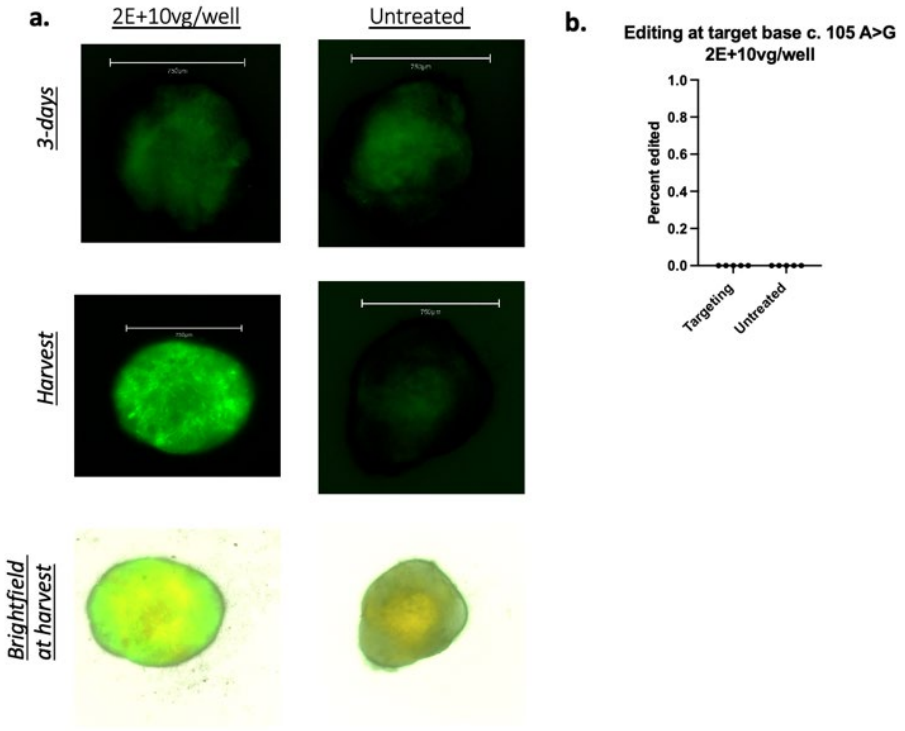

Figure 5-9: Retinal organoid transduction to introduce c.105 A>G at low dose (2E+10vg).
a. Digital imaging and brightfield imaging of the treated and untreated retinal organoids 3-days post-transduction and the day of harvest, 42-days post-transduction. GFP is strongly expressed by harvest, with no GFP or autofluorescence visible in the untreated samples. **b.** Despite high observed vector expression, deep sequencing revealed no editing at the target site, c.105.

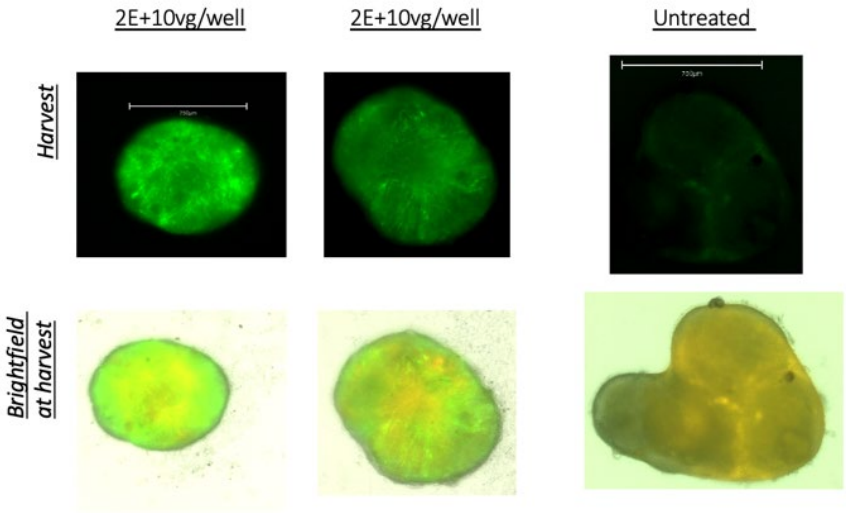

Figure 5-10: Transduction variability between retinal organoids.
Organoids that received the same dose demonstrated variable GFP expression at the same dose. Images were the day of harvest, 42 days post-transduction. Large sample size required to account for such variation.

5.3.2.4 Inducing a nearby mutation, c.105 A>G via dual vector dPspCas13b-ADAR$_{DD}$ editing - 5E+10vg/organoid

Following widespread transduction at the low dose (2E+10vg) but no observed editing at the target site, a higher dose of 5E+10vg/organoid was tested using 2.5E+10vg of each AAV2QM-RK-dCas13b-ADAR$_{DD}$(E488Q) and AAV2QM-U6-gRNA-CAG-GFP. As with the low dose, expression increased over time, reaching much of the organoid. However, the high dose was harvested at 30 days post-transduction, reducing the time for the vector to express and likely contributing to the reduced observed GFP expression (Figure 5-11).

Despite the higher dose, no on- or off-target editing was observed (Figure 5-11). Again, no confirmation of dCas13b-ADAR expression was confirmed, perhaps contributing to the lack of activity at the target site or throughout the amplicon. IHC of sectioned organoids revealed GFP expression above background, however, this was less than observed at the low dose (Figure 5-12and Figure 5-13). Further testing at higher doses with longer incubation time alongside targeting different regions is required to establish effective base editing in organoids.

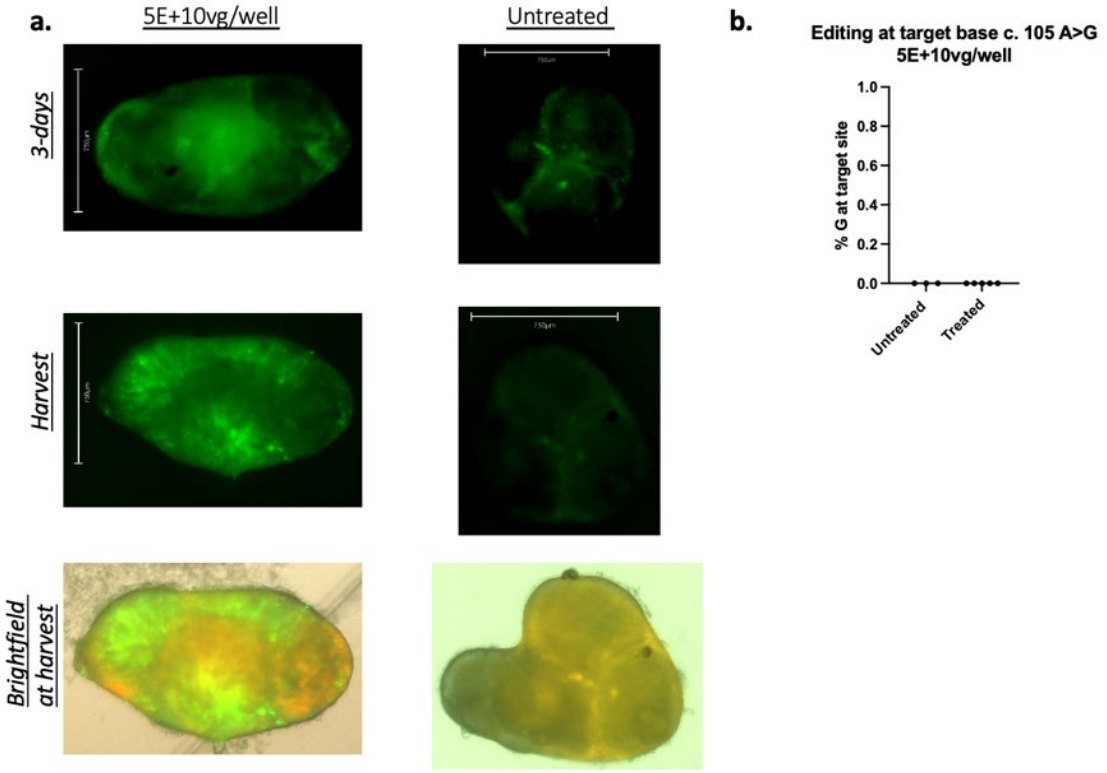

Figure 5-11: Retinal organoid transduction to introduce c.105 A>G at low dose (5E+10vg).
a. Digital microscopy and brightfield images (EVOS FL Auto2) of treated and untreated retinal organoids at 3-days post-transduction and the day of harvest, 30-days post-transduction. Treated organoids showed progressively increased GFP expression over time compared to the untreated organoids. **b.** Deep sequencing showed no on-target editing.

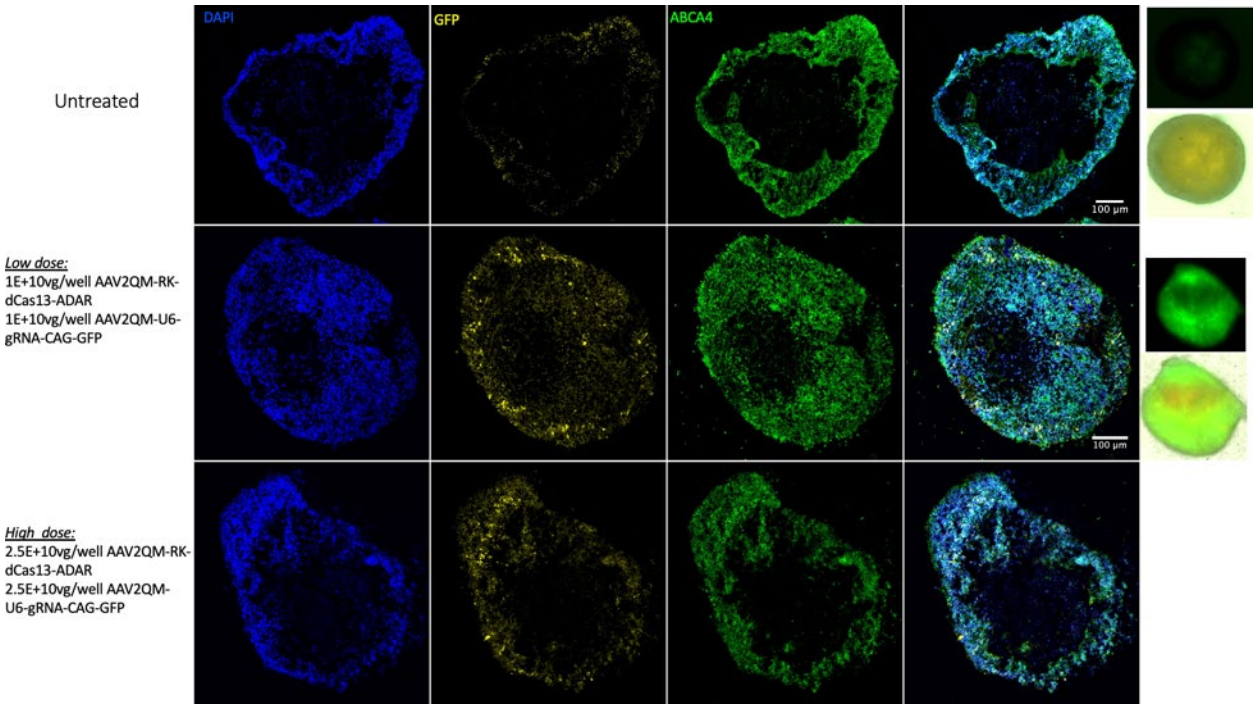

Figure 5-12: IHC of retinal organoid sections at both the low (2E+10vg) and high (5E+10vg) dose at 10x magnification.
Sectioned and stained organoids treated with no virus (top), 2E+10vg (middle) and 5E+10vg (bottom). GFP at both doses was higher than the background, with the strongest signal detected at the low dose but with longer treatment time. ABCA4 was consistent across all three conditions, although staining was not as anticipated. Digital microscopy images of the same sample as the section shown on the far right for the untreated and low dose samples.

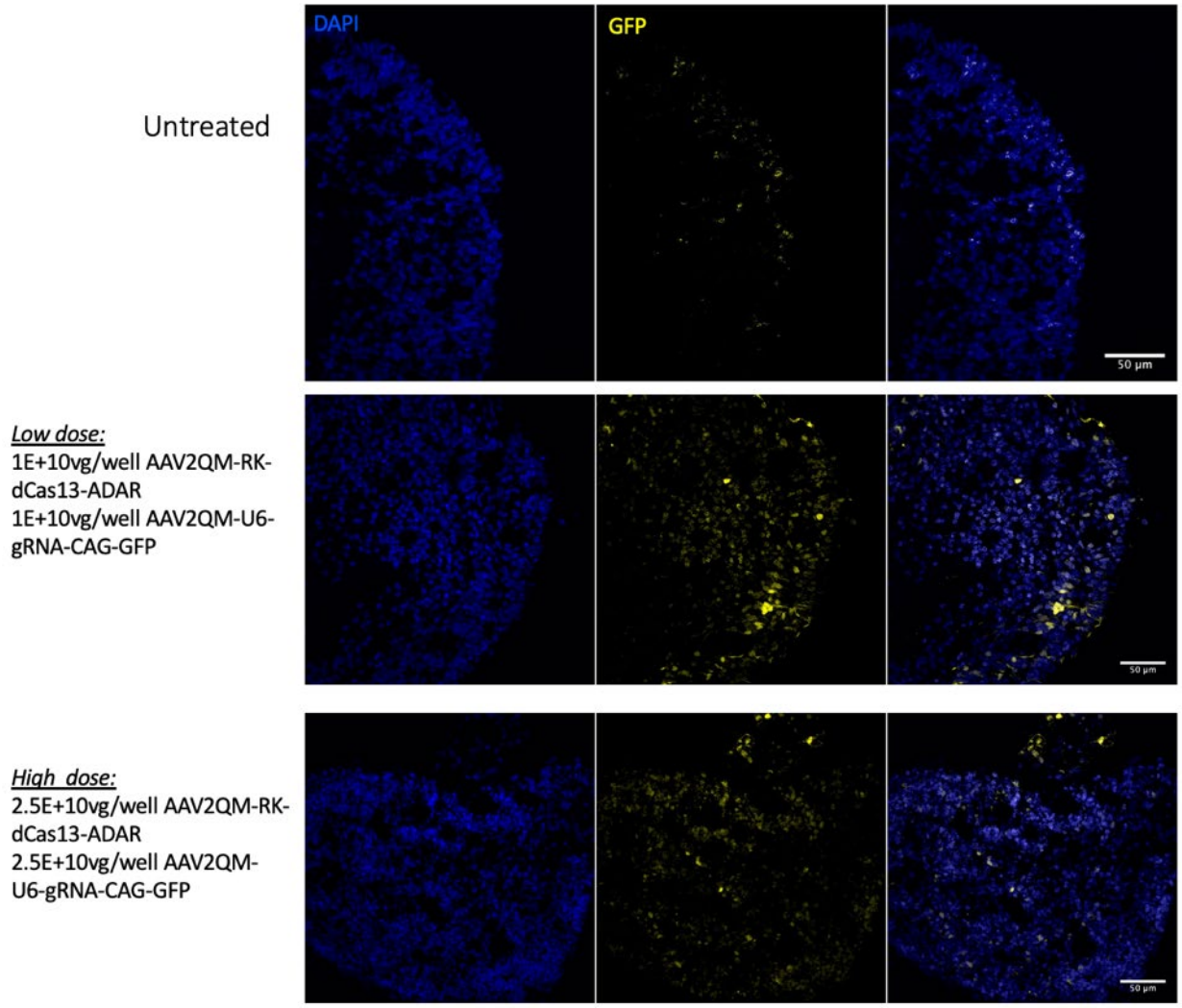

Figure 5-13: IHC of treated and untreated retinal organoids at the high and low dose - 40x magnification. At the higher magnification GFP was difficult to detect, although both doses showed expression above background. As seen in digital microscopy and brightfield images (EVOS FL Auto2), and in IHC, the low dose with longer treatment time showed the highest GFP expression.

5.4 Discussion

The initial aim to compare DNA and RNA base editors in patient-derived retinal organoids was unfortunately not possible within the time of this PhD. Indeed, efforts are ongoing to develop retinal organoids with the c.93 G>A mutation to complement a humanised mouse model that is in development also containing the c.93 G>A mutation. An alternative approach was undertaken targeting nearby sites to determine if the region is targetable by DNA and RNA base

editors and if base editing systems can successfully be applied in a retinal organoid model. This data aimed to provide insight for the longer-term translational models.

Establishing and optimising DNA and RNA base editing strategies may be useful for conditions such as Stargardt where the majority of mutations are amenable to editing and high heterogeneity is observed. However, due to the known site specificity of both the Cas and the deamination domain, three further sites were targeted in this chapter following the equal editing rates observed in Chapter 4. Since *in silico* prediction tools are typically designed for SpCas PAM sites,[286,311,312] not SaKKHABE8e or dCas13b-ADAR$_{DD}$, testing a variety of targets provides a more thorough comparison of DNA and RNA base editors.

Lastly, Cas13-ADAR was tested in retinal organoids to target the c.105 site and establish whether RNA base editing was possible in a pre-clinical model that more closely recapitulates human retinal physiology and genetics.

5.4.1 Luciferase assay

An overall analysis of the luciferase assay as a guide screening method is presented in the general discussion. Broadly, the luciferase assay does not recapitulate the biological transcript context. In the previous chapter, the discrepancy between transcript analysis and the luciferase assay outputs were observable but minimal. Here, multiple variations were tested with continued truncation of the c.93 target cassette to improve Firefly expression levels. Initially, it seemed that the hairpin secondary structure that was formed with the two longer cassettes inhibited expression. However, the shortest cassette continued to show substantially reduced Firefly expression when compared to the 206-wildtype cassette, despite ablation of the hairpin secondary structure. This suggests an alternative structure may be interfering in translational efficiency, such as an observed stem-loop remaining in the smallest cassette. Given the proximity of the c.93 site to the Kozak sequence, RNA secondary structures to regulate expression levels, such as stem loops and hairpins, may be more likely early-on in the transcript.[313] Alternatively, given the lack of native context even in the largest cassette, it is possible the cassette is misfolding and becoming a rate-limiting structure.[314]

It is possible that the predicted secondary structure is not accurate given that multiple folding outcomes can result in the same energy score.[315] Additionally, factors other than RNA secondary structure may be affecting expression level, such as codon usage.[316-318] Future work

may include codon optimisation of the cassettes to enable investigation of the effects of both codon usage and RNA secondary structure on downstream Firefly expression levels.

Despite the lack of assay function for the c.93 region, the luciferase assay can provide an easy, cost-effective way to screen guides.

5.4.2 Comparison of DNA and RNA base editing at c.93 site *in vitro*

It is unclear why editing at this site was so variable. Cas13-ADAR revealed substantial mean editing at the target site in the c.93 G>A mutant plasmid with two guides screened, although this fluctuated by ~30% between replicates. Interestingly, when comparing this to the same two guides targeting the luciferase plasmid with the shortest c.93 cassette, editing rates were more consistent and, on average, higher than when targeting the c.93 G>A mutant *ABCA4* plasmid, suggesting an altered ability in binding or deamination. Alternatively, sequence preference may have played a role in the ability to target the c.93 G>A mutation, where a 5'-GAN-3' is the least preferred ADAR motif.[198,199,215] When analysing production of full-length protein, no ABCA4 was detected, indicating either that no editing occurred or that the editing was insufficient for detection. Based on the fluctuations seen between replicates, either is possible.

Similarly, bystander edits were prominent but fluctuated significantly (~30%). Nonetheless, given the overall higher editing rates achieved at bystander sites of up to 56%, attempts were made to induce these edits in the *ABCA4* plasmid with re-designed guides. This resulted in consistent editing of 20-30%. However, since these were silent missense variants, confirmation other than Sanger sequencing was not possible.

The lack of editing in the non-targeting control suggests editing due to Cas13-ADAR rather than ADAR recruitment. Altered guide design for other RNA base editing approaches such endogenous or exogenous ADAR recruitment, may result in improved editing outcomes and requires future investigation. Alternative applications of Cas13 may enable targeting of difficult regions. For example, CRISPR (Cas13) Assisted mRNA Fragment Trans-splicing mRNA (CRAFT) may allow for complete replacement of *ABCA4* exons 1 and 2 (or more) using more easily and consistently targetable sites. Initial *in vitro* data using CRAFT showed promising editing of up to ~24% with the best performing guide targeting *DMPK.*[319]

DNA base editing resulted in no base editing at the plasmid or genomic level, despite the multitude of PAM sites tested (Figure 5-6). This contradicted the 21% editing predicted at c.93 G>A by *in silico* software (BE-dict) (Figure 5-14), although this is based on SpCas base editors. The lack of editing could be due to inefficient guide binding or insufficient sequence consensus for the deaminase. Indeed, targeting genomic *ABCA4* with SaCas9 at the same site as SaABE8e (~c.118) revealed low-level activity between 4-9%, potentially indicating an inefficient deaminase. *In silico* prediction tools designed for SpABEs predicted editing of 8% at site c.118 (Figure 5-14), reflecting the SaCas9 editing efficiency.

While deaminase sequence preference plays a role, other factors likely contribute. First, the GC content at this site of 30% is lower than the preferred 40-60%, likely affecting binding efficiency.[320] Second, repetitive regions such as the observed thymine triplicates, particularly near the 3' end of the guide, have been shown to decrease Cas9 cleavage.[312,321] R-loop generation and maintenance affects deaminase efficiency, where position within the R-loop with respect to the deaminase can affect target-base accessibility.[285,322] Further testing at the remaining PAM sites with SaKKHCas9 may shed light on whether deamination or gRNA binding is the limiting factor. Furthermore, alternative Cas9 and base editors such as SpCas, could be tested to further interrogate this site. Lastly, disrupting the surrounding PAM sites may shed light on the effects of steric hinderance due to the high number of PAM sites in the area.[163,323]

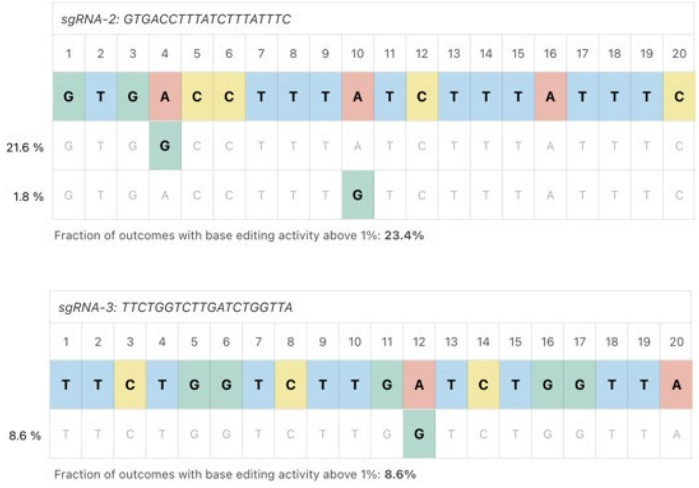

Figure 5-14: *In silico* editing in the c.93 region using BE-dict: predicted outcomes.
Editing of c.93 G>A (top, 'sgRNA-2') was predicted to be 21.6% with 1.8% bystander editing. The downstream SaABE/SaCas9 PAM site (bottom; 'sgRNA-3') was predicted to show 8.6% editing. *In vitro,* no base editing occurred at either site but the sgRNA-3 did reveal cleavage by SaCas9, with editing efficiencies ranging between 4-

9% depending on whether outputs were analysed by TIDE or EditR. At this site, predictive tools did not align with experimental data and even predicted the relative inverse output, demonstrating the limitations of predictive tools.

These unexpected outcomes shed light on the need for experimental screening and the site specificity observed with gene editing tools. Moreover, this highlights the diversity of tools available and suggests that different gene editing technologies may be better suited for different target sites.

5.4.3 RNA base editing does not edit in wild-type retinal organoids

Base editing by dCas13b-ADAR$_{DD}$ did not work at either dose tested when targeting c.105A in retinal organoids. Initially, the lack of editing was surprising given the uniformity and strength of GFP expression observed at both doses. However, this was similar to the outcome *in vivo,* where despite strong GFP expression by retinal imaging, dCas13b-ADAR$_{DD}$ targeting the *ABCA4* start codon did not show any editing (Chapter 6). The lack of editing in retinal organoids could have been due to several reasons and requires future investigation.

First, although observed GFP expression was robust in the organoids, dCas13b-ADAR expression was not confirmed due to time constraints. RT-PCR of the transgene would have revealed if AAV packaging was correct or resulted in a truncated gene. In addition, targeting the FLAG-tag at the 3'-end of ADAR2 during IHC would have confirmed Cas13-ADAR expression and allowed for visualisation of protein localisation within the organoid. Lastly, single cell sequencing analysis may shed light on Cas13 and guide expression levels, and allow for correlation with expression levels observed by microscopy.

While the fluorescence microscopy images showed robust GFP expression, IHC revealed substantially reduced detection of GFP (Figure 5-12 and Figure 5-13). This may be due to out-of-focus fluorescence observed by fluorescence microscopy, which, when filtered out by the confocal microscope, revealed true GFP expression levels.

Another factor affecting editing outcomes may be the highly variable transduction efficiencies seen between organoids. However, this is unlikely since none of the sequencing outputs revealed editing, regardless of observed GFP expression in the corresponding sample or dose.

An alternative reason for lack of editing may be the observed editing variability when targeting this region. *In vitro,* editing rates varied by up to 30% between replicates when targeting c.93 G>A at both on-target and off-target sites. This is also possible at the c.105A target site, potentially resulting in no editing or undetectable levels of editing. One solution would be to test higher doses and increase incubation times. For example, one study targeting c.5882 G>A in *ABCA4* in retinal organoids used 1E+11vg/organoid, which is twice the high dose used in this study.[102] As observed in this experiment, the low dose samples expressed as much or more GFP than the high dose possibly due to 12 extra days incubation. This may increase the chances for detectible editing to occur. However, for Cas13-ADAR this is unlikely to make a difference due to targeting mRNA which is continually produced and transient.

Given the reduced expression with this region *in vitro* perhaps due to secondary structure of the RNA, Cas13-ADAR guide binding may also be affected. Different editing approaches may circumvent this due to the altered guide design. The circular gRNAs (carRNAs) and ADAR recruiting gRNAs (arRNAs) use a guide at least 60nt long, with guides 110-151nt in length showing editing between 25-50% depending on the target and cell type.[324] Future testing could include ADAR recruitment with exogenous ADAR2 delivery or endogenous ADAR. However, this could largely be affected by ADAR motif preference.

Taken together, it is difficult to discern the reason for the lack of editing in the retinal organoids by dCas13b-ADAR. Further, it is unclear why *in vitro* editing remains relatively high across all target sites but results in no editing in more complex pre-clinical models.

Nonetheless, while transduction of AAV2QM-RK-dCas13b-ADAR did not result in editing, there is a growing body of research showing successful use of gene editing in retinal organoids. A recent study achieved significant knockdown of VEGF in retinal organoids using Cas13bt which achieved transduction efficiencies of up to 18.8% and significant editing of VEGF with the targeting guide.[207] Knockdown was determined by single cell sequencing. In future work targeting a nonsense mutation in *ABCA4* in a patient-derived organoid model, single-cell RNA sequencing may enable sensitive testing of editing.

Editing of *ABCA4* by DNA base editing (SpABE) in organoids has also proven successful with 4-12% editing of the c.5882G>A mutation.[102] Interestingly, the organoids were not stained for ABCA4 in IHC and no reason was provided, perhaps due to the high observed background. Another study successfully used CRISPR/Cas9 to correct an *RPGR* mutation in patient-derived

retinal organoids, resulting in healthy retinae and providing proof-of-principle of target mutation correction and a functional effect in organoids. It was further hypothesised that the corrected retinae are potentially valuable for retinal regeneration applications without fear of immunological rejection since they are patient-derived, shedding light on an alternative gene editing treatment path.[325,326] Similarly, two mutations in *ABCA4* were successfully edited by CRISPR-Cas9 homology-directed repair with no detectable off-target edits in patient-derived iPSCs.[168] Future work includes investigation of DNA base editing in targeting alternative mutations in *ABCA4* in patient-derived retinal organoids.

The rapid continued development of retinal organoid models will enable future testing of therapeutics in an environment increasingly similar to the human retina. In combination with other pre-clinical models, such as mouse models, the understanding of the efficacy and response to novel therapeutics can be vastly improved.

5.4.4 Toxicity and off-targets

In vitro toxicity was observed in the luciferase assay, where addition of Cas13-ADAR significantly reduced Firefly and *Renilla* expression. Conversely, the western blot revealed sustained signal in both wildtype ABCA4 samples with and without Cas13-ADAR. Further testing is required to determine a toxic effect due to the base editors *in vitro.*

In organoids, published reports of 1E+11vg/organoid showed healthy organoids with no signs of toxicity.[102] Thus, it is unlikely that either the low (1E+10vg/organoid) or high (5E+10vg/organoid) dose used would result in toxicity.[102] To determine a healthy metabolic state of the organoids, GFAP staining or an ATP-viability assay could have been performed.

Sections stained during IHC, did not result in clear lamellar structures (Figure 5-12Figure 5-13). In addition, fluorescence microscopy did not reveal obvious outer segments. This could be due to poor sectioning or required optimisation of the staining protocol. Toxicity may also contribute to altered organoid structure.

Since there was no on-target editing, off-target editing was unlikely. Indeed, analysis of bystander editing and off-target editing within the amplicon revealed no activity. This may indicate a lack of Cas13-ADAR expression, given that *in vivo,* despite no observed on-target editing, promiscuous off-target activity was observed throughout the amplicon. Off-target activity would be expected with expression of ADAR2 due to its notoriety for hyperactivity at

off-target adenosines particularly at favoured recruitment motifs throughout the transcriptome.[198,215,327,328]

5.4.5 Insights from retinal organoid model

The development of retinal organoids as a pre-clinical model has revolutionised studies of the retina, in particular retinal development, understanding disease mechanisms, and as a tool for screening of potential therapeutics in a native human context. Retinal organoids mimic human retinal development and resemble the molecular and cellular profile of the retina, where there is a laminated structure of retinal ganglion cells in the inner layer and photoreceptor cells (rods and cones) in the outer layer.[92,329] In addition, the mature photoreceptors have photosensitivity.[304,329] However, for applications such as *ABCA4*-related retinopathies which affect the outer segment and RPE, ROs have significant limitations.

First, retinal organoids have poorly defined outer segments and retinal pigment epithelium.[93] This was seen in the imaging and staining of the retinal organoids, where no clear and consistent outer segments were observed. Recent studies have enabled efficient development of outer segment bearing photoreceptors with better organisation and structures resembling stacked discs.[310] However, this was not achieved across all photoreceptors. Moreover, *in vivo,* outer segments undergo continued renewal as part of the visual transduction cascade,[11] which, at present, cannot be recapitulated in organoids. This requires the support of the RPE*,* given that the RPE is responsible for the phagocytosis of outer discs alongside providing other essential support such as nutrient transport and removal of waste.[310] However, one advantage of the absence of an RPE monolayer surrounding the organoid is the likely improved AAV transduction of photoreceptors due to greater photoreceptor accessibility.

Second, over time, the inner nuclear layer and retinal ganglion cells are gradually lost, influencing the study of age-related retinal degenerations with organoid models.[93,330,331] This may be due to the retina being a highly energy-demanding tissue,[332-334] typically supplemented by the choroid and RPE (discussed above) and vasculature to the eye.[93] The lack of vascularisation of retinal organoid models poses an issue post-maturation in the longevity of organoids, where nutrients and oxygen struggle to penetrate the organoid core. Alternatively, the lack of inner retina organisation may be causal in RGC loss.[330,331] In the context of Stargardt disease, where disease progression is hugely variant dependent,[23] this could influence the study of pathogenic mutations and their functional effects.

Third, the retinal organoids demonstrated extreme variability. This was observed in fluorescence imaging of organoids treated with the same dose, where GFP expression ranged from minimal to strong expression seen throughout the whole organoid (Figure 5-10). To overcome this, a larger sample size is required which is costly.

Fourth, although organoids contain Müller glial cells to respond to stress, retinal organoids lack immune cells. However, a recent publication co-cultured microglia-like cells with retinal organoids, showing functional integration and response to endotoxin.[335] Specifically, an upregulation of pro-inflammatory markers ILα, IL-12/IL-23p40, IL-15, IL-16, TNF-β, IL-1β, IL-8 and TNF-α, and anti-inflammatory markers IL-10 and IL-13 was observed. This would enable the well-documented crosstalk between microglia and Müller glial cells, more fully recapitulating immune responses in the eye.[336,337] In the future, this would enable improved evaluation of innate immune response to AAV in the eye or other potential therapeutics in a 'human' environment.

Despite these shortcomings, ROs provide a unique and important ability to test therapeutics in a molecular, genetic, and physiological setting resembling a human retina. Furthermore, retinal organoids are rapidly advancing to include other complex systems such as immune cells,[335] the RPE,[338-340] and vascularisation,[341] enabling improved measures in evaluating potential therapeutics.

5.4.6 Translational considerations

Multiple notable conclusions can be drawn from this chapter in regard to translation. First, gene editing technologies require significant screening to establish the targetability of specific sites. Nonetheless, the *in vitro* results are promising in that they indicate that through diverse testing of a plethora of editing technologies, there is likely a method that enables editing with optimisation. The continued development and rapid advancement of existing and novel gene editing methods will likely continue improving the targetability of mutations.

Second, it is difficult to determine why no Cas13-ADAR activity was observed in a more complex pre-clinical model. Further optimisation of transduction, dose, expression, and guide design will work toward improving editing outcomes and shed light on the reason behind the lack of editing and continue the path toward therapeutic potential.

Lastly, retinal organoids, despite their shortcomings, provide immense potential for screening novel therapeutics and provide an insight into disease progression on a

mutation/patient specific level. Additionally, the continued improvements to organoid models will enable increasingly accurate screening due to greater recapitulation of the native human retina.

5.5 Conclusion

This chapter presented a continued holistic comparison of DNA and RNA base editing at a variety of sites, revealing the need for continued screens and optimisations at complex sites. Further, testing of dCas13b-ADAR$_{DD}$ in a wildtype retinal organoid highlighted that in its current state, there is no therapeutic potential. Significant optimisation and continued testing is necessary to establish transgene expression and editing activity.

6 *In vivo* comparison of DNA vs RNA base editing knockdown of *ABCA4* start codon

6.1 Introduction

As established throughout the thesis, mutations in *ABCA4* are one of the most common causes of IRDs and no treatment exists, to date. Further, many gene supplementation and therapy methods have been tested with no success thus far in clinical trials.[35] An *ABCA4* mouse model comparing the efficacy of SaKKHABE8e DNA and Cas13-ADAR RNA base editors targeting the same point mutation could demonstrate *in vivo* proof of principle that base editors can potentially target pathogenic *ABCA4* mutations. *In vitro* data suggest that targeting mutations using both base editors is possible at a high efficiency (Chapter 4). However, it has also shown that editing can be highly site-specific (Chapter 5).

Evidence suggests that DNA base editing with SpCas is possible *in vivo* and has been used in photoreceptors targeting *ABCA4* c.5882 G>*A*.[175,187,342] RNA base editing has been tested *in vivo* with varying success, including recently in photoreceptors.[210-212,343,344] To date, there are eleven *ABCA4* mouse models commercially available which have been invaluable for evaluating the efficacy and safety of novel therapeutics. However, all of these have significantly altered cassettes to facilitate knockdown and are thus not suitable for assessing base editing of point mutations. Existing gene editing technologies have broadened the scope and ease of creating

novel mouse models, such as two non-commercial *ABCA4* mouse models containing homozygous pathogenic point mutations, p.N965S or pL541P, A1038V.[76,101] Unfortunately, these could not be used for this project since they do not contain the required G>A mutation to compare DNA and RNA base editing.

Since no existing mouse models could be used to compare DNA and RNA base editors effectively and it was not possible to develop a clinically relevant model containing the necessary G>A point mutation, a proof-of-principle comparison was conducted knocking down the *ABCA4* start codon in a heterozygous mouse containing one wild-type allele and one knocked-down allele. The model design is described fully in the methods. Although inducing a mutation is not directly translationally relevant as a potential novel therapeutic or model, the c.1 A>G mutation is reported 41 times in LOVD and is classified as severely pathogenic in ClinVar, making the site clinically relevant. Future DNA base editing strategies, including SaKKHABE8e, could be tested to correct c.1A>G on the reverse strand. For this project, to enable comparisons of DNA and RNA base editing, the A of the *ABCA4* start codon was targeted for conversion to G to determine (1) the relative levels of editing achieved by DNA and RNA base editors at the same *ABCA4* target, (2) to identify if the editing could influence ABCA4 protein levels in the retina, and (3) demonstrate the first proof-of-principle application of the dual vector and all-in-one size minimised SaKKHABE8e in photoreceptors.

This chapter details targeting the *ABCA4* start codon (ATG->GTG) by both DNA and RNA base editors *in vitro* and *in vivo.* Specifically, dPspCas13b-ADAR$_{DD}$(E488Q), a dual vector SaKKHABE8e, and an all-in-one SaKKHABE8e were tested at multiple doses to determine the safety and efficacy of AAV-mediated delivery of these base editors. Use of the all-in-one SaKKHABE8e has yet to be demonstrated in photoreceptors and provides exciting clinical potential due to single vector delivery. Further, this work will establish the relative efficacy of the different base editors and determine the targetability of this site. This may shed light on which base editor is more suitable for treatment of *ABCA4* retinopathies given the rapid outer segment turnover time of ~10 days.[11,280]

6.1.1 Chapter aims

The overall aim of this chapter is to compare dCas13b-ADAR$_{DD}$ (E488Q) and SaKKHABE8e targeting the *ABCA4* start codon using the workflow established in Chapter 4.

Guides were first screened *in vitro,* and the best performing guides were packaged within an AAV and tested *in vivo.* Specifically, the aims are:

1. To screen guides *in vitro* for DNA and RNA base editors targeting the *ABCA4* start codon and evaluate the best performing guides by functional luciferase assay and transcript analysis.
2. Clone base editors tested in Chapter 4 for *in vivo* photoreceptor-specific targeting and generate AAV vectors: RK-SaKKHABE8e, U6-gRNA-CAG-mChery, RK-SaKKHABE8e-U6-gRNA, RK-dCas13b-ADAR$_{DD}$(E488Q), and U6-gRNA-CAG-GFP.
3. Assess vector expression and efficacy of vectors in knocking down *ABCA4* at the RNA, DNA, and protein level to enable comparison of DNA and RNA base editing targeting the same site.
4. Determine safety and tolerability of the vectors by analysis of retinal structure and investigation of off-target effects.

6.2 Materials and methods

6.2.1 Mouse model design and breeding

Since it was not possible to develop a clinically relevant mouse model within the time of this PhD, an alternative, proof-of-principle model knocking down *ABCA4* was tested. Specifically, the ‘A’ of the ATG start codon was chosen as the target site given that it is targetable by both dPspCas13b-ADAR and SaKKH, enabling a comparison of both editing efficiency and its consequence on RNA and protein levels *in vivo*. Fortunately for SaKKH, an ideal PAM-site placed the target ‘A’ within the optimal editing window aTnd had no potential bystander ‘A’s (Figure 6-2). Even the Cas13-ADAR only had three potential bystander sites in a 50bp guide. To maximise potential measurable knockdown, a heterozygous (het) mouse was bred using the homozygous knockout *Abca4*^{tm1Ght}/J mouse on a 129S background (strain 023725, Jackson Laboratory) and the wildtype 129S2/SvHsd (Envigo), respectively. The 129S2/SvHsd was the mouse with the most similar background commercially available.

6.2.2 Molecular Biology

6.2.2.1 *In vitro* assay design

An *in vitro* assay using the Dual-Glo® system was designed to screen base editing guides and ensure that the *ABCA4* start codon is targetable by both DNA and RNA base editors. A psiCHECK™-2 plasmid (kind gift of Michelle McClements, Promega) was used to clone constructs for base editing reporting when targeting a start codon where the reading frame changes upon editing (Figure 6-1). This assay still functions using *Renilla* and Firefly luciferase but the target cassette is upstream of *Renilla* driven by an SV40 promoter and is normalised to Firefly luciferase on an HSV-TK promoter (Figure 6-1). The wild-type 'ATG' target cassette puts *Renilla* out-of-frame and *Renilla* is thus not expressed. The mutant 'GTG' target cassette results in readthrough where *Renilla* is in the correct reading frame and is thus expressed; upon knockdown of ATG to GTG by base editing, *Renilla* is produced. The ratio of *Renilla:*Firefly estimates the editing efficiency and was used to screen guides for RNA editing. Editing calculations are described in Section 6.2.3.

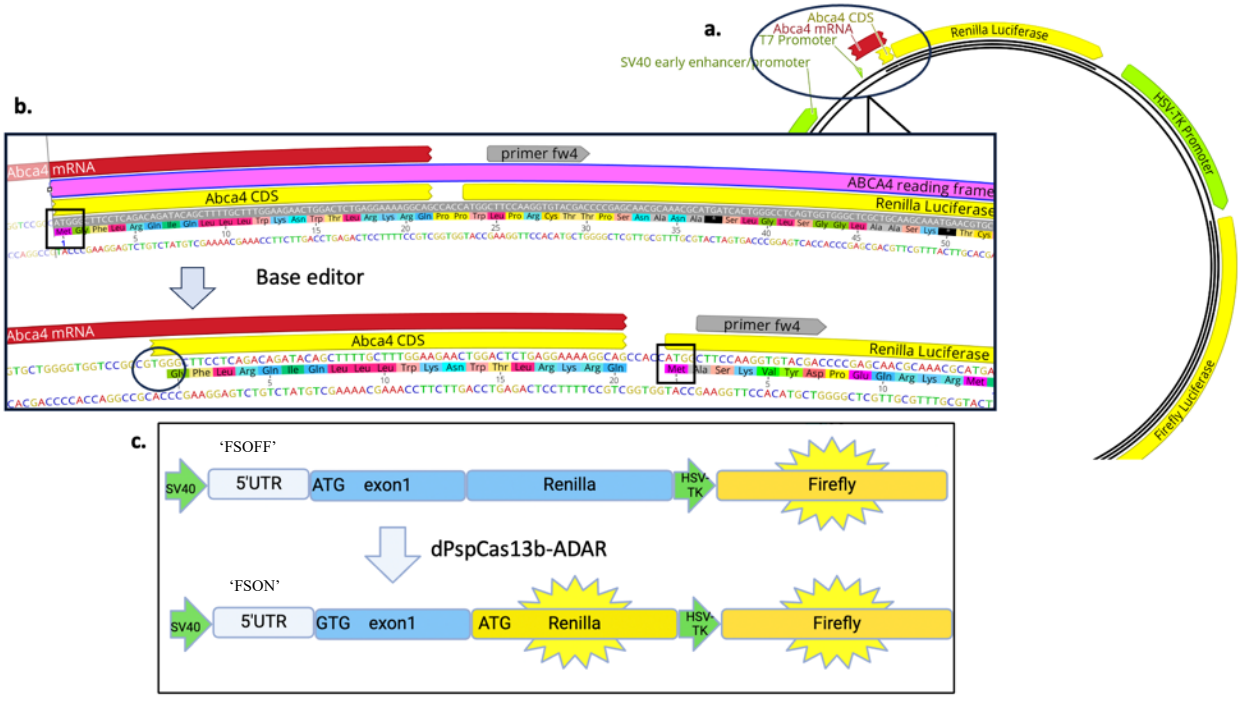

Figure 6-1: PsiCheck2 Dual-Glo® luciferase assay design for targeting mouse abca4 start codon.
a) PsiCheck2 plasmid design where mouse *abca4* precedes Renilla luciferase which is normalized to Firefly luciferase. **b)** The reading frame shifts from *abca4* to Renilla (outlined in boxes) upon editing of the c.1A due to readthrough of the start codon. **c)** the presence of the *abca4* start codon results in an out-of-frame Renilla and thus

no Renilla expression. Upon editing of the start codon, readthrough occurs putting Renilla in frame and enabling expression.

6.2.2.2 Cloning luciferase assay for *in vitro* testing

The final target cassette consisted of 88bp of the 5' UTR plus exon 1 of mouse *ABCA4 (mABCA4)* and was commercially synthesized as a double stranded DNA fragment from IDT. The fragments were amplified by PCR using KOD Hotstart Polymerase Master Mix (Sigma-Aldrich), an annealing temperature of 65°C, and a 20 second extension time for a 175bp fragment length. The primers for PCR are listed in Table 6-1 and all cassettes and plasmid sequences are listed in the appendix. The psiCHECKDB8-2 plasmid was digested with NheI and treated with rSAP as per the general methods. The NEBuilder® HiFi DNA Assembly Kit was used to insert the fragment in the digested backbone using 25bp overhangs complementary to the insertion site. Transformation, colony selection, and plasmid extraction and amplification were done per the general methods.

6.2.2.3 Cloning DNA and RNA base editing guides

Guides were cloned as per the general methods and as in Chapter 4. Fifteen sgRNAs for dPspCas13b-ADAR RNA base editing were cloned into the pC0043-PspCas13b crRNA backbone (Addgene #103854) to screen in the luciferase assay. The three best performing guides were cloned into a backbone containing ITRs and GFP for downstream *in vivo* experiments. Guides were cloned into pAAV.U6-PspgRNA-CAG-GFP (Kind gift of Lewis Fry) using the BspMI/BveI restriction enzyme (NEB/ThermoFisher). The same annealed and phosphorylated guide oligos were used for cloning into both the pC0043 and the pAAV guide plasmids since the restriction site overhangs were the same. Prior to virus production, guides were transfected to test for GFP expression and underwent an XmaI digest to confirm correct ITRs.

SaKKH DNA base editing guides ranging in length from 19-23bp were cloned into the pAK212 plasmids using the SapI restriction enzyme for screening and the dual vector approach. The two best performing guides were cloned into the all-in-one SaKKH plasmid using the BsmBI-v2 restriction enzyme (NEB). For this, guides were re-designed in reverse in alignment with the U6 promoter and SaCas scaffold (Figure 6-2b). Guides were cloned into two plasmids containing either the EFS or GRK1 promoter to enable testing of the vector *in vitro* (EFS) prior to *in vivo* (GRK1) experiments.

All guides were amplified and extracted as described in the general methods and sequence confirmed using a nanopore based NGS service, Plasmid-EZ (Genewiz).

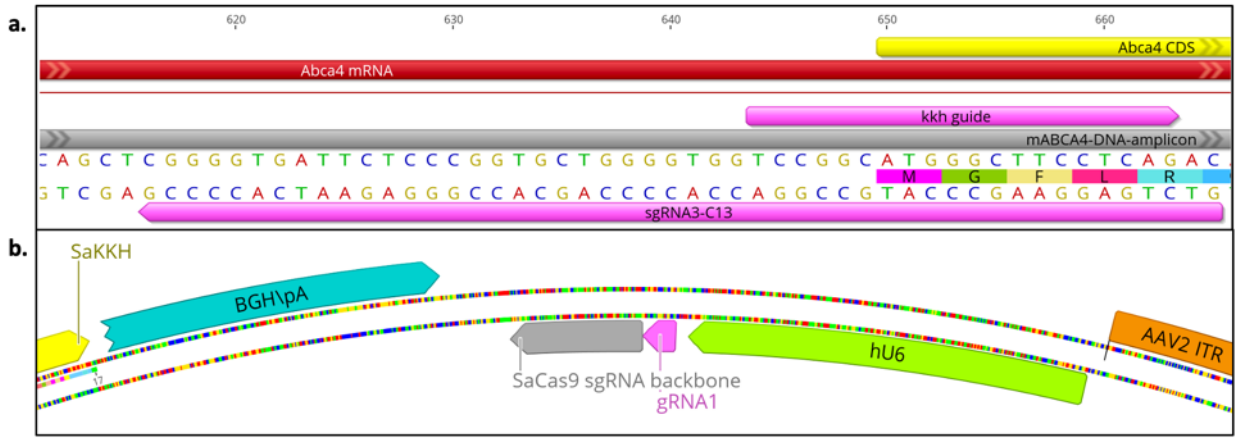

Figure 6-2: Target region of mouse abca4 and all-in-one KKH guide cloning.
a) Both the DNA and RNA base editing guides shown within mouse abca4. KKH guide applies for both the all-in-one and dual vector SaKKH. The sgRNA3-C13 is for dPspCas13b-ADAR$_{DD}$. The yellow 'Abca4 CDS' is exon1 and the red region upstream is the 5' UTR. The m-ABCA4-DNA-amplicon indicates the amplicon sent for sequencing. **b)** the all-in-one gRNA cloning orientation is in reverse.

6.2.2.4 Cloning AAV base editor plasmids

6.2.2.4.1 Addition of GRK1 promoter for the all-in-one SaKKHABE8e

The all-in-one SaKKH-ABE8e plasmid is described in detail in the general methods. For *in vitro* work, the all-in-one SaKKH-ABE8e with the EFS promoter was used. For *in vivo* work, the EFS promoter was replaced with the rhodopsin-kinase promoter (GRK1), a 197bp, photoreceptor-specific promoter (Figure 6-3c). Fortunately, the plasmid already contained the necessary ITRs for virus production. To replace EFS with GRK1, the all-in-one SaKKH-ABE8e plasmid underwent a double digest with NheI and Kpn2I (NEB) at 37°C, which removed both the EFS promoter and the TadA domain (Figure 6-3d). There were no available restriction sites for the removal of only EFS. A double stranded DNA fragment containing the GRK1 promoter, the TadA domain and 25 bp overlap with the digested backbone were commercially synthesised (IDT). Samples were amplified by PCR using KOD Hot Start Master mix (NEB) with annealing at 70°C and supplemented with 1% DMSO (NEB) (Figure 6-3d). The NEBuilder® HiFi DNA Assembly Kit (NEB) was used to assemble the plasmid. Transformation, colony selection, and

plasmid expansion were done per the general methods. Plasmids were fully sequenced using Plasmid-EZ (Genewiz).

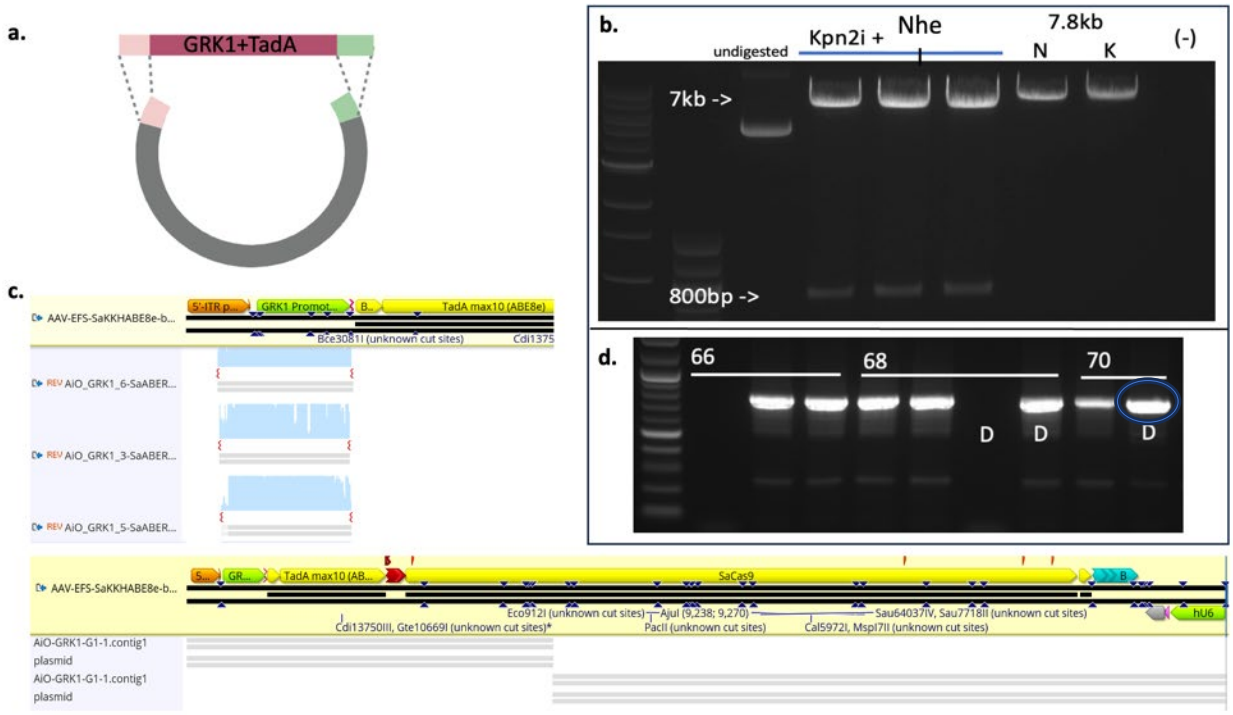

Figure 6-3: GRK1 promoter cloning in all-in-one SaKKH.
a) The overall NEBuilder® HiFi DNA assembly strategy for replacing the EFS promoter with GRK1. EFS and the TadA domain were removed and replaced with a GRK1 and TadA fragment with 25bp overlap on each side. **b)** EFS-AiO-SaKKHABE8e digest with Kpn2i and NheI. The 7kb backbone was excised and used for downstream cloning with the GRK1+TadA insert. N = NheI only control, K= Kpn2i only control. **c)** Successful insertion of the GRK1+TadA fragment as shown by Sanger sequencing (top) and NGS PlasmidEZ (bottom). **d)** PCR gradient amplifying the GRK1+TadA insert (764bp). 'D' indicates addition of DMSO to minimise non-specific amplification. Blue circle indicates fragment used for cloning.

6.2.2.4.2 Addition of ITRs and GRK1 promoter for dual vector SaKKHABE8e

The SaKKHABE8e dual vector construct (guide delivered separately) is described in detail in the general methods. The plasmid used *in vitro* carried a CMV promoter and did not contain ITRs for virus production. To enable *in vivo* delivery, a construct containing both ITRs and a GRK1 promoter was cloned. A plasmid containing ITRs and a GRK1 promoter was digested with AgeI and NotI at 37°C. The 3.2kb band was excised, purified using the QIAquick® Gel Extraction Kit (Qiagen), and used as the backbone in downstream steps. The base editor was split into four fragments by gradient PCR amplification from the SaKKHABE8e plasmid using primers that created 25bp overhangs with neighbouring fragments or the ITR-GRK1 backbone

(Figure 6-4a). The PCR was run using KOD Hot Start Master Mix at 65°C, 67°C, and 69°C (Figure 6-4b). Note, two fragment fours were tested where 's' denotes short and 'l' denotes long. Both the 4s and 4l fragment lengths allowed for a transgene under the ~4.7kb AAV packaging limit. The four fragments and the ITR-GRK1 backbone were assembled using the NEBuilder® HiFi DNA Assembly Kit (NEB) according to manufacturer protocol (Figure 6-4c). Transformation, colony selection, and plasmid expansion were done as described in the general methods. Sequence confirmation was done using Plasmid-EZ (Genewiz).

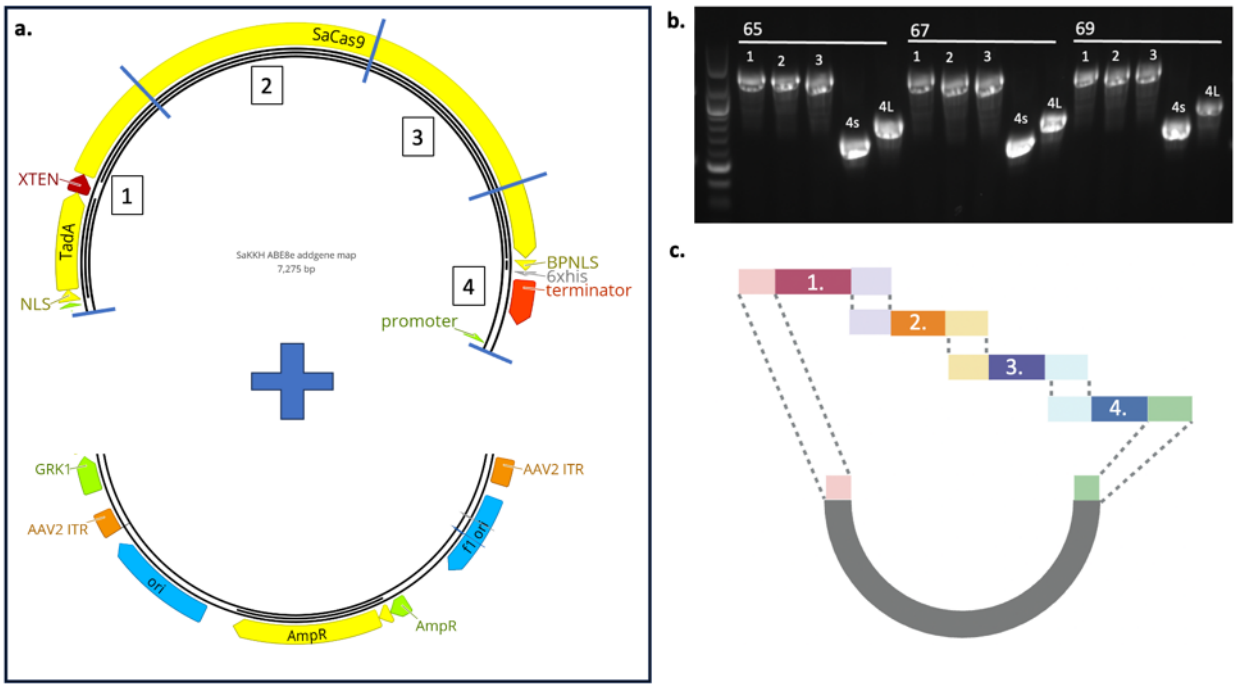

Figure 6-4: Cloning strategy for addition of ITRs and GRK1 promoter in dual vector SaKKH. **a)** The insert SaKKH was split into four fragments with 25bp overlap on each end. This was cloned using NEBuilder® HiFi DNA assembly into an ITR and GRK1 containing backbone. **b)** PCR gradient amplifying the four fragments. 4s and 4l refer to a short (s) and long (l) version of fragment 4 containing varying amounts of sequence after the terminator. 4L cloned more successfully (4.68kb total) and was used in downstream experiments. **c)** Cloning strategy showing overlap regions.

6.2.3 Cell culture for *in vitro* DNA and RNA editing

All cell culture was conducted as described in the general methods. dPspCas13b-ADAR$_{DD}$ guides were screened using the Dual-Glo® luciferase assay and run as described in Chapter 4. Calculations for estimated editing efficiency differed given the differing assay design (Figure 6-1). Duplicate or triplicate wells of each condition were averaged. Untransfected wells

were used to describe a mean background luminescence and subtracted from mean values for each experimental condition. *Renilla* was then normalised to Firefly. To determine relative expression, all values were taken as a proportion of the 'FSON' (wild-type expression) value, resulting in 'FSON' as one ie 100%.

Once RNA editing guides were screened, DNA and RNA editing constructs were screened further by transcript analysis. HEK293T cells were maintained as described in the general methods and seeded in 12-well Corning cell culture plates at 4.5 x 10^5 cells/well. After 24 hours or 70-80% confluence, cells were triple transfected using 100ng target plasmid (luciferase with mouse *abca4* exon 1), a base editor, and the guide plasmid. For dPspCas13b-ADAR$_{DD}$, a 2:1 guide:editor ratio was maintained where 333ng guide and 167ng editor were used. For SaKKHABE8e, a 1:1 guide:editor ratio was used – 250ng of each. Plasmids were diluted, aliquoted by condition into a PCR plate, incubated at a 3:1 TransIT-LT1(Mirus Bio):DNA ratio for 15-20 minutes and added to the corresponding well on the plate. Plates were left to incubate for 48hrs at 37°C. Cells were harvested as described in the general methods and used downstream or frozen at -80°C.

6.2.4 Detection of DNA and RNA editing

Extraction of DNA and RNA from cell pellets and cDNA synthesis is described in the general methods and Chapter 4. PCR amplification of the target regions was done using KOD Hot Start Master Mix (NEB). For cDNA samples, annealing was conducted at 60 °C with an extension time of 20s. DNA samples were PCR amplified at 55°C for annealing with a 20s extension time. Both cDNA and DNA were cycled 25 times. Primers are shown in Table 6-1. 5 μL of samples were run on a gel, after which the remaining sample was PCR purified, nanodropped, and sent for sequencing (Genewiz). To detect editing, chromatograms were analysed in EditR.

DNA and RNA extraction from neural retinal tissue was done with a combination of the AllPrep DNA/RNA/Protein Mini Kit (Qiagen) and the Monarch® Total RNA Miniprep Kit (NEB). (Only DNA and RNA were extracted from the same sample, not protein). The AllPrep manufacturer protocol was followed for tissue lysis and initial gDNA removal. RNA was subsequently extracted first, while columns containing gDNA were stored at 4°C for later use. The flow-through containing the RNA (post-gDNA removal) had 400μL 99% ethanol (Sigma-

Aldrich) added, mixed well, and transferred to the Monarch® RNA purification columns. From this point on, the Monarch® manufacturer protocol was followed including the optional DNAse treatment. RNA was eluted with 30μL nuclease-free water. RNA samples were immediately used for cDNA synthesis and the remaining sample frozen at -80°C. For DNA extraction, the AllPrep manufacturer protocol was followed. Samples were eluted with 2x 40μL elution buffer pre-heated to 70°C. Samples were stored at -20°C for downstream use.

DNA and cDNA samples were PCR amplified using KOD Hot Start Master Mix. Primers are listed in Table 6-1. PCR was run using 2 μL cDNA with an annealing temperature of 55°C and DNA samples were run using 100ng genomic DNA with an annealing temperature of 60°C. Both samples had a 10 second extension time and were cycled 35 times. Samples were run on gel electrophoresis and bands excised and processed using the Monarch® DNA Gel Extraction Kit (NEB) according to manufacturer protocol. Incubation was conducted at 50°C and samples eluted with 8 μL elution buffer. Samples were sent for Illumina short-read NGS using the amplicon-EZ service (Genewiz) which provides ~40-60,000 reads, but up to 100,000x reads. Paired-end sequencing outputs were analysed in Crispresso2 with the Base Editor parameters. The amplicon reference sequence and gRNA region were input for analysis, enabling alignment of sequencing reads to the reference sequence and determination of base changes and modifications within the amplicon.

Primer	Sequence	Application
mABCA4F1	GACGTGGTCCTAGC	*In vitro* – PCR, sequencing
psiCheck2F1	GTGTAGCCGTAGTTAGG	*In vitro* - PCR
psiCheck2F2	ACCTCTGACTTGAG	*In vitro* - Sequencing
PCseqRv3	TTAGGCAGATCGTCGC	*In vitro* - PCR, sequencing
mABCA4F5	CTTTGTGTCCGGTGCTTGC	*In vivo* - PCR
mABCA4rv2	CCAGCAGGTGTCGAAGC	*In vivo* - PCR
mABCA4RNArv2	CCATGAACTGCGACAAGG	*In vivo* - PCR

Table 6-1: Primers for detection of DNA and RNA base editing.
Primers for *in vitro* and *in vivo* work differed, indicated on the right.

6.2.5 Detection of editing with quantitative PCR

All quantitative PCR probes and protocols are listed in the general methods. To calculate gene expression, all target samples (abca4, sacas9, Sacas scaffold, rho) were normalised to the geometric mean of gapdh and beta-actin. Rhodopsin was used as an indicator of photoreceptor health in uninjected versus injected eyes. SaCas9 and guide scaffold expression are presented in two ways. First, the dCt values were graphed where the bars approach 0, the expression increases. In instances where there was no expression, such as in uninjected eyes, a Ct of 41 was used in calculations as this is the latest cycle. Second, relative expression was calculated and graphed as a visual representation of expression. However, since it is relative to PBS injected eyes where there is no expected expression, the values are arbitrary but provide more intuitive curves.

6.2.6 Western blot

Western blots were run according to the general methods. Whole neural retina was lysed with a handheld homogeniser in 56 μL Lysis buffer (1xRIPA, protease inhibitor pellet, PBS) on ice. To determine total protein concentration, a bicinchoninic acid assay (BCA) was conducted with an albumin standard curve. 50μg protein (10μg of Hek293T controls) was loaded/well and run for ~1.5 hours at 115V. Samples were transferred and blocked, then gently rocked at 4°C overnight in the primary antibody solution. All samples were targeted with two anti-ABCA4 antibodies targeting the N- and C-terminals. The membrane was washed and gently rocked in secondary antibody solution at room temperature for ~1.5 hours and washed again. Lastly, the membrane was left to dry covered from light for 10 mins and imaged on the Odyssey Fc imaging system. Antibodies are listed in the general methods.

6.2.7Immunohistochemistry

Eyecups soaking in 30% sucrose were embedded in OCT for long term storage at -80°C. For this, handmade eye containers were constructed from aluminium foil and filled with OCT. Containers were placed in isopentane on dry ice to allow for slow freezing of OCT. Eyecups were gently covered in OCT, held in the cooling OCT until frozen, and stored at -80°C.

Samples were sectioned in a Leica CM1860 UV cryostat set to -20°C into 10-14μm slices and immediately placed on a slide. Once dry, slides were placed at -20°C for storage. For IHC, samples were removed from -20°C storage and thawed to room temperature for at least one hour. Slides were washed, stained, and stored as described in the general methods, alongside all primary and secondary antibodies used.

6.2.8Detection of transgene

The qPCR protocol was applied to determine expression of the transgene for SaCas9 and the scaffold as previously described. Given no samples with which to normalise, expression was calculated relative to the negative control in fold increases. dCt values were also compared. For Cas13, since no qPCR probes were custom designed, cDNA samples (RNA was DNase treated) were amplified by PCR using primer pairs in Table 6-2 spanning the transgene from the transcriptional start site to the poly A tail, gel extracted, and Sanger sequence confirmed. Similarly, in instances where DNA was extracted from samples, the transgene was amplified from DNA by PCR using the primers in Table 6-2 as well and run on a gel. The correct band was excised, purified, and sent for Sanger sequencing. PCR was conducted with Platinum™ SuperFi II with an annealing temperature of 55°C and an extension time of 2 minutes 20 seconds.

Primer	Sequence
F1-RK	CCTTCTTGCCACTCCTAAGC
ADAR-R1	ATCAGCGAGCTCTAGGAATTC
C13F7	CAGGCACAGATGTTAAAGATGC
C13F5	AGCGGAAGTTCTACCTGACC
C13F2	AAGTCCCAAGTGAATACCGG
KKHpA-R	CCAGCATGCCTGCTATTGTC
KKH-R4	CGATCTGCTTCAGTGTAGGC
KKH-F4	GGCCATCAATCTGATCCTGG

Table 6-2: Primers for transgene confirmation.

6.2.9 *In vivo* procedures

All mice were housed and all animal work was carried out at the Biomedical Sciences Division, University of Oxford compliant with: the Animals (Scientific Procedures) Act 1986, UK, the University of Oxford policy on animal use in scientific research, and the Association for Research in Vision and Ophthalmology Statement for the Use of Animals in Ophthalmic and Vision Research. Animal procedures were conducted under UK Home Office Project license PP3038118 (Expiry Dec 2025) and Personal License I97298205. Mice were kept in individually ventilated cages on a normal mouse chow diet and water freely available with a 12-hour light/dark cycle.

6.2.9.1 Anaesthesia and pupil dilation

Mice were anaesthetised by intraperitoneal injection with ketamine (Narketan, Vetoquinol, final concentration 8mg/mL) and xylazine (Rompun, Bayer, final concentration 1mg/mL) in 0.9% normal saline at a dose of 0.15mL/10g bodyweight, and pupils dilated by application of phenylephrine hydrochloride 2.5% followed by tropicamide 1% topical eye drops. Anaesthesia was reversed at the end of the procedure by subcutaneous injection of atipamezole (Antisedan, Zoetis, final concentration 0.2mg/mL) at a dose of 0.15mL/10g bodyweight in 0.9% normal saline. To prevent drying and infection of the cornea during recovery, 0.5% chloramphenicol topical drops and Viscotears® Liquid Gel (0.2mg/g polyacrylic acid) were applied. Mice were placed in a 33°C temperature-conturolled chamber for recovery.

6.2.9.2 Subretinal injections

Mice were anaesthetised and pupils dilated as described above. Once asleep, mice were placed on a ‘custom’ foam operating mat to stabilise the head for surgery (Figure 6-5a) under an ophthalmic surgical microscope (Leica Biosystems), which was used throughout. For corneal anaesthesia, topical proxymetacaine (Minims, Bausch and Lomb) was applied.

Paracentesis was performed with a 33G needle (TSK laboratory) to lower intraocular pressure for subretinal injections. Injections were carried out with a NanoFil 10μL syringe and a 35G bevelled NanoFil needle (both World Precision Instruments), with 1 μL of AAV suspension or PBS drawn up in preparation for injection. Following paracentesis, for a direct view of the fundus, the eye was covered with Viscotears® and a 6mm round cover slip (Figure 6-5c/d).

Notched forceps were used to stabilise the eye by holding the superior rectus muscle, while the needle was introduced into the subretinal space (Figure 6-5b). The needle bevel became visible beneath the retina and the superior rectus was released for injection (Figure 6-5c). The plunger was gently depressed and, in a successful subretinal injection, created a bleb as seen in Figure 6-5d. The needle was withdrawn, the coverslip removed, and the mouse ear-notched and recovered (Figure 6-5f) as described above. Mice experiencing complications were recorded and, depending on severity, excluded from analysis. Each injected cohort included PBS injected controls, which were pooled and used as a control across all cohorts (N=22). Additional mice were not injected and used as uninjected controls. Subretinal injections were carried out by two members of the lab very experienced in the protocol. Both are mentioned in the acknowledgements and Ahmed is pictured below.

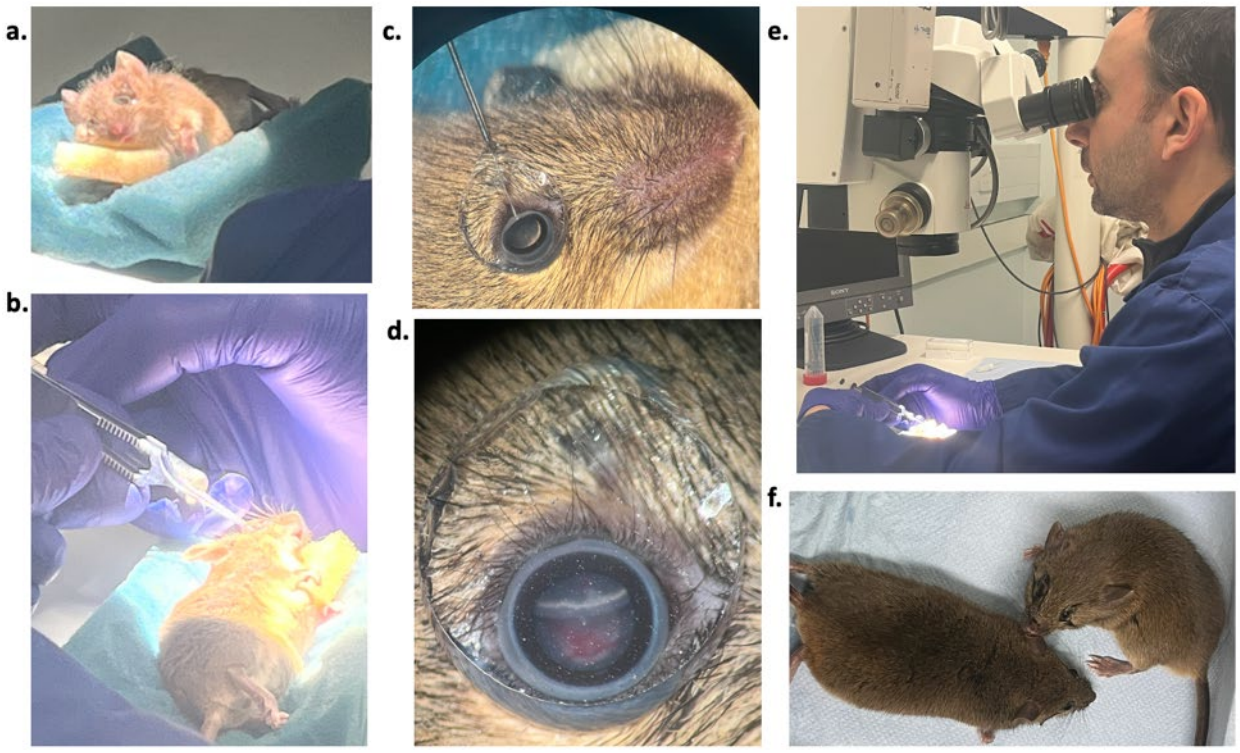

Figure 6-5: Subretinal injections for *in vivo* work.
a) the mouse was placed on the custom foam operating mat with Viscotears® liberally applied to the eye. **b)** the superior rectus was held while a 10 μL Nanofil syringe was used to inject 1 μL AAV suspension. **c)** the syringe was gently twisted back and forth until the end was in the subretinal space. **d)** the plunger was depressed, forming a hemiretinal detachment. **e)** Ahmed performing an operation using the Leica operating microscope. **f)** the mice in the recovery chamber.

6.2.9.3 Retinal imaging

The Spectralis™ ophthalmic imaging platform (Heidelberg Engineering) with a 55° lens was used for retinal imaging. Mice were anaesthetised, pupils dilated, and coupling fluid (Hypromellose 0.3%, Blumont Healthcare ltd) applied to the cornea to prevent drying of the lens to the cornea. A custom-made mouse contact lens (polymethyl methacrolate mouse lens, Cantor and Nissel) with a back optic zone radius of 1.7mm, total diameter of 3.2 mm, and a centre thickness of 0.4mm was placed on the centre of the cornea. The mouse was positioned for imaging by placing it on a platform mounted on the chin rest (Figure 6-6). Mice were imaged at 3-4 weeks and 9-11 weeks post-injection.

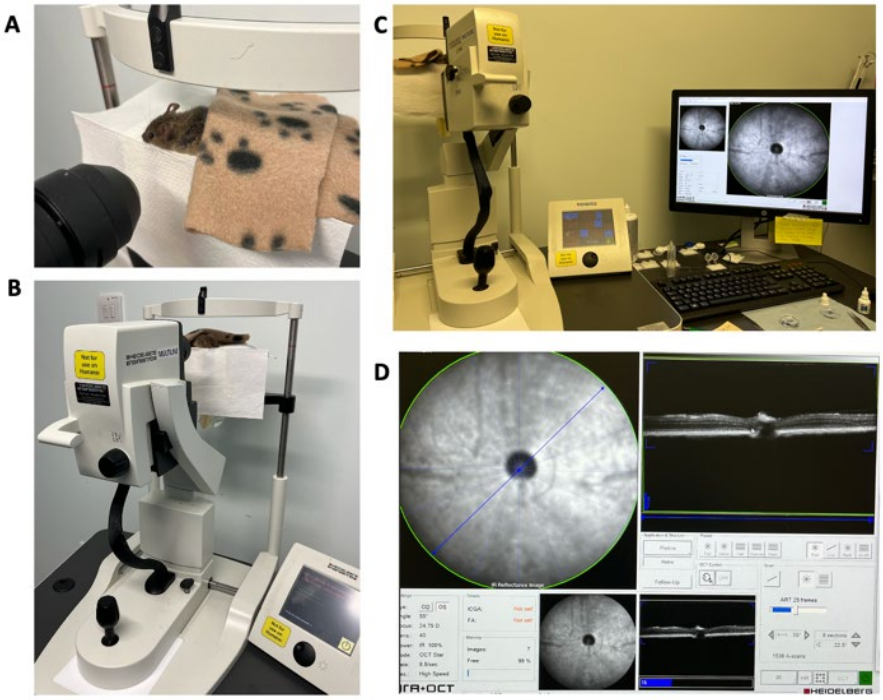

Figure 6-6: Mouse imaging process.
a) mouse was positioned with the jaw line along the edge of the imaging block and covered with a blanket to maintain temperature. **b)** the whole camera could be moved along the horizontal metal bar or up and down with the lever. The joystick allowed for smaller adjustments. The small screen was used to switch between imaging channels. **c)** the camera relative to the screen. **d)** Example of OCT imaging in the Spectralis program. The left is the photoreceptor layer and on the right are the layers of the retina. The bottom right shows the number of frames.

6.2.9.4 Confocal Laser Scanning Ophthalmoscopy

Confocal laser scanning ophthalmoscopy (cSLO) was used to generate a high-resolution retinal image.[345] For imaging, a standard mouse retinal imaging protocol in 'High Resolution' mode of 1536x1536 pixels and 8 bits/pixel was used.[346] To account for mouse respiratory

movement, automatic real-time (ART) averaging set to 20 images with normalisation turned off was applied, enabling higher resolution merged images (Figure 6-6). Careful alignment was required for optimal imaging. In instances of sudden mouse movements/waking-up, imaging would be re-started.

Images were acquired in near infrared reflectance (NIR), blue autofluorescence (BAF), green autofluorescence (GAF), and infrared autofluorescence (IRAF) modes. The optic disc was centred in NIR mode, ensuring uniform illumination and exposure across all quadrants. Using the focus and sensitivity, the nerve fibre layer and photoreceptor layer were captured first. For EGFP, BAF mode was used with a 488nm laser and for mCherry, GAF mode was used with a 532nm laser. Fluorescence images were captured at sensitivities from 107-60. Images in the 'Results' section typically show high fluorescence images to demonstrate the extent of fluorescent protein expression.

6.2.10 Optical Coherence Tomography

Spectral domain optical coherence tomography (SD-OCT) images were a continuation of the cSLO imaging and were thus captured with the Spectralis OCT module with a 55º lens to produce a cross-sectional B scan of the retina. A standard OCT protocol using ART averaging of 25 images captured eight-line scans extending from the optic nerve head. In instances where mice began recovering from anaesthesia during imaging, the Fast ART protocol was used. Images were analysed using HEYEX software, where total retinal thickness and the photoreceptor layer (PRL) were measured at 3mm from the optic disc. An Early Treatment of Diabetic Retinopathy Treatment Study (EDTRS) grid was centred on the optic disc to allow for consistent measurements. Exported images vary in size likely due to slight variations in field of view and have been adjusted for better configuration.

6.2.11 Retinal tissue collection post-imaging

After imaging the second timepoint, mice under anaesthesia were injected with pentobarbital (Pentoject), death was confirmed by cervical dislocation, and eyes were harvested and placed in PBS. Eyes were immediately dissected under a dissecting microscope (Leica). Using a 23G needle, the cornea was punctured and then cut around the edge with Vannas scissors for removal. The lens was gently removed. The neural retina was subsequently removed from the

eyecup using forceps and was snap frozen on dry ice and stored at -80°C for downstream applications.

For IHC, whole eyes were placed in 4% PFA on ice for fixation for 10-15 minutes. Eyes were moved into ice cold PBS and carefully dissected to remove the cornea and lens. The eyecup containing the retina was placed in 4% PFA on ice for a further 30 minutes after which the eyecup was moved through a sucrose gradient (10%-30%) at 4°C. Starting with 10% sucrose, eyecups were incubated for 2 hours or until the eyecup sank to the bottom of the well. This was repeated for 20% sucrose. Lastly, the eyecup was placed in 30% sucrose at 4°C overnight or up to a week. Sectioning and IHC for mouse retina is described further in the general methods and 6.2.7.

6.2.12 Confocal Microscopy

Confocal imaging was performed as described in the general methods for stained mouse eyecup sections. Laser strength and power were first established using a secondary only control. This was followed by a knockout control, the wild-type control, and lastly the heterozygous control to determine background staining levels.

6.3 Results

6.3.1 *In vitro* screen of gRNAs targeting *mABCA4* start codon

6.3.1.1 RNA base editing with dPspCas13b-ADAR$_{DD}$

6.3.1.1.1 Dual-glo luciferase assay for RNA base editing

As in Chapter 4, the C-terminally truncated, hyperactive dPspCas13b-del984-1090-ADAR$_{DD}$(E488Q) was used to edit the target site given the smaller size and higher editing rates.[199] Fifteen 50nt guides were screened where the A-C mismatch occurred between positions 17-39 from the scaffold. The FS luciferase vectors were screened with and without dCas13bdel-ADAR2$_{DD}$(E488Q) and with targeting and non-targeting guides. This demonstrated an encouraging output, where all guides showed activity, and seven of fifteen guides showed >20% editing. The three best performing guides, G3, G7, and G11, showed editing efficiencies of 23.6%, 24.4% and 21.1% $\pm$ 3.7% ($p<0.0001$), respectively (Figure 6-7b). The ‘C’ mismatch occurred at positions 36 (G3), 31 (G7), and 24 (G11). Low levels, ~4.7%, of background

expression were observed in samples transfected with dCas13bdel-ADAR2$_{DD}$(E488Q) and the non-target control, which is accounted for in the targeting guide editing efficiencies. The FSON positive controls with and without dPspCas13b-del984-1090-ADAR$_{DD}$(E488Q) showed strong expression relative to the original psiCHECK2 vector. Like prior luciferase assays, the addition of Cas13 shows low levels of toxicity indicated by decreased Firefly expression across all samples (Figure 6-7a). While some background was observed, the significant increase in Renilla expression in samples with targeting guides relative to both positive and negative controls supports the conclusion that this is due to targeted editing by dCas13bdel-ADAR2$_{DD}$(E488Q) rather than expression due to a secondary mechanism. The luciferase assay did not include controls for endogenous ADAR activity; however, this was controlled for in the transcript analysis in 6.3.1.1.2.

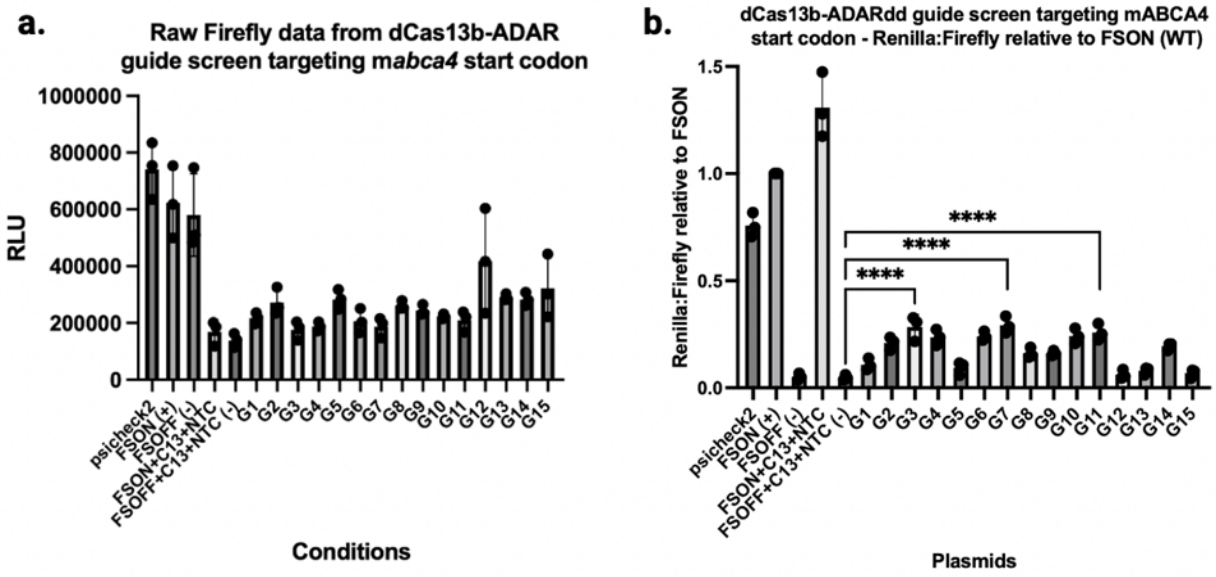

Figure 6-7: Luciferase assay dCAs13b-ADAR buide screens targeting m*abca4* start codon.
a) Raw Firefly data showing a drop in expression with the addition of Cas13 (N=3) **b)** Ratio of Renilla to Firefly proportional to FSON (positive control). One-way ANOVA with subsequent Tukey's multiple comparisons indicated that guides 3, 7, and 11 showed the most significant editing. FSOFF with and without Cas13 and a non-targeting guide showed low, non-significant levels of background. N=3. ($p<0.0001$).

6.3.1.1.2 Transcript analysis in EditR

To confirm editing results observed in the luciferase assay guide screen, the dCas13b-ADAR$_{DD}$ was transfected with the three best performing guides. Using RT-PCR sequencing,

editing rates were determined in EditR, which determines base frequency at each position within the guide using fluorescence intensity provided in Sanger sequenced '.ab1' files.[270]

Tukey's multiple comparisons showed on target editing rates for the best performing guides, 7, relative to the non-target control for samples transfected with dCas13bdel-ADAR2$_{DD}$(E488Q) (Figure 6-8). No on-target editing was detected in samples transfected with the non-target control or in samples with a targeting guide but without dCas13bdel-ADAR2$_{DD}$(E488Q) indicating no endogenous ADAR activity. These results reflected the luciferase assay data.

Bystander editing was not observed by Sanger sequencing within the guide sequence. However, local off-target editing was seen at one site in *Renilla* with significant editing rates of up to 68.7% $\pm$ 1.5% ($p<0.0001$) for both the targeting and non-targeting guides transfected with dCas13bdel-ADAR2$_{DD}$(E488Q) (Figure 6-8). The samples consisting of only the target construct or only the target construct and the guide did not show this off-target edit. This suggests the off-target editing occurred due to exogenous Cas13-ADAR$_{DD}$(E488Q) independent of the gRNA and that the off-target editing was not due endogenous ADAR activity. The mutation was an AGA>GGA (Arginine-Glycine) missense variant. Fortunately, this off-target edit occurred in *Renilla* and was therefore deemed unproblematic for downstream *in vivo* work. Deep sequencing by NGS would likely reveal widespread, low-level off-target editing in agreement with previous reporting.[199,213] Off-target editing is expanded upon in the discussion.

Based on these results, guides 3 (G3) and 11 (G11) were initially selected for *in vivo* experiments to compare guides predominantly binding the 5'-UTR (G3) versus exon 1 (G11). However, due to the impurity of G11 AAV (SDS-PAGE in appendix), only G3 was used in downstream work.

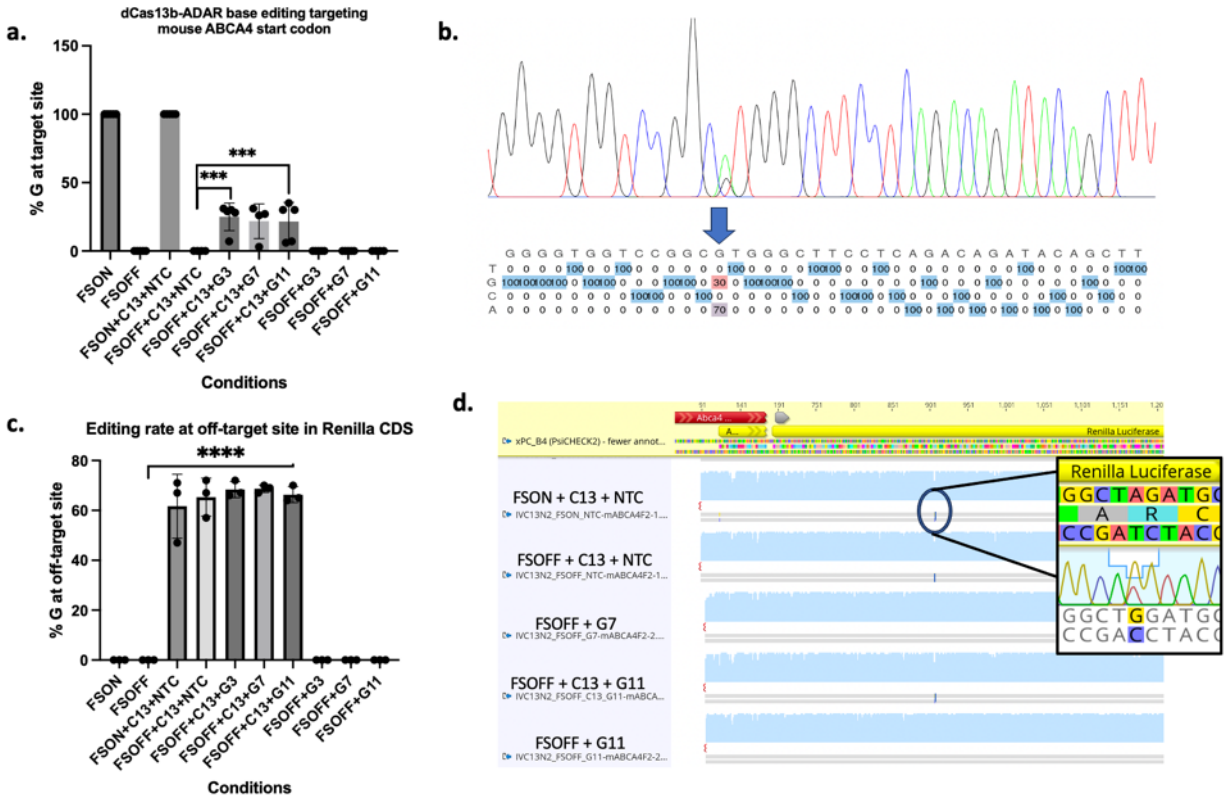

Figure 6-8: dCas13b-ADARdd *in vitro* transcript analysis targeting the m*abca4* start codon.
a) Transcript analysis of RT-PCR amplicons analysed in EditR showed similar levels of editing for guides 3, 7, and 11. While guide 11 showed the highest rate at 25 ± 13.9%, guide 3 showed the most consistent editing rate of 21.6 ± 10.1%. Each guide had on**e** replicate that yielded significantly lower editing rates of 3-7% as seen on the graph. **b)** An example of an EditR output with the chromatogram on the top and the guide region base call percentages on the bottom. **c)** Percentage editing at the off-target site in Renilla. The editing rate is consistent across non-targeting and targeting guides. **d)** The off-target site as seen in the Sanger sequence output aligned to the target plasmid sequence.

6.3.1.2 DNA base editing using dual vector and all-in-one SaKKH-ABE8e

To test DNA base editing activity, a guide screen was conducted by Sanger sequencing transcript analysis in EditR. A luciferase assay was not used given the smaller number of possible guide designs. Five guides ranging in length from 19-23bp were screened initially using the dual vector (DV) approach to minimise cloning. For analysis, DNA was extracted and purified, and PCR sequenced to derive editing efficiencies in EditR.

Editing rates by SaKKH-ABE8e were much higher than the observed dPspCas13b-del984-1090-ADAR$_{DD}$(E488Q) RNA editing. All five guides achieved significant levels of editing relative to the non-targeting guide, ranging from 24.3 ± 4.5 % - 44.7 ± 7% ($p<0.0001$), with G1 (20bp) showing the highest editing (Figure 6-9). This was expected as the known preferred guide length for SaKKH is 20bp. The 19bp guide showed similar levels of editing to

the 21bp and 22bp guides, despite putting the target 'A' at a more optimal position within the editing window. G5 (23bp) showed the lowest editing at nearly half the efficiency of G1.

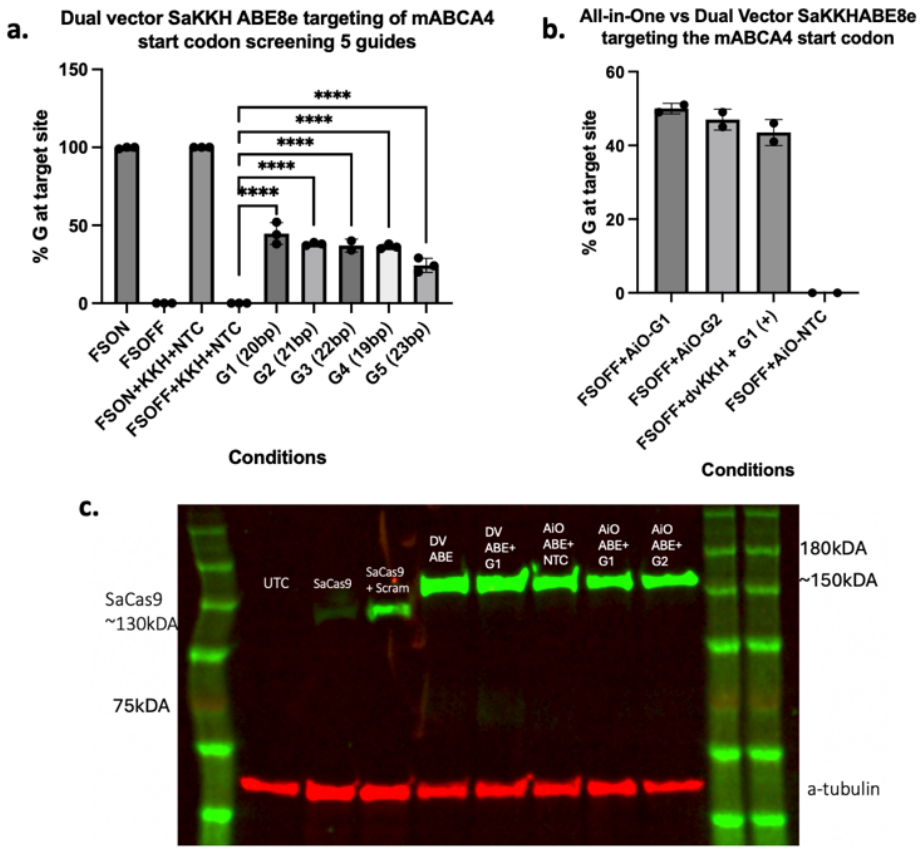

Figure 6-9: SaKKH-ABE8e targeting mouse *ABCA4* start codon *in vitro*.
a) A dual vector approach screening five SaKKH guides targeting the m*ABCA4* start codon ranging in size from 19-23bp in length. Sanger sequenced amplicons were analysed in EditR. G1 showed the highest editing rate of 44.7 ± 7%. N=3, $p<0.0001$. **b)** Comparison of the all-in-one (AiO) SaKKH to the dual vector SaKKH approach. The EFS-AiO-G1 showed higher rates of editing than G1 using the dual vector approach, at 50 ± 1.4%. N=2. **c)** A western blot confirming **SaKKH protein** using an **anti-SaCas9 antibody**. UTC= untransfected control, SaCas9 + scram = non-targeting guide + SaCas9; DV ABE= SaKKH ABE8e; DV ABE + G1 = SaKKH ABE8e + G1; AiO ABE + NTC/G1/G2 = all-in-one SaKKH-ABE8e + nontargeting guide, guide1, or guide2. Transfection of a guide with Cas9 results in increased band intensity. This is shown with the SaCa9 and SaCas9+scram controls. However, this same pattern is not observed for the SaKKH-ABE8e base editors where all five conditions show strong bands. A-tubulin was the housekeeping control.

An all-in-one SaKKH-ABE8e (AiO-SaKKHABE8e) consisting of both the DNA base editor and the guide was compared to the dual vector delivery approach. The two best performing guides by dual vector delivery, guides 1 and 2, were redesigned given the reverse orientation and cloned into the EFS-AiO-SaKKHABE8e for the *in vitro* screen. Both samples transfected with the AiO-SaKKHABE8e performed marginally better than the dual vector

delivery when transfected with the same quantity of total DNA, achieving 50 ± 1.4% and 47 ± 2.8% editing for G1 and G2, respectively (Figure 6-9). The dual vector G1 remained consistent with prior transfections at 43.5±3.5% editing. Bystander editing at this site is unlikely given there is only one other targetable A at position 20 – no bystander editing was seen at this site in the *in vitro* screens.

To confirm expression of the AiO and dual vector SaKKH base editors, samples were run on a western blot (Figure 6-9) using an anti-SaCas9 antibody. An SaCas9 lysate with and without a guide were used as a positive control, but interestingly both the dual vector and AiO SaKKH showed stronger bands. The high rates of editing in the transcript analysis alongside strong observed protein levels of the base editors supports that the editing is likely from the DNA base editors rather than a secondary mechanism. Unfortunately, no mouse *ABCA4* plasmid was available for use in the lab to test for *ABCA4* knockdown by western blot.

6.3.2 Characterisation of mouse baseline measures

A baseline *ABCA4* expression profile of the wildtype 129S2/SvHsd, heterozygous, and *abca4*^{tm1Ght}/J knock-out mice was determined by qPCR, western blot and immunohistochemistry. RT-qPCR data showed a significant reduction (>50%) in *ABCA4* in the heterozygous mice compared to the wildtype mice ($p<0.0001$). Rhodopsin was targeted as a control and showed no significant difference between wildtype, heterozygous, and *mAbca4 -/-* mice (Figure 6-10a). Western blot analysis of neural retina extracts showed decreased ABCA4 protein levels in the heterozygous mouse relative to the wildtype (Figure 6-10c). Quantitation of western blot signal reflected the qPCR results, showing a substantial decrease in ABCA4 relative to the wildtype (Figure 6-10c).

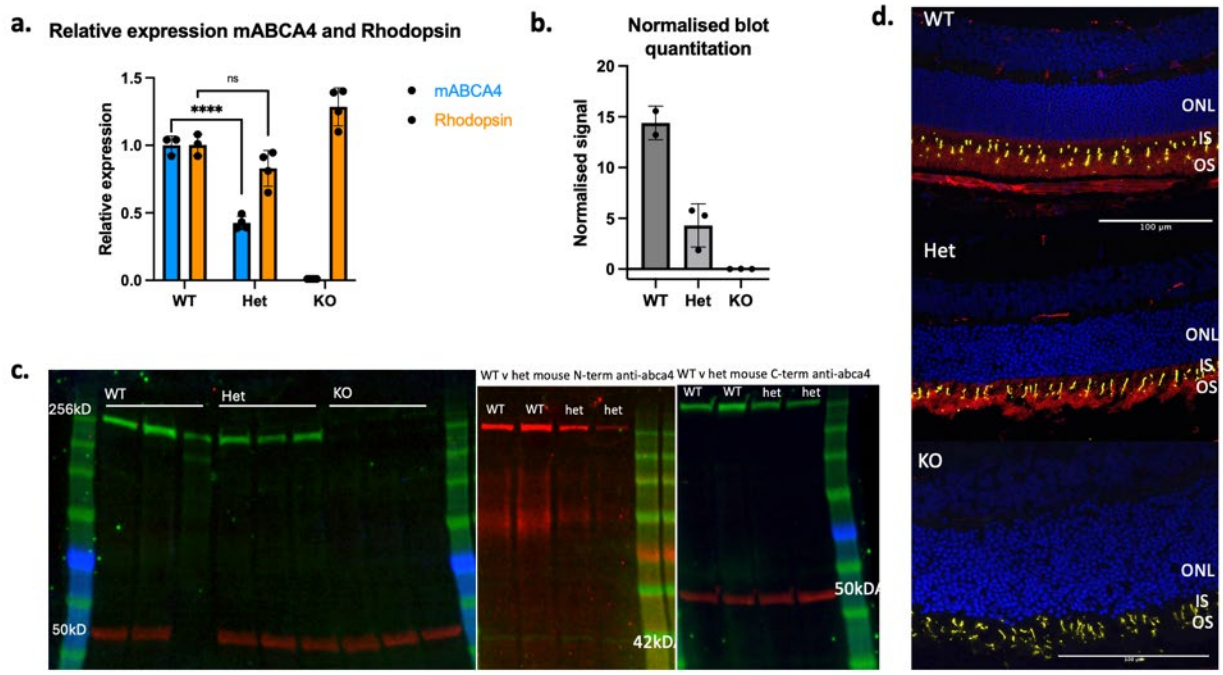

Figure 6-10: Baseline mouse model measures.
a. QPCR of *mABCA4* and Rhodopsin expression in wildtype (WT), het, and *Abca44 -/-* (KO) mice. *mABCA4* expression was significantly reduced ($p<0.0001$), whereas rhodopsin revealed no significant difference. Knockout mice showed no *mABCA4* but normal Rhodopsin expression. **b.** Western blot signal quantitation data normalised to the housekeeping protein showing substantially decreased mABCA4 in heterozygous mice and no mABCA4 in *mAbca4 -/-* mice. **c.** Western blots with observable reduction in mABCA4 in heterozygous mice and no mABCA4 in *mAbca4 -/-* mice. **d.** IHC staining detected mABCA4 in the outer segments of WT and het mice and no mABCA4 in *mAbca4 -/-* mice. All three show robust l-opsin staining (yellow). Mouse 3F4 monoclonal anti-ABCA4 (red). *note: gain may vary and partially explain the difference in observed background. This is discussed further in the Discussion.

Immunohistochemistry suggested potentially reduced staining of the outer segments using two different anti-ABCA4 antibodies (Figure 6-10d and Figure 6-11). For IHC, a dilution series was tested to determine the optimal antibody concentration (Figure 6-12). The 1:500 showed greater signal specificity, however, the 1:100 dilution showed stronger signal and had been successfully used in prior publications.[65] Due to this, the 1:100 antibody concentration was used in further experiments. The control samples, WT, het, KO samples typically exhibited less background than experimental samples.

While reduction in *ABCA4* expression in het mice was anticipated, such significant reduction was surprising. The knockout samples consistently showed no *ABCA4* expression or protein across qPCR, western blot, and IHC.

Lastly, PBS injected heterozygous eyes (injection control) showed robust ABCA4 staining (Figure 6-13). All experimental cohorts were compared to the pooled PBS-injected eyes (N=22).

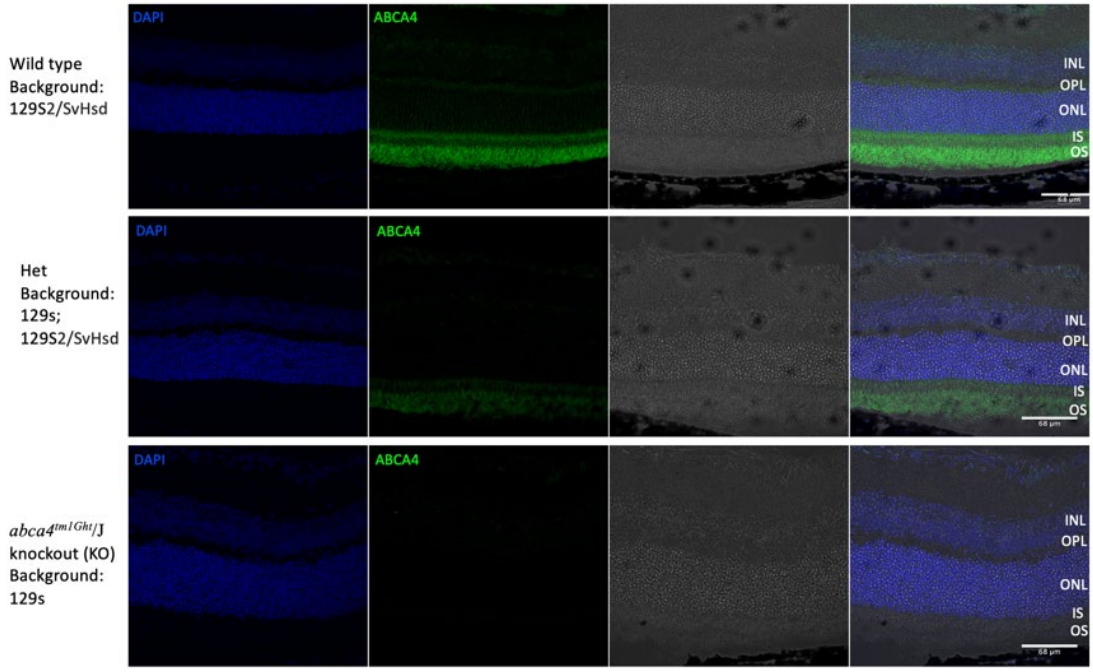

Figure 6-11: Baseline immunohistochemistry of mouse model using rabbit anti-ABCA4.
Retinal sections stained with rabbit anti-ABCA4 (ab72955) showing strong ABCA4 signal in the wildtype, reduced signal in the heterozygous mouse, and no signal in the knockout mouse. Typically, background was notably less in the control samples, including these, than in the experimental samples.

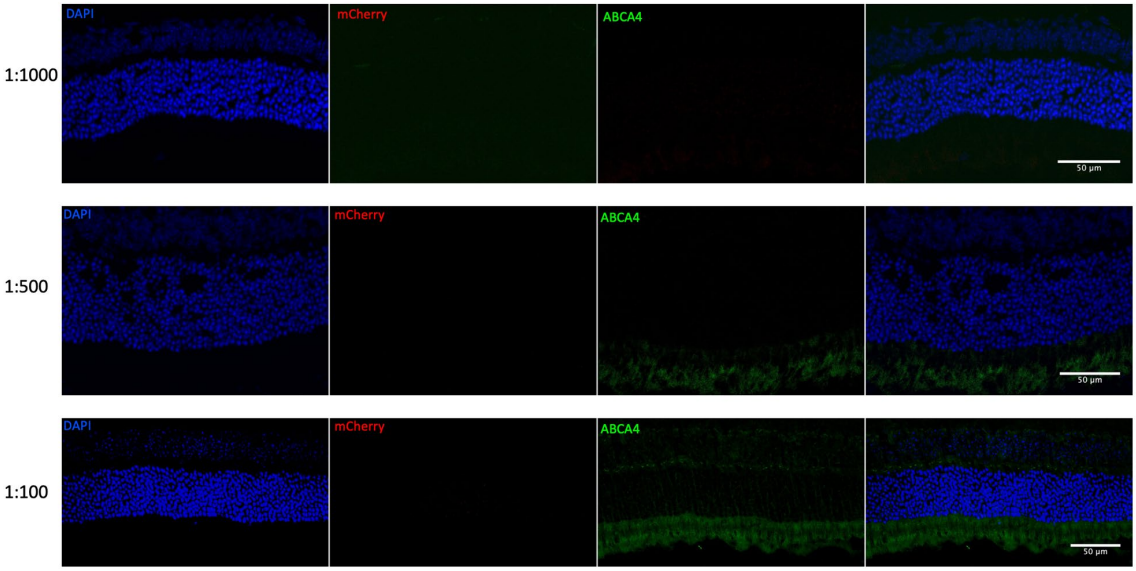

Figure 6-12: Dilution series in IHC staining with rabbit anti-ABCA4.

To determine an optimal antibody concentration to use for IHC, a dilution series was performed. While 1:500 shows greater specificity, the 1:100 samples showed stronger signal.

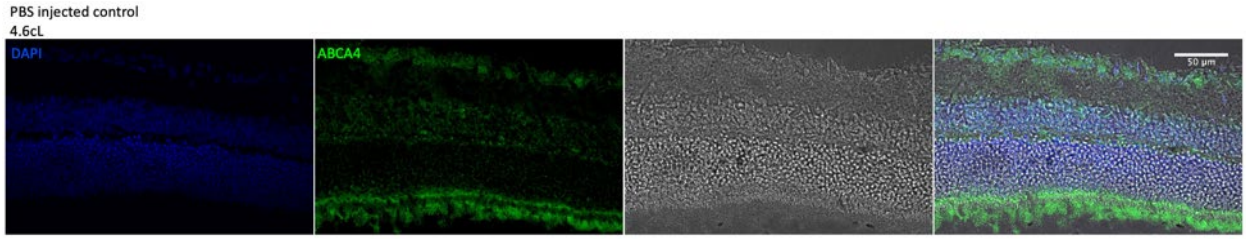

Figure 6-13: PBS injected control IHC.
The PBS injected eyes showed robust ABCA4 staining. All experimental samples were compared to the pooled PBS injected eyes. This is a representative example of the observed high background and mislocalisation seen in control samples, which requires further optimisation.

6.3.3 *In vivo* RNA base editing using dual vector RK-dPspC13b-del-ADAR$_{DD}$ to knock down *ABCA4*

6.3.3.1 On-target editing of *mABCA4* start codon by dual vector GRK1-dPspCas13b-ADAR$_{DD}$ and U6-gRNA-CAG-GFP strategy

A pilot study using a dual vector GRK1 driven dCas13b-del-ADAR$_{DD}$(E488Q) was undertaken to target the *mABCA4* start codon *in vivo*. A cohort of 16 heterozygous *abca4*$^{wt/KO}$ mice received bilateral injections of 1E+9vg/eye AAV-RK-dCas13b-del-ADAR$_{DD}$(E488Q) and 2.5E+8vg/eye AAV-U6-gRNA-CAG-GFP of either the targeting (G3) or non-targeting guide, or PBS. Injections were not paired. The dose was established by prior work done in the lab which observed GFP-related toxicity at 5E+8vg.[210] It was hypothesised that using a lower dose to reduce inflammation may enable editing rates consistent with the 5E+8vg dose given improved cell health. Imaging for vector-related inflammation was performed at 3-4 weeks post-injection. Eyes were imaged again at 9-11 weeks post-injection to allow for complete outer segment turnover post-AAV expression. Eyes were harvested and processed at this time point.

Deep sequencing by targeted NGS of cDNA amplicons was analysed in Crispresso2. Eyes injected with the targeting guide showed no detectable editing of the target ‘A’ to a ‘G’ to knockdown *mABCA4.* When comparing ‘modified’ to ‘unmodified’ reads which include background noise, there was no significant editing relative to the non-targeting and PBS controls (Appendix). Analysis by Crispresso2 of local off-target editing throughout the amplicon showed low level activity reaching a maximum of 2% for any given base, even in non-targeting controls (Figure 6-14a and e). QPCR of relative *mABCA4* expression indicated a decrease in relative

expression in both the targeting and non-targeting samples. Interestingly, the mean relative expression was lower in the non-targeting group than in the targeting eyes partly due to an outlier caused by surgical trauma. The lack of *mABCA4* expression reduction indicates both no observed knockdown and vector tolerance at a relatively high dose (1.25E+9vg/eye) (Figure 6-14b).

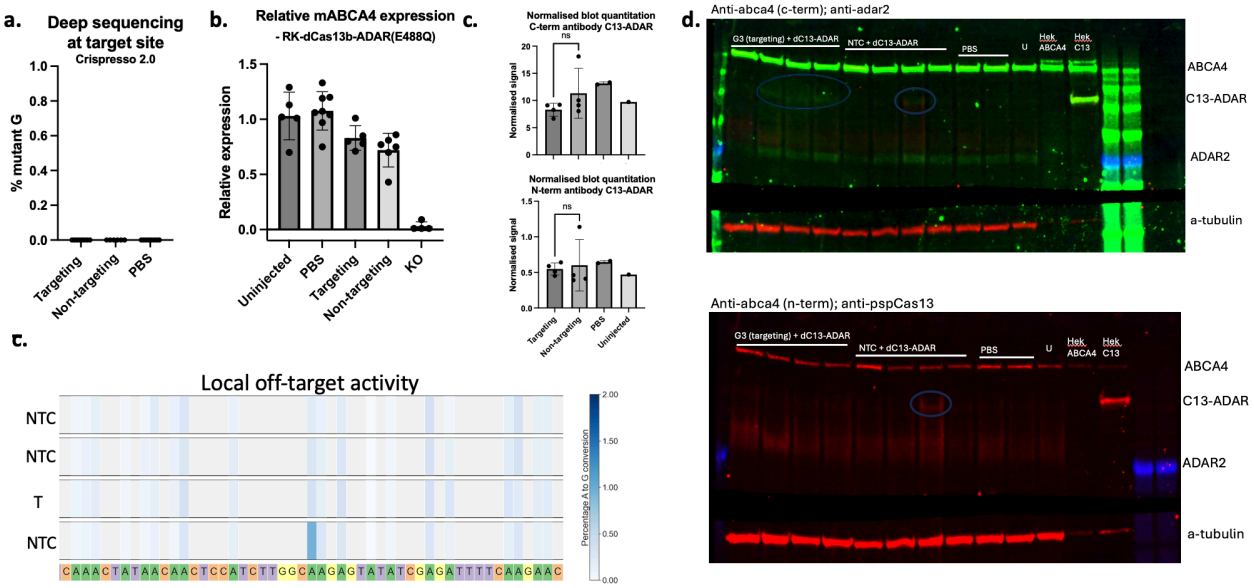

Figure 6-14: dCas13b-ADARdd(E488Q) analysis of targeting *ABCA4* start codon in vivo.
a. Deep sequencing of target amplicon at RNA level showing no on-target editing. **b.** QPCR of relative *mABCA4* expression normalised to *GAPDH* and *ACTB*. Both the targeting and non-targeting groups showed decreased relative expression, with the non-targeting samples showing a greater reduction. **c.** Quantitation of western blot signal for the C- and N- terminal anti-ABCA4 antibodies. There was no significant difference observed between targeting and non-targeting injected eyes. Samples were normalised to alpha-tubulin. **d.** Both: Western blots show no observable difference between targeting and non-targeting, PBS, and uninjected (U) eyes. (p=0.4857; p=0.2504) Top: Endogenous ADAR2 signal is seen in all retinal samples. Cas13-ADAR is seen in 4/8 injected eyes and the HEK293 containing Cas13-ADAR control (HekC13). Bottom: PspCas13b antibody works well for the cell sample (HekC13) but not *in vivo* samples with only one sample showing signal. e. Snapshot of local off-target activity throughout the amplicon in four samples. NTC= non-target control, T= targeting injected.

To explore the effect on mABCA4 protein levels, immunohistochemistry and western blot were performed on injected retinas. Western blots of both C-terminal and N-terminal anti-ABCA4 antibodies showed no observable knockdown between targeting and non-targeting, PBS, or uninjected eyes (Figure 6-14d). Fluorescence quantitation of western blots revealed no significant difference between targeting and non-targeting injected eyes with both the N- and C-terminal antibodies (p=0.4857; p=0.2504). Samples of HEK293T cells transfected with *ABCA4* or dCas13b-del-ADAR$_{DD}$(E488Q) were used as experimental controls. The anti-ADAR2 (RED1) antibody detected endogenous ADAR2 in all retina samples and faint bands corresponding to the

dCas13b-del-ADAR$_{DD}$(E488Q) HEK control band in 4/8 injected samples. The anti-dPspCas13b antibody had not been tested *in vivo* and only detected 1/8 injected samples, but robust signal in the Cas13-ADAR HEK293 control (Figure 6-14c).

Analysis by immunohistochemistry showed decreased levels of mABCA4 at the site of injection in both targeting and non-targeting injected eyes. In the non-targeting eye, mABCA4 reduction was likely due to high levels of GFP expression. The targeting injected eye showed substantially less GFP than the non-targeting injected eye, likely due to injection variability. The inferior retina exhibited robust mABCA4 expression and no GFP expression (Figure 6-15).

Taken together the data indicate that dPspCas13b-ADAR$_{DD}$(E488Q) did not edit the *mABCA4* start codon efficiently and thus did not knockdown *mABCA4* expression at this dose.

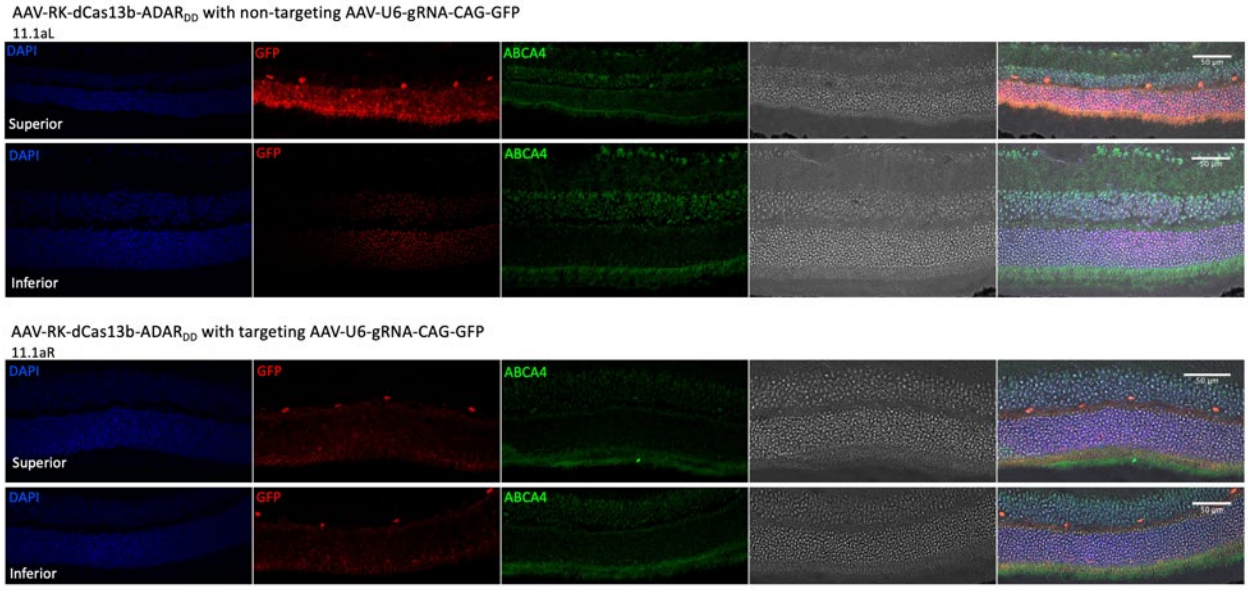

Figure 6-15: Immunohistochemistry of dCas13b-ADARdd injected eyes.
Top: Non-targeting injected eye showing strong GFP expression and reduced mABCA4 expression superiorly. Inferiorly, mABCA4 was observed with no GFP signal. **Bottom:** Targeting injected eye showing substantially less GFP than the non-targeting sample. A robust mABCA4 signal is seen both superiorly and inferiorly, linking mABCA4 signal with vector/GFP toxicity.

6.3.3.2 Analysis of expression of RK-dPspCas13b-del-ADAR$_{DD}$(E488Q) and U6-gRNA-CAG-GFP vectors

Since no editing at the target site was detected, experiments were undertaken to test for transgene expression. As described in 6.3.3.1, western blots of retinal lysates using two different antibodies targeting either dPspCas13b or ADAR2 were tested. Anti-ADAR2 detected what is presumed to be endogenous ADAR2 in all retina samples and faintly detected Cas13-ADAR

protein in 4/8 injected retina samples. The anti-dPspCas13b, however, only detected protein in 1/8 injected eyes (Figure 6-14d). Expression levels were likely influenced by surgical factors such as bleb size and the degree of surgical trauma.

To further confirm expression, Cas13-ADAR transcripts were amplified by RT-PCR from transduced retina from the RK promoter to the 3' end of ADAR2. The initial gel indicated bands of the correct size, but these were not sequenced due to band faintness (Figure 6-16b). A subsequent RT-PCR of the same samples indicated stronger amplification (Figure 6-16a) but shorter amplicons, including the positive control. These samples were Sanger sequenced and indicated full coverage except for the first ~200bp (Figure 6-16c). This may indicate a truncated vector amplified from contaminant DNA. However, Cas13-ADAR protein expression was observed by western blot in half of the samples, indicating likely full-length vector expression.

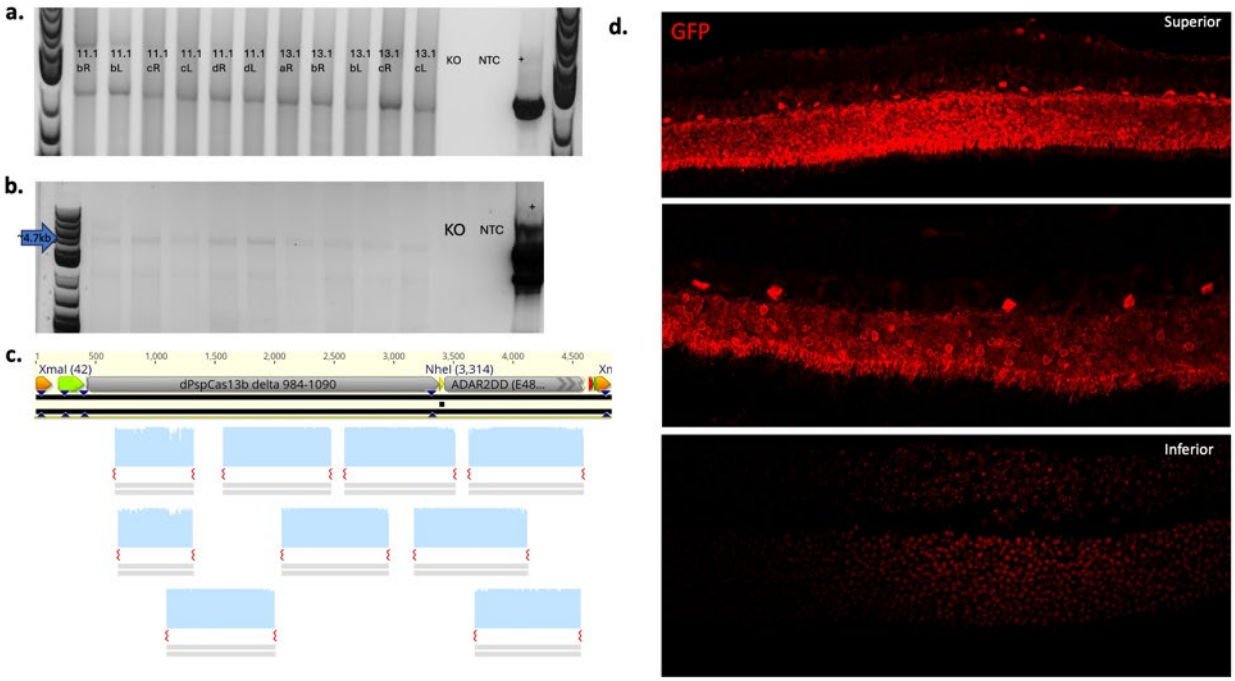

Figure 6-16: dCas13b-ADARdd expression confirmation.
a. RT-PCR of dCas13b-ADAR injected eyes. Number-letter code is the mouse ID. KO=knockout, NTC=non-target control, +=plasmid control. These stronger bands were excised and sent for Sanger sequencing **b.** Initial RT-PCR showing a faint but longer amplicon. **c.** Sanger sequence confirmation of dCas13b-ADAR injected eye. **d.** Strong GFP signal in IHC of dCas13b-ADAR with the non-targeting guide. Signal decreases with distance from the injection site.

U6-gRNA-CAG-GFP (gRNA-GFP) was detected by retinal imaging at 3-4 weeks post-injection and 9-11 weeks post-injection. GFP expression was further confirmed by IHC with robust expression in the outer segments and penetration into the outer nuclear layer. Stronger

expression was observed in the non-target control than the targeting guide (Figure 6-15 and Figure 6-16d).

6.3.3.3 Analysis of retinal structure in dual vector RK-dPspCas13b-del-ADAR$_{DD}$(E488Q) pilot

Imaging was performed at 3-4 weeks and 9-11 weeks post-injection. At the first timepoint, an expected surgery-related photoreceptor layer thinning in the injected superior retina relative to the inferior retina was observed in eyes injected with both the targeting (-16.27 $\pm$ 6.6%) and non-targeting guides (-19.8 $\pm$ 8.2%) (Figure 6-17). This was less than observed in the PBS injected eyes (-26.63 $\pm$ 7%). Although significant ($p<0.0001$), this was not surprising given the high occurrence of subretinal bleeds and haemorrhage seen in these mice despite a decreased injection volume of 1μL. Seven of the 22 PBS-injected eyes had a strong surgical response. At the second timepoint, targeting injected eyes showed negligible thinning compared to the first timepoint of -0.25 $\pm$ 1.9% ($p=0.9$) and non-targeting injected eyes showed signs of recovery with a significant +9.57 $\pm$ 2.8% ($p=0.0019$) gain in superior retinal thickness (Figure 6-17). Robust GFP expression was observed at both timepoints from the gRNA-GFP vector (Figure 6-18 and Figure 6-19). Inflammatory response was mouse dependent (Figure 6-18 Figure 6-19).

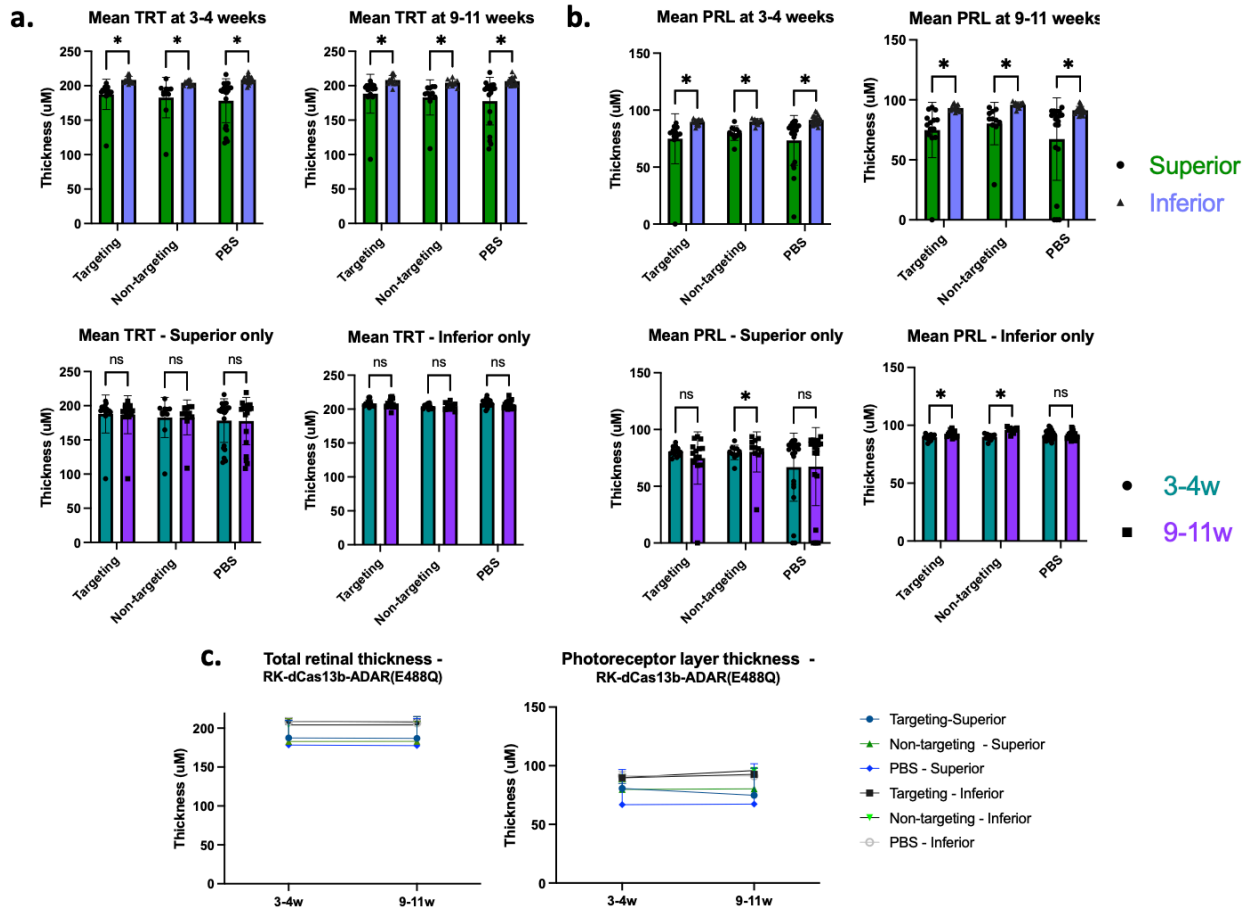

Figure 6-17: Retinal thickness measurements of dCas13b-ADARdd cohort.
a. Mean total retinal thickness measurements. Top: comparison of superior to inferior retina at each timepoint. All injection groups showed a significant difference at both timepoints. At 3-4 weeks, targeting (N=14, $p<0.0001$), non-targeting (N=11, $p=0.0005$), and PBS (N=22, $p<0.0001$), and at 9-11 weeks ($p<0.0001$). Bottom: Comparison of 3-4 week to 9-11 week timepoint of the superior and inferior retina. No significant difference was observed. **b.** Mean photoreceptor layer measurements. Top: comparison of superior to inferior retina at each timepoint. All groups showed a significant difference at both timepoints ($p<0.0001$). Bottom: Comparison of 3-4 week to 9-11 week timepoint of the superior and inferior retina. Comparison between timepoints resulted in a significant difference in non-targeting injected eyes ($p=0.002$) superiorly and a significant difference in targeting (0.021) and non-targeting ($p=0.00098$) injected eyes inferiorly between the timepoints. This was due to retinal thickening over time. Top: Mann-Whitney test, Bottom: Wilcoxon test. Data = mean ± SEM. **c.** A visual of superior and inferior measurements over time.

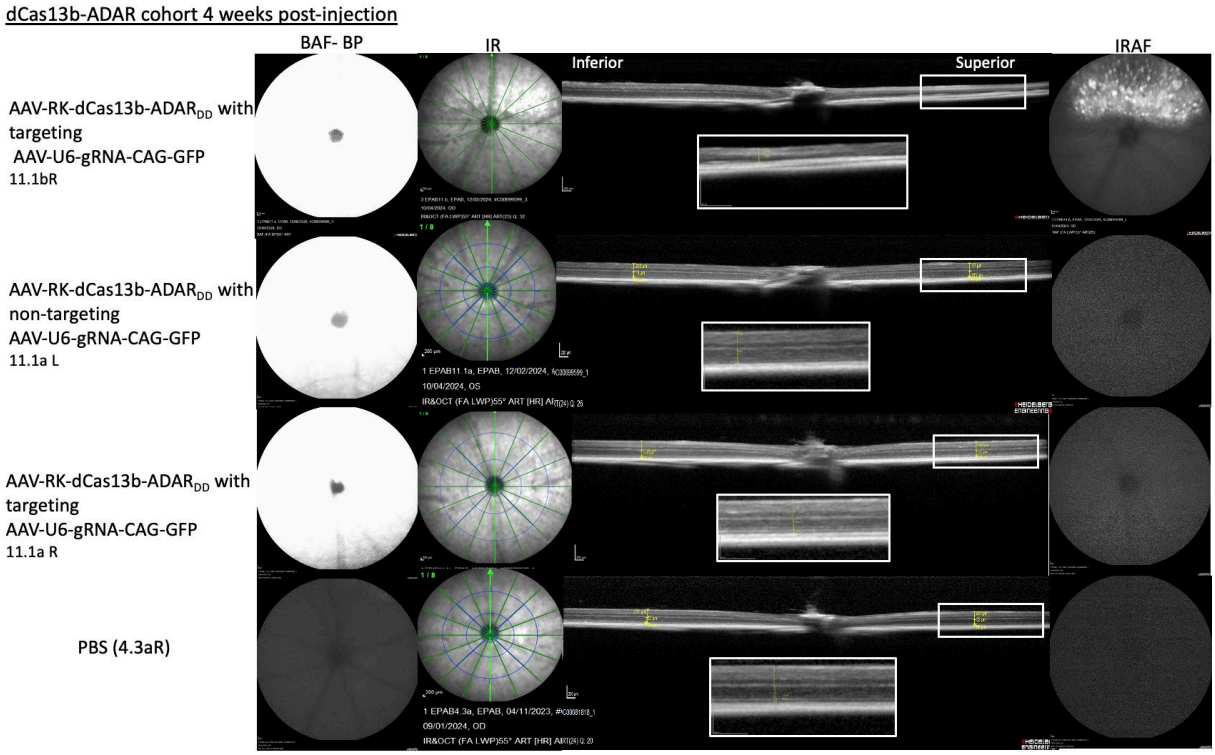

Figure 6-18: Representative images of dCas13b-ADARdd injected eyes 3-4 weeks post-injection.
OCT b-scans and *en face* cSLO images of representative targeting, non-targeting, and PBS injected eyes using blue autofluorescence (BAF), infrared (IR) reflectance, and infrared autofluorescence (IRAF) channels at 3-4 weeks post-injection. The top panel is a representative inflammatory response. The BAF channel showed strong GFP expression in all eyes injected with AAV-U6-gRNA-CAG-GFP and no fluorescence in the PBS injected eye. In the IR channel, the injection bleb was clearly visible in the top panel. The other vector-injected eyes showed no difference to the PBS injected eyes. Similarly, the OCT scans showed superior thinning and inflammation in the IRAF channel in the top panel. 11.1aL and 11.aR vector-injected eyes showed no observed difference to the PBS injected eye. The number-letter code is the mouse ID.

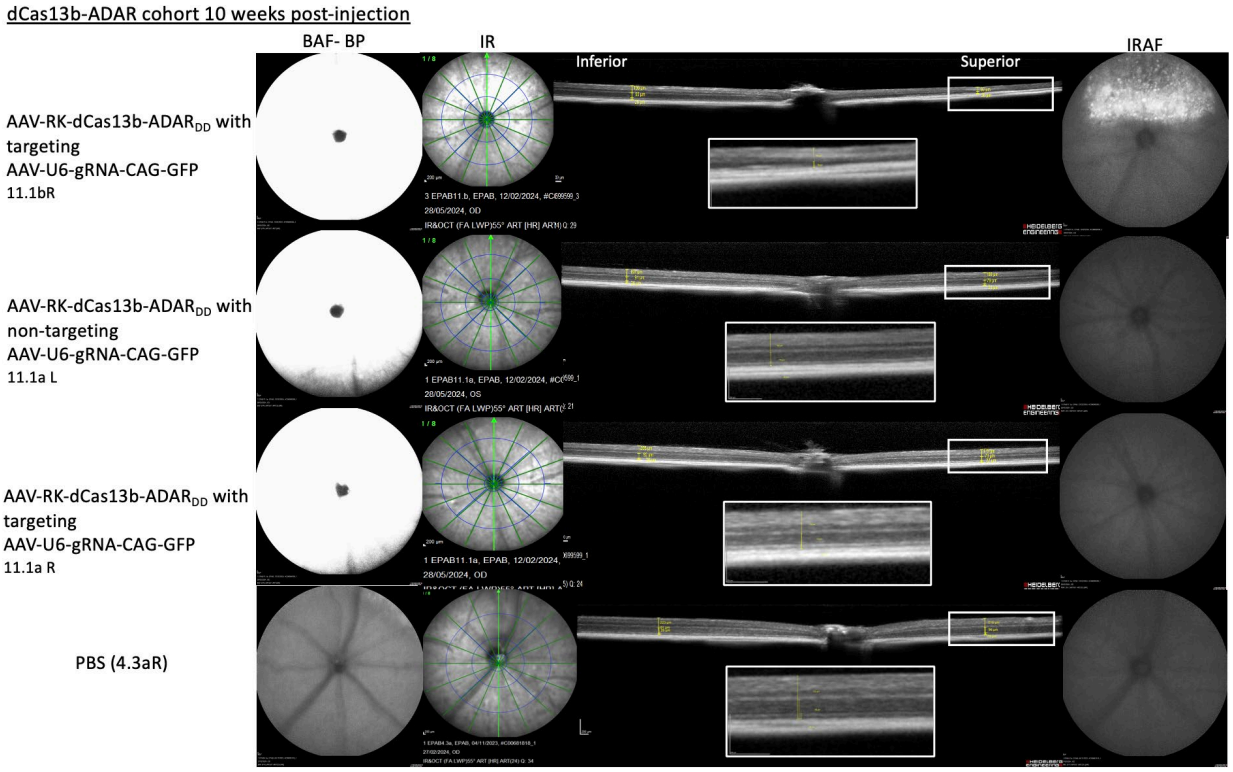

Figure 6-19: Representative images of dCas13b-ADARdd injected eyes 9-11 weeks post-injection. OCT b-scans and *en face* cSLO images of representative targeting, non-targeting, and PBS injected eyes using blue autofluorescence (BAF), infrared (IR) reflectance, and infrared autofluorescence (IRAF) channels at 9-11 weeks post-injection. GFP expression remained robust in all vector-injected eyes as seen by BAF channel. No observed inflammation or thinning relative to the PBS injected eyes in 11.1aL and 11.aR. The top row shows the injection bleb in the IR channel, continued superior retinal thinning (OCT), and continued inflammation (IRAF).

6.3.4 *In vivo* DNA base editing using a dual vector SaKKH-ABE8e to knock down *mABCA4*

To compare DNA and RNA base editing at the same target, a dual vector RK-driven SaKKH-ABE8e was tested. This was used alongside an AAV-U6-gRNA-SaScaff containing CAG-mCherry as the fluorescent marker. Two cohorts of mice received bilateral injections of RK-SaKKHABE8e and either the targeting or non-targeting guide, or PBS. The first cohort (high dose) received a mixture of 5E+8vg/eye of each AAV-RK-SaKKHABE8e and AAV-U6-gRNA-SaScaff-CAG-mCherry (U6-gRNA-SaScaff), totalling at 1E+9vg/eye. The second cohort (low dose) received a mixture of 5e+8vg/eye AAV-RK-SaKKHABE8e and 2.5E+8vg/eye AAV-U6-gRNA-SaScaff-CAG-mCherry totalling at 7.5E+8vg/eye. The slightly lower dose of the gRNA vector in the second cohort was a result of observed toxicity in the high dose cohort (6.3.4.4) and minimal observed toxicity with the all-in-one vector (6.3.5.4), suggesting toxicity due to

mCherry. Mice were imaged for toxicity at 3-4 weeks post-injection and at 9-11 weeks post-injection to allow for complete outer segment renewal post-treatment. Eyes were harvested and processed post-imaging at 9-11 weeks.

6.3.4.1 On-target editing of *mABCAa4* start codon by dual vector RK-SaKKHABE8e (5E+8vg/eye) and U6-gRNA-CAG-mCherry (5E+8vg/eye) strategy – high dose

Deep sequencing of retinal DNA amplicons from eyes injected with the targeting guide indicated significant editing of 6.17 ± 2.35% A>G (p=0.026) at the target site compared to the non-target control. Editing was highly injection dependent, though, with editing rates for the targeting guide ranging from 0.26-17.22%. At the cDNA level, deep sequencing of the same samples revealed an increased downstream effect, where 8.75 ± 3.7% of reads showed the desired A>G edit (p=0.0004). The non-target and PBS controls showed no editing at the target site at the DNA and cDNA levels (Figure 6-20a-b). Graphs showing background noise looking at modified versus unmodified sequencing reads can be found in the appendix. Analysis in Crispresso2 of local off-target editing within the amplicon indicated no off-target editing. Four samples showed low levels of ~1.8% off-target editing 40bp downstream of the editing window. However, this was not observed at the cDNA level.

Relative *mABCA4* expression analysis by qPCR revealed no significant difference in *mABCA4* expression between targeting and non-targeting samples (p=0.079) or PBS samples (p=0.15). However, this is likely due to injection variability. To distinguish between real knockdown of *mABCA4* and toxicity and surgical trauma, relative rhodopsin expression was also analysed. Eyes injected with the targeting guide showed equally decreased rhodopsin expression, indicating toxicity or surgical trauma as the likely reason for decreased expression. The non-target control showed relative *mABCA4* and Rhodopsin expression on par with PBS and uninjected samples (Figure 6-20d). Interestingly, cSLO imaging showed notably less vector expression in 4/14 non-targeting samples (Figure 6-29) and substantial retinal thinning (Figure 6-30).

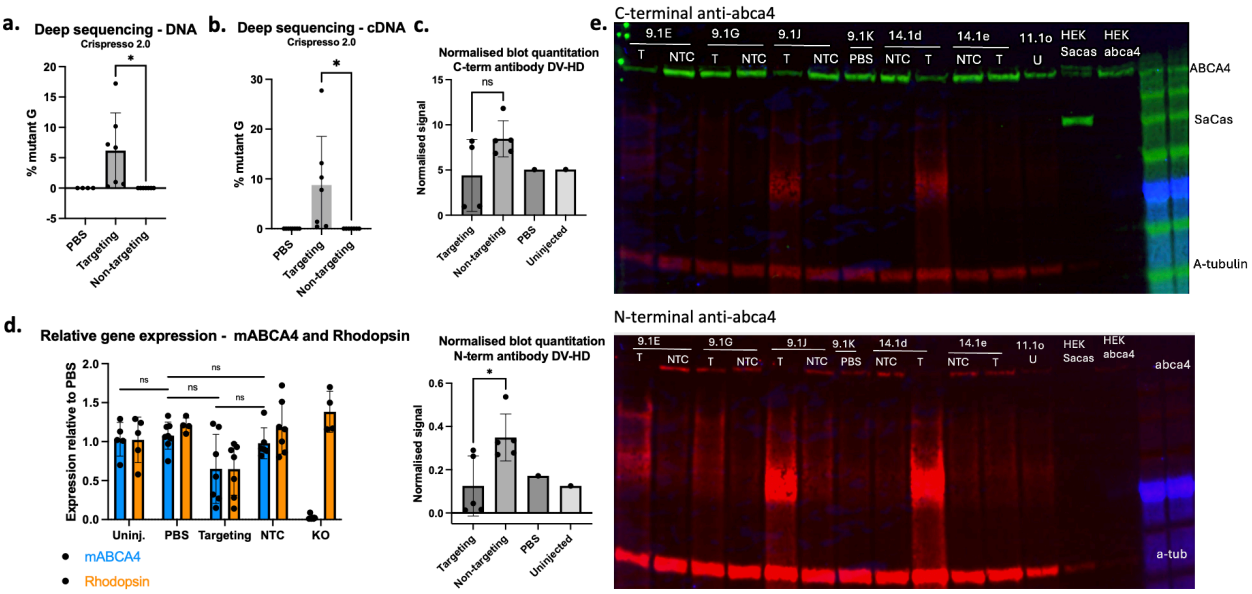

Figure 6-20: Molecular analysis of dual vector SaKKHABE8e high dose cohort.
a. NGS amplicon deep sequencing of editing at the DNA level showed significant editing of 6.17 ± 2.35% (p=0.026) compared to the non-target control. N=7. **b.** Analysis of the downstream effect of DNA editing at the RNA level, which showed 8.75 ± 3.7% of transcripts with the target A>G (p=0.0004). N=7. **c.** Quantitation of western blot signal for the C-terminal (top) and N-terminal (bottom) anti-ABCA4 antibody. No significant difference was observed between targeting (N=4) and non-targeting (N=5) samples with the C-terminal antibody (p=0.086). The N-terminal antibody did show a significant difference (p=0.0207). Unpaired t-test. **d.** QPCR relative gene expression of *mABCA4* and Rhodopsin. No significant difference was observed between targeting (N=7) and non-targeting (N=7) or PBS (N=6) samples, despite lower mean relative expression in targeting samples for both *mABCA4* and rhodopsin. Statistics performed on dCt values with one-way ANOVA. e. Western blot signals were visually reduced in most targeting samples relative to non-targeting samples. See quantitation. SaKKH was not seen in any samples. Number-letter codes are mouse IDs. T=targeting, NTC=non-targeting control, U=uninjected, Hek=hek293 control samples expressing *abca4* and/or SaKKH.

Analysis of protein levels by western blot showed strongly reduced mABCA4 bands in 3/5 mice relative to the non-targeting, PBS, and uninjected controls. Fluorescence quantitation revealed 47.8 % and 64.2 ± 17.78% mean reduction of signal in targeting injected eyes for the C- and N- terminal antibodies, respectively. This was not significant relative to the non-targeting control with the C-terminal antibody (p=0.0317) but was significant with the N-terminal antibody (p=0.0207). Given the SLO-OCT imaging results and the relative expression of *mABCA4* and rhodopsin, protein reduction was likely due to vector toxicity and inflammation. Specifically, the mice with reduced signal on the blot had no remaining photoreceptor layer. Interestingly, 9.1G indicated no reduction but also lost the photoreceptor layer. Further, no SaKKH was detected.

IHC showed no mABCA4 expression at the injection site of both targeting and non-targeting injected eyes due to extreme toxicity. The outer nuclear layer became progressively thinner until

absent, reflecting the observed thinning in OCTs (6.3.4.3). MCherry was not detected with the microscope possibly due to cell death (Figure 6-21). Inflammation build-up was visible when inspecting with the eye through the ocular lens (Figure 6-28). Inferiorly, staining of mABCA4 in the outer segments was stronger in the targeting eye than the non-targeting eye, contrary to western blot and qPCR outputs (Figure 6-21 and Figure 6-22). While background staining with the anti-ABCA4 antibody was strong, staining of the outer segments does not occur in knockout mice even with strong background.

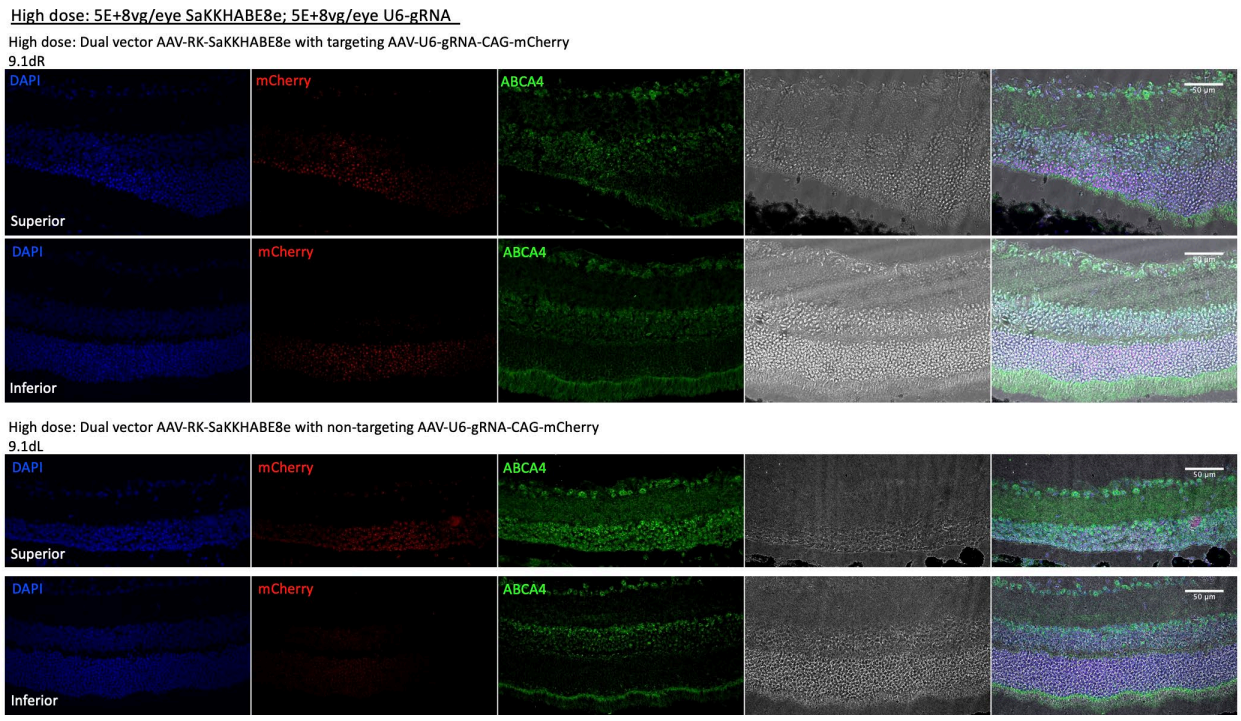

Figure 6-21: Dual vector SaKKHABE8e high dose cohort IHC at 40x.
Both targeting and non-targeting injected eyes displayed superior retinal thinning until complete extinction. Inferiorly, outer segment staining was observed more strongly in the targeting eye than the non-targeting eye.

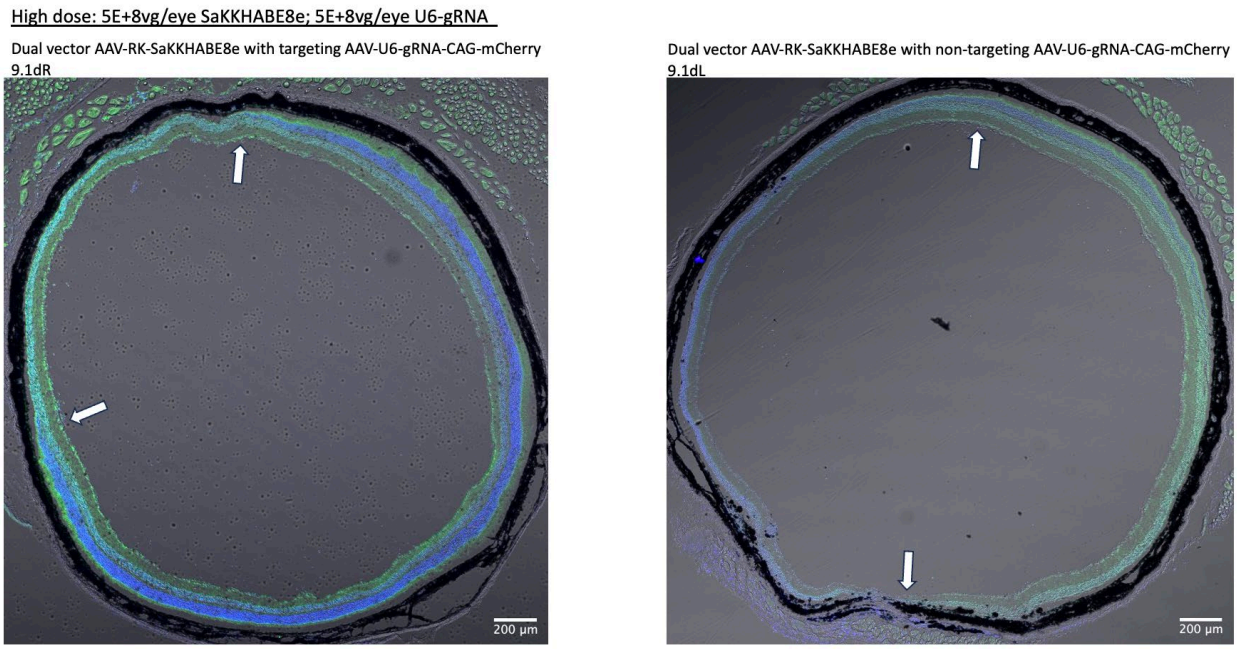

Figure 6-22: Dual vector SaKKHABE8e high dose IHC at 4x.
Both targeting (left) and non-targeting (right) eyes showed extreme thinning of the OS and ONL, indicated by the white arrows. Outer segment ABCA4 staining was seen inferiorly more robustly in the targeting eyes than non-targeting eyes.

6.3.4.2 On-target editing of *mABCA4* start codon by dual vector RK-SaKKHABE8e (5E+8vg/eye) and U6-gRNA-CAG-mCherry (2.5E+8vg/eye) strategy – low dose

Given the observed toxicity of the dual vector high dose hypothesised to be due to mCherry, a lower dose of 2.5E+8vg/eye of the gRNA-mCherry was tested. Deep sequencing of DNA amplicons of eyes injected with the targeting guide showed an expected reduction in editing compared to the higher dose, at 4.55 ± 1.99% on target editing (p=0.037). This corresponded to 8.07 ± 4.22% of the A>G edit at the cDNA level in the same samples (p=0.005) (Figure 6-23). The percentage of edited transcripts at the low dose was roughly the same as the high dose (8.75 ± 3.7%). The non-targeting control showed no editing at the target site or modifications above background. Analysis of local off-targets indicated low levels of activity at the DNA and cDNA level in 2/10 samples (Figure 6-23).

Relative expression of *mABCA4* and rhodopsin showed significantly decreased expression of *mABCA4* in targeting and non-targeting injected eyes, suggesting a toxic effect (p=0.0141; p=0.0164). This was reflected in SLO and OCT data between targeting and non-targeting eyes at both doses (Figure 6-30Figure 6-31). Although rhodopsin showed a notable reduction in mean

relative expression, this was not significant (Figure 6-23). The reductions reflected the observed thinning.

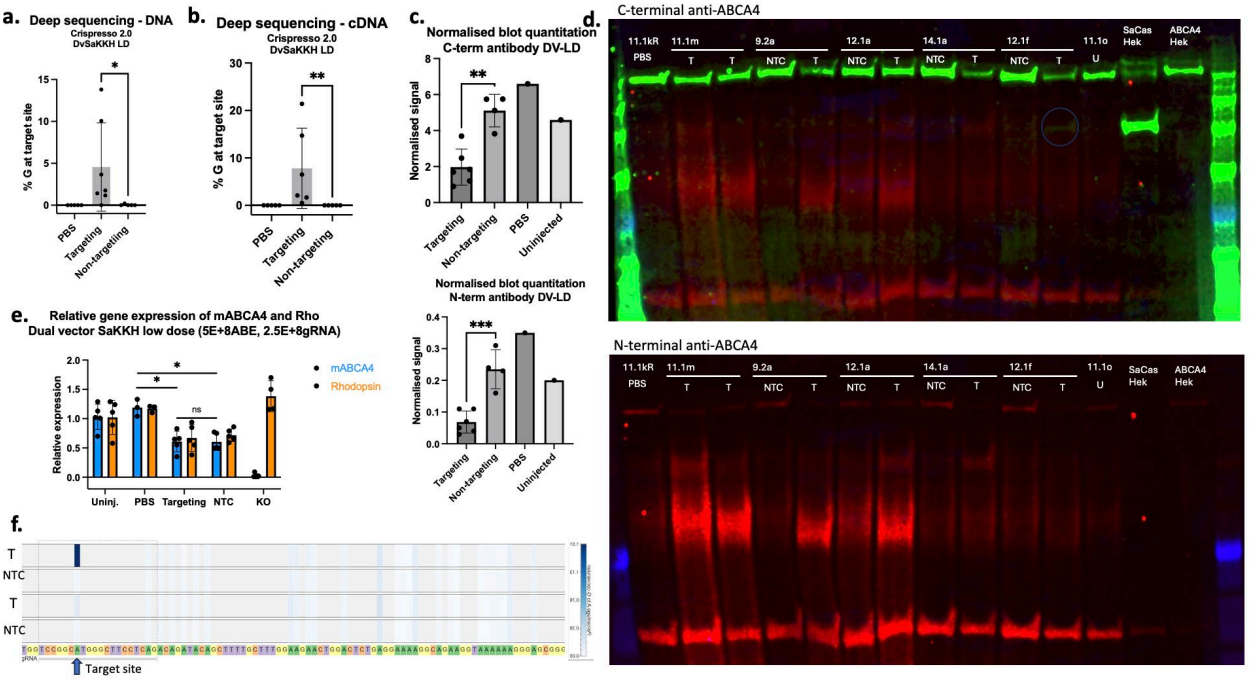

Figure 6-23: Molecular analysis dual vector SaKKHABE8e low dose cohort.
a. Deep sequencing revealed significant editing in targeting eyes relative to non-targeting eyes of 4.55 ± 1.99% (p=0.037, N=7). **b.** Analysis of the downstream effect of DNA editing at the RNA level, showed 8.07 ± 4.22% of transcripts with the target A>G (p=0.005, N=6). Kruskal-Wallis test was used for editing rate analysis. **c.** Western blot quantitation indicated a significant reduction in ABCA4 in targeting (N=6) compared to non-targeting (N=5) injected eyes with both the C- and N-terminal antibodies (p=0.001, p=0.0005). Unpaired t-test. **d.** Western blots of both C- and N- terminal antibodies with visible reduction in ABCA4 compared to non-targeting and PBS injected eyes. SaKKH was detected in one sample. HEK293 samples were used as positive controls. **e.** Relative *mABCA4* and rhodopsin expression. Targeting (N=5) and non-targeting (N=5) injected eyes showed significant reduction in *mABCA4* expression compared to PBS eyes (p=0.0141, p=0.0164; one-way ANOVA). Rhodopsin showed similar reductions, but this was not significant (p=0.5136, p>0.99; Kruskal-Wallis test). Statistics performed on dCt values. **f.** Crispresso2 output of a portion of the amplicon exhibiting off-target activity. The grey dotted box indicates the guide region. T=targeting, NTC= non-targeting, U= uninjected.

Western blots using N- and C- terminal anti-ABCA4 antibodies showed observable reduced fluorescence signal in targeting samples, albeit not as notably as in the high dose samples. Interestingly, fluorescence quantitation showed a significant difference in signal between targeting and non-targeting injected eyes with both antibodies (p=0.0005, p=0.001). The mean signal showed a 61.5 ± 19.7% and 70.9 ± 6.06% mean reduction in the targeting injected eye relative to non-targeting injected eyes for the C- and N- terminal antibodies, respectively. SaKKH was detected in 1 of 8 samples (Figure 6-23).

Further protein analysis with immunohistochemistry displayed outcomes as seen in the higher dose. Both targeting and non-targeting injected eyes similarly showed minimal ABCA4

staining, reduced DAPI, and complete thinning of the ONL at the site of injection. The inferior retina exhibited substantially greater ABCA4 staining and robust DAPI staining. However, as seen previously, background was high (Figure 6-24 and Figure 6-25).

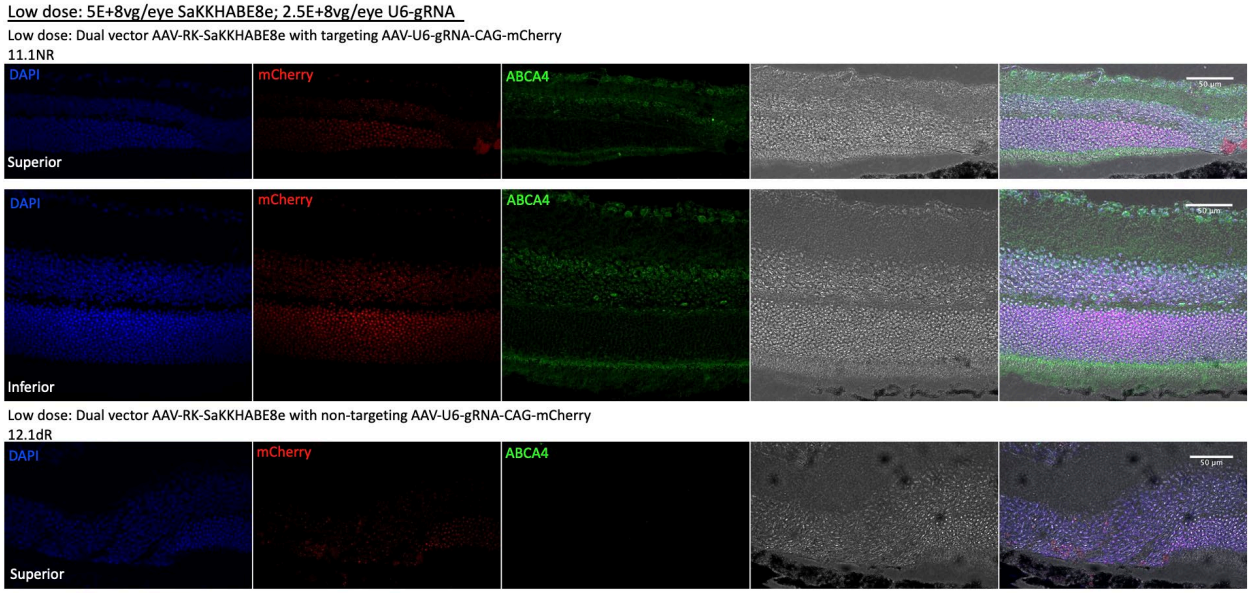

Figure 6-24: Dual vector SaKKHABE8e low dose cohort IHC at 40x.
Both the targeting and non-targeting eyes showed thinning of the ONL until complete extinction, as seen in the high dose. No mABCA4 signal was detected in the non-targeting eye, whereas there was significant background in the targeting eye. The targeting eye showed potential mCherry expression. The inferior retina showed stronger ABCA4 signal and consistent staining.

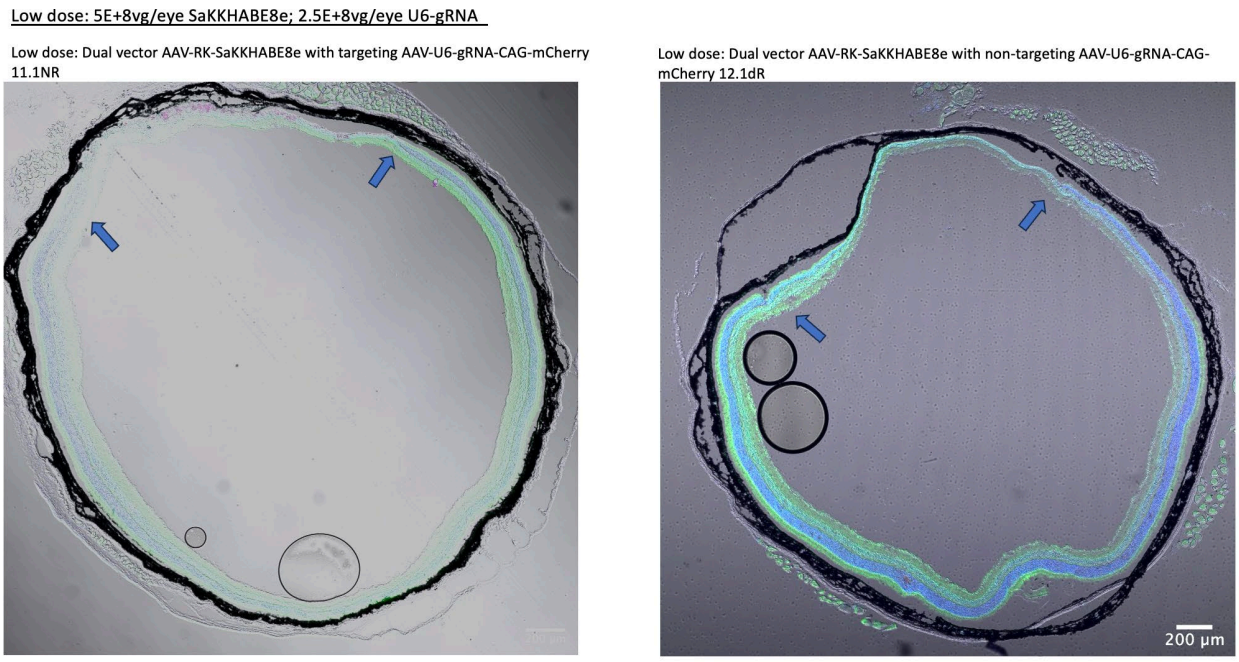

Figure 6-25:Dual vector SaKKHABE8e low dose cohort IHC at 4x.

Both eyes displayed substantial thinning indicated by blue arrows, as seen in the high dose samples. Inferiorly, outer segment staining of mABCA4 was robust. Samples displayed high background; however, this was not observed in the secondary only or knockout samples.

6.3.4.3 Analysis of vector expression – dual vector SaKKHABE8e

Expression of the transgene was confirmed at the DNA, RNA, and protein level. The SaKKH transgene was amplified from extracted retinal DNA and sequenced to determine transduction. Sequencing results of both ends of the transgene showed alignment without error (Figure 6-41). Subsequent qPCRs at both doses indicated significant expression of both the SaCas and guide scaffold in targeting and non-targeting eyes relative to PBS and uninjected eyes (Figure 6-28) ($p<0.0001$; $p=0.0004$). Specifically, the high and low dose both received 5E+8 of SaKKH, which was reflected in the roughly equal mean observed expression across doses in the targeting (7.55 ± 0.68; 8.18 ± 1.03) and non-targeting samples (8.96 ± 1.2; 7.81 ± 0.85). Interestingly, the expression of the gRNA was higher in the low dose than in the high dose, possibly due to marginally improved retinal health and thus expression (Figure 6-28). The PBS samples showed occasional low-level expression of SaCas and scaffold, indicating a small degree of contamination in some qPCRs, however, this was not significant ($p=0.96$).

At the protein level, western blot revealed signal of SaKKH in one low dose sample and none in the high dose samples indicating low expression levels in surviving cells and injection variability (Figure 6-23). MCherry was visible when harvesting the retina (Figure 6-28). Further, strong expression of mCherry was observed in imaging and likely resulted in retinal thinning. Interestingly, mCherry did not fluoresce in immunohistochemistry, albeit an mCherry specific antibody was not used. This was due to presumed cell death given that DAPI signal was also lower near the injection site compared to the inferior retina.

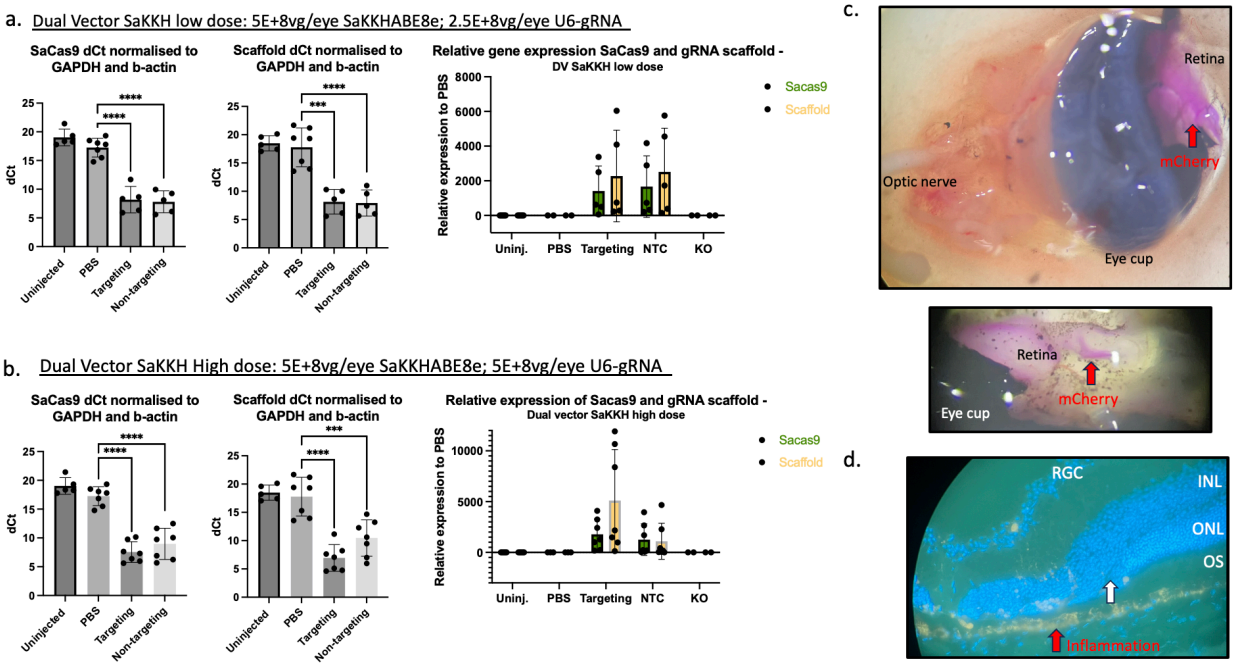

Figure 6-26: Molecular analysis of AAV expression - dual vector SaKKHABE8e.
a. qPCR analysis at the low dose showed significant expression of SaCas and gRNA-Scaffold in both targeting (N=5; p<0.0001) and non-targeting (N=5; p<0.0001) samples. Closer to zero equates to greater expression. **b.** qPCR analysis at the high dose showed significant SaCas and gRNA scaffold expression in both targeting (N=7; p<0.0001) and non-targeting (N=7; p<0.0001; p=0.0004) samples. Guide expression was greater in the low dose samples. Normalised to *GAPDH* and *ACTB*. Relative expression shown for easier visualization. Statistics performed on dCt values. **c.** mCherry expression was visible during dissections – injection/expression variability also visible between eyes. **d.** Thinning of the ONL and OS, alongside inflammation build-up.

6.3.4.4 Analysis of retinal structure – dual vector SaKKHABE8e

Imaging was performed at 3-4 weeks and 9-11 weeks post-injection. Eyes injected with the targeting and non-targeting guides showed robust mCherry expression at both the high and low dose (Figure 6-27 and Figure 6-28). MCherry was typically tolerated at the first timepoint but became increasingly toxic over time and resulted in extreme thinning. While this could also be due to SaKKH, the observed toxicity in the all-in-one SaKKHABe8e injected eyes was significantly less than in the dual vector injected eyes (Discussed more below). Vector impurity could have a toxic effect.

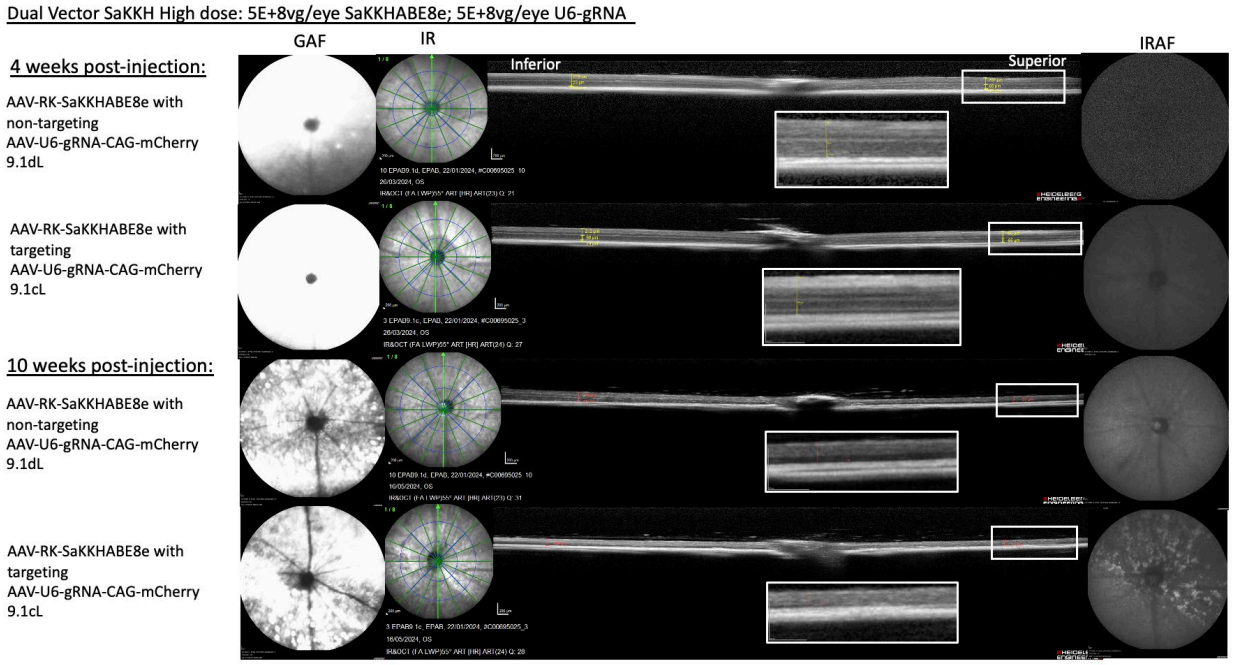

Figure 6-27: Representative cSLO and OCT images of dual vector SaKKH at the high dose.
CSLO and OCT images of representative high dose targeting and non-targeting dual vector SaKKH injected eyes at both timepoints. Robust mCherry was seen at 4 weeks and 10 weeks post-injection with the GAF channel. (Note: week 10 GAF images are at a lower sensitivity to show that the expression is in the inferior retina. At full sensitivity (106), the image was completely white). This was observed by OCT alongside extreme superior and inferior retinal thinning. Autofluorescence due to inflammation is not visible (IRAF) at 4 weeks but seen at 10 weeks. In 9.1cL, the IR channel shows the outline of the bleb at both timepoints, with damage seemingly forming by 10 weeks.

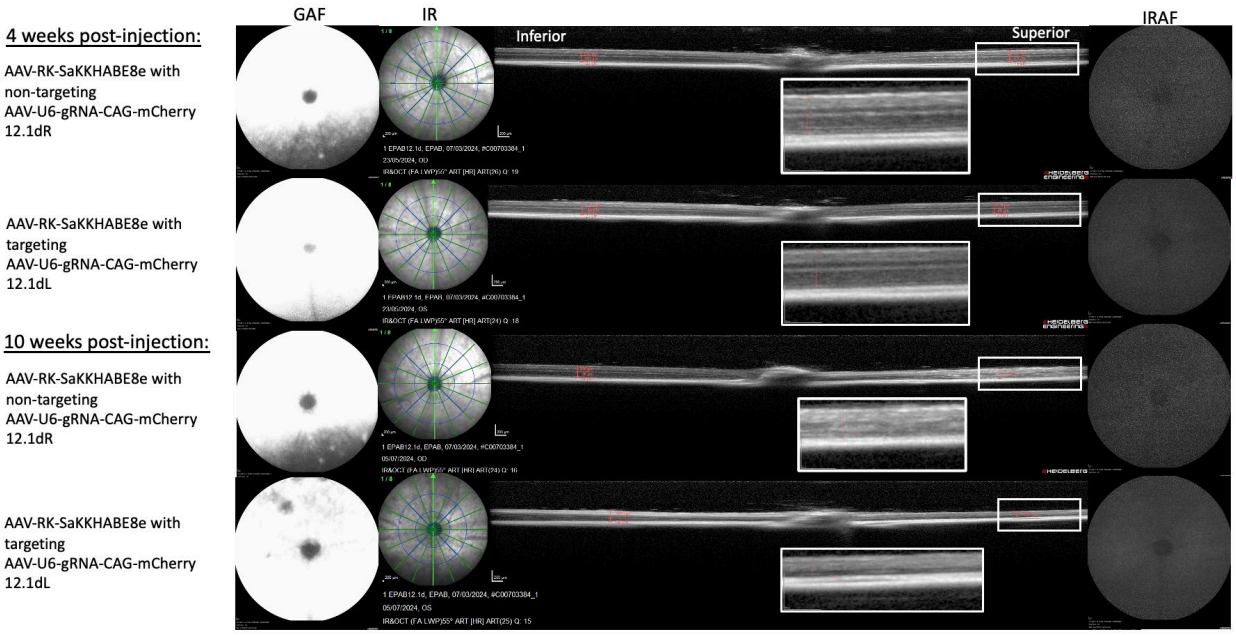

Figure 6-28: Representative cSLO and OCT images of dual vector SaKKH at the low dose.
CSLO and OCT images of representative low dose targeting and non-targeting dual vector SaKKH injected eyes at both timepoints. Robust mCherry expression is seen across both timepoints, although non-targeting expression is

less than the targeting vector**.** Outlines of blebs are visible in the IR channel. Significant retinal thinning is seen by OCT superiorly by 10 weeks. Inferior thinning is not as drastic as seen at the high dose. The IRAF channel shows no signs of inflammation.

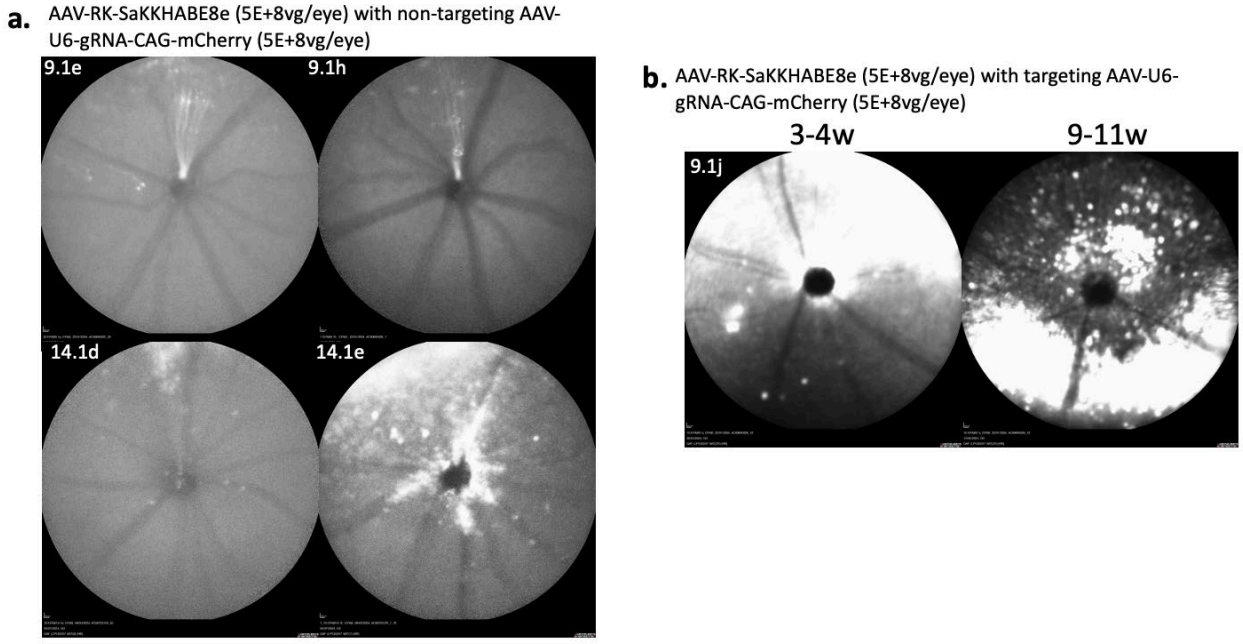

Figure 6-29: Dual vector SaKKH high dose cSLO images of injection variability.
a. The non-targeting vector showed substantial injection variability where 4/14 injected eyes minimally expressed in a cone shape. This could be due to failed injections going intravitreally**.** 14.1e is shown as an in-between expression level to demonstrate the degree of possible injection variability. This may have hit the optic nerve due to the unusual spread. **b.** At the high dose, mCherry expression could be seen strongly expressed inferiorly by 10 weeks.

Surgical thinning occurred at both doses in the targeting (High: 15.64 ± 4.5%; Low: 24.96 ± 8%) and non-targeting (High 13.33 ± 4.2%; Low: 20.95 ± 9.1%) samples (Figure 6-30 and Figure 6-31). Although more than accepted (~10%) surgical thinning, these were at or below the observed surgical thinning in PBS samples. Over time the targeting and non-targeting samples had a highly toxic effect resulting in photoreceptor layer thinning of 75.15 ± 12.98% ($p=0.002$) and 34.04 ± 13.7% ($p=0.2$) at the high dose (Figure 6-30) and 76.1 ± 8.3% ($p<0.0001$) and 44.2 ± 13.6% ($p=0.098$) at the low dose, respectively (Figure 6-31). However, only the targeting guide resulted in significant thinning. There was no significant difference in thinning between the low and high dose at either timepoint (Appendix).

In addition, substantial thinning was seen in the inferior retina at both doses, with greater thinning observed at the high dose. Specifically, the high dose (Figure 6-30) showed thinning of 28.62 ± 11.3% in the targeting ($p=0.007$) and 3.92 ± 3.94% in the non-targeting ($p=0.64$) eyes compared to 20.94 ± 6.3% ($p<0.0001$) and 13.19 ± 9.01% ($p=0.066$) at the low dose (Figure

6-31). This suggests a more toxic effect from the targeting vector. Similarly, there was no significant difference between the high and low dose in inferior photoreceptor layer thickness at both timepoints (Appendix).

Inflammation of the RPE seen in the IRAF channel on cSLO was observed at the high dose in 8/14 targeting and 3/14 non-targeting eyes at 9-11 weeks. At the low dose, 4/9 non-targeting and 11/16 targeting eyes exhibited autofluorescence due to inflammation of the RPE.

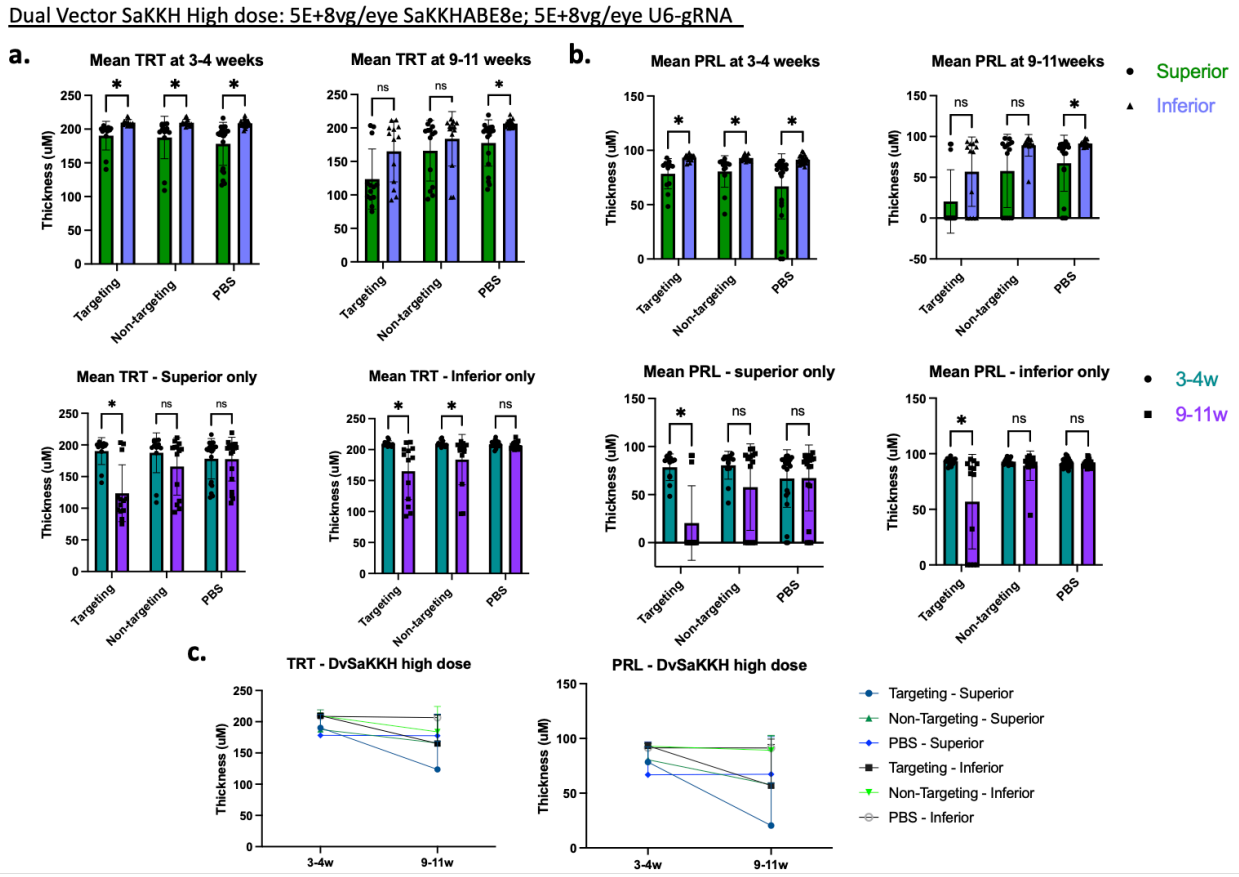

Figure 6-30: Dual vector SaKKH high dose retinal structure analysis.
a. Mean total retinal thickness (TRT) comparing superior to inferior thickness (top) and between timepoints (bottom). Significant thinning was seen particularly by 10 weeks, where this extended to inferior thinning. **b.** Mean photoreceptor layer (PRL) thinning comparing superior to inferior (top) and between timepoints (bottom). Significant thinning was observed in all groups at 3-4 weeks comparing superior to inferior thickness. Comparing between the timepoints, only the targeting guide showed significant thinning but both superiorly (p=0.002) and inferiorly (p=0.007). **c.** Visual representation of superior and inferior measurements at both timepoints. a. and b. Top: Mann-Whitney test Bottom: Wilcoxon test.

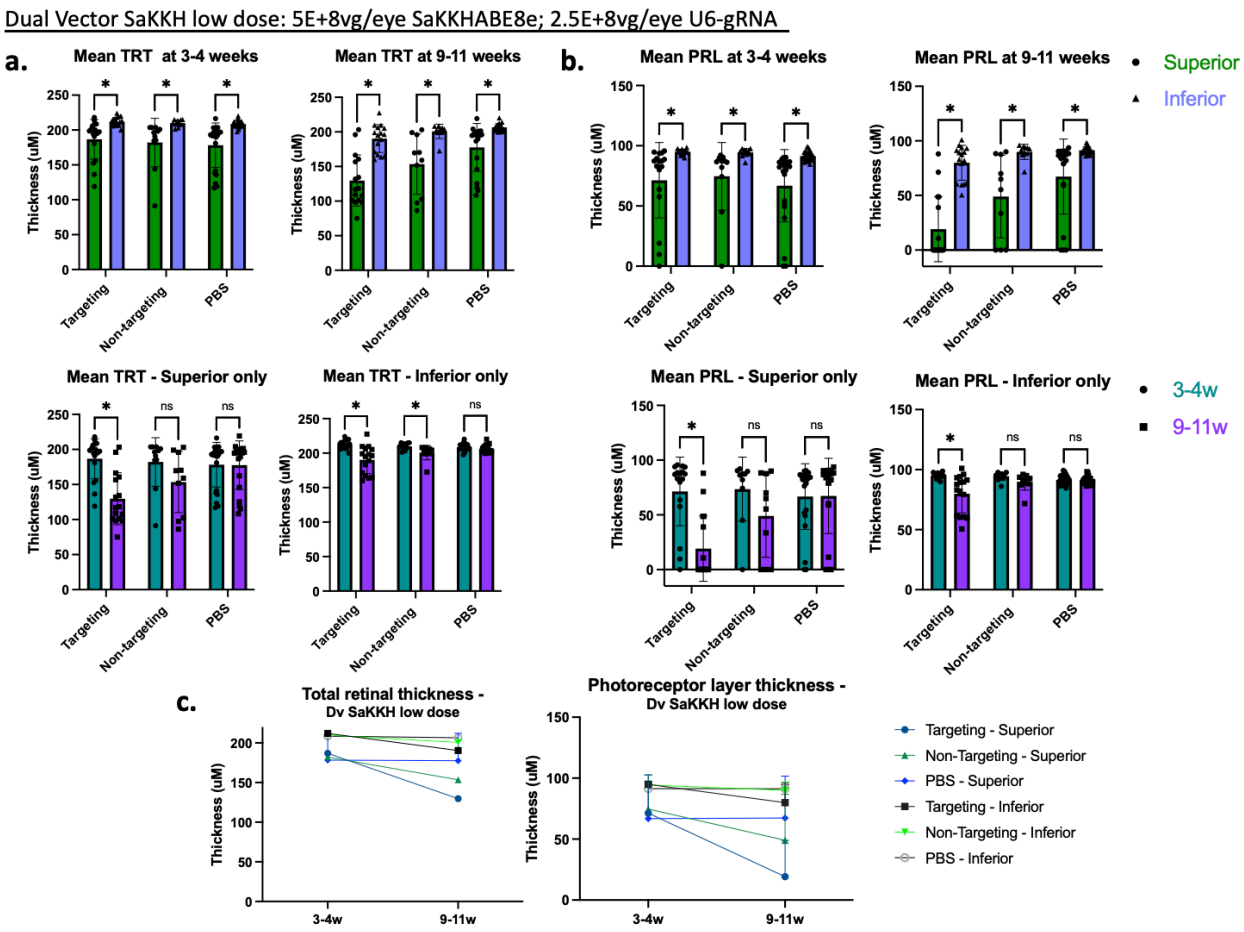

Figure 6-31: Dual vector SaKKH low dose retinal structure analysis.
a. Mean total retinal thickness (TRT) comparing superior to inferior thickness (top) and between timepoints (bottom). Top: All groups at both timepoints showed significant thinning when comparing the superior to inferior mean TRT. Bottom: The targeting injected eye showed significant thinning both superiorly and inferiorly. Interestingly, the non-targeting guide only showed significant thinning inferiorly. **b.** Top: Mean PRL also showed significant thinning when comparing superior to inferior thickness in all groups, including PBS injected eyes. Bottom: Only the targeting guide showed significant thinning both superiorly ($p<0.0001$) and inferiorly ($p<0.0001$). **c.** Visual representation of superior and inferior measurements at both timepoints. a. and b. Top: Mann-Whitney test Bottom: Wilcoxon test.

Lastly, to investigate the toxicity of the individual vectors, eyes were injected bilaterally with the targeting guide in one eye and the SaKKH in the other eye, each at 1E+9vg/eye. Eyes were imaged at 3-4 weeks. Minimal inflammation was observed (Figure 6-32).

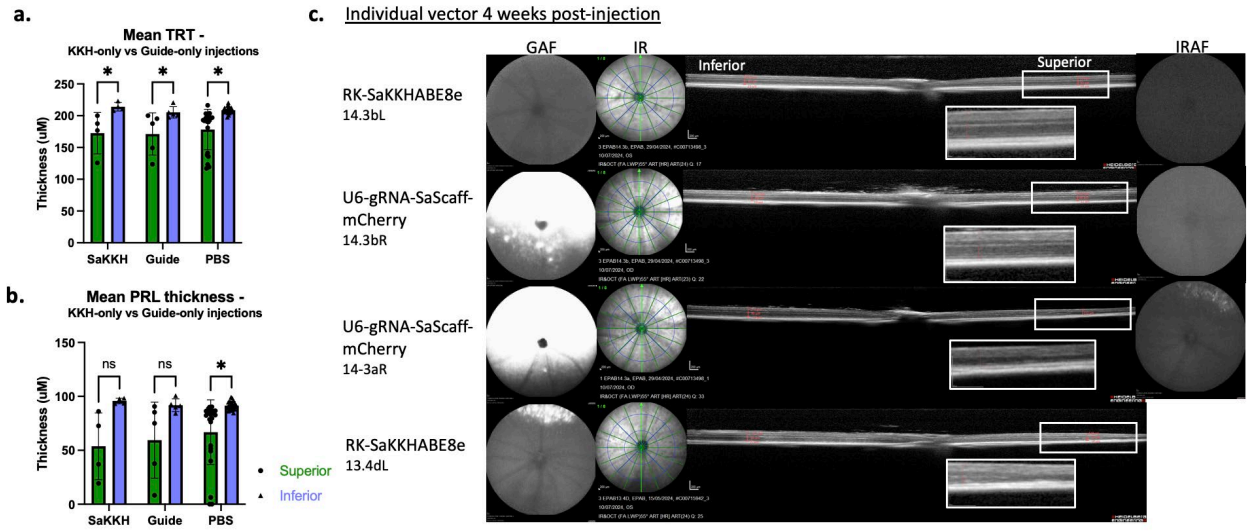

Figure 6-32: Representative images of toxic response of individual vectors SaKKH and U6-gRNA-SaScaff. **a.** Mean total retinal thickness (TRT) comparing superior to inferior TRT. All groups exhibited a significant difference, although this was consistent with PBS eyes. **b.** Mean photoreceptor layer thickness comparing superior to inferior PRL. Only PBS eyes showed a significant difference (N=22), however, the SaKKH-only and gRNA-only eyes showed notable injection variability. a. and b. Injections consisted of only SaKKH or only U6-gRNA-SaScaff at 1E+9vg/eye. Measurements were taken at 4 weeks post-injection. c. cSLO images at 4 weeks post-injection. SaKKH eyes showed no mCherry expression but inflammation and thinning in 13.4dL. The U6-gRNA injected eyes showed robust mCherry expression. One eye exhibited inflammation and thinning.

6.3.5 *In vivo* DNA base editing using an all-in-one SaKKH-ABE8e to knock down *mABCA4*

Ideally, a retinal gene therapy would be delivered in one vector for optimised efficiency and allow for a lower possible dose. Here, a size-optimised all-in-one RK-SaKKHABE8e-U6-gRNA was tested targeting the *mABCA4* start codon to compare to the dCas13b-ADAR$_{DD}$(E488Q) and dual vector SaKKHABE8e approaches. The construct is described in detail in the general methods and Chapter 6 methods. Two cohorts of mice received bilateral injections of either a non-targeting or targeting guide, or PBS. The first cohort received 1E+9vg/eye (high dose) and, after observed inflammation, the second cohort received a reduced dose of 5E+8vg/eye (low dose). A fluorescent protein was not co-delivered due to the hypothesised toxicity and to enable apt testing of the delivery of a single vector. The same protocol was followed where imaging was performed at 3-4 weeks and 9-11 weeks post-injection, and eyes were harvested and processed.

6.3.5.1 On-target editing of *mABCA4* start codon by all-in-one RK-SaKKHABE8e-U6-gRNA – high dose 1E+9vg/eye

Deep sequencing at the target site detected 15.29 ± 4.28% mean editing (N=9, p=0.0019), with editing at the target site reaching up to 32.35% at the DNA level. This corresponded to a significant mean of 23.41 ± 5.68% (N=9, p=0.0004) of the intended A>G edit at the cDNA level but reached up to 47.25% (Figure 6-33). Target-site specific analysis showed no editing in PBS or non-targeting injected eyes. Editing rates varied likely due to injection variability. When analysing modified versus unmodified reads, eyes injected with targeting guides showed significant editing above background observed in PBS and non-targeting injected eyes (Appendix).

Relative expression of both *mABCA4* and rhodopsin decreased in the targeting and non-targeting control. However, only the reduction in *mABCA4* with the targeting guides showed significance (N=9, p=0.037) when compared to PBS-injected eyes. None of the reductions in rhodopsin were significant (Figure 6-33), as in the dual vector cohorts (Figure 6-23 Figure 6-20). However, the mean reductions were notably less, reflecting the improved tolerability of this vector.

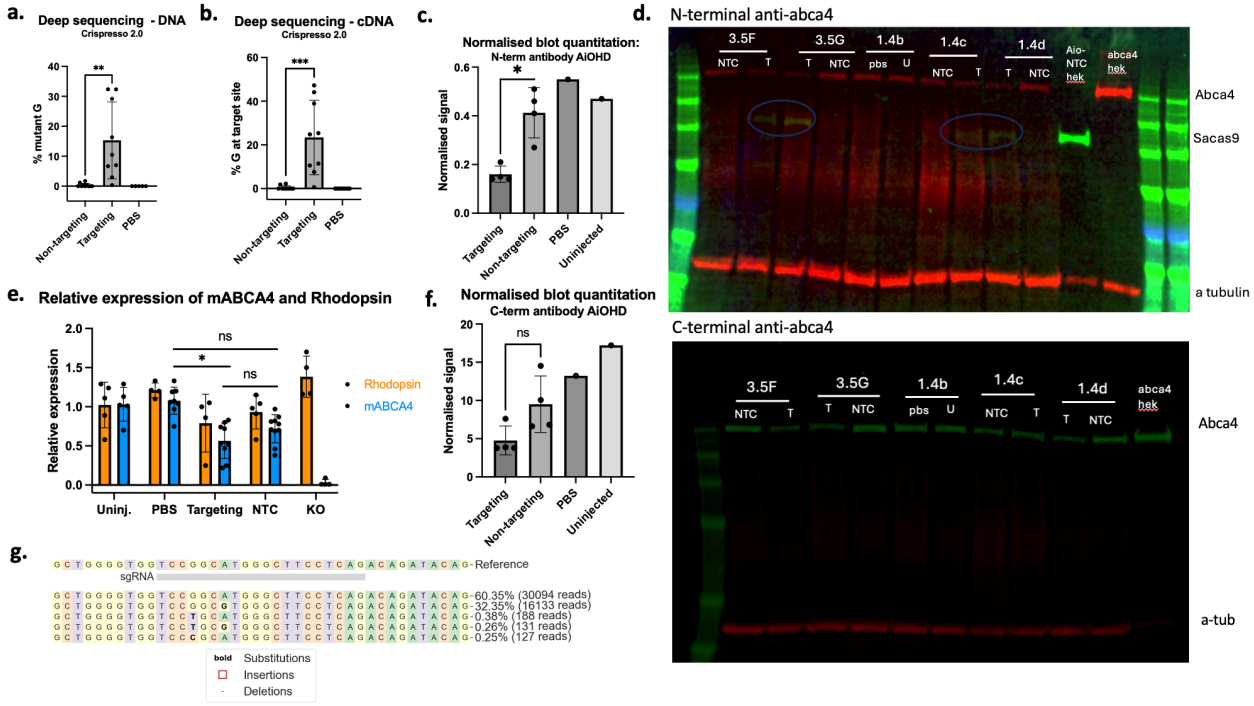

Figure 6-33: Molecular analysis of all-in-one AAV-RK-SaKKHABE8e-U6-gRNA high dose (1E+9vg/eye). **a.** Deep sequencing at the DNA level, showing significant editing of 15.29 ± 4.28% (N=9, p=0.0019) compared to the non-target control. **b.** at the cDNA level, a mean 23.41 ± 5.68% of transcripts showed the A>G edit (N=9,

p=0.0004) compared to the non-target control. a. and b. Kruskal-Wallis test. Data= mean ± SEM. **c.** Western blot quantitation of ABCA4 N-terminal antibody signal normalised to a-tubulin signal, resulting in a significant decrease in **m**ABCA4 signal in the targeting eyes compared to the non-targeting eyes. (N=4, p=0.0286). Mann-Whitney test. **d.** N- (top) and C- (bottom) terminal western blots showing decreased ABCA4 signal in targeting (T) eyes compared to non-targeting eyes (NTC). This was less apparent in the C-terminal blot. All four targeting eyes show robust SaKKH signal. Aio-NTC hek and abca4 hek = HEK293 cell control sample containing SaCas or abca4. Number-letter codes are mouse IDs **e.** QPCR relative gene expression of *mABCA4* and rhodopsin. Only the targeting eyes showed a significant decrease in *mABCA4* expression (N=9, p=0.037). **f.** Western blot quantitation of the mABCA4 C-terminal antibody signal. The mean reduction observed in the targeting eyes was not significant compared to the non-targeting eyes. (N=4, p=0.114). Mann-Whitney test. **g.** Example of bystander activity in an eye with high editing rates. Crispresso2 output.

Protein levels were analysed by western blot and immunohistochemistry. The N-terminal antibody showed an observable decrease in levels of *mABCA4* in targeting eyes relative to PBS and non-injected eyes. Band signal quantitation demonstrated a significant difference between targeting and non-targeting samples, with a 61% reduction in mean signal. (N=4, p=0.0286) Further, the targeting injected samples demonstrated robust SaKKH signal (Figure 6-33). However, when run with a C-terminal antibody and quantified, no significant difference was demonstrated between targeting and non-targeting injected eyes despite a 49.9% reduction in mean signal. (N=4, p=0.114) The targeting injected outlier, 1.4c, exhibited lower SaCas signal than the other three samples likely affecting the observed knockdown (Figure 6-33). This is likely due to injection variability.

IHC data show both targeting and non-targeting injected eyes exhibited no ABCA4 signal at the injection site due to retinal thinning seen in the retinal sections (Figure 6-34 and Figure 6-35). However, in targeting injected eyes, a gradient of ABCA4 signal was observed where signal decreased with proximity to the injection site when analysing images at 40x and 10x (Figure 6-34 and Figure 6-36). Analysis at 4x looking at the whole section proved difficult to draw conclusions from given the high level of background. At 4x, the signal reduction occurred in both targeting and non-targeting injected eyes. This could be due to vector toxicity or inflammation, which further imaging with co-staining of another photoreceptor protein may shed light on. Taken together with the observed editing rates and western blot results, ABCA4 knockdown is plausible.

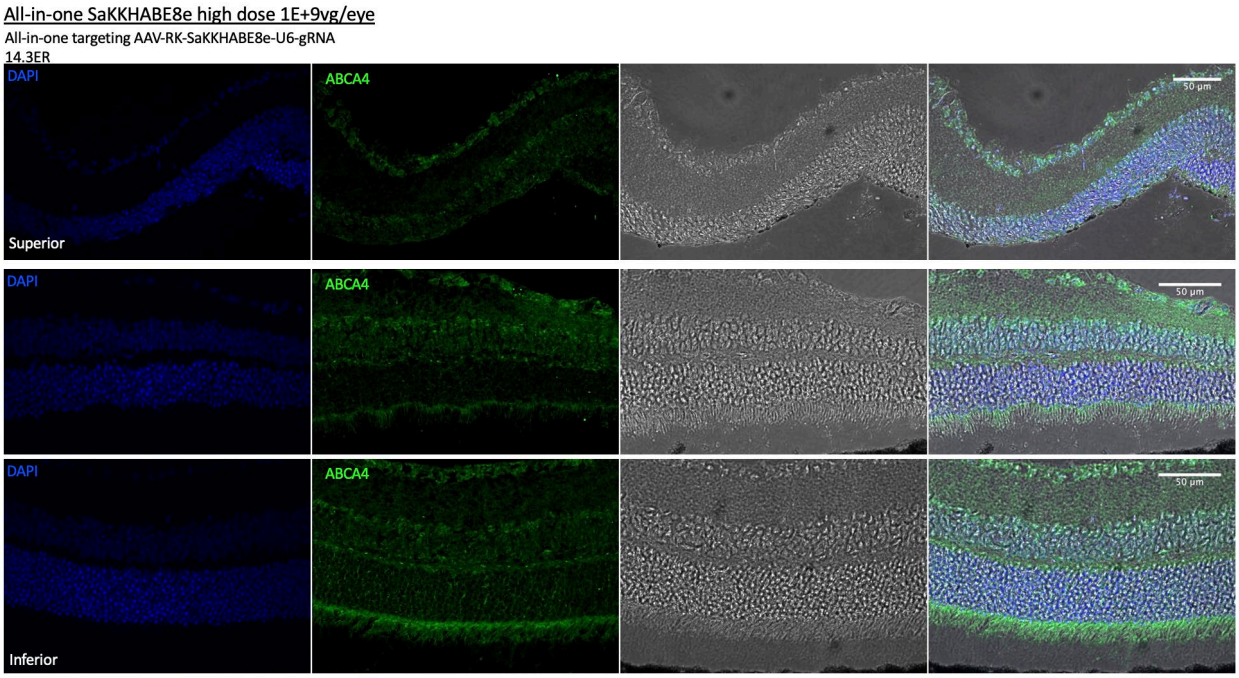

Figure 6-34: IHC all-in-one SaKKHABE8e high dose (1E+9vg/eye) targeting injected eye at 40x.
ABCA4 signal superiorly was non-existent due to complete ONL and outer segment reduction. As the images progress inferiorly, ABCA4 signal improved, suggesting knockdown due to targeted editing or vector toxicity.

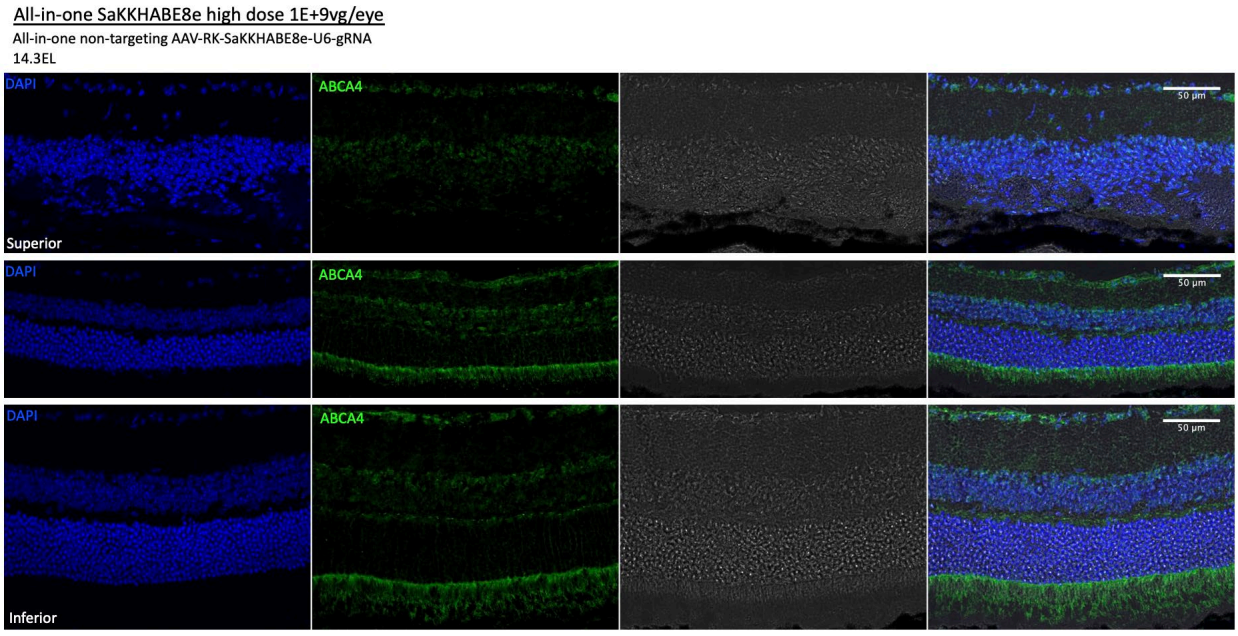

Figure 6-35: IHC all-in-one SaKKHABE8e high dose (1E+9vg/eye) non-targeting injected eye at 40x.
As in the targeting injected eye, the ONL and OS completely reduced superiorly. As the image progresses inferiorly, ABCA4 signal improves.

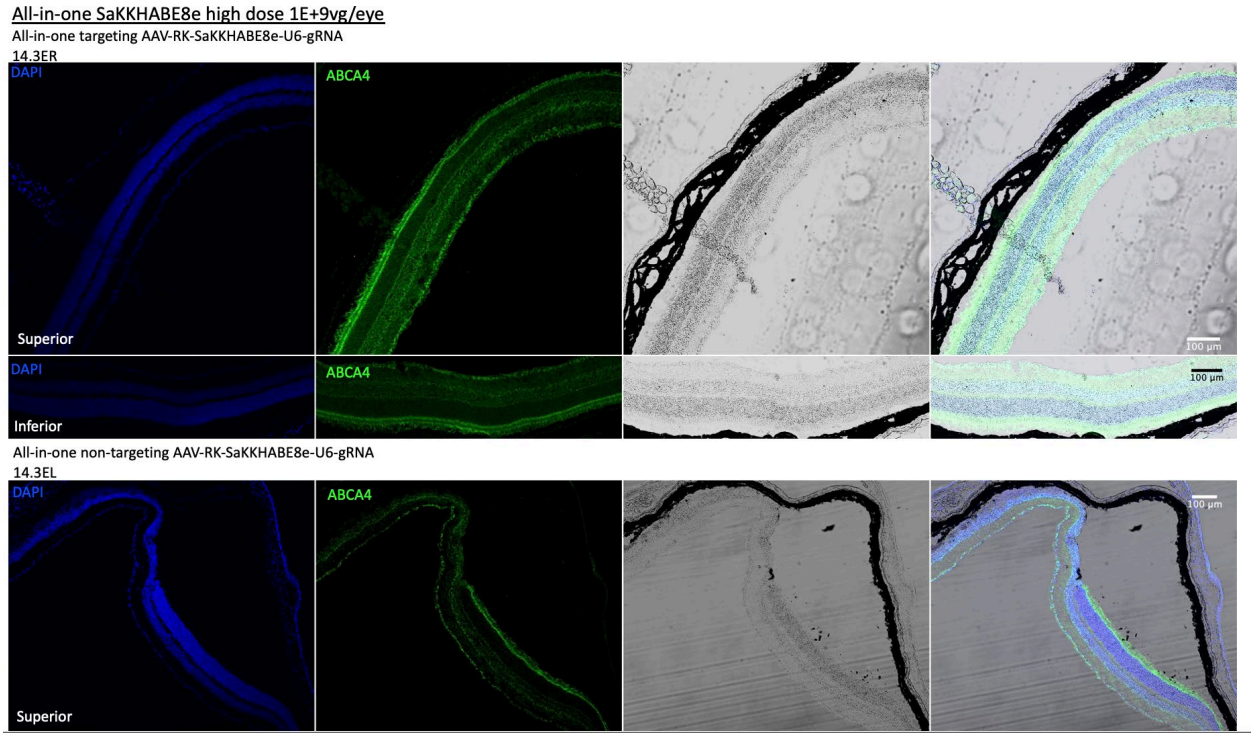

Figure 6-36: IHC all-in-one SaKKHABE8e high dose (1E+9vg/eye) targeting and non-targeting injected eyes at 10x.
As at 40x, the injection site reveals no OS or ONL. The targeting injected samples (top), show a gradient of ABCA4 expression. The non-targeting eye (bottom) shows ABCA4 signal immediately after the injection site. However, at 4x (below) this signal is less robust around the remaining section.

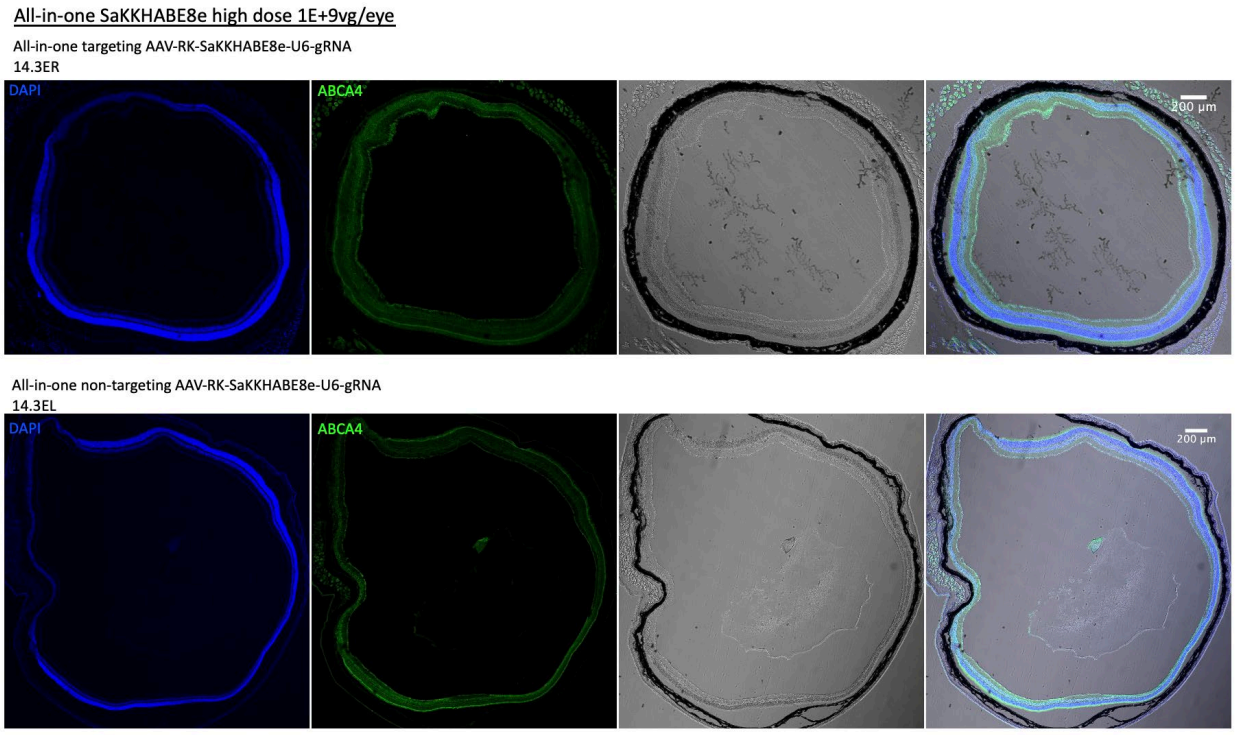

Figure 6-37: IHC all-in-one SaKKHABE8e high dose (1E+9vg/eye) targeting and non-targeting injected eyes at 4x.
Superiorly, no ONL or OS are visible (top left of images). Determining ABCA4 signal at this magnification proved difficult given the high levels of background. Further imaging is required. However, from these images, it is likely the observed signal reduction is due to vector toxicity given that both the targeting and non-targeting eyes show reduced ABCA4.

6.3.5.2 On-target editing of *mABCA4* start codon by all-in-one RK-SaKKHABE8e-U6-gRNA – low dose 5E+8vg/eye

Surprisingly, deep sequencing of low dose eyes at the target site detected a greater mean editing rate than the high dose, with 16.16 ± 3.16% editing (N=9, $p<0.0001$). At the cDNA level, this resulted in a mean of 24.51 ± 4.29% of transcripts with the intended A>G edit (N=9, $p<0.0001$). Editing at the DNA level reached up to 35.08% with a downstream effect of up to 40.3% (Figure 6-38). Analysis of PBS or non-targeting injected eyes showed no editing at the target site. Local off-target editing was not observed across any of the groups. Modified versus unmodified read analysis revealed a significant difference between targeting guides and background observed in PBS and non-targeting injected eyes (Figure 6-38).

Relative *mABCA4* expression by qPCR showed no significant difference between targeting and non-targeting or PBS injected eyes (Figure 6-38). Unfortunately, these samples were not targeted with rhodopsin probes, so no comparison can be shown.

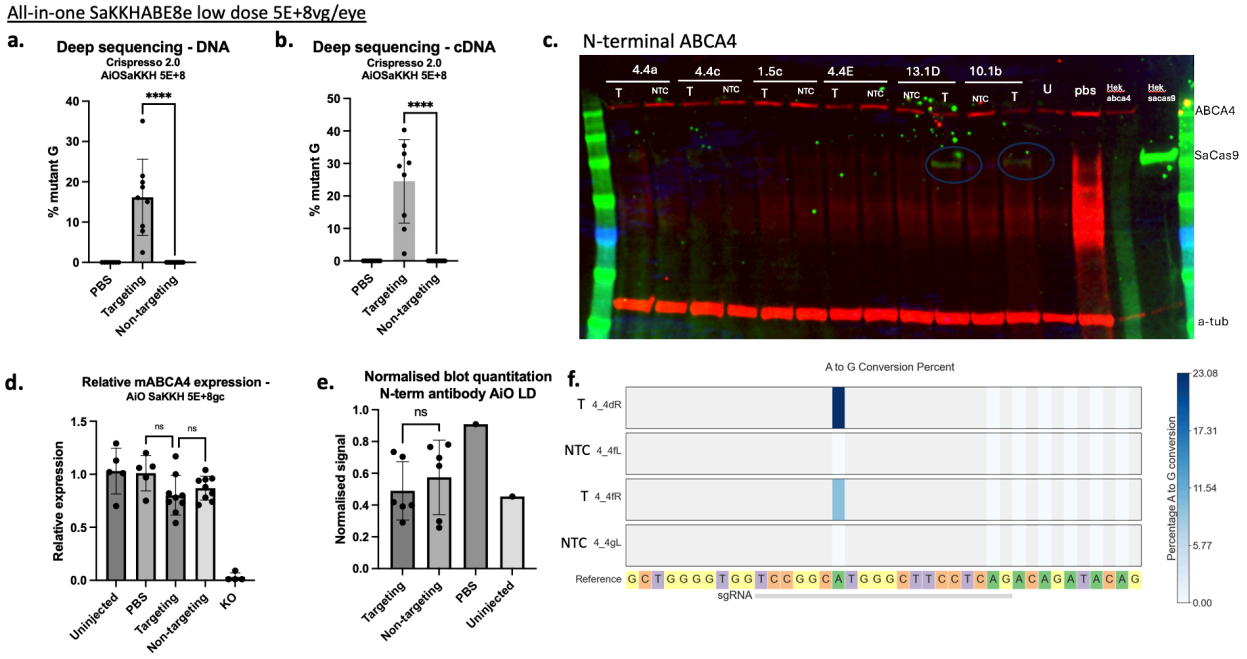

Figure 6-38: Molecular analysis of all-in-one AAV-RK-SaKKHABE8e-U6-gRNA at the low dose (5E=8vg/eye). **a.** DNA deep sequencing revealed mean editing of 16.16 ± 3.16% (N=9, p<0.0001) in targeting injected eyes – a higher rate than the high dose. **b.** Deep sequencing of transcripts resulted in 24.51 ± 4.29% (N=9, p<0.0001) containing the desired A>G edit. Kruskal-Wallis test. **c.** Western blot of retinal lysate using the N-terminal antibody showed reduced mABCA4 signal in the targeting eyes compared to non-targeting eyes. In 2/6 eyes robust SaKKH expression was detected, suggesting a threshold point between the low (5E+8vg/eye) and the high dose (1E+9vg/eye). The number-letter code is the mouse ID. T=targeting, NTC=non-targeting control, U=uninjected, Hek= HEK293 hek controls containing *ABCA4* or SaCas. **d.** QPCR data of relative *mABCA4* expression normalised to the geomean of GAPDH and beta-actin. There was no significant difference between the targeting-injected eyes and PBS or non-targeting injected eyes. DCt values were used for statistics; one-way ANOVA. **e.** Quantitation of western blot signals normalised to a-tubulin housekeeping protein. No significant difference between targeting and non-targeting injected eyes was observed (N=6, p=0.426). **f.** Crispresso2 output showing editing at the target site but not at nearby adenosines. T= targeting, NTC= non-targeting control.

Protein output analysis was done by western blot and immunohistochemistry. Western blot showed protein expression reduction was highly injection dependent with some samples showing observable reduction in *mABCA4* expression. Band quantitation revealed 11% mean reduction in targeting samples compared to non-targeting samples, however, this was not significant (Figure 6-38) (N=6, p=0.426). When the two outliers were removed, the protein reduction became significant (p=0.039) and revealed a 50.5% reduction in protein signal in the targeting injected samples.

IHC analysis demonstrated no mABCA4 expression at the site of injection in both targeting and non-targeting injected eyes as in all previous cohorts. The non-targeting samples showed retinal thinning, whereas targeting eyes revealed a robust ONL structure (Figure 6-39Figure 6-40). The non-targeting eyes demonstrated stronger mABCA4 signal in the outer

segment throughout the rest of the section, particularly in the inferior retina (Figure 6-40). The targeting injected eyes, however, exhibited weak mABCA4 signal even in the inferior retina (Figure 6-39). Further sectioning and staining are required.

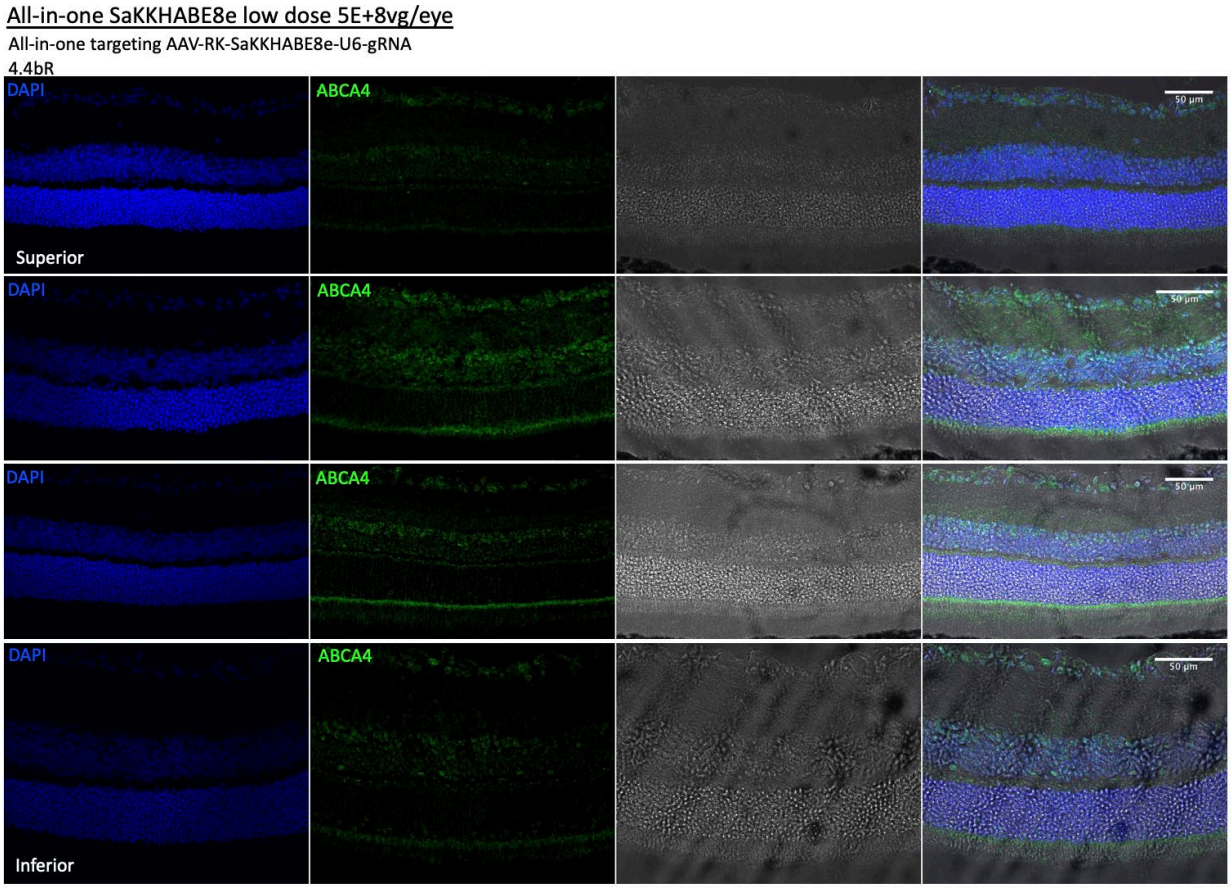

Figure 6-39: IHC of all-in-one AAV-RK-SaKKHABE8e-U6-gRNA targeting injected eyes at the low dose (5E+8vg/eye) 40x.
Superiorly, there was no ABCA4 signal. Throughout the retina, mABCA4 signal remained minimal, but retinal structure was preserved.

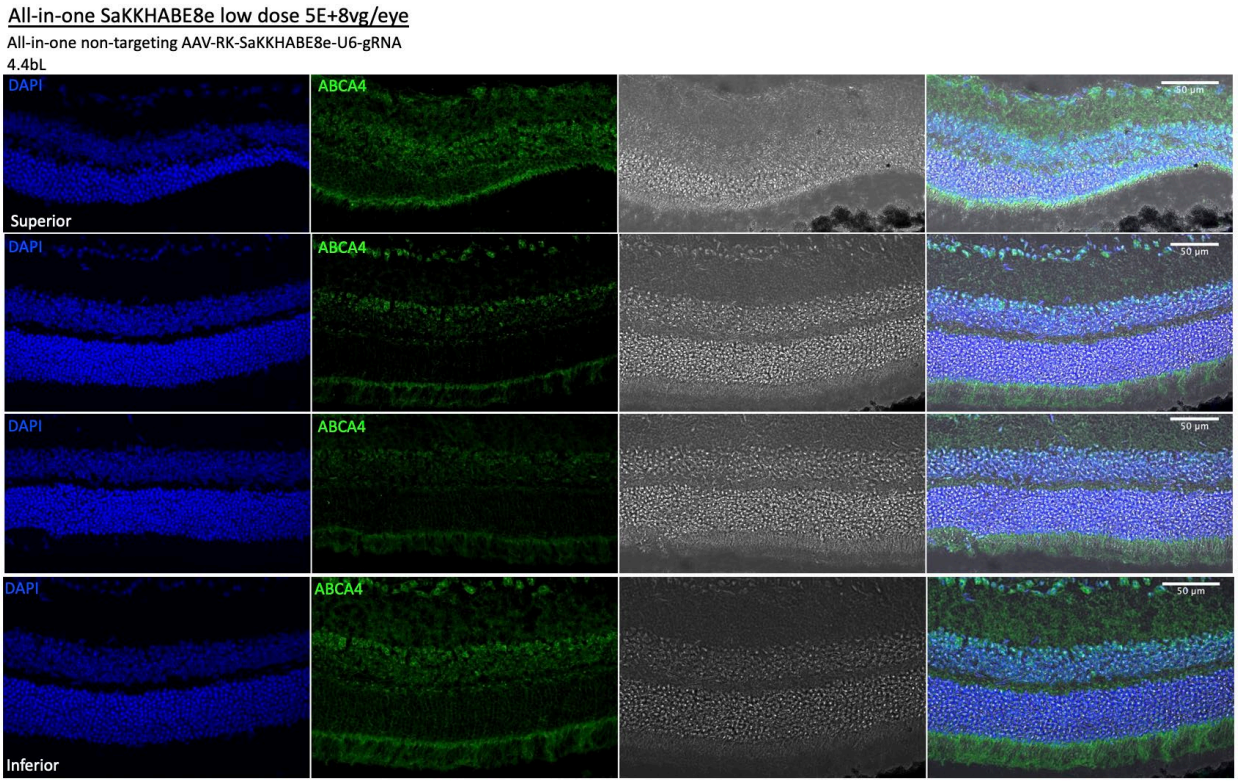

Figure 6-40: IHC of all-in-one AAV-RK-SaKKHABE8e-U6-gRNA targeting injected eyes at the low dose (5E+8vg/eye) 40x.
At the site of injection, the ONL and OS were lost and did not exhibit any mABCA4 signal. Inferiorly, there was strong ABCA4 staining but high background.

6.3.5.3 Analysis of vector expression – all-in-one SaKKHABE8e

Vector expression was determined at the DNA, RNA and protein level. DNA extracted from retina was amplified targeting the SaKKH transgene and sequenced (Figure 6-41). Samples at both doses were tested and indicated correct sequencing for SaKKH. However, this may be amplified from virus in the eye, not necessarily from transduced cells.

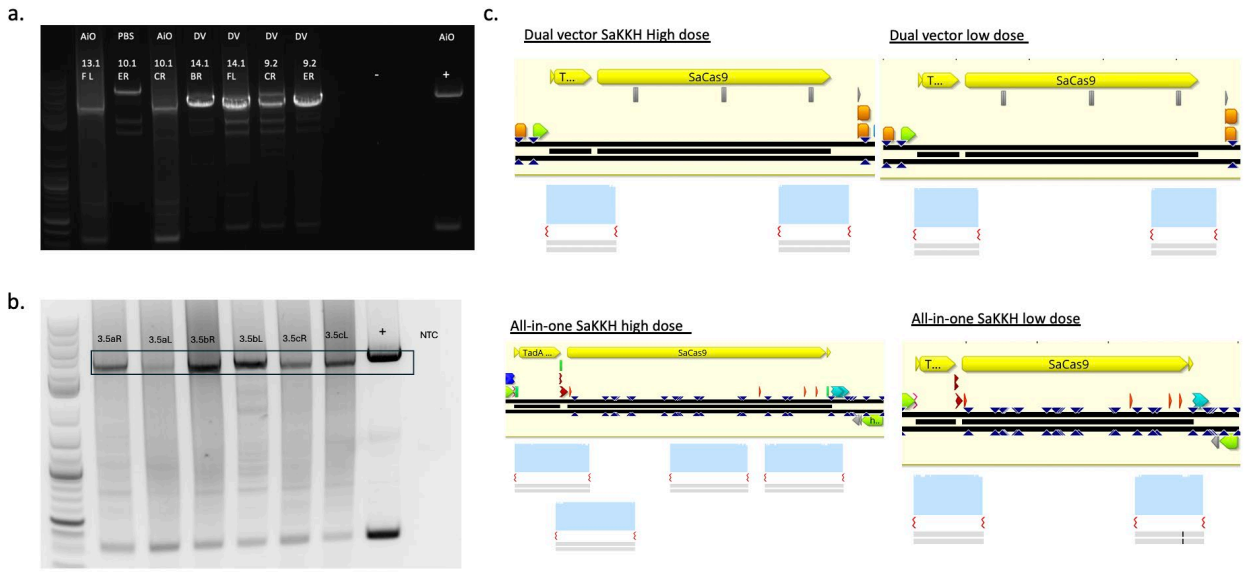

Figure 6-41: Transgene amplification and Sanger sequencing confirmation from extracted DNA.
Both doses of the dual vector and all-in-one SaKKH were amplified from DNA extracted from mouse retina. a. gel electrophoresis showing successful amplification. b. gel electrophoresis of the all-in-one high dose sample PCR. c. Sanger sequencing of representative samples indicating the full-length of the SaKKH. Number-letter code is the mouse ID.

QPCR analysis showed significant SaKKH expression in both targeting and non-targeting samples at both doses ($p<0.0001$), whereas guide scaffold expression was only significant in non-targeting samples (high dose: $p=0.028$, low dose: $p=0.015$) (Figure 6-42). This could be due to injection variability. Alternatively, since AAV are packaged from the 3' and the 5' end, there is a possibility that the U6 promoter, scaffold, and/or guide were truncated. Future RT-PCR of this region would shed light on this.

At the protein level, samples with the targeting guide at both doses showed robust SaKKHABE8e expression where 6/10 samples had signal (Figure 6-33 and Figure 6-38). Interestingly, no samples with the non-targeting guide showed expression at the protein level but showed equal transcript levels by qPCR. This could be due to truncation, degradation, inefficient translation, or reduced antibody binding to non-targeting samples. Lastly, since no fluorescent protein was co-delivered, no fluorescence was observed by SLO-OCT. Retinal structure was much better preserved across timepoints, likely due to the lack of a fluorescent protein and lower dose.

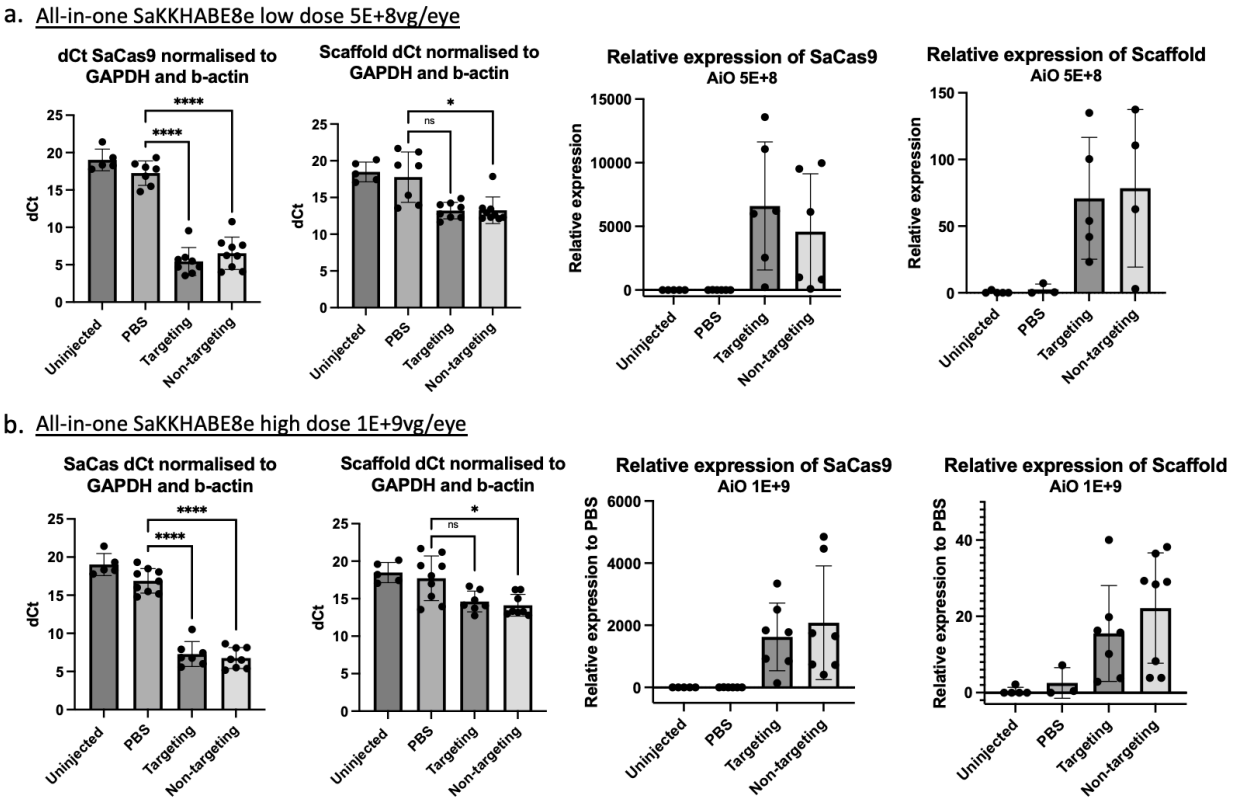

Figure 6-42: QPCR analysis of SaKKH and gRNA expression in all-in-one SaKKHABE8e eyes in both doses. qPCR analysis of the low dose (a.) eyes (N=9) and the high dose (b.) (N=9). Both doses showed significant levels of SaKKH expression for targeting and non-targeting injected eyes ($p<0.0001$). The gRNA-Scaffold only showed significant expression in the non-targeting guide (high dose: $p=0.028$, low dose: $p=0.015$). Relative expression graphs are for easier visualisation. Statistics were performed on dCt values normalised to GAPDH and beta-actin. One-way ANOVA and Kruskal-Wallis test were used.

6.3.5.4 Analysis of retinal structure - all-in-one DNA base editors

Overall, the all-in-one vector was the most tolerated at both the low and high dose. Both doses showed photoreceptor layer thinning for both the targeting and non-targeting vectors due to surgical trauma.

At the low dose, the targeting injected eyes showed -13.92 ± 5.2% thinning and the non-targeting injected eyes showed -23.49 ± 7.3% thinning ($p<0.0001$) (Figure 6-43). This was at, or below, the observed -26.63 ± 7% thinning in the PBS injected eyes. Comparing the superior retina at the two timepoints, there was no significant change. The targeting injected eyes showed signs of recovery, gaining +6.66 ± 9.5% retinal thickness, whereas the non-targeting injected eyes showed minimal change with -3.97 ± 13.42% thinning. The inferior retina showed no significant difference over time (Figure 6-43).

The low dose (5E+8vg/eye) cohort retained robust retinal structure with clearly visible retinal layers. This was mostly consistent over time. Inflammation was seen in 5/17 non-targeting injected eyes and 1/17 targeting injected eyes (Figure 6-44). Overall, this was the most tolerated vector-dose combination.

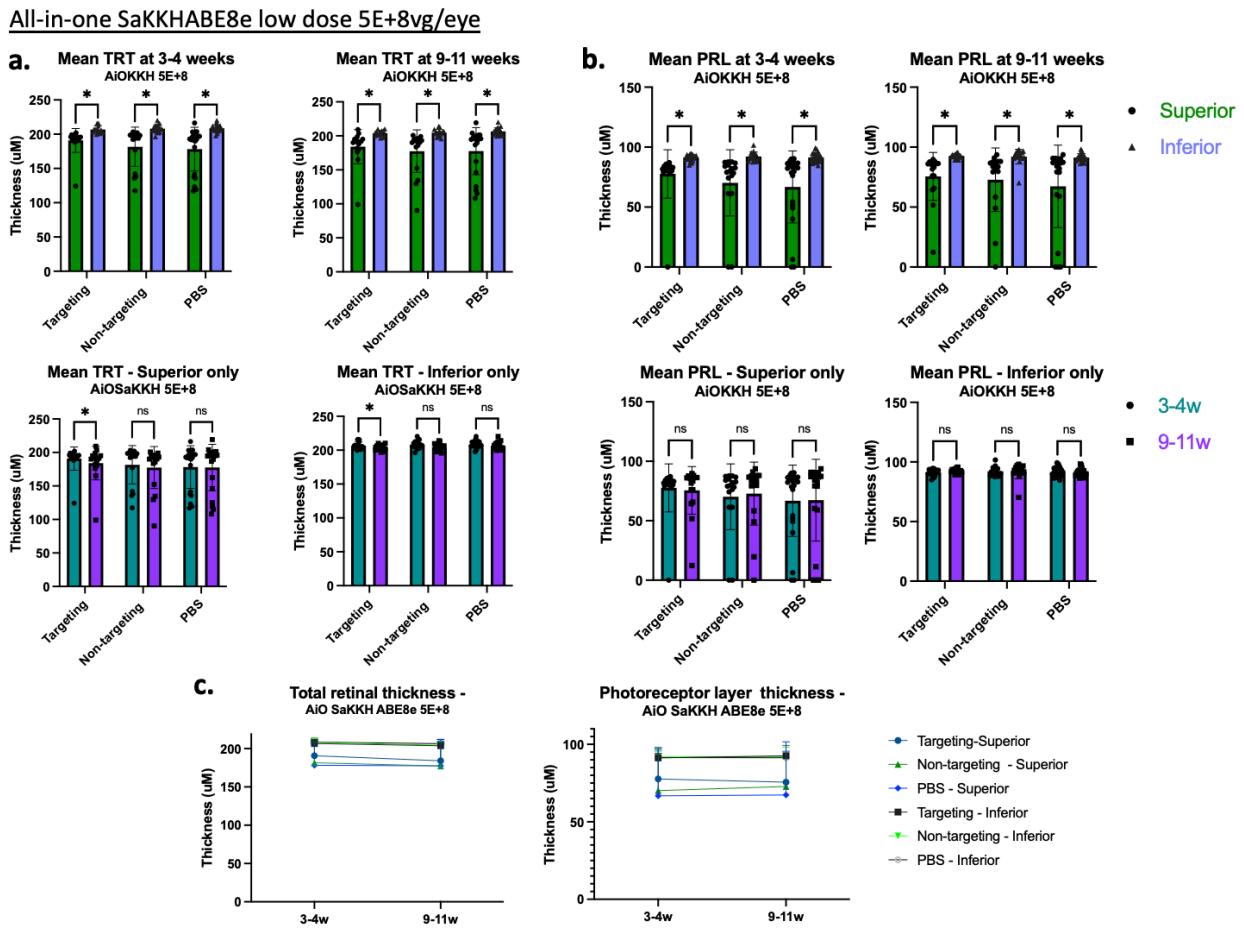

Figure 6-43: Analysis of retinal thickness of all-in-one AAV-RK-SaKKH-U6-gRNA at low dose (5E+8vg/eye). **a.** Mean total retinal thickness (TRT) measurements comparing superior to inferior retinal thickness (top) and superior or inferior measurements over time (bottom). A significant difference was seen in all samples when comparing superior to inferior measures. When comparing over time, only the targeting injected eyes showed a significant difference. (p=0.011, p=0.006) **b.** Mean photoreceptor layer measurements comparing superior to inferior thickness (top) and superior or inferior measurements over time (bottom). As with TRT, all samples comparing superior to inferior thickness showed a significant difference. Comparison over time showed no significant difference. Top: Mann-Whitney test, Bottom: Wilcoxon test. **c.** visual representation superior and inferior measurements over time.

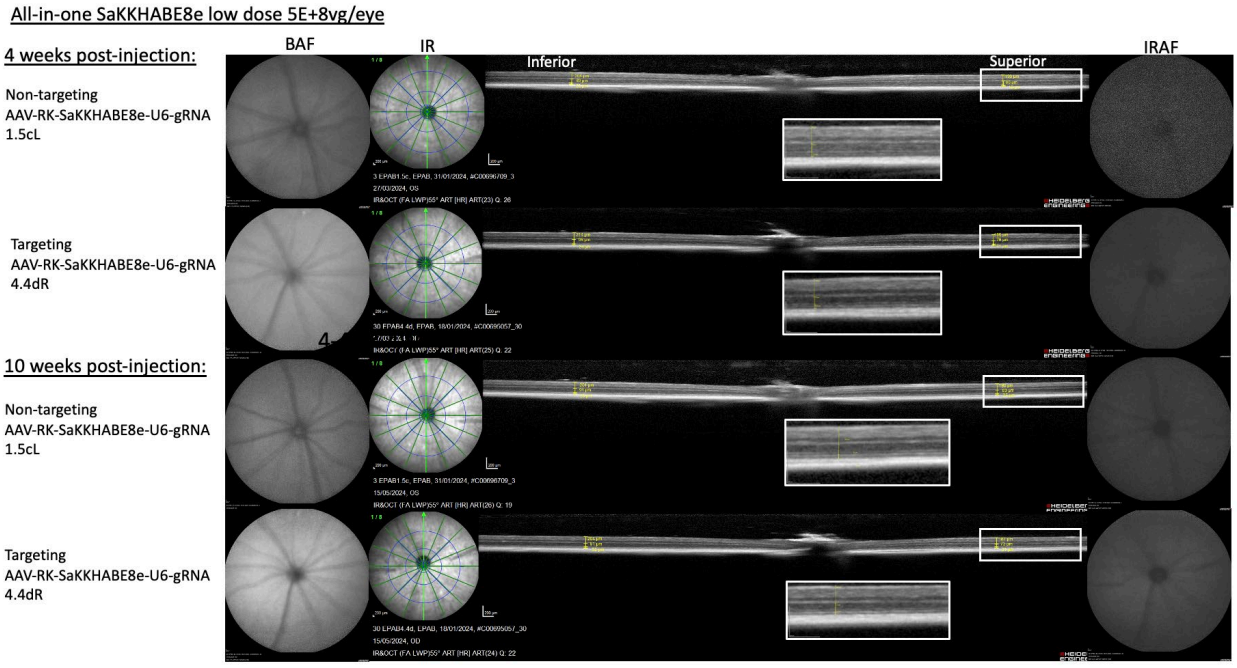

Figure 6-44: Representative cSLO images and OCT b scans of all-in-one AAV-RK-SaKKH-U6-gRNA at low dose (5E+8vg/eye).
The low dose all-in-one SaKKH vector was tolerated well over time. Given no fluorescent protein, no signal was seen in the BAF channel. *En face* images of the back of the eye (IR) and infrared autofluorescence show no observed differences or inflammation. Retinal thickness and structure remained robust.

The high dose showed greater thinning due to surgical trauma and vector toxicity than the low dose (Figure 6-47). At the first timepoint, the targeting injected eyes demonstrated -24 ± 4.67% thinning and the non-targeting injected eyes -34.8 ± 8.1% ($p<0.0001$). The targeting eyes reflected the -26.6 ± 7% observed in the PBS injected eyes. When comparing the superior retina across the timepoints, the targeting injected eyes showed no significant further thinning, however thinning was still -26.6 ± 10% ($p=0.02$) (Figure 6-45). This was more than the -13.85 ± 8.4% seen in the PBS eyes. Interestingly, the non-targeting injected eyes showed no mean change, with -0.08 ± 14.96% thinning. The inferior mean photoreceptor layer thickness showed a significant increase in the non-targeting injected eyes ($p=0.008$) (Figure 6-45). Eyes with thinning due to surgery did not maintain the thickness reported at 4 weeks post-injection and often showed continued thinning over time, however this was not significant.

Retinal images exhibited inflammation in 6/16 targeting and 7\16 non-targeting eyes. This was observed in the BAF and IRAF channels of cSLO (Figure 6-46). The retinal structure remained robust, with some thinning as described (Figure 6-45Figure 6-46).

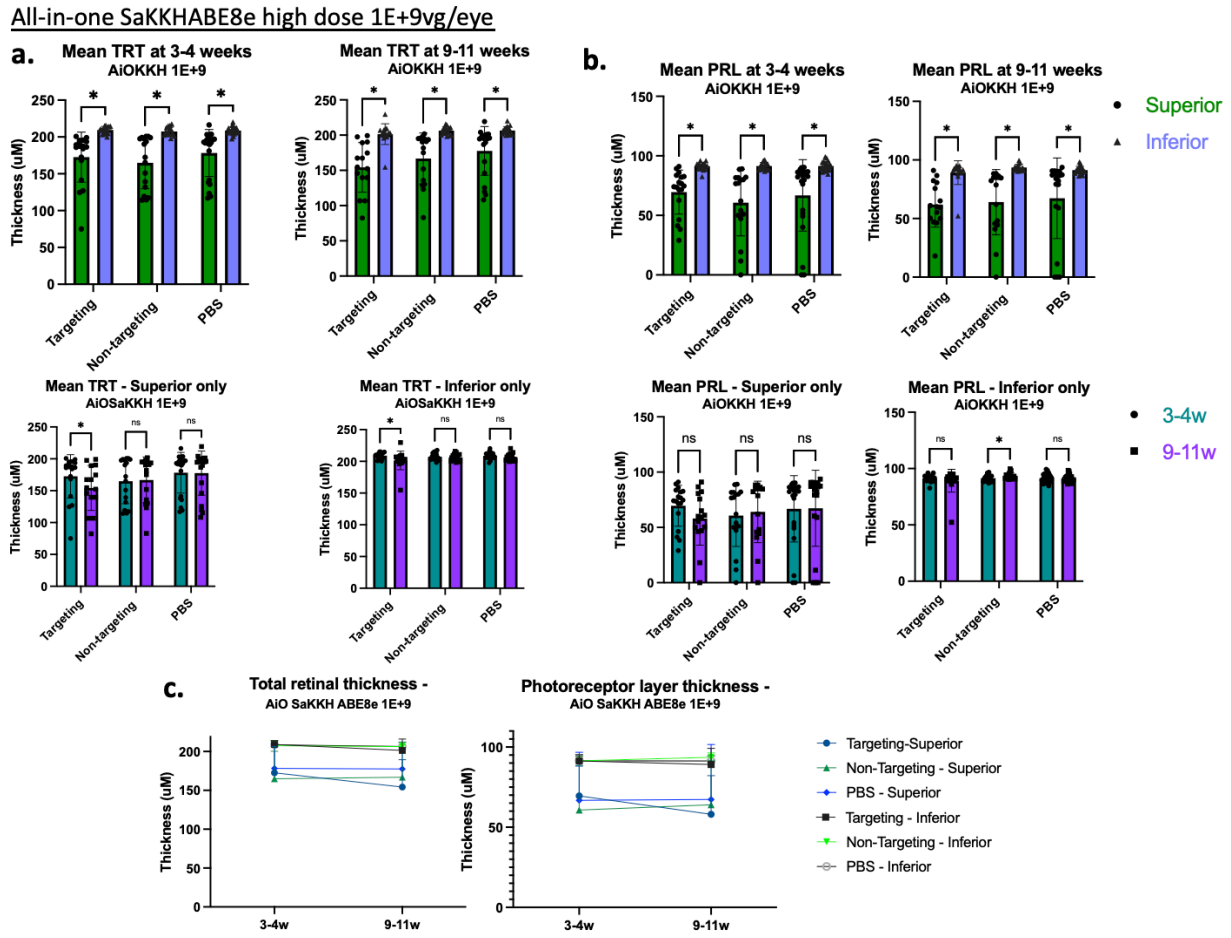

Figure 6-45: Analysis of retinal thickness of all-in-one AAV-RK-SaKKH-U6-gRNA at high dose (1E+9vg/eye). **a.** Mean total retinal thickness (TRT) measurements comparing superior to inferior retinal thickness (top) and superior or inferior measurements over time (bottom). A significant difference was seen in all samples when comparing superior to inferior measures. When comparing over time, only the targeting injected eyes showed a significant difference. **b.** Mean photoreceptor layer measurements comparing superior to inferior thickness (top) and superior or inferior measurements over time (bottom). As with TRT, all samples comparing superior to inferior thickness showed a significant difference. Comparison over time showed no significant difference, except for the inferior non-targeting measurements due to gain in thickness (p=0.008). Top: Mann-Whitney test, Bottom: Wilcoxon test. **c.** visual representation superior and inferior measurements over time.

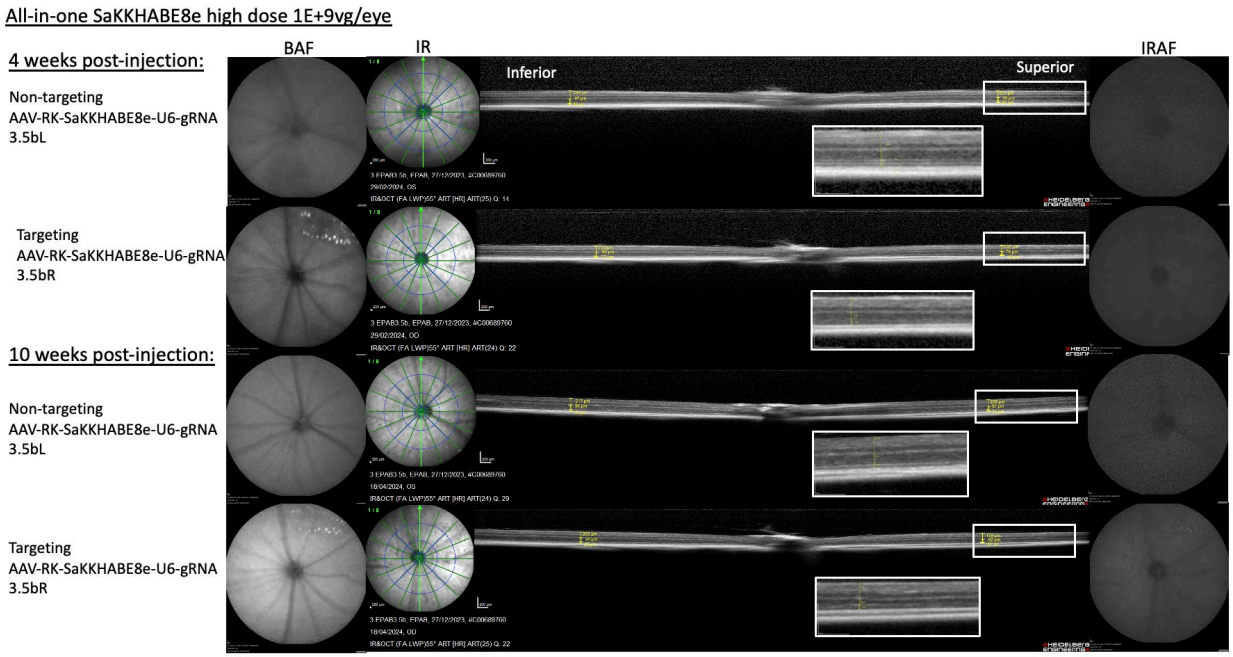

Figure 6-46: Representative cSLO images and OCT b scans of all-in-one AAV-RK-SaKKH-U6-gRNA at high dose (1E+9vg/eye).
The high dose all-in-one SaKKH vector was tolerated well over time. Given no fluorescent protein, no strong fluorescent signal was seen in the BAF channel. Autofluorescence due to inflammation was observed in the targeting (3.5bR) eye over time. *En face* images of the back of the eye (IR) and infrared autofluorescence (IRAF) showed no observed differences except for the targeting eye at the 10 week timepoint. Retinal thickness and structure remained robust.

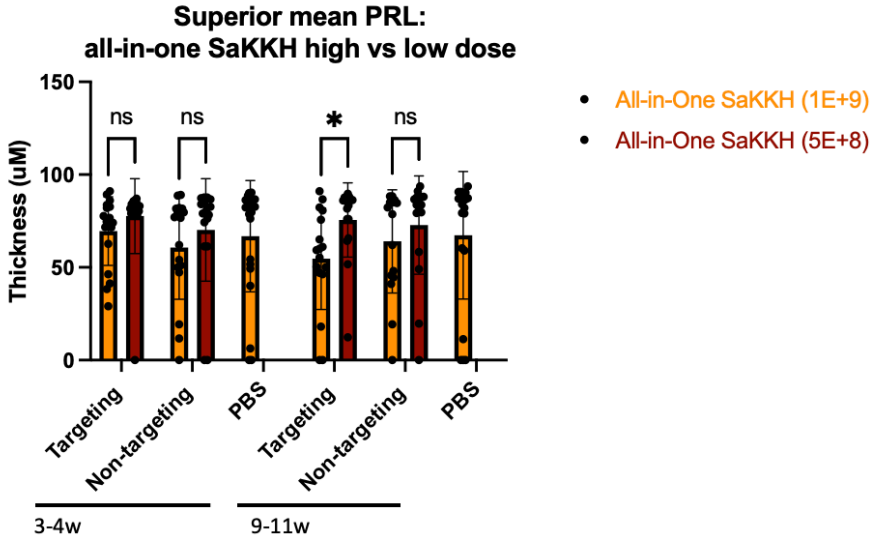

Figure 6-47: Comparison of retinal thickness of the all-in-one SaKKHABE8e at the low and high doses.
The mean photoreceptor layer (PRL) thickness of the high and low dose were compared at both timepoints. There was no significant difference between the doses except for in the targeting injected eyes at 9-11 weeks (p=0.0059). Greater injection variability was evident in the high dose compared to the more tightly clustered low dose measurements. Some variability was always observed as seen in the PBS injected eyes (N=22).

It is unclear why the non-targeting injected eyes showed such high thinning compared to the PBS and targeting injected eyes at both doses. This suggests vector toxicity or impurity. However, over time, the non-targeting vector at both doses was well-tolerated with minimal further thinning or thickening of the PRL.

When comparing how well tolerated the doses were at both timepoints, there was no significant difference between the doses except for in the targeting injected eyes at 9-11 weeks. Here, the high dose showed significantly greater thinning (-26.6%) than at the low dose, where the retina gained thickness (+6.6). Overall, the low dose tended to reflect the PBS injected eyes more closely than the high dose, where greater variability and lower mean thickness were observed (Figure 6-47).

6.3.6 Bystander editing and off-target analysis

Given the 50bp length of the Cas13-ADAR guides, the likelihood of bystander editing was increased. In addition, Cas13-ADAR has a propensity for bystander and off-target activity, particularly with the hyperactive E488Q variant.[199] As expected, low-level activity was observed throughout the guide sequence (Figure 6-14) for both the targeting and non-targeting samples. Local off-target editing also showed low-level activity (<~1.5%) throughout the whole amplicon (Figure 6-14). Whole RNA-seq would shed light on site-specific off-target activity.

Fortunately, due to the design of the SaKKH guide, bystander editing was extremely unlikely given the lack of alternative targetable adenosines within the spacer. No bystander editing was observed in Crispresso2 analyses of the guide region. Further, no off-target activity was observed within the amplicon except for in two samples. Similar to the Cas13-ADAR, this was low-level activity across adenosines throughout the amplicon (Figure 6-23). Whole genome sequencing or site-specific analysis using *in silico* predictions will be investigated in the future to determine off-target effects.

6.4 Discussion

This chapter aimed to compare the efficacy and safety of AAV-delivered DNA and RNA base editors targeting the *mABCA4* start codon *in vitro* and *in vivo* to provide a holistic comparison of the editing systems across multiple target sites in a variety of models. Most encouragingly, it found that the all-in-one DNA base editor SaKKHABE8e demonstrated the

highest editing, with both cohorts achieving 15-16% mean editing and reaching up to ~35% editing at the DNA-level. Despite the promising editing rates, knockdown of *mABCA4* was difficult to demonstrate further due challenges in delineating knockdown from toxic effect.

6.4.1 Comparison of AAV-dCas13b-ADAR$_{DD}$(E488Q) and AAV-SaKKHABE8e *in vitro* targeting the *mABCA4* start codon

The all-in-one SaKKH performed best in targeting the *mABCA4* start codon *in vitro* compared to Cas13-ADAR and the dual vector SaKKH. This was expected given previous publications indicating higher *in vitro* and *in vivo* performance.[180] Guide screens enabled efficient determination of which guides to bring forward into *in vivo* experiments. For Cas13-ADAR, both G3 and G11 were considered for testing to establish if the proportion of the guide bound to the 5'-UTR affected *in vivo* editing efficiency. However, due to virus prep impurity for G11, G3 was chosen for subsequent experiments.

Further *in vitro* testing would have included replacing exon 1 in the human *ABCA4* plasmid with *mABCA4* to enable determination of protein knockdown and potential protein truncation. While multiple stop codons arise when nearby alternate start sites are screened, likely leading to nonsense mediated decay, *in vitro* testing would have shed light on other possible outcomes such as alternative splicing.

Lastly, given plasmid overexpression, these editing rates were expected to be substantially higher than in ensuing *in vivo* work. Off-target editing is discussed in 6.4.4. Use of the luciferase assay as a screening method is discussed fully in the general discussion.

6.4.2 Mouse model and editing strategy

Initially, a screen of *ABCA4* patient databases in Oxford and Moorfields was conducted for homozygous G>A stop mutations with suitable PAM sites. Patient databases were screened to allow for the development of patient-derived organoids to enable comparison across multiple models (Chapter 6). This c.93 G>A mouse model would have been an ideal, clinically relevant model, as sufficient mutation repair should allow for detection of *ABCA4* expression. Unfortunately, the mouse model could not be developed in time (still in production). As described in the introduction, no alternative *ABCA4* mouse models with a G>A stop mutation

were available. To enable comparison of the DNA and RNA base editors, the start codon was targeted to measure knockdown of *ABCA4.*

Targeting a splice site to knockdown or truncate *ABCA4* was an alternative considered editing strategy. Although variations of Cas13 have been used to target splice sites, a splice variant was not targeted given the uncertainty of efficient dPspCas13b-ADAR$_{DD}$ editing at splice sites.[205,319,347-349] Specifically, using Cas13-ADAR to target a splice site presented many challenges due to several unknowns. First, the competitive binding of splice factors, particularly at the exon-junction, could inhibit dPspCas13-ADAR guide binding.[350-353] Second, whether there is a sufficient window prior to splicing in which editing could occur due to localisation.[198,216,354] Third, it is unclear if these are the factors inhibiting editing or if it is target or orthologue dependent.[198,350,354] While Cas13 derived editors have been used at splice sites, Cas13-ADAR has not.[205,319,349,350]

A heterozygous mouse with one knockout allele and one wild-type allele was bred to improve knockdown sensitivity by only requiring editing of one allele. A similar approach using one knockout allele has been applied in other *ABCA4* mouse models.[102] Molecular characterisation of the heterozygous mouse showed reduced expression of *mABCA4* by qPCR, western blot, and immunohistochemistry relative to the wildtype. This was ideal for increased sensitivity of *ABCA4* knockdown by base editors. Further, age-matched, uninjected mice showed robust retinal structure at 3-4 months of age (N=3).

While this was the best way to compare base editors, the model had several shortcomings. First, knockdown is significantly more difficult to determine than restoration of a protein, given that high editing is required to observe a knockdown effect. Second, discerning knockdown from a toxic effect or inflammatory response proved challenging.

Despite the shortcomings, this mouse model provides the opportunity to see if the Stargardt phenotype is inducible and inversely providing optimisim that editing a pathogenic mutation could result in a therapeutically beneficial outcome. In the short-term future, mice injected with the all-in-one SaKKH at the high dose will be imaged every 3 months until 9-12 months post-injection to determine any lipofuscin build-up. If possible, eyes will be sent for electron microscopy for further analysis of lipofuscin accumulation. This study would also enable long-term vector-tolerance analysis.

Lastly, c.1A>G is a clinically relevant mutation listed 41 times in LOVD and is severely pathogenic. Future production of a mouse model with the c.1 A>G mutation would allow for testing with cytosine base editors or prime editors, enabling a potentially clinically relevant downstream application. In the immediate future, Cas-editors will be tested targeting c.93 G>A.

6.4.3 Comparison of AAV-dCas13b-ADAR$_{DD}$(E488Q) and AAV-SaKKHABE8e *in vivo* targeting the *ABCA4* start codon

6.4.3.1 DNA base editors show greater efficacy than RNA base editors *in vivo* in photoreceptors

Data from this chapter demonstrates greater efficacy of DNA base editors over Cas13-ADAR RNA base editing *in vivo* in photoreceptors. Further, it is the first demonstration of using size-minimized SaKKH (dual and all-in-one) DNA base editors in targeting photoreceptors. A comparison of three AAV-RK-base editors at a range of doses demonstrated up to 35% editing with a mean of 16% at the target site using a size-minimised all-in-one SaKKHABE8e. This had an encouraging downstream effect at the RNA level of up to 47% edited transcripts with a mean of 24.51%. This corresponded with reduced ABCA4 signal in eyes injected with the targeting guide. In other studies investigating the use of DNA base editors *in vivo*, mean editing rates of 13.06% at the DNA level resulted in protein restoration in the outer segment.[186] This suggests that the mean editing rate of 16% achieved with the all-in-one SaKKH would likely restore ABCA4 protein in a disease model.

There were several notable findings in comparing DNA and RNA base editors at the same target site. First, the relative performance of the different base editors *in vivo* reflected the *in vitro* data. The all-in-one SaKKH had the highest editing rates, followed by the dual vector SaKKH and Cas13-ADAR. Second, the effects of knockdown are difficult analyse, thereby complicating the establishment of a minimum threshold dose or delineating between vector toxicity and the effects of editing. Third, Cas13-ADAR RNA editing did not work at the dose used, 2.5E+8vg/eye gRNA. Prior work done in the lab showed editing of a different target *in vivo* when using 5E+8vg/eye of gRNA,[210] potentially indicating this as a minimum required dose of gRNA. Fourth, DNA base editing with only 5E+8vg/eye base editor and 2.5E+8vg/eye gRNA resulted in ~8% editing, suggesting an overall lower required dose when targeting DNA. This

was hypothesised given the large number of mRNA transcripts relative to targetable DNA. Further, the editing rate would have likely been higher without mCherry induced toxicity. Lastly, the lower all-in-one SaKKH dose of 5E+8gc/eye resulted in minimal toxic effect and demonstrated similar editing rates to the high dose where inflammation was observed. This suggests that a lower dose without observed inflammation can work as well as a substantially higher dose, however, this requires further testing.

While Cas13-ADAR RNA base editing did not edit at this dose, successful *in vivo* knockdown of *VEGFA* has been achieved using an active, truncated CRISPR-Cas13bt by intravitreal injection. The editing was highly specific, where human *VEGFA* mRNA saw a reduction of 50%, but not mouse *VEGFA*.[207] (However, it is worth noting that the greatest effect was observed in the RPE). Dose optimisation to reflect *in vitro* ratios and administering higher doses, alongside GFP-free vectors may improve Cas13-ADAR RNA base editing outcomes, and requires future testing.

In addition, many clinically relevant alternative RNA editing technologies are emerging. Endogenous ADARs harnessed with chemically modified guides achieved editing efficiencies of up to 50% in non-human primate hepatocytes.[344] Alternatively, circular ADAR-recruiting guide RNAs (cadRNAs) enabled 53% editing of mPCSK9 *in vivo*.[215] Given that expression levels of ADAR in photoreceptors is unknown, exogenous ADAR delivery alongside an ADAR harnessing guide has also been explored.[213] These systems provide potential alternatives in targeting pathogenic *ABCA4* mutations by RNA editing.

6.4.4All-in-one SaKKH achieved more optimal outcomes than dual vector SaKKH

Further comparison of the DNA base editors revealed that the all-in-one SaKKHABE8e at both doses showed higher editing at the target site and less toxicity than the dual vector approach. This was expected given the decreased likelihood of two AAVs transducing the same target cells across a large area at a high efficiency.[355] This was observed in the study that developed the all-in-one SaKKHABE8e, where dual vector delivery resulted in lower editing rates than the all-in-one constructs.[180] However, the reduced editing by the dual vector approach could likely be partially attributed to mCherry toxicity. Further experiments comparing the all-in-

one construct and the dual vector delivery excluding a fluorescent marker are required to accurately discern the efficacy and tolerability between the delivery approaches.

The low dose all-in-one SaKKH was the most tolerated DNA base editing cohort, resulting in minimal retinal thinning, while achieving the greatest mean editing efficiency. This suggests that vector induced retinal thinning impinges upon editing efficiency. A further dose escalation of the all-in-one SaKKH would aid in establishing an upper threshold of a toxic effect and a lower threshold at which editing is achieved.

In this study, the dual vector likely had a substantial decrease in editing efficiency due to the toxic effect of the mCherry reporter. While some toxicity was expected, this degree of toxic effect was not. Future work will include replacing mCherry with a less toxic fluorescent marker or an HA tag, or switching the fluorescent-marker promoter to a photoreceptor specific promoter such as RK or PDE6B. Using tissue-specific promoters has been reported to result in less toxicity.[356]

This adds to continually emerging literature demonstrating the potential of DNA base editing and other DNA editing technologies in the retina and in humans. A dual AAV-SpRY-ABE8e targeting a mutation in *rd10* mice achieved up to 17.5% editing at the target adenine. More recent dual AAV delivered prime editors resulted in 76% correction in retinal cells *in vivo.*[357] Most recently, a baby was effectively cured of a rare and debilitating carbamoyl phosphate synthetase 1 (CPS1) deficiency.[358] Utilising an all-in-one DNA base editor may enable higher rates of editing with minimal toxic effect, which is highly relevant for therapeutic applications.

Perhaps, similar to the DNA base editor, a high dose of the all-in-one size-minimised dCas13-ADAR, dCas13bt-ADAR or mxABE, may have shown greater efficacy *in vivo* than the dual vector delivery containing GFP. While dCas13bt-ADAR shows decreased activity, this would have increased the concentration of the gRNA and abolished any GFP-related toxicity, likely improving outcomes. More recently, the size-minimised Cas13 mxABE has shown successful editing *in vivo* targeting two different genes in the ear, MYO6 and OTOF.[211,212]

6.4.5 Base editing to knockdown a gene is difficult to determine

Although this thesis aimed to compare DNA and RNA base editing at the same site in *ABCA4,* an unintentional analysis that emerged is the applicability of base editing in knocking down gene expression. This has been successfully tested *in vitro* and *in vivo* with both cytosine

and adenine base editors, CRISPR-STOP/iSTOP[359,360] and i-Silence,[361] respectively. These systems were tested to more safely develop gene knockout models without the risk of DSB-induced toxicity.[362-364] In this thesis, it was determined that the all-in-one SaKKH showed editing of up to 35% with downstream effects of up to 47% at the cDNA level. Confusingly, this corresponded with significant knockdown at the protein level compared to the non-target control when using an N-terminal antibody, but no significant difference when using a C-terminal antibody. Further, given the observed toxicity, discerning between knockdown and toxicity in IHC was not possible. While the editing rates are promising, the toxic effects will need be to overcome to better understand the true degree of knockdown.

Further investigation could enable applying base editors as a gene knockdown method as an alternative to the typical CRISPR-Cas9 approach, particularly due to the reduced risk of off-target editing with ABEs.[365] Clinically, this may be less relevant given that CRISPR-Cas9 has allele specificity in knocking down a gene with far fewer parameters than would be required for base editing. Nonetheless, this could be applicable in mutant dominant gain-of-function scenarios, such as Fuchs' endothelial corneal dystrophy (FECD).[366]

6.4.6Challenges with immunohistochemistry of ABCA4

To enable a visual demonstration of knockdown, IHC staining for ABCA4 in retinal sections was undertaken. This proved challenging, with all four antibodies tested at various concentrations using previously published protocols[42,65,101] demonstrating strong background staining across all samples. Confusingly, the *ABCA4 -/-* controls did not display the background staining, which may be due to differing gain. Interestingly, the staining in Lenis et al[65] and Molday et al,[101] revealed a similar trend across three different ABCA4 antibodies (3F4, 5B4, ab72955), although to a lesser extent. Other publications, however, have shown minimal background and strong localisation to the outer segments,[42,367] suggesting continued protocol optimisation and improved imaging techniques are required.

6.4.7Off-target effects

Given the overexpression of all plasmids *in vitro,* off-targets were not investigated extensively. Local off-target analysis within the amplicon revealed a prominent off-target site in Cas13-ADAR treated samples in *Renilla* (Figure 6-8). This site achieved much higher editing

rates than on-target editing with both targeting and non-targeting guides. Further, samples without Cas13-ADAR showed no editing at the on- or off-target site, suggesting ADAR recruitment to this site due to Cas13-ADAR overexpression. While it is unknown what specifically results in ADAR recruitment, the most pronounced sequence preference is the RNA motif 5'- TAG -3' which is the off-target sequence in this instance.[198,327,328] Interestingly, despite the prominent off-target activity, no bystander editing was observed.

In vivo analysis of local off-target editing by Cas13-ADAR revealed an expected low-level, promiscuous editing profile throughout the amplicon in both targeting and non-targeting injected eyes (Figure 6-14). No specific off-target site was observed as seen in the *in vitro* samples. Given the overexpression of ADAR, analysis of preferred ADAR sites (ie 5'-TAG) would be hypothesised to reflect *in vitro* data and show off-target activity. Whole genome sequencing was not performed given the lack of on-target editing, but it can be hypothesised that off-target editing occurred throughout the transcriptome with the hyperactive variant.[199,213,265,368]

In vitro analysis of local off-targets in SaKKH treated samples did not reveal any off-target or bystander activity within the amplicon. No bystander editing was likely given that there is only one other adenine at position A_{19}. Similarly, *in vivo* analysis of local off-targets did not indicate any sites throughout the amplicon. However, two samples did show low-level (<1%), promiscuous activity. This was unexpected given the low expression levels compared to the *in vitro* samples but could be due to greater sequencing depth in the *in vivo* samples. Further, samples with high levels of on-target editing also had low-levels of invalid bystander (G>T/C) edits (~0.89%) at position G_4. While ABEs cannot make G>T/C substitutions, these substitutions are reported at low levels.[221,369] At the cDNA level, these substitutions were not observed, suggesting background noise or that these variants are not transcribed. Future investigations would undertake whole genome sequencing to establish off-target sites and editing efficiencies at these sites.

A multitude of developments have emerged to minimise off-target effects for DNA and RNA editing. One of the leading factors in the development of off-targets in DNA editing is continued expression of the vector. To reduce expression time, alternative delivery methods/formats have been tested such as ribonucleoproteins in hit-and-run virus-like particles.[370] Other approaches including combinatorial engineering and PA(N)CE systems allow for rational design and evolution of existing base editors to minimise bystander activity, such as NG-ABE9e.[185,371,372]

Similar evolution has been applied to RNA base editors, where further mutagenesis has reduced off-target activity.[199] Novel guide designs that introduce G-A mismatches may reduce both bystander and local off-target editing.[324] For both DNA and RNA editing, testing new orthologues may enable greater on-target specificity.[180,199,205]

6.4.8 AAV-vector expression

Relative *in vivo* editing rates reflected the relative *in vitro* editing rates of the base editors. However, overall editing rates *in vivo* were much lower. This was likely due to a combination of expression levels of the transgene, injection variability, and vector toxicity (6.4.9). Base editor expression was determined at multiple levels.

At the low dose, dual vector SaKKH had a notable absence of SaKKH protein detection by western blot. SaKKH signal was observed in the only targeting injected eye that retained the photoreceptor layer, suggesting vector toxicity. At the high dose, no eyes showed vector expression, even in instances where the retina was preserved. Interestingly, the qPCR data showed significant SaCas expression in both the low dose and the high dose, with greater expression in the low dose as seen on western blot. The observed qPCR data indicate that transcription of the base editor persists, but the lack of corresponding protein suggest inefficient translation or degradation, perhaps due to cellular toxicity from mCherry expression. Alternatively, western blot sensitivity may not be sufficient to detect SaKKH protein in the neural retina lysate sample.

The all-in-one SaKKH showed robust SaKKH protein expression in the targeting samples at both the low (2/6 eyes) and high doses (4/4 eyes). This establishes a minimum threshold, where injection variability at the low dose (5E+8vg/eye) may or may not result in protein detection, whereas at the high dose (1E+9vg/eye) protein expression was consistent. Interestingly, the qPCR data revealed similar SaKKH expression levels at the low and high dose.

Both the all-in-one doses showed protein detection in targeting injected eyes but not in non-targeting injected eyes. This is contrary to qPCR data which shows similar transcript expression levels between non-targeting and targeting injected eyes. This could be due to truncations during viral packaging of the non-targeting sample resulting in insufficient scaffold for the nCas9 to complex with. Alternatively, upon not finding the target sequence, the gRNA:Cas de-complexes, resulting in greatly decreased SaCas antibody sensitivity (Figure 6-9). Amplification of the

gRNA by RT-PCR would shed light on this. This was not observed in the dual vector blot given the lower protein-level expression.

Cas13-ADAR showed protein detection in 4/8 injected eyes at 1E+9vg/eye. The injection variability suggests a threshold for Cas13-ADAR protein expression, with further studies needed to optimise dosing. Despite Cas13-ADAR protein signal in 3/4 targeting injected eyes, no editing was seen in the deep sequencing results, which could have multiple contributing factors. First, the gRNA dose of 2.5E+8vg/eye is likely insufficient to enable editing. *In vitro* assays were optimised with a 2:1 gRNA:Cas13-ADAR ratio, implying an optimal guide concentration of 2E+9vg/eye. While this would more than likely result in toxicity, a higher gRNA dose without a GFP reporter may improve editing outcomes. Second, although protein signal was detected, this was variable, indicating that a higher dose may enable more consistent protein detection, as seen with the all-in-one SaKKH. The Cas13-ADAR was well-tolerated, indicating that a higher dose would be possible.

Where the dual vector approach was used, guide vector presence was confirmed by fluorescent marker. Additional qPCR was performed in SaKKH injected eyes. In dual vector SaKKH eyes qPCR data showed robust guide expression. The all-in-one SaKKH showed lower guide expression (dCt) than the dual vector. This could indicate a truncated vector given the proximity to the 3' ITR and subsequent insufficient expression. However, as tested *in vitro,* the western blot signal of the all-in-one SaKKH was robust in targeting injected eyes, suggesting a complexed protein rather than solely the base editor (Figure 6-9). As previously mentioned, amplification of the gRNA-scaffold would shed light on transcription.

Lastly, across all base editing cohorts, future analysis by single cell sequencing of transduced eyes would enable correlation of base editor and guide expression to *ABCA4* expression. Moreover, analysis of cell-health markers may provide quantitative insight into the toxic effect.

6.4.9 Toxicity

Toxicity had a likely effect on transgene expression and may have been caused by various factors. Determining toxic effect was done by *in vivo* SLO and OCT imaging, and IHC. Reductions in photoreceptor layer thickness and the presence of inflammation-induced autofluorescence were measures of toxicity. IHC analysis showed further evidence of retinal structure disruption and expression of fluorescent markers.

Surgical trauma was a major source of inflammatory response in the 129 background mice resulting in ~25% thinning – substantially higher than the accepted 10% threshold. This was injection material independent, with PBS injected eyes also suffering excessive post-injection trauma. Multiple physiological and immunological differences have been reported in inbred mouse strains, including 129S, and may be causal in this response to subretinal injections.[373-375] This likely contributed to downstream effects including the variability of retinal thinning and inflammation between mice.

The dual vector SaKKH and gRNA-mCherry vectors showed the strongest toxic response, with significant thinning extending into the inferior retina. This was addressed iteratively by maintaining the SaKKH dose (5E+8gc/eye) but reducing the dose of the guide vector to 2.5E+8vg/eye. This minimally improved thinning given the small dose de-escalation. Both doses reflected the observed thinning seen on OCT in the immunohistochemistry performed, where the ONL was completely lost at the injection site. Redesigning the guide-containing construct without CAG-mCherry may help establish the cause of toxicity and allow for dose escalation.

The all-in-one SaKKH resulted in a milder response in which the majority of high dose (1E+9vg/eye) injections resulted in visible inflammation by SLO but with thinning comparable to the PBS control. Subsequently, a lower dose of 5E+8gc/eye was tested which substantially reduced the toxicity observed. Interestingly, the Cas13-ADAR injected eyes showed less overall thinning than other cohorts and PBS injected eyes and exhibited minimal inflammation despite a combined dose of 1.25E+9vg/eye.

A proportion of the extreme toxicity in dual vector SaKKH samples was likely due to the gRNA-mCherry vector. Far less toxicity was seen in the all-in-one SaKKH samples than the dual vector samples, suggesting this is due to gRNA-mCherry. Studies have conflicting outcomes regarding mCherry toxicity. Ubiquitous mCherry expression in mice looking at expression across a multitude of organs (excluding eyes) found strong expression and no signs of toxicity.[376] However, a study investigating fluorescent protein fusions in frog eye development found GFP only slightly more toxic than uninjected controls, whereas mCherry led to a decrease of the average eye size and had indicators of abnormal eye development.[377] The latter was reflected in the relative vector toxicity between cohorts, where mCherry injected eyes (dual vector SaKKH cohort) showed 44-76% mean PRL thinning and gRNA-GFP (Cas13-ADAR cohort) showed -

0.25% - +9.57% retinal thickness change. The non-targeting mCherry injections showed lower expression than the targeting eyes.

Another toxic factor may be the CAG-promoter, which has shown toxicity in delivering GFP in photoreceptors and RPE as well as other broadly active promoters. When photoreceptor-specific promoters were used to deliver GFP, they were found to be non-toxic at all doses.[356] This may have enhanced the toxicity of mCherry, but interestingly not GFP.

To further delineate toxicity due to SaKKH versus gRNA-mCherry, paired injections were undertaken at 1E+9vg/eye, the combined dual vector high dose. Unfortunately, images were only analysed at 3-4 weeks due to time constraints, revealing no significant difference. The strong toxic effect was typically seen at the second timepoint, which could be tested in future work. Excluding mCherry from the gRNA construct would have likely reduced toxicity and enabled a more apt comparison to the all-in-one SaKKH vectors. Alternatively, driving fluorescent expression with a *PDE6B* promoter would improve specificity to photoreceptors and potentially decrease toxicity.[356]

A portion of the observed inflammation is also likely due to the base editor since they are bacteria-derived proteins. Given that *S. aureus* are facultative colonisers of skin and can cause infection, it is likely the immune system would recognise SaKKH proteins as an antigen.[378] It has been shown *in vivo* that Cas9 proteins are recognised as antigens and mount corresponding immune responses in mice.[379] Further, this has been demonstrated in humans, where 79% of samples (n=34) exhibited anti-SaCas9 antibodies.[380] The first CRISPR-Cas clinical trial, Edit-101, delivered SaCas9 to target a CEP290 mutation and showed a favourable safety profile.[167,381] However, specific immune response data is not yet available. The immunogenicity of KKH orthologue requires further investigation.

Although active PspCas13b non-specifically cleaves RNA, with detrimental effects on cell health, this has not typically been associated with the deactivated dPspCas13b form. Nonetheless, an immune response to the Cas13b protein has been reported in mice, where transient immunosuppression resulted in a reduced immune response in Cas13b treated mice.[382]

The deaminases may contribute to observed toxicity, as well. The hyperactive $ADAR_{DD}$(E488Q) has been associated with deleterious effects from off-target editing, likely affecting cell physiology.[213] The effects of the ecTadA deaminase domain of the SaKKHABE8e require further investigation.

Lastly, a proportion of the toxicity was likely AAV-related, given in-house production variability. Studies have successfully delivered substantially higher doses of AAV8.[120,356] Unfortunately, variables such as full-to-empty capsid ratios, effective packaging, and purification variability were difficult to control and likely affected the toxic and inflammatory response.[127] Outsourcing virus production would likely reduce variability and potentially reduce costs, enabling successful delivery of higher doses and improve reproducibility.

Overall, determining the relative effects of virus production and response to the various transgene components on toxic response is not possible. Continued research in understanding and enhancing the safety of these editors is needed, as well improving production consistency between experiments to better discern the source of toxicity. The encouraging safety profile of SaCas9 used in the Edit-101 clinical trial are a positive indicator for the translational capabilities of SaKKH base editors.

6.4.10 Translational considerations

This chapter has demonstrated successful editing of the *ABCA4* start codon by the SaKKHABE8e base editor using dual vector or all-in-one delivery. However, it was difficult to draw conclusions about the knockdown effect beyond the toxicity. These toxic effects need to be addressed before any knockdown or downstream rescue in a clinical model can be demonstrated. Further, given the phenotype development of *ABCA4* knockout mice, observing the functional effect has not been possible within the time of the PhD. Work to observe lipofuscin build-up over 6-9 months and the long-term toxic effect is currently underway.

Required levels of editing for a functional effect are unknown, but it would be hypothesised that 100% editing of one allele would be required for a fully curative effect. In the instance of other IRDs such as choroideremia, only ~5% of wildtype *REP1* transcripts were associated with a slower progression of degeneration, however this likely does not describe required editing of *ABCA4* given the differing expression levels.[383] Indeed, in a dual vector *ABCA4* gene augmentation study, treated eyes with <20% of wildtype levels of *ABCA4* led to a significant reduction in A2E. However, these A2E levels remained substantially higher than the mean wildtype levels.[41] Other studies have estimated a minimum of 12.5% editing.[102]

Given the high rate of turnover of *ABCA4* due to outer segment phagocytosis, the minimum rate of RNA editing would be hypothesised to be significantly higher for sufficient

targeting of mRNA transcripts than required in DNA base editing. While no editing was achieved with dCas13b-ADAR$_{DD}$ at this dose, alternative RNA base editing methods have achieved significantly higher *in vivo* editing that may result in a functional effect.[213,215] However, DNA editing would likely require lower editing rates since all downstream transcripts would contain the edit. While promising DNA base editing efficiencies were achieved, further investigation is required to determine if these lead to a functional effect. The 6-9 month follow-up will hopefully shed light on this. Based on the success of targeting *mABCA4 in vivo* in this project, future work would test these systems in a clinically relevant model.

As with most CRISPR systems, targeting is extremely site dependent. This model and data have determined this murine site is targetable *in vivo* using the guides that were screened for. Designing a clinically relevant, humanised model containing the c.1 A>G mutation or other nonsense mutations would indeed enable establishing a protein-level and functional threshold. However, this presents further challenges including PAM site availability, guide sequence specificity and the potential effects of methylation. Further testing of therapeutically relevant guides would be required in other models, such as retinal organoids.

6.5 Conclusion

This chapter presented an iterative screen of DNA and RNA base editors targeting the same mutation, first undertaken *in vitro* followed by *in vivo* tests in the *mABCA4* mouse model. This was the first test of SaKKHABe8e in photoreceptors, establishing the translational potential of these technologies. Importantly, promising levels of on-target editing were achieved but also underscored the trade-off between dose and transgene expression, and the associated effects on off-target editing and toxicity.

7 General Discussion

7.1 Summary and reflection on thesis aims

ABCA4 has ~1200 known pathogenic mutations, of which ~63% are transition mutations targetable by base editors with potential for clinical translation. While base editors can hypothetically target the majority of mutations based on PAM availability established in Chapter 3, sequence and deaminase specificity are still difficult to predict.[277,286] Large datasets and machine learning are being developed to predict editing outcomes with improved accuracy as model development continues. However, these are often designed for the SpCas 5'-NGG PAM site.[286,384]

Given the high number of targetable mutations in *ABCA4* with an SaKKH PAM site, the development of an all-in-one SaKKHABE8e deliverable by single AAV, the known site specificity of editing efficiencies across all editing technologies, and the lack of prediction tools available for Sa, SaKKH, and Cas13 base editors, multiple mutations and sites were targeted throughout this thesis in a variety of models to determine a holistic understanding and comparison of the applicability of base editors. This was undertaken as a comparison of DNA and RNA base editors to determine which is more relevant for translational purposes for *ABCA4* given the high turnover rate of outer segment discs, and thus *ABCA4.* In an *Abca4 -/-* mouse model, SaKKHABE8e achieved mean editing of 16% in the best performing cohort, whereas dPspCas13b-ADAR$_{DD}$(E488Q) resulted in no editing at the dose tested.

This discussion first reflects on the four thesis aims and then on the greater context of novel therapeutics for *ABCA4* and CRISPR editing.

1. **To characterise the genetic landscape of *ABCA4* mutations and establish the relevance of base editing for *ABCA4*.**

Using variant databases and published patient cohort variants, a systematic investigation was conducted to determine the relevance of DNA base editors based on PAM site prevalence in *ABCA4.* This confirmed the complexity of the *ABCA4* genetic landscape and concluded that DNA base editors are highly relevant for *ABCA4* gene therapy due to heterogeneity. The analysis identified a variant for use in aim 2. As gene editing technologies continue to develop (ie prime editors, transversion editors, etc) continued analyses can be conducted to explore all *ABCA4* variants. Lastly, this also shed light on the data gap regarding common variants across continental Asia, Africa, and South America.

2. **Develop a pipeline to compare DNA and RNA base editing in targeting the same *ABCA4* mutation.**

   An SaCas9 nickase KKH orthologue fused to an ecTadA deaminase domain (DNA base editor, SaKKHABE8e) and dPspCas13b fused to a hyperactive ADAR2$_{DD}$(E488Q) (RNA base editor, Cas13-ADAR) were compared *in vitro* in HEK293T cells targeting the c.206 G>A stop mutation in *ABCA4.* Guides were screened using a luciferase reporter assay. The best performing guides for each base editor were then used in a side-by-side comparison of the base editors looking at DNA, RNA, and protein level analysis. The editing rate at the DNA-level for the DNA base editor resulted in a 2x downstream transcript-level effect. Overall, editing rates at c.206 G>A were roughly equal between the DNA and RNA base editors by all measures except for qPCR. Off-target editing and toxicity were also investigated, with SaKKH surprisingly showing a higher degree of bystander editing than the well-documented promiscuity of Cas13-ADAR.[199,215] The toxic response to SaKKHABE8e was greater than to Cas13-ADAR in HEK cells.

3. **Screen a clinically relevant mutation and transduce retinal organoids to target *ABCA4***

An *ABCA4* patient database from Moorfield's was screened for a clinically relevant mutation from which to produce patient-derived organoids. The c.93 G>A nonsense mutation was chosen due to the numerous PAM sites. The patient kindly consented; however, organoid production was unsuccessful. Nonetheless, to establish editing at a wide variety of sites and target a clinically relevant mutation, c.93 G>A was targeted by both DNA and RNA base editors *in vitro*. Editing at this site resulted in extremely variable RNA base editing and no successful DNA base editing, in contrast to the editing observed at the target sites in aims 2 and 3. This outcome highlighted the known site specificity of gene editing technologies[285-287] and the subsequent importance of thorough screening at target sites.

Nearby sites, c.99 and c.105, were also targeted *in vitro* for downstream testing of DNA and RNA base editors in wildtype retinal organoids. Targeting by SaKKHABE8e, again, resulted in no successful editing at either site, whereas editing by Cas13-ADAR was successful at both sites. Due to this, only Cas13-ADAR was taken forward for testing in wildtype organoids at the c.105 site. Unfortunately, as in the *in vivo* experiments, this resulted in no editing. The reason for the discrepancy between Cas13-ADAR editing outcomes *in vitro* and *in vivo* is unclear and requires further investigation. In addition, the editing outcomes underscore the need for testing in complex pre-clinical models. Lastly, this suggests that RNA base editing using dCas13b-ADAR is not therapeutically viable for *ABCA4* at this stage and requires significant optimisation to achieve editing beyond *in vitro* screens.

4. **Test AAV-delivered DNA and RNA base editors in targeting *ABCA4 in vivo.***

   Given that no clinically relevant mouse model could be produced within the time of the PhD, a heterozygous mouse with one wildtype and one knockout *ABCA4* allele was bred. The base editors were used to target the *ABCA4* start codon and knockdown *ABCA4.* Three cohorts investigating multiple doses were undertaken to compare the three base editors *in vivo*:

   a. RK driven dPspCas13b-ADAR$_{DD}$(E488Q) in a dual vector approach with the gRNA delivered on a separate vector
   b. RK driven SaKKHABE8e in a dual vector approach with the gRNA delivered on a separate vector

c. An all-in-one RK driven size-minimised SaKKHABE8e with the guide in reverse included in the same vector

The *in vitro* screens did not predict the *in vivo* outcomes. The SaKKHABE8e dual vector and all-in-one delivery were each tested at two doses. The dPspCas13b-ADAR$_{DD}$(E488Q) was only tested at one dose. The best performing cohort, the all-in-one SaKKHABE8e at the low dose (5E+8vg/eye), demonstrated the highest mean editing of 16% with a mean transcript-level effect of 24.5%. The highest single editing rate achieved was with the all-in-one SaKKHABE8e high dose (1E+9vg/eye) editing of DNA reached up to 32.3% with a downstream effect of 47% at the RNA level. These results were highly encouraging for the single-AAV SaKKHABE8e and highlighted the need for further dose optimisation and testing in a clinically relevant mouse model. Work is ongoing to establish a functional effect. The dual vector SaKKHABE8e demonstrated low-level editing and extreme toxicity. This was likely due to the mCherry reporter, presenting the need for future testing without fluorescent markers or using alternative tags. In comparison, the dPspCas13b-ADAR$_{DD}$(E488Q) showed no detectable editing at the tested dose. Although less encouraging, both dual vector approaches would benefit from continued testing with no fluorescent marker to improve editing rates and reduce toxic effect. Taken together, at the doses tested and considering the toxic effect of the fluorescent protein, DNA base editing using single AAV delivery resulted in the most promising outcomes.

7.2 *In vitro* assays for detection of editing

Relative editing rates of the guides determined by Sanger sequencing and EditR correlated with the luciferase assay output. However, the luciferase assay typically underreported editing rates by 5-10% compared to sequencing outputs, and it is unclear why. While the assay is highly sensitive, one possibility is the multitude of steps required for luciferase assay output.[385] Taken together, these may result in a cumulative, measurable inefficiency. Alternatively, unedited transcripts may undergo nonsense mediated decay, increasing the relative percentage of edited transcripts and thereby skewing editing rates determined by sequencing. However, this is unlikely due to splice mechanisms and NMD machinery, and sequencing validation. [270,327,386-388]

Overall, the sequencing to luciferase assay output discrepancy largely depended on the target site and typically never exceeded 10%.

When using the luciferase assay to measure knockdown, an assay design was used where a change in reading frame enabling expression provided evidence for on-target activity. An alternative of knocking down the start codon and thus *Renilla* was considered to reflect the exact biology of the *in vivo* experiment, however, this outcome would have been highly dependent on assay conditions such as cell-health, transfection efficiency, etc despite the orthogonal design. A positive result outcome ensured that activity was due to editing, rather than assay conditions.[385]

For both luciferase assay designs, multiple positive controls were used, including a universal control used across all experiments that placed the Firefly in-frame and a site-specific control containing the wildtype (ie 'corrected') sequence. This allowed for analysis of the effect of the sequence on expression levels, as seen with the c.93 region. Samples were compared and normalised to the site-specific control to account for the effect of the sequence on expression.

The assays targeting mutant *ABCA4* plasmids allowed for testing of the best-performing guides in a more biologically relevant context, particularly for dCas13-ADAR editing. This system still did not fully recapitulate endogenous expression, such as expression levels, folding and structure, methylation, protein interactions, or localisation. However, production of mutant *ABCA4* plasmids allowed for cheaper, faster *in vitro* screening than developing mutant cell-lines or using patient fibroblasts. Further, it enabled analysis of DNA and RNA level editing, alongside full-length protein production. Future testing would have included protein functional assays[389-391] and targeting in cell-lines which endogenously express *ABCA4*, such as in hair follicle stem cells and keratinocytes.[66]

The combined analysis from the luciferase assay and from targeting *ABCA4* plasmids allowed for comprehensive screening of base editors and guides prior to testing in more complex models.

7.3 Insights from pre-clinical models

There was a notable discrepancy when moving from *in vitro* HEK cell assays to more complex pre-clinical models, such as *in vivo* mouse models or retinal organoids. This was expected given the plasmid overexpression in HEK cells allied to the increased complexity of

mouse models and organoids, and is similarly reflected in the transition from pre-clinical models to clinical trials. Although it seemed as if dPspCas13b-ADAR$_{DD}$(E488Q) had the strongest decrease when going from *in vitro* to *in vivo* or organoids, the incremental difference was similar between the DNA and RNA base editors. Targeting the *mABCA4* start codon, c.1, dPspCas13b-ADAR$_{DD}$(E488Q) showed 21.8% editing *in vitro* and 0% editing *in vivo,* whereas SaKKHABE8e showed 45-50% editing *in vitro* and mean editing of 16% *in vivo,* a 34% reduction in efficiency. In the organoid model, dPspCas13b-ADAR$_{DD}$(E488Q) also showed no editing, despite 34.7% editing at the c.105 site *in vitro*.

These results underscore the importance of testing editing technologies in a wide variety of pre-clinical models to gain a more realistic look at real editing rates and secondary effects. While more clinically relevant models were intended for this project targeting the same site in retinal organoids and a mouse model, the models used provided valuable insights. Future experiments would include targeting the same mutation across all models tested.

Quantifying knockdown or editing of a missense variant was challenging. For knockdown, while absolute editing rates, protein analysis, and expression analysis were undertaken, determining the effect of knockdown versus toxicity was not fully possible. Ongoing work investigating a functional effect through induction of a phenotype at 6-9 months post-injection will enable continued examination of *ABCA4* knockdown, as well as studying the long-term on- and off-target rates and effects. Additional experiments such as single cell sequencing and more IHC may aid in delineating knockdown from toxicity in these long-term outlooks.

Similarly, inducing a silent missense variant in organoids to determine site targetability was difficult to quantify beyond sequencing output. Future experiments targeting clinically relevant stop mutations would allow for more definitive and sensitive analysis of editing in both models.

Nonetheless, each model offered valuable information. *In vivo* work enabled analysis of the effect of injection, toxic components, vector tolerability, and observation of immune response in a fully formed retina. However, given the species differences, this does not fully recapitulate the human response. In addition, mice lack a macula and have physiological peculiarities due to inbreeding, thus affecting studies of macular degeneration such as Stargardt disease.[96] Conversely, retinal organoids do provide a human genetic and physiological environment for testing of therapeutics that can be personalised to an individual. However, as discussed in

Chapter 5, retinal organoids do not contain key tissues such as an RPE monolayer, vascularisation, or immune cells such as microglia.[93] This may hamper the ability to study *ABCA4* given the dependence of the outer segments on the RPE. Nonetheless, organoids are rapidly developing, enabling improved representation of the human retina.

Clinically relevant models containing specific mutations tend to be time-consuming and costly to produce. Nevertheless, both mouse and retinal organoid models are necessary to provide critical and in-depth analysis of the diverse measures required in therapeutics screening.

7.4 Comparison of dCas13b-ADAR and SaKKHABE8e

Based on the results of the three experimental chapters, cumulatively targeting six different sites in *ABCA4,* it is clear that editing efficiencies are extremely site dependent.[285,286,311] Further, it is difficult to predict editing efficiencies with existing predictive tools, especially since they are typically designed for SpCas base editors.[353,384,392,393] Moreover, editing efficiencies, particularly for dPspCas13b-ADAR$_{DD}$(E488Q), dropped significantly when moving from *in vitro* conditions to a complex pre-clinical model. As stated previously, it is unclear why this happened. Both the varied editing efficiencies and model differences are discussed in greater detail in each of the sections below.

7.4.1 Guide design, specificity, and efficiency

The known variation in editing efficiencies across different target sequences is a major limitation of gene editing tools.[286] This was reflected in thesis results which revealed notable editing variability at the different targets in the DNA and RNA base editors tested. Two factors influencing this are the binding efficiency of the gRNA[286,287,353] and the consensus sequence preference of the deaminase.[198,215,216,285] The context of the sites targeted are analysed based on known guide design preferences.

7.4.2 SaKKHABE8e

For DNA base editing, this thesis focussed on an SaKKHABE8e base editor due to the small size and the improved PAM flexibility. Interestingly, as seen in Chapter 3, *ABCA4* has a high proportion of pathogenic transition mutations with an SaKKH PAM site of ~44%, likely due

to the larger editing window. Due to PAM site requirements, DNA base editing of specific pathogenic mutations does not allow for flexibility in guide design. Nonetheless, 3-5 guides varying in length from 19-23bp were tested at most target sites to put the target mutation at positions 4-12 within the spacer. Previous reports indicate 20nt guides for SaABE, but optimal guide lengths of 21-23nt for SaCas9.[158,250] At the sites tested, guides 20 or 21nt in length demonstrated the highest editing rates with minimal difference between the two lengths.

The discrepancy in site specificity was stark, where editing rates ranged from 0-45% across target sites. Editing of the start codon, c.1, resulted in the highest editing of 44.7%, followed by 24.3% at c.206 G>A and 0% at c.93 G>A, c.99, and c.105. Interestingly, SaCas9 showed 4-9% cleavage activity using the same guide as the SaCas base editor (SaABE8e). It is hypothesised that deaminase consensus sequence preference may be the reason for no base editing at c.93, c.99, and c.105 but successful cleavage at c.124. This requires further investigation of cleavage by SaKKHCas9 at sites c.105, c.99, and c.93.

Location within the guide sequence likely did not affect editing efficiency since positions 5-12 were screened across the six targets. Although the sites at which editing occurred placed the target at positions 5 and 7, sites c.93, c.99, and c.105 also had guides placing the target at positions 6-12 (Table 7-1).

One major factor affecting editing rates is gRNA binding efficiency. This is partly affected by GC content,[312,321,394,395] where 40-60% is considered optimal and <35% reduces efficiency. Indeed, at all sites where no editing occurred, c.93, c.99, and c.105, %GC was between 30-33%. Conversely, c.206 and c.1 had 60 and 65% GC content, respectively. An additional sequence-related factor influencing activity is a high proportion of Ts,[321] which is seen in the c.93, c.99, and c.105 guides where this ranges from 55-60% (Table 7-1). This is significantly less in the c.206 and c.1, at 23-25%. Lastly, PAM multiplicity can affect Cas activity, where a greater number of PAM sites in a region can reduce activity.[323] The c.93 region has three SaKKH PAM sites in short succession, perhaps contributing to reduced guide binding. While it is still difficult to predict editing efficiencies and guide binding, taken together, the c.93 region has multiple factors that would likely decrease binding and activity, whereas c.1 and c.206 have favourable factors for activity and binding.

Site	Editing % *in vitro*	Position	Multiple PAMs	% GC	% T
c.1	44.7	7	No	65	25
c. 93	0	6-8	Yes; 4	33	55
c.99	0	6, 12	Yes; 4	30-33	55-60
c.105	0	7, 12	Yes; 4	30-33	55
c. 206	24.3	5	Yes; 2	60	23

Table 7-1: Factors affecting SaKKH gRNA binding and editing efficiency.
Four factors affecting binding and editing at the target site: target site position, number of SaKKH PAM sites, %GC content of guide, and % T content of guide. Position within the spacer can influence editing rates, particularly in relation to the deaminase domain. The editing window for SaKKH is positions 4-12, with optimal editing at positions 4-8. PAM multiplicity affects activity, where multiple PAM sites in an area can hinder activity. Low GC (<35%) and high GC (>80%) inhibit guide binding. High T% (not specified) reduces activity. All editing rates listed are *in vitro.*

7.4.3dCas13b-ADAR$_{DD}$

The dPspCas13b-ADAR$_{DD}$(E488Q) was selected to undertake RNA base editing. Given the lack of PAM sites required and the longer optimal guide length of 50nt for dPspCas13b-ADAR$_{DD}$(E488Q) editing, guide design was much more flexible. Due to this, as described throughout the thesis, fifteen guides were screened per site.

In the original paper, an A-C mismatch distance of 32-36nt was shown to be optimal.[199] The three sites that underwent a full guide screen showed consistently high activity at positions 30 and 31 (guides 6 and 7) and had another peak at positions 24-26. The one exception to this is at c.93 where position 37 (guide 2) showed the highest on-target and lowest off-target activity. While the active positions remained constant across target sites, editing rates varied and, as for SaKKHABE8e, were likely affected by sequence context and deaminase sequence consensus. However, the variability was notably less than for DNA base editing, ranging from 16-47%, where editing was seen at all target sites *in vitro*. C.206 showed the highest editing at 47% and c.93 the lowest, at 16% (Table 7-2).

Site	Editing achieved %	Position	Bystander/ Off-target	Target motif (5'-3')
c.1	21.6	24	Yes	CAT
c. 93	16	37	Yes	GAC
c.99	28.3	30	No	TAT
c.105	34.7	24	No	TAT
c. 206	47	31	No	TAG
c.5882	29	32	Yes	GAA

Table 7-2: Summary of dCas13b-ADAR$_{DD}$(E488Q) editing rates at target sites.
Editing rates, position within the spacer, bystander or off-target editing, and the target motif for each site targeted throughout the thesis by dCas13b-ADAR. The motifs followed the expected ADAR2 preferences where 5'-TAG-3' is the most preferred and 5'-GAC-3' is the least preferred.

Although sequence preferences of Cas13 guides and ADARs are not well understood, target sequence context influences editing efficiency, as with DNA base editors.[353] RNA structures such as mismatches, bulges, and stem-loops play an important role in ADAR activity, suggesting that evolutionarily preserved RNA secondary[275] and tertiary structure[396] play a major role in recruitment and activity.[276,397] In Lehmann et al, four radio-labeled adenosines were interrogated by either ADAR1 or ADAR2. The percentage of deamination was the same regardless of the enzyme used, suggesting the RNA substrate determines selectivity.[398] However, it has been shown that the dsRNA-binding-motifs (dsRBMs) across a family of proteins targeting dsRNA show a high degree of sequence selectivity specific to the protein.[399] This is the same for ADAR, where exchange of the catalytic domain between ADAR1 and ADAR2 resulted in sequence specificity associated with the catalytic domain identity.[400]

Sequence motif preferences for ADAR2 have been established to be U>A>C>G at the 5' end and G>C>U≈A at the 3' end, which differs from ADAR1.[198,327,328,398] This suggests that sequence specificity is indeed largely due to enzyme sequence preference. Conversely, multiplicative models analysing sites beyond nearest neighbour bases indicated that editing was influenced by more distant bases as well as nearest neighbours ie the RNA substrate context.[327] Overall, the understanding of what affects editing is limited and multifactorial.

Using the published ADAR2 sequence preferences, analysis of the targeted sites throughout this thesis showed that editing efficiencies reflected the preferences. The c.206 stop codon with a 5'-TAG-3' motif was the favoured editing site and c.93 motif, 5'-GAC-3,' a less

preferred site. In Cox et al,[199] a screen of Cas13-ADAR motif preferences at the same target site where the 5' and 3' flanking bases where changed, showed that 5'-UAU-3' had the greatest editing. C.99 and c.105 which both had this motif showed substantial editing rates, however, editing at c.206 was notably higher. Sequence context likely contributed, which was observed with the varied editing rates between c.93, c.99, and c.105, where small differences in the guide made a remarkable difference in editing. A factor contributing to the stronger ADAR2 preferences may be the independent effect of the ADAR, considering that previous publications have shown that 20-60% of editing is possible without the DR scaffold ie independent of dPspCas13b.[272] This was particularly prominent at the off-target site in *Renilla* which had the preferred 5'-UAG-3' and the highest editing throughout the whole thesis.

Novel ADAR recruitment methods are enabling high efficiency dsRNA editing without dCas13b either with endogenous ADAR or exogenous ADAR delivery. This exciting novel development is discussed more below.

7.4.4 Vector expression

The on-target editing variability between dPspCas13b-ADAR$_{DD}$(E488Q) and SaKKHABE8e were substantial and site-dependent, as previously discussed. The most notable difference was in the more complex models, where dPspCas13b-ADAR$_{DD}$(E488Q) did not result in editing, regardless of dose. One of the main contributing factors for this is low expression levels. *In vivo,* while dPspCas13b-ADAR$_{DD}$(E488Q) was sufficiently expressed to be detected by western blot, the dose of gRNA was particularly low. Inversely, in the organoids, at both doses the gRNA expressed strongly, but dPspCas13b-ADAR$_{DD}$(E488Q) expression was not confirmed. Editing may be possible with more optimised doses and confirmed expression. For example, applying the *in vitro* optimised 2:1 gRNA:base editor ratio may improve outcomes *in vivo.* Interestingly, in a recent study targeting the OTOF gene in inner hair cells of the ear in mice, an RNA base editor, mini-dCas13x (mxABE), achieved 80% editing and resulted in expression in 100% of inner hair cells, suggesting that therapeutic levels of RNA base editing are achievable at an optimal dose.[212] In contrast, another recent study targeting the *MYO6* in the inner ear with mxABE, editing of 4.22% was achieved.[211]

Overall, the DNA base editing, particularly the all-in-one delivered SaKKHABE8e, showed reliable on-target editing *in vivo.* This is likely due to factors such as targeting DNA and thus fewer gene copies, being delivered in one vector, and sufficient vector expression as seen by

western blot. Going forward, testing the all-in-one SaKKHABE8e in organoids and further optimising the dose *in vivo* may enable improved editing outcomes.

Future investigation of expression levels of the transgenes, the target gene, and indicators of cell health through GFAP staining and single cell RNA sequencing may provide a more definitive understanding of base editor expression and corresponding cellular expression levels.

7.4.5 Off-target editing

Bystander and off-target editing present a major safety concern in the application of gene editing technologies, due to undesired changes to the genome or transcriptome. Although machine learning tools are being developed to predict where these sites might arise, confirmation of off-target editing through *in vitro* assays or WGS is necessary.[220,401,402] This may require personalised screens in a therapeutic context given that genetic diversity may alter likely off-target sites.[403]

Fortunately, adenine base editors, such as ABE8e, exhibit desirable properties for precision gene editing. This includes greater single nucleotide editing precision[178,311] and lower levels of Cas-independent off-target editing.[178,179,372,404] A recent study investigating off-target editing of ABE8e in tomatoes found no evidence of guide-independent deamination, suggesting no Cas-independent off-target editing by ecTadA.[405] Further, ABEs have undergone continued evolution to improve higher on-target editing efficiency and reduced off-target editing efficiencies, or guide modifications to improve target specificity, such as ABE9e.[406-408] Despite these advantages and advancements, for DNA base editing, off-target edits may accumulate over time and thus pose a greater risk with long-term expression due to targeting of the genome. Minimising expression time could drastically decrease the chances of off-target editing. Alternative delivery methods may offer a solution to temporally control transgene expression and are discussed further in section 7.6.1. Further, off-target editing is highly sequence dependent, where guides with stronger binding affinity may show reduced off-target editing at the expense of editing rate.[277]

The SaKKHABE8e used throughout this thesis has advantages in a more flexible PAM site and increased editing window, enabling targeting of more mutations. However, this increases the risk of bystander editing, for example, this was observed at site c.206, where the bystander A was edited at nearly the rate of on-target editing. A recent study using ABE8e to target a nonsense mutation (c.130C>T) in *RPE65 in vivo* found that introduction of missense bystander

edits resulted in impeded restoration of visual function.[409] Fortunately, bystander edits can be anticipated and the consequences analysed in programs such as AlphaFold.[410] Future work would include investigation of genome-wide off-targets by whole-genome sequencing for *in vivo* samples. The continued work looking at the functional effects of the SaKKHABE8e on *ABCA4* knockdown will also shed light on the effects of long-term expression on off-target editing.

While RNA base editing by dPspCas13b-ADAR$_{DD}$(E488Q) has a minimal risk of irreversible off-target edits (ie genome) due to targeting the transcriptome, off-target editing can still lead to altered expression or protein misfunction, in addition to generation of immunogenic epitopes.[411] This is a particular risk with exogenous ADAR2 overexpression,[215,411] such as with dPspCas13b-ADAR$_{DD}$(E488Q), where protein interactions can be altered, thus affecting cellular physiology.[20] Directed evolution and rational mutagenesis have led to orthologues with substantially decreased off-target activity, such as the addition of the T375G mutant.[199] Transcriptome-wide off-target analysis was not undertaken for dPspCas13b-ADAR$_{DD}$(E488Q) *in vivo* due to the lack of on-target editing. Inspection of local off-targets within the amplicon revealed low-level promiscuity throughout.

One novel method of reducing the effect/risk of off-target editing is the recruitment of endogenous ADARs, given the native expression levels.[199,215] Indeed, initial attempts resulted in a 2-3 fold magnitude decrease in off-targets in a study recruiting endogenous ADAR using circular ADAR recruiting RNAs (cadRNAs). Notably, 80% of this was bystander editing in the target transcript, which the outcomes of are significantly easier to predict.[215]

Bystander editing with dPspCas13b-ADAR$_{DD}$(E488Q) or other RNA base editing methods are substantially more likely due to the increased guide length of at least 50nt. While no modifications for this have been made with dPspCas13b-ADAR$_{DD}$(E488Q) apart from the C mismatch, ADAR recruiting methods have significantly reduced bystander editing by creating bulges in the guide sequence. Bystander editing was substantially reduced by this method, but on-target editing saw significant reductions as well.[215,412] Additional novel guide modificiations introducing A-A mismatches at the N$_{10}$ site[413] and hairpin guide structures[414] have been shown to reduce bystander and off-target editing.

Bystander and off-target editing were only observed at three of the six sites targeted, c.1, c.93, and c. 5882. Interestingly, these were the less-preferred binding motifs (Table 7-2),

suggesting that off-target and bystander editing is less likely proximal to preferred motifs due to greater on-target activity, however, this requires extensive further investigation.

7.5 Toxicity and immunogenicity

Toxicity due to the Cas constructs and the viral vectors was observed throughout this project. *In vitro* both the dPspCas13b-ADAR$_{DD}$(E488Q) and SaKKHABE8e resulted in decreased *ABCA4* expression as seen in the luciferase assay and western blot. Translationally, this raises the concern that the Cas components are bacterially derived and could thus result in immune responses.[378] As discussed in Chapter 6, pre-existing antibodies to SaCas9 are common. Despite this, in the Edit-101 clinical trial injecting SaCas9 to treat LCA, by one-year post-injection, no serious adverse events had been reported. An immune response was detected in patients both with and without pre-existing immunity. Lastly, no SaCas9-binding antibodies were detected before or after treatment.[415] These results are promising but require continued long-term monitoring.

Prevalence of pre-existing antibodies to dPspCas13b-ADAR$_{DD}$(E488Q) has not been studied in humans. A study investigating pre-existing immunity against RfxCas13d found reactive antibodies and CD4 and CD8 T cell responses in most donors. This was comparable to the responses to SaCas9 and SpCas9.[416] Similarly, in a study looking at a PspCas13b knockdown strategy in mice, an immune response that was improved with the administration of immunosuppressants was observed.[382] Based on this, it can be assumed that an immune response against dPspCas13b-ADAR$_{DD}$(E488Q) is likely in humans.

Surprisingly, *in vivo,* dPspCas13b-ADAR$_{DD}$(E488Q) and SaKKHABE8e were well-tolerated at specific doses. Higher dose and construct-specific toxicity were observed, for which further investigation of the immune responses is required. Longer-term analysis of vector tolerance both *in vivo* and in retinal organoids would shed light on this. Analysis by GFAP staining may enable observation of cellular sensitivity. *In vivo,* single cell RNA sequencing, IHC, and flow cytometry may shed light on immune markers to determine if these are upregulated in response to AAV dose-escalation and across base editor types. Overall, toxicity and immunogenicity require longer-term investigation and observation to establish a robust safety profile.

Immunogenicity of the virus is also an important consideration in regard to inflammation or toxic-effect, particularly in a translational context. The immune response to AAV in the eye is poorly understood and highly variable. Some reports show no toxicity due to the vector or transgene,[126,417-420] whereas other reports do show a toxic response and inflammation.[230,421,422] It is unclear how an ocular toxic response is triggered, but it is observable that surgery, the AAV vector, the transgene, or the combination can result in a toxic response. Additional factors such as gene overexpression may affect overall retinal health, resulting in a toxic downstream effect.[423] This will require monitoring in the long-term *in vivo* follow-up. Further, AAV can activate innate and adaptive immune responses.[126] Indeed, some reports have shown ~70% of people have antibodies to AAV2 due to natural exposure to wildtype AAV. Fortunately, pre-existing antibodies to the serotypes that transduce photoreceptors, AAV5 and AAV8, are some of the least prevalent.[424-426]

7.6 AAV delivery

Delivery methods such as lentivirus, nanoparticles, eVLPs, and naked DNA delivery demonstrate low transduction beyond the RPE.[427] Thus, AAV vectors continue to be the preferred delivery method for targeting the retina for several reasons. First, the non-pathogenic, episomal nature of the vector provides a robust safety profile. Second, they can transduce dividing and non-dividing cells, enabling transduction of photoreceptors. Third, multiple serotypes have shown strong transduction of the RPE and photoreceptors, enabling transduction of both key cell types in Stargardt Disease.[56,65,428,429] Thus, AAVs are the main candidate for the delivery of gene therapeutics, ranging from gene augmentation to CRISPR-Cas, despite packaging capacity limitations.

Continued evolution of gene editing technologies enables circumventing of the AAV packaging capacity. A wide variety of compact Cas orthologues have been fused to base editing effectors to create size-minimised ABEs deliverable in a single AAV, including CjCas, Nme2Cas, SauriCas, and Sa(KKH)Cas. These have shown robust editing *in vivo,* achieving editing rates of up to 59% in the liver.[180] Indeed, this was demonstrated with the all-in-one SaKKHABE8e in this thesis with up to 32% editing, or mean editing rates of 16%, in the retina. Similarly, an RNA base editor has been created using a compact orthologue, Cas13bt[204] and Cas13X.1.[206] These have shown successful base editing in the inner ear targeting OTOF, achieving up to 80% editing.[212]

In instances where targeting using a single AAV is not possible, alternative methods, such as the trans-splicing or split-intein approaches have been applied with great success. Larger Cas orthologues, like SpCas9, or prime editors have shown editing rates of 15.9%[175] and 11.4%,[192] respectively, in the RPE and photoreceptors. The dual vector approaches also offers the benefit of delivering multiple guides to target multiple mutations where needed. This would not be possible with the all-in-one SaKKHABE8e, for example.

One shortcoming of AAV mediated delivery is the transgene expression time. At its conception and in the context of gene augmentation, continued transgene expression was key, particularly to enable single administration.[31,56] Similarly, for RNA editing, sustained expression is required given the transient nature of the mRNA target. Fortunately, all-in-one Cas13-ADAR orthologues and novel endogenous and exogenous ADAR approaches are small enough for AAV delivery.[215,216] However, although single AAV delivery is possible for DNA base editing, long-term expression increases the likelihood of developing off-target editing.[257] While it has been hypothesised that transgene expression may decrease over time,[230,231] alternative delivery methods have been investigated to reduce gene editor expression time.

7.6.1 Alternative delivery options

A wide variety of alternative delivery options have been developed to enable efficient delivery of a larger cargo size with limited immune response, including lipid nanoparticles (LNPs),[427,430] virus-like particles (VLPs),[370,431,432] and lentiviruses.[35] These are described in greater detail in the general introduction. Novel packaging methods such as eVLPs enable tissue-specific delivery of ribonucleoproteins (RNPs) instead of genes. This would enable reduced expression time due to protein degradation in instances of genome editing, such as Cas9, DNA base editors, and prime editors, and likely reduce off-target editing as a result. In addition, given the lack of DNA delivered and expressed, the risk of genetic material integration[131,249,433] and gene overexpression[423] are avoided.

A recent report of *in vivo* delivery of a prime editor RNP by eVLP demonstrated efficient editing in the RPE. Two genes, *Mfrp* and *Rpe65,* were targeted and resulted in 15% and 7.2% editing, respectively. Moreover, *in vitro* the on-target to off-target ratio improved 3-fold when comparing eVLP to plasmid transfection at two highly edited off-target sites. *In vivo,* analysis by deep sequencing of the top 10 off-target sites revealed no editing above the limit of detection. This is hypothesised to be due to a combination of prime editing site specificity and the transient

nature of RNPs.[131] An additional study reported direct delivery of a Cas9 RNP and DNA base editor RNP to photoreceptors, however, high concentrations led to retinal toxicity. Nonetheless, Cas9 editing of 7.2% and ABE editing of 10.7% was reported in the photoreceptors.[434]

Although promising, with both studies showing sufficient RPE transduction, photoreceptor transduction is still lacking and is not comparable to AAV-delivered editing activity. A major factor inhibiting efficient transduction by non-AAV mediated delivery is retinal structure, where the photoreceptor outer segment is difficult to penetrate due to the phospholipid bilayer of the discs. This is compounded by the continued phagocytosis of the outer discs, which may also phagocytose or degrade the delivered therapeutic.[435,436]

Continued research into vector structure and make-up in relation to improved understanding in retinal structure and interactions will enable exciting developments in gene editing technology delivery.

7.7 Novel gene editing tools

7.7.1 DNA editing

The discovery of the Cas editing systems has enabled straightforward, efficient editing of the genome. Fusing the guide-directed Cas to a variety of effectors has allowed for a wide scope of editing and flexibility in targeting mutations. Initial iterations of this included CRISPR inhibitors and activators to influence gene regulation.[437] Adenine and cytosine base editors next enabled site-specific editing,[176] and have since undergone directed evolution to create a wide-variety of orthologues with improved PAM flexibility and site-specificity, such as the ones used throughout this thesis. This has resulted in at least 9 clinical trials as of 2024, showcasing the therapeutic potential of base editors.[438]

Further fusion of effectors to Cas9 has expanded editing tools to include prime editors,[190] a highly versatile editing tool that can edit all 12 point mutations and small indels. Prime editing has proven to be highly effective *in vivo,* resulting in up to 42% editing in mouse brain with no detectable off-target edits.[439] In the retina, 16% editing was achieved in targeting a mutation in *RPE65.*[192] Although promising, given the complexity of prime editing, editing efficiencies are extremely variable depending on the target site, complicating its application.[440]

More recently, transversion base editors have enabled single base correction of transversion mutations. Editing rates in mouse embryos and human cell lines resulted in 44-56%

average A-to-C editing, expanding the possibilities of base editing technologies.[188] Glycosylase base editors and modified ABEs (CABE-T) are further broadening site-specific editing tools.[182,189] The combined Cas9-based toolbox has rapidly widened the scope of gene editing strategies, providing an exciting outlook for therapeutics and permanent treatments.

7.7.2 RNA editing

Early methods of targeting RNA have included antisense oligo therapies and RNA interference.[441-443] RNA base editing, particularly by Cas13, is a relatively novel RNA editing tool that enables precision targeting of the transcriptome through guide-directed A>G deamination. This thesis investigated editing using dPspCas13b-ADAR$_{DD}$(E488Q) with little success. However, new reports using a size-minimised Cas13 RNA base editor (mini-dCas13X) achieved up to 80% editing *in vivo,* restoring OTOF expression in inner hair cells.[212] Alternative RNA editing Cas orthologues have also been reported, such as Cas13Y and Cas7-11.[444,445] However, these are yet to be used *in vivo.*

Methods using ADAR recruitment via modified guides have made structural improvements by circularising the guide and thus mitigating degradation of the guide. These designs have resulted in significant *in vivo* editing efficiencies using both exogenously delivered and endogenous ADAR. Endogenous ADAR recruitment, in particular, shows promise given the native expression levels of ADAR, thus reducing the likelihood of negative physiological effects from altered ADAR expression levles.[213,215,216]

Lastly, a newly started clinical trial applies pre-mRNA-trans splicing to enable successful replacement of the mutant 5’ or 3’ half of a transcript with correct synthetic RNA. This would enable native expression levels of the target gene and does not require mutation-specific editing, but likely still requires high efficiency for a treatment effect. Clinical trial data will shed light on safety and long-term efficacy.[260]

The wide variety of editing tools, as with DNA editing, collectively enable editing of the majority of genetic mutations. Although it is unlikely there will be a one-size-fits all approach, these gene editing tools provide great therapeutic potential.

7.8 Therapeutics for ABCA4-related disease

Mutations in *ABCA4* are the most common cause of inherited macular degeneration and have thus been a central candidate in gene therapy development.[23,446] A multitude of approaches have been tested in pre-clinical and clinical trials, including lentiviral deliver,[35] dual AAV,[41,42] lipid nanoparticles,[43] (pre)mRNA trans-splicing,[58,125] split-intein,[447,448] and Cas-mediated mutation correction.[102] However, due to the complexity of the gene in terms of size (6.8kb),[68] mutation number (~1200),[23] the high percentage of complex alleles (10-16% of patients),[23,69] and the expression profile (photoreceptors, minimally RPE),[65] no treatment or therapy is available yet. Further, the high degree of heterogeneity would likely require high editing efficiencies by site-specific editors for a treatment effect, given that only one allele is targetable.

A new clinical trial (NCT06467344) utilising pre-mRNA *trans*-splicing to join a synthetic mRNA to an endogenous pre-mRNA target may enable amelioration of most *ABCA4* variants by delivering either the 5'- or 3'- half of the *ABCA4* coding sequence.[125,260] Further, given that RNA is edited, any potential off-target effects are transient in nature. Although promising, the clinical trial is only in the pre-screening stages so the efficacy in humans is yet to be determined, where high transduction and editing efficiency are required.

The listed technologies have rapidly advanced in the last 10 years, providing many exciting prospects for an *ABCA4* treatment or therapy. In this thesis, DNA base editing in particular, proved an exciting *in vivo* candidate for targeting *ABCA4*. Although promising, overall, base and prime editing may prove to be a tedious approach in addressing *ABCA4*-related retinopathies given the sheer number of targetable mutations.[23] Further, the risk of bystander editing is elevated given the relatively high likelihood of inducing a pathogenic variant. In instances of targeting common mutations, such as c.5882 G>A and c.5160-10 T>C, base and prime editing may be suitable options.

Three clinical trials beginning in 2024-2025 focus on gene supplementation therapy. Two trials will aim to deliver *ABCA4* by dual vector delivery (SB007, AAVB-039).[121] A third approach uses a novel method of genomic *ABCA4* insertion by transposition (SGT-1001).[129,130] All three provide a promising outlook for treating *ABCA4,* however, due to the delivery methods by dual-vector and LNP, efficiency may be reduced.[41,42,180,427] Saliogen has since shut down.

Base editing may also offer a solution for patients homozygous for complex alleles with transition mutations in both the 5' and 3' end of *ABCA4*. Although such variant combinations are rare, DNA base editors can target multiple mutations simultaneously when delivered with multiple guides, enabling a therapeutic possibility in complex genetic situations.

7.9 Future of gene therapy for IRDs

The first retinal gene therapy, voretigene neparvovec (Luxturna), was approved only 8 years ago. The road to approval established gene therapy efficacy, clinical endpoint measures, surgical technique, AAV safety, and long-term studies of AAV expression, paving the way for future gene therapies.[233,449] Since then, many retinal gene augmentation therapeutics have been developed pre-clinically and tested in clinical trials with varying success.

The advent of CRISPR gene editing tools coincided with the approval of Luxturna, enabling genomic or transcriptomic editing as an alternative, potentially more sustainable solution, to gene augmentation therapies. Moreover, previously untargetable genes, such as large[450,451] or dominantly inherited IRDs, may be addressed by gene editing. Although there are logistical challenges due to the guide design process, screening delivery methods, and determining the best gene editor for a target-site, this would allow for a personalised treatment option. Further, machine learning and artificial intelligence may enable fast and reliable screening and optimised delivery methods, complemented by testing in patient-derived retinal organoids.[394,452]

Continued evolution of gene therapies has led to innovations such as pre-mRNA trans-splicing, which would be particularly applicable in cases such as *ABCA4*, as described above. However, for larger genes, such as *Ush2a* (15kb)[453] or *EYS* (~9-10kb),[454] treatment would still require multiple strategies since the synthetic RNA is still limited by AAV packaging capacity (4.7kb).[125] In diseases such as age-related macular degeneration which have a complex pathogenesis, gene editing may replace or function alongside molecular therapies as a long-term treatment.[455,456]

Novel gene therapeutic technologies have provided an exciting future in potentially treating disease causing genetic mutations. DNA and RNA base editing, prime editing, and (pre)mRNA trans-splicing have all demonstrated immense promise. Consequently, this requires careful consideration in responsible use of these technologies.

Existing therapeutic development has an enormous price-tag largely due to the immense cost of research and development, where only 10-20% of clinical trials achieve approval.[457] For retinal gene therapies specifically, only one gene therapy and one cell therapy have been FDA approved to date (https://www.fda.gov/vaccines-blood-biologics/cellular-gene-therapy-products/approved-cellular-and-gene-therapy-products; accessed Jul 30, 2025), but the number of past or ongoing trials has reached 209 globally. However, trials rarely move from Phase I/II to Phase III/IV. [458] A key factor is the difficulty and complexity in designing clinical trials and establishing effective clinical endpoints for gene therapies given variable disease presentation, wide treatment window, slow disease progression resulting in long and costly trials, and the inability of photoreceptors to regenerate, limiting visual improvements. Post-approval, patients require effective policy implementation and regulation by governments to enable access and patient priority.[459-462] Further, ensuring responsible research applications and collaboration both by governments, private companies, and throughout the wider research community will be critical for the continued application of gene therapy. [459,463] However, the existing approval process for Cas-derived therapies for a gene such as *ABCA4,* with ~1200 known variants, may be difficult to fund, particularly for rare variants, given the degree of heterogeneity. While a carefully regulated approval process is necessary for ethical use, amending the approval process to enable more widespread application of personalised, Cas-derived therapies may be required. This may be on the horizon for life-threatening conditions, as seen recently with the personalised base editing treatment developed in 6-months for a baby with mutations in *CPS-1.*[358]

7.10 Conclusion

Throughout this thesis a comparison of DNA and RNA base editing was undertaken to target the genetically complex *ABCA4.* This included exploring the genetic landscape of *ABCA4* and determining the applicability of base editing *in silico,* followed by side-by-side comparison of the base editors at six target sites and across two preclinical models – retinal organoids and *in vivo.* Application of the all-in-one SaKKHABE8e represents the first use in photoreceptors *in vivo*. This shed light on the successes and limitations of the tested methods and techniques, and highlighted areas for continued research. Further, this work has led to two peer-reviewed review articles,[50,67] a successful grant application, eight presentations, and an additional manuscript in preparation.

Within the time of this thesis, gene editing experienced major development in application and continued evolution, with extensive progress of these technologies in the clinic. These data contribute to the translational realm of gene editing technologies, particularly in screening across pre-clinical models. It has given me an appreciation of both the speed and impact of innovation and the complexity of effective application of these potential therapies. From my time in the MacLaren group, I gained insight, experience, and a foundation in gene editing technologies, which will continue to inspire and drive me in my future.

8 References

1 Sung, C. H. & Chuang, J. Z. The cell biology of vision. *Journal of Cell Biology* **190**, 953-963 (2010). https://doi.org/10.1083/jcb.201006020

2 Curcio, C. A., Sloan, K. R., Kalina, R. E. & Hendrickson, A. E. Human Photoreceptor Topography. *J Comp Neurol* **292**, 497-523 (1990). https://doi.org/DOI 10.1002/cne.902920402

3 Rahman, N., Georgiou, M., Khan, K. N. & Michaelides, M. Macular dystrophies: clinical and imaging features, molecular genetics and therapeutic options. *Brit J Ophthalmol* **104**, 451-460 (2020). https://doi.org/10.1136/bjophthalmol-2019-315086

4 Masland, R. H. The Neuronal Organization of the Retina. *Neuron* **76**, 266-280 (2012). https://doi.org/10.1016/j.neuron.2012.10.002

5 Remington, L. A. *Clinical anatomy and physiology of the visual system*. 2. edn, (Elsevier, Inc., 2021).

6 Stern, J. & Temple, S. Retinal pigment epithelial cell proliferation. *Exp Biol Med* **240**, 1079-1086 (2015). https://doi.org/10.1177/1535370215587530

7 Wu, J. M., Seregard, S. & Algvere, P. V. Photochemical damage of the retina. *Surv Ophthalmol* **51**, 461-481 (2006). https://doi.org/10.1016/j.survophthal.2006.06.009

8 Slijkerman, R. W. *et al.* The pros and cons of vertebrate animal models for functional and therapeutic research on inherited retinal dystrophies. *Prog Retin Eye Res* **48**, 137-159 (2015). https://doi.org/10.1016/j.preteyeres.2015.04.004

9 Mustafi, D., Engel, A. H. & Palczewski, K. Structure of cone photoreceptors. *Prog Retin Eye Res* **28**, 289-302 (2009). https://doi.org/10.1016/j.preteyeres.2009.05.003

10 Anderson, D. H., Fisher, S. K. & Steinberg, R. H. Mammalian Cones - Disk Shedding, Phagocytosis, and Renewal. *Invest Ophth Vis Sci* **17**, 117-133 (1978).

11 Young, R. W. The renewal of photoreceptor cell outer segments. *J Cell Biol* **33**, 61-72 (1967). https://doi.org/10.1083/jcb.33.1.61

12 Wang, J. S. & Kefalov, V. J. The Cone-specific visual cycle. *Prog Retin Eye Res* **30**, 115-128 (2011). https://doi.org/10.1016/j.preteyeres.2010.11.001

13 Ingram, N. T., Fain, G. L. & Sampath, A. P. Elevated energy requirement of cone photoreceptors. *P Natl Acad Sci USA* **117**, 19599-19603 (2020). https://doi.org/10.1073/pnas.2001776117

14 Tworak, A. *et al.* Rapid RGR-dependent visual pigment recycling is mediated by the RPE and specialized Muller glia. *Cell Rep* **42** (2023). https://doi.org/ARTN 112982 10.1016/j.celrep.2023.112982

15 Daiger, S. P., Sullivan, L. S., Cadena, E. L. & Bowne, S. J. History of Finding Genes and Mutations Causing Inherited Retinal Diseases. *Csh Perspect Med* **14** (2024). https://doi.org/ARTN a041287 10.1101/cshperspect.a041287

16 Hu, M. L. *et al.* Gene therapy for inherited retinal diseases: progress and possibilities. *Clin Exp Optom* **104**, 444-454 (2021). https://doi.org/10.1080/08164622.2021.1880863

17 Cremers, F. P. M., Boon, C. J. E., Bujakowska, K. & Zeitz, C. Special Issue Introduction: Inherited Retinal Disease: Novel Candidate Genes, Genotype-Phenotype Correlations, and Inheritance Models. *Genes-Basel* **9** (2018). https://doi.org/ARTN 215 10.3390/genes9040215

18 Hejtmancik, J. F. & Daiger, S. P. Understanding the genetic architecture of human retinal degenerations. *P Natl Acad Sci USA* **117**, 3904-3906 (2020). https://doi.org/10.1073/pnas.1922925117

19 Verbakel, S. K. *et al.* Non-syndromic retinitis pigmentosa. *Prog Retin Eye Res* **66**, 157-186 (2018). https://doi.org/10.1016/j.preteyeres.2018.03.005

20 Lee, W. *et al.* -acting modifiers in the locus contribute to the penetrance of the major disease-causing variant in Stargardt disease. *Hum Mol Genet* **30**, 1293-1304 (2021). https://doi.org/10.1093/hmg/ddab122

21 Tatour, Y. & Ben-Yosef, T. Syndromic Inherited Retinal Diseases: Genetic, Clinical and Diagnostic Aspects. *Diagnostics* **10** (2020). https://doi.org/ARTN 779 10.3390/diagnostics10100779

22 den Hollander, A. I., Black, A., Bennett, J. & Cremers, F. P. M. Lighting a candle in the dark advances in genetics and gene therapy of recessive retinal dystrophies (vol 120, pg 3042, 2010). *J Clin Invest* **121**, 456-457 (2011). https://doi.org/10.1172/Jci45855

23 Cremers, F. P. M., Lee, W., Collin, R. W. J. & Allikmets, R. Clinical spectrum, genetic complexity and therapeutic approaches for retinal disease caused by mutations. *Prog Retin Eye Res* **79** (2020). https://doi.org/ARTN 100861 10.1016/j.preteyeres.2020.100861

24 Britten-jones, A. C. *et al.* The Diagnostic Yield of Next Generation Sequencing in Inherited Retinal Diseases: A Systematic Review and Meta-analysis. *Am J Ophthalmol* **249**, 57-73 (2023). https://doi.org/10.1016/j.ajo.2022.12.027

25 Carss, K. J. *et al.* Comprehensive Rare Variant Analysis via Whole-Genome Sequencing to Determine the Molecular Pathology of Inherited Retinal Disease. *Am J Hum Genet* **100**, 75-90 (2017). https://doi.org/10.1016/j.ajhg.2016.12.003

26 Nuzbrokh, Y., Ragi, S. D. & Tsang, S. H. Gene therapy for inherited retinal diseases. *Ann Transl Med* **9** (2021). https://doi.org/ARTN 1278 10.21037/atm-20-4726

27 Kang, C. & Scott, L. J. Voretigene Neparvovec: A Review in Mutation-Associated Inherited Retinal Dystrophy. *Mol Diagn Ther* **24**, 487-495 (2020). https://doi.org/10.1007/s40291-020-00475-6

28 McClements, M. E., Elsayed, M. E. A. A., Major, L., de la Camara, C. M. F. & MacLaren, R. E. Gene Therapies in Clinical Development to Treat Retinal Disorders. *Mol Diagn Ther* **28**, 575-591 (2024). https://doi.org/10.1007/s40291-024-00722-0

29 Drag, S., Dotiwala, F. & Upadhyay, A. K. Gene Therapy for Retinal Degenerative Diseases: Progress, Challenges, and Future Directions. *Invest Ophth Vis Sci* **64** (2023). https://doi.org/ARTN 39 10.1167/iovs.64.7.39

30 Taylor, A. W. Ocular immune privilege. *Eye* **23**, 1885-1889 (2009). https://doi.org/10.1038/eye.2008.382

31 Petit, L., Khanna, H. & Punzo, C. Advances in Gene Therapy for Diseases of the Eye. *Hum Gene Ther* **27**, 563-579 (2016). https://doi.org/10.1089/hum.2016.040

32 Biber, J., Gandor, C., Becirovic, E. & Michalakis, S. Retina-directed gene therapy: Achievements and remaining challenges. *Pharmacol Therapeut* **271** (2025). https://doi.org/ARTN 108862
10.1016/j.pharmthera.2025.108862
33 Amato, A. *et al.* Gene Therapy in Inherited Retinal Diseases: An Update on Current State of the Art. *Front Med-Lausanne* **8** (2021). https://doi.org/ARTN 750586
10.3389/fmed.2021.750586
34 Parker, M. *et al.* Six-year results of a Phase Illa gene therapy trial in patients with Usher Syndrome Type-1B (USH1B). *Invest Ophth Vis Sci* **65** (2024).
35 Parker, M. A. *et al.* Three-Year Safety Results of SAR422459 (EIAV-ABCA4) Gene Therapy in Patients With ABCA4-Associated Stargardt Disease: An Open-Label Dose-Escalation Phase I/IIa Clinical Trial, Cohorts 1-5. *Am J Ophthalmol* **240**, 285-301 (2022). https://doi.org/10.1016/j.ajo.2022.02.013
36 Kuzmin, D. A. *et al.* The clinical landscape for AAV gene therapies. *Nature Reviews Drug Discovery* **20**, 173-174 (2021). https://doi.org/10.1038/d41573-021-00017-7
37 Wang, D., Tai, P. W. L. & Gao, G. P. Adeno-associated virus vector as a platform for gene therapy delivery. *Nature Reviews Drug Discovery* **18**, 358-378 (2019). https://doi.org/10.1038/s41573-019-0012-9
38 Agbandje-McKenna, M. & Kleinschmidt, J. AAV Capsid Structure and Cell Interactions. *Adeno-Associated Virus: Methods and Protocols* **807**, 47-92 (2011). https://doi.org/10.1007/978-1-61779-370-7_3
39 Li, C. W. & Samulski, R. J. Engineering adeno-associated virus vectors for gene therapy. *Nat Rev Genet* **21**, 255-272 (2020). https://doi.org/10.1038/s41576-019-0205-4
40 Maheshri, N., Koerber, J. T., Kaspar, B. K. & Schaffer, D. V. Directed evolution of adeno-associated virus yields enhanced gene delivery vectors. *Nature Biotechnology* **24**, 198-204 (2006). https://doi.org/10.1038/nbt1182
41 Dyka, F. M., Molday, L. L., Chiodo, V. A., Molday, R. S. & Hauswirth, W. W. Dual
-AAV Vector Treatment Reduces Pathogenic Retinal A2E Accumulation in a Mouse Model of Autosomal Recessive Stargardt Disease. *Hum Gene Ther* **30**, 1361-1370 (2019). https://doi.org/10.1089/hum.2019.132
42 McClements, M. E. *et al.* An AAV Dual Vector Strategy Ameliorates the Stargardt Phenotype in Adult
Mice. *Hum Gene Ther* **30**, 590-600 (2019). https://doi.org/10.1089/hum.2018.156
43 Sun, D. *et al.* Effective gene therapy of Stargardt disease with PEG-ECO/pGRK1-ABCA4-S/MAR nanoparticles. *Mol Ther-Nucl Acids* **29**, 823-835 (2022). https://doi.org/10.1016/j.omtn.2022.08.026
44 Kaltak, M. *et al.* QR-1011 restores defective ABCA4 splicing caused by multiple severe ABCA4 variants underlying Stargardt disease. *Sci Rep-Uk* **14** (2024). https://doi.org/ARTN 684
10.1038/s41598-024-51203-7
45 Biasutto, P. *et al.* Allele specific knock-down of human P23H rhodopsin mRNA and prevention of retinal degeneration in humanized P23H rhodopsin knock-in mouse, following treatment with an intravitreal GAPmer antisense oligonucleotide (QR-1123). *Invest Ophth Vis Sci* **60** (2019).
46 Girach, A. *et al.* RNA-based therapies in inherited retinal diseases. *Ther Adv Ophthalmol* **14** (2022). https://doi.org/Artn 25158414221134602

10.1177/25158414221134602
47 Chen, H. Y. *et al.* Reserpine maintains photoreceptor survival in retinal ciliopathy by resolving proteostasis imbalance and ciliogenesis defects. *Elife* **12** (2023). https://doi.org/ARTN e83205
10.7554/eLife.83205
48 Song, H. B. *et al.* Attenuation of photoreceptor degeneration in P23H rhodopsin transgenic rats by reserpine, previously discovered in a photoreceptor survival screen of CEP290 retinal ciliopathy. *Invest Ophth Vis Sci* **64** (2023).
49 Wilschanski, M. *et al.* Chronic ataluren (PTC124) treatment of nonsense mutation cystic fibrosis (vol 38, pg 59, 2011). *Eur Respir J* **38**, 996-996 (2011). https://doi.org/10.1183/09031936.50120910
50 Piotter, E., McClements, M. E. & MacLaren, R. E. Therapy Approaches for Stargardt Disease. *Biomolecules* **11** (2021). https://doi.org/ARTN 1179
10.3390/biom11081179
51 Orlans, H. O., Barnard, A. R., Patricio, M. I., McClements, M. E. & MacLaren, R. E. Effect of AAV-Mediated Rhodopsin Gene Augmentation on Retinal Degeneration Caused by the Dominant P23H Rhodopsin Mutation in a Knock-In Murine Model. *Hum Gene Ther* **31**, 730-742 (2020). https://doi.org/10.1089/hum.2020.008
52 Pelletier, R., Caron, S. O. P. & Puymirat, J. RNA based gene therapy for dominantly inherited diseases. *Curr Gene Ther* **6**, 131-146 (2006). https://doi.org/Doi 10.2174/156652306775515592
53 Cideciyan, A. V. *et al.* Mutation-independent rhodopsin gene therapy by knockdown and replacement with a single AAV vector. *P Natl Acad Sci USA* **115**, E8547-E8556 (2018). https://doi.org/10.1073/pnas.1805055115
54 Deyle, D. R. & Russell, D. W. Adeno-associated virus vector integration. *Curr Opin Mol Ther* **11**, 442-447 (2009).
55 McCarty, D. M., Young, S. M. & Samulski, R. J. Integration of adeno-associated virus (AAV) and recombinant AAV vectors. *Annu Rev Genet* **38**, 819-845 (2004). https://doi.org/10.1146/annurev.genet.37.110801.143717
56 Leroy, B. P. *et al.* Gene therapy for inherited retinal disease: long-term durability of effect. *Ophthalmic Res* **66**, 179-196 (2023). https://doi.org/10.1159/000526317
57 Maeder, M. L. *et al.* Development of a gene-editing approach to restore vision loss in Leber congenital amaurosis type 10. *Nat Med* **25**, 229-+ (2019). https://doi.org/10.1038/s41591-018-0327-9
58 Riedmayr, L. M. *et al.* mRNA trans-splicing dual AAV vectors for (epi)genome editing and gene therapy. *Nat Commun* **14** (2023). https://doi.org/ARTN 6578
10.1038/s41467-023-42386-0
59 Kiser, P. D., Golczak, M. & Palczewski, K. Chemistry of the Retinoid (Visual) Cycle. *Chem Rev* **114**, 194-232 (2014). https://doi.org/10.1021/cr400107q
60 Scortecci, J. F. *et al.* Cryo-EM structures of the ABCA4 importer reveal mechanisms underlying substrate binding and Stargardt disease. *Nat Commun* **12** (2021). https://doi.org/ARTN 5902
10.1038/s41467-021-26161-7
61 Quazi, F. & Molday, R. S. ATP-binding cassette transporter ABCA4 and chemical isomerization protect photoreceptor cells from the toxic accumulation of excess 11--retinal. *P Natl Acad Sci USA* **111**, 5024-5029 (2014). https://doi.org/10.1073/pnas.1400780111

62 Abudayyeh, O. O. *et al.* RNA targeting with CRISPR-Cas13. *Nature* **550**, 280-+ (2017). https://doi.org/10.1038/nature24049

63 Farnoodian, M. *et al.* Retina and RPE lipid profile changes linked with ABCA4 associated Stargardt's maculopathy. *Pharmacol Therapeut* **249** (2023). https://doi.org/ARTN 108482
10.1016/j.pharmthera.2023.108482

64 Farnoodian, M. *et al.* Cell-autonomous lipid-handling defects in Stargardt iPSC-derived retinal pigment epithelium cells. *Stem Cell Rep* **17**, 2438-2450 (2022). https://doi.org/10.1016/j.stemcr.2022.10.001

65 Lenis, T. L. *et al.* Expression of ABCA4 in the retinal pigment epithelium and its implications for Stargardt macular degeneration. *P Natl Acad Sci USA* **115**, E11120-E11127 (2018). https://doi.org/10.1073/pnas.1802519115

66 Sciezynska, A. *et al.* Role of the
Gene Expression in the Clearance of Toxic Vitamin A Derivatives in Human Hair Follicle Stem Cells and Keratinocytes. *Int J Mol Sci* **24** (2023). https://doi.org/ARTN 8275
10.3390/ijms24098275

67 Piotter, E., McClements, M. E. & MacLaren, R. E. The Scope of Pathogenic ABCA4 Mutations Targetable by CRISPR DNA Base Editing Systems-A Systematic Review. *Front Genet* **12** (2022). https://doi.org/ARTN 814131
10.3389/fgene.2021.814131

68 Allikmets, R. A photoreceptor cell-specific ATP-binding transporter gene (ABCR) is mutated in recessive Stargardt macular dystrophy (vol 15, pg 236, 1997). *Nat Genet* **17**, 122-122 (1997). https://doi.org/DOI 10.1038/ng0997-122b

69 Lin, S. Y. *et al.* Spectrum of Genetic Variants in the Most Common Genes Causing Inherited Retinal Disease in a Large Molecularly Characterized United Kingdom Cohort. *Ophthalmol Retina* **8**, 699-709 (2024). https://doi.org/10.1016/j.oret.2024.01.012

70 Jaakson, K. *et al.* Genotyping microarray (gene chip) for the
(
) gene. *Hum Mutat* **22**, 395-403 (2003). https://doi.org/10.1002/humu.10263

71 Yatsenko, A. N., Shroyer, N. F., Lewis, R. A. & Lupski, J. R. Late-onset Stargardt disease is associated with missense mutations that map outside known functional regions of
(
). *Hum Genet* **108**, 346-355 (2001). https://doi.org/DOI 10.1007/s004390100493

72 Sparrow, J. R., Wu, Y. L., Kim, C. Y. & Zhou, J. L. Phospholipid meets all-
-retinal: the making of RPE bisretinoids. *J Lipid Res* **51**, 247-261 (2010). https://doi.org/10.1194/jlr.R000687

73 Molday, R. S. & Zhang, K. Defective lipid transport and biosynthesis in recessive and dominant Stargardt macular degeneration. *Prog Lipid Res* **49**, 476-492 (2010). https://doi.org/10.1016/j.plipres.2010.07.002

74 Issa, P. C., Barnard, A. R., Herrmann, P., Washington, I. & MacLaren, R. E. Rescue of the Stargardt phenotype in
knockout mice through inhibition of vitamin A dimerization. *P Natl Acad Sci USA* **112**, 8415-8420 (2015). https://doi.org/10.1073/pnas.1506960112

75 Cornelis, S. S. *et al.* Functional Meta-Analysis of 5,962
Variants in 3,928 Retinal Dystrophy Cases. *Hum Mutat* **38**, 400-408 (2017). https://doi.org/10.1002/humu.23165

76 Zhang, N. *et al.* Protein misfolding and the pathogenesis of
-associated retinal degenerations. *Hum Mol Genet* **24**, 3220-3237 (2015). https://doi.org/10.1093/hmg/ddv073
77 Wolock, C. J. *et al.* A case-control collapsing analysis identifies retinal dystrophy genes associated with ophthalmic disease in patients with no pathogenic
variants. *Genet Med* **21**, 2336-2344 (2019). https://doi.org/10.1038/s41436-019-0495-0
78 Maugeri, A. *et al.* The
2588G > C Stargardt mutation:: Single origin and increasing frequency from South-West to North-East Europe. *Eur J Hum Genet* **10**, 197-203 (2002). https://doi.org/10.1038/sj.ejhg.5200784
79 Maugeri, A. *et al.* The 2588G→C mutation in the
gene is a mild frequent founder mutation in the western European population and allows the classification of ABCR mutations in patients with Stargardt disease. *Am J Hum Genet* **64**, 1024-1035 (1999). https://doi.org/Doi 10.1086/302323
80 Westeneng-van Haaften, S. C. *et al.* Clinical and Genetic Characteristics of Late-onset Stargardt's Disease. *Ophthalmology* **119**, 1199-1210 (2012). https://doi.org/10.1016/j.ophtha.2012.01.005
81 Zernant, J. *et al.* Frequent hypomorphic alleles account for a significant fraction of ABCA4 disease and distinguish it from age-related macular degeneration. *J Med Genet* **54**, 404-412 (2017). https://doi.org/10.1136/jmedgenet-2017-104540
82 Bax, N. M. *et al.* Heterozygous Deep-Intronic Variants and Deletions in
in Persons with Retinal Dystrophies and One Exonic
Variant. *Hum Mutat* **36**, 43-47 (2015). https://doi.org/10.1002/humu.22717
83 Lindner, M. *et al.* Differential Disease Progression in Atrophic Age-Related Macular Degeneration and Late-Onset Stargardt Disease. *Invest Ophth Vis Sci* **58** (2017). https://doi.org/10.1167/iovs.16-20980
84 Albert, S. *et al.* Identification and Rescue of Splice Defects Caused by Two Neighboring Deep-Intronic
Mutations Underlying Stargardt Disease. *Am J Hum Genet* **102**, 517-527 (2018). https://doi.org/10.1016/j.ajhg.2018.02.008
85 Bauwens, M. *et al.* ABCA4-associated disease as a model for missing heritability in autosomal recessive disorders: novel noncoding splice, cis-regulatory, structural, and recurrent hypomorphic variants. *Genet Med* **21**, 1761-1771 (2019). https://doi.org/10.1038/s41436-018-0420-y
86 Cherry, T. J. *et al.* Mapping the
-regulatory architecture of the human retina reveals noncoding genetic variation in disease. *P Natl Acad Sci USA* **117**, 9001-9012 (2020). https://doi.org/10.1073/pnas.1922501117
87 Cremers, F. P., Maugeri, A., den Hollander, A. I. & Hoyng, C. B. The expanding roles of ABCA4 and CRB1 in inherited blindness. *Novartis Found Symp* **255**, 68-79; discussion 79-84, 177-178 (2004). https://doi.org/10.1002/0470092645.ch6
88 Burke, T. R. *et al.* Retinal Phenotypes in Patients Homozygous for the G1961E Mutation in the
Gene. *Invest Ophth Vis Sci* **53**, 4458-4467 (2012). https://doi.org/10.1167/iovs.11-9166
89 Guymer, R. H. *et al.* Variation of codons 1961 and 2177 of the Stargardt disease gene is not associated with age-related macular degeneration. *Arch Ophthalmol-Chic* **119**, 745-751 (2001). https://doi.org/DOI 10.1001/archopht.119.5.745

90 Garces, F. *et al.* Correlating the Expression and Functional Activity of ABCA4 Disease Variants With the Phenotype of Patients With Stargardt Disease. *Invest Ophth Vis Sci* **59**, 2305-2315 (2018). https://doi.org/10.1167/iovs.17-23364

91 Sangermano, R. *et al.* midigenes reveal the full splice spectrum of all reported noncanonical splice site variants in Stargardt disease. *Genome Res* **28**, 100-110 (2018). https://doi.org/10.1101/gr.226621.117

92 Cheng, Y. M., Ma, C., Jin, K. X. & Jin, Z. B. Retinal organoid and gene editing for basic and translational research. *Vision Res* **210** (2023). https://doi.org/ARTN 108273
10.1016/j.visres.2023.108273

93 Singh, R. K. & Nasonkin, I. O. Limitations and Promise of Retinal Tissue From Human Pluripotent Stem Cells for Developing Therapies of Blindness. *Front Cell Neurosci* **14** (2020). https://doi.org/ARTN 179
10.3389/fncel.2020.00179

94 Volland, S., Esteve-Rudd, J., Hoo, J., Yee, C. & Williams, D. S. A Comparison of Some Organizational Characteristics of the Mouse Central Retina and the Human Macula. *Plos One* **10** (2015). https://doi.org/ARTN e0125631
10.1371/journal.pone.0125631

95 Peichl, L. Diversity of mammalian photoreceptor properties: Adaptations to habitat and lifestyle? *Anat Rec Part A* **287a**, 1001-1012 (2005). https://doi.org/10.1002/ar.a.20262

96 Fletcher, E. L. *et al.* Studying Age-Related Macular Degeneration Using Animal Models. *Optometry Vision Sci* **91**, 878-886 (2014). https://doi.org/Doi 10.1097/Opx.0000000000000322

97 Nadal-Nicolás, F. M. *et al.* True S-cones are concentrated in the ventral mouse retina and wired for color detection in the upper visual field. *Elife* **9** (2020). https://doi.org/ARTN e56840
10.7554/eLife.56840

98 Ortín-Martínez, A. *et al.* Number and Distribution of Mouse Retinal Cone Photoreceptors: Differences between an Albino (Swiss) and a Pigmented (C57/BL6) Strain. *Plos One* **9** (2014). https://doi.org/ARTN e102392
10.1371/journal.pone.0102392

99 Issa, P. C. *et al.* Fundus Autofluorescence in the

Mouse Model of Stargardt Disease-Correlation With Accumulation of A2E, Retinal Function, and Histology. *Invest Ophth Vis Sci* **54**, 5602-5612 (2013). https://doi.org/10.1167/iovs.13-11688

100 Sparrow, J. R. *et al.* Quantitative Fundus Autofluorescence in Mice: Correlation With HPLC Quantitation of RPE Lipofuscin and Measurement of Retina Outer Nuclear Layer Thickness (vol 54, pg 2812, 2013). *Invest Ophth Vis Sci* **55** (2014). https://doi.org/10.1167/iovs.12-11490a

101 Molday, L. L., Wahl, D., Sarunic, M. V. & Molday, R. S. Localization and functional characterization of the p.Asn965Ser (N965S) ABCA4 variant in mice reveal pathogenic mechanisms underlying Stargardt macular degeneration. *Hum Mol Genet* **27**, 295-306 (2018). https://doi.org/10.1093/hmg/ddx400

102 Alissa, M. *et al.* High-efficiency base editing for Stargardt disease in mice, non-human primates, and human retina tissue. *bioRxiv*, 2023.2004.2017.535579 (2023). https://doi.org/10.1101/2023.04.17.535579

103 Morival, C. *et al.* Generation of a compound heterozygous ABCA4 rat model with pathological features of STGD1. *Hum Mol Genet* **34**, 1040-1056 (2025). https://doi.org/10.1093/hmg/ddaf057

104 Ferla, R. *et al.* Retinal gene therapy for Stargardt disease with dual AAV intein vectors is both safe and effective in large animal models. *Sci Adv* **11** (2025). https://doi.org/ARTN eadt9354
10.1126/sciadv.adt9354

105 Ekesten, B., Mäkeläinen, S., Ellis, S., Kjellström, U. & Bergström, T. F. Abnormal Appearance of the Area Centralis in Labrador Retrievers With an Loss-of-function Mutation. *Transl Vis Sci Techn* **11** (2022). https://doi.org/ARTN 36
10.1167/tvst.11.2.36

106 Mäkeläinen, S. *et al.* An ABCA4 loss-of-function mutation causes a canine form of Stargardt disease. *Plos Genet* **15** (2019). https://doi.org/ARTN e1007873
10.1371/journal.pgen.1007873

107 Ma, Y. *et al.* Juvenile macular degeneration in nonhuman primates generated by germline knockout of ABCA4 gene. *Sci Bull (Beijing)* (2025). https://doi.org/10.1016/j.scib.2025.04.077

108 Lu, Q. & Reynolds, A. L. 219-223 (Springer Nature Switzerland).

109 Noel, N. C. L., Allison, W. T., MacDonald, I. M. & Hocking, J. C. Zebrafish and inherited photoreceptor disease: Models and insights. *Prog Retin Eye Res* **91** (2022). https://doi.org/ARTN 101096
10.1016/j.preteyeres.2022.101096

110 Willoughby, J. J. & Jensen, A. M. Abca4, mutated in Stargardt disease, is required for structural integrity of cone outer segments. *Dis Model Mech* **18** (2025). https://doi.org/ARTN dmm052052
10.1242/dmm.052052

111 Sassone, F. *et al.* Interruption of the visual cycle in a novel animal model induces progressive vision loss resembling Stargardts Disease. *Sci Rep-Uk* **14** (2024). https://doi.org/ARTN 30880
10.1038/s41598-024-81869-y

112 Szel, A. & Rohlich, P. Two cone types of rat retina detected by anti-visual pigment antibodies. *Exp Eye Res* **55**, 47-52 (1992). https://doi.org/10.1016/0014-4835(92)90090-f

113 Verra, D. M., Sajdak, B. S., Merriman, D. K. & Hicks, D. Diurnal rodents as pertinent animal models of human retinal physiology and pathology. *Prog Retin Eye Res* **74** (2020). https://doi.org/ARTN 100776
10.1016/j.preteyeres.2019.100776

114 Radu, R. A. *et al.* Accelerated accumulation of lipofuscin pigments in the RPE of a mouse model for -mediated retinal dystrophies following vitamin A supplementation. *Invest Ophth Vis Sci* **49**, 3821-3829 (2008). https://doi.org/10.1167/iovs.07-1470

115 Weng, J. *et al.* Insights into the function of Rim protein in photoreceptors and etiology of Stargardt's disease from the phenotype in knockout mice. *Cell* **98**, 13-23 (1999). https://doi.org/Doi 10.1016/S0092-8674(00)80602-9

116 Sahel, J. A., Marazova, K. & Audo, I. Clinical Characteristics and Current Therapies for Inherited Retinal Degenerations. *Csh Perspect Med* **5** (2015). https://doi.org/ARTN a017111
10.1101/cshperspect.a017111
117 Grieger, J. C. & Samulski, R. J. Packaging capacity of adeno-associated virus serotypes: Impact of larger genomes on infectivity and postentry steps. *J Virol* **79**, 9933-9944 (2005). https://doi.org/10.1128/Jvi.79.15.9933-9944.2005
118 Dong, B. A., Nakai, H. & Xiao, W. D. Characterization of Genome Integrity for Oversized Recombinant AAV Vector. *Mol Ther* **18**, 87-92 (2010). https://doi.org/10.1038/mt.2009.258
119 Lai, Y., Yue, Y. P. & Duan, D. S. Evidence for the Failure of Adeno-associated Virus Serotype 5 to Package a Viral Genome ≥8.2kb. *Mol Ther* **18**, 75-79 (2010). https://doi.org/10.1038/mt.2009.256
120 Trapani, I. *et al.* Effective delivery of large genes to the retina by dual AAV vectors. *Hum Gene Ther* **25**, A33-A33 (2014).
121 Ghenciu, L. A., Hategan, O. A., Stoicescu, E. R., Iacob, R. & Sisu, A. M. Emerging Therapeutic Approaches and Genetic Insights in Stargardt Disease: A Comprehensive Review. *Int J Mol Sci* **25** (2024). https://doi.org/ARTN 8859
10.3390/ijms25168859
122 Kong, J. *et al.* Correction of the disease phenotype in the mouse model of Stargardt disease by lentiviral gene therapy. *Gene Ther* **15**, 1311-1320 (2008). https://doi.org/10.1038/gt.2008.78
123 Binley, K. *et al.* Transduction of Photoreceptors With Equine Infectious Anemia Virus Lentiviral Vectors: Safety and Biodistribution of StarGen for Stargardt Disease. *Invest Ophth Vis Sci* **54**, 4061-4071 (2013). https://doi.org/10.1167/iovs.13-11871
124 Puppo, A. *et al.* Retinal transduction profiles by high-capacity viral vectors. *Gene Ther* **21**, 855-865 (2014). https://doi.org/10.1038/gt.2014.57
125 Doi, A., Delaney, C., Tanner, D., Burkhart, K. & Bell, R. D. RNA exon editing: Splicing the way to treat human diseases. *Mol Ther Nucl Acids* **35** (2024). https://doi.org/ARTN 102311
10.1016/j.omtn.2024.102311
126 Bucher, K., Rodríguez-Bocanegra, E., Dauletbekov, D. & Fischer, M. D. Immune responses to retinal gene therapy using adeno-associated viral vectors-Implications for treatment success and safety. *Prog Retin Eye Res* **83** (2021). https://doi.org/ARTN 100915
10.1016/j.preteyeres.2020.100915
127 Chandler, L. C. *et al.* Characterizing the cellular immune response to subretinal AAV gene therapy in the murine retina. *Mol Ther-Meth Clin D* **22** (2021). https://doi.org/10.1016/j.omtm.2021.05.011
128 Sun, D. *et al.* Formulation and efficacy of ECO/
-
-
nanoparticles for nonviral gene therapy of Stargardt disease in a mouse model. *J Control Release* **330**, 329-340 (2021). https://doi.org/10.1016/j.jconrel.2020.12.010
129 LeBlanc, M. *et al.* ABCA4 gene replacement in a mouse model of Stargardt disease using a mammalian transposon system. *Invest Ophth Vis Sci* **65** (2024).

130 LeBlanc, M. E. *et al.* Efficacy and Integration of a Non-Viral
Transposon in Treating Stargardt Disease: Evidence from Mice and Primate Studies. *Mol Ther* **32**, 6-7 (2024).
131 An, M. R. *et al.* Engineered Virus-Like Particles for Transient Delivery of Prime Editor Ribonucleoprotein Complexes. *Mol Ther* **32**, 118-118 (2024).
132 Scholl, H. P., DeBartolomeo, G., Washington, I. & Saad, L. ALK-001 (C20-D3-Vitamin A) slows the growth of atrophic lesions in
-related Stargardt Disease: Results of a Phase 2 placebo-controlled clinical trial (TEASE study). *Invest Ophth Vis Sci* **63** (2022).
133 Grigg, J. R. *et al.* Safety, Tolerability, and Efficacy of Tinlarebant from the 24-Month Phase 2 study in Adolescent Patients Affected by Stargardt Disease. *Invest Ophth Vis Sci* **65** (2024).
134 BeliteBio. *Belite Bio Announces FDA Granting of Breakthrough Therapy Designation for Tinlarebant for the Treatment of Stargardt Disease*, <https://investors.belitebio.com/news-releases/news-release-details/belite-bio-announces-fda-granting-breakthrough-therapy> (2025).
135 Kubota, R. *et al.* Phase 1, Dose-Ranging Study of Emixustat Hydrochloride (Acu-4429), a Novel Visual Cycle Modulator, in Healthy Volunteers. *Retina-J Ret Vit Dis* **34**, 603-609 (2014). https://doi.org/DOI 10.1097/01.iae.0000434565.80060.f8
136 Kubota, R., Birch, D. G., Gregory, J. K. & Koester, J. M. Randomised study evaluating the pharmacodynamics of emixustat hydrochloride in subjects with macular atrophy secondary to Stargardt disease. *Brit J Ophthalmol* **106**, 403-408 (2022). https://doi.org/10.1136/bjophthalmol-2020-317712
137 Marks, E., Anugu, A., Bisiani, J. & Pentyala, S. Stem cell therapy as treatment for Stargardt disease. *Ther Adv Ophthalmol* **17** (2025). https://doi.org/Artn 25158414251320592
10.1177/25158414251320592
138 Gonzalez, V. H. *et al.* MCO-010 intravitreal optogenetic therapy in Stargardt disease. 6-month outcomes from the Phase 2 STARLIGHT trial. *Invest Ophth Vis Sci* **64** (2023).
139 Wang, L., Shah, S. M., Mangwani-Mordani, S. & Gregori, N. Z. Updates on Emerging Interventions for Autosomal Recessive
-Associated Stargardt Disease. *J Clin Med* **12** (2023). https://doi.org/ARTN 6229
10.3390/jcm12196229
140 MacDonald, I. M. & Sieving, P. A. Investigation of the effect of dietary docosahexaenoic acid (DHA) supplementation on macular function in subjects with autosomal recessive Stargardt macular dystrophy. *Ophthalmic Genet* **39**, 477-486 (2018). https://doi.org/10.1080/13816810.2018.1484931
141 Prokopiou, E. *et al.* Eicosapentaenoic acid-rich omega-3 fatty acids supplementation may improve vision in dry age-related macular degeneration or Stargardt disease, as shown in MADEOS, a prospective, randomized, multicentre, double-blind, placebo-controlled pilot study. *Pharmanutrition* **29** (2024). https://doi.org/ARTN 100400
10.1016/j.phanu.2024.100400
142 Piccardi, M. *et al.* Antioxidant Saffron and Central Retinal Function in ABCA4-Related Stargardt Macular Dystrophy. *Nutrients* **11** (2019). https://doi.org/ARTN 2461
10.3390/nu11102461

143 Urnov, F. D., Rebar, E. J., Holmes, M. C., Zhang, H. S. & Gregory, P. D. Genome editing with engineered zinc finger nucleases. *Nat Rev Genet* **11**, 636-646 (2010). https://doi.org/10.1038/nrg2842
144 Bibikova, M. *et al.* Stimulation of homologous recombination through targeted cleavage by chimeric nucleases. *Mol Cell Biol* **21**, 289-297 (2001). https://doi.org/Doi 10.1128/Mcb.21.1.289-297.2001
145 Boch, J. *et al.* Breaking the Code of DNA Binding Specificity of TAL-Type III Effectors. *Science* **326**, 1509-1512 (2009). https://doi.org/10.1126/science.1178811
146 Carroll, D. Genome engineering with targetable nucleases. *Faseb J* **28** (2014).
147 Moscou, M. J. & Bogdanove, A. J. A Simple Cipher Governs DNA Recognition by TAL Effectors. *Science* **326**, 1501-1501 (2009). https://doi.org/10.1126/science.1178817
148 Carlson, D. F., Fahrenkrug, S. C. & Hackett, P. B. Targeting DNA With Fingers and TALENs. *Mol Ther-Nucl Acids* **1** (2012). https://doi.org/ARTN e3 10.1038/mtna.2011.5
149 Epstein, B. E. & Schaffer, D. V. Combining Engineered Nucleases with Adeno-associated Viral Vectors for Therapeutic Gene Editing. *Precision Medicine, Crispr, and Genome Engineering: Moving from Association to Biology and Therapeutics* **1016**, 29-42 (2017). https://doi.org/10.1007/978-3-319-63904-8_2
150 Doudna, J. A. & Charpentier, E. The new frontier of genome engineering with CRISPR-Cas9. *Science* **346**, 1077-+ (2014). https://doi.org/ARTN 1258096 10.1126/science.1258096
151 Ishino, Y., Shinagawa, H., Makino, K., Amemura, M. & Nakata, A. Nucleotide-Sequence of the Iap Gene, Responsible for Alkaline-Phosphatase Isozyme Conversion in Escherichia-Coli, and Identification of the Gene-Product. *J Bacteriol* **169**, 5429-5433 (1987). https://doi.org/DOI 10.1128/jb.169.12.5429-5433.1987
152 Jinek, M. *et al.* A Programmable Dual-RNA-Guided DNA Endonuclease in Adaptive Bacterial Immunity. *Science* **337**, 816-821 (2012). https://doi.org/10.1126/science.1225829
153 Urnov, F. D. Genome Editing B.C. (Before CRISPR): Lasting Lessons from the "Old Testament". *Crispr J* **1**, 34-46 (2018). https://doi.org/10.1089/crispr.2018.29007.fyu
154 Cho, S. W., Kim, S., Kim, J. M. & Kim, J. S. Targeted genome engineering in human cells with the Cas9 RNA-guided endonuclease. *Nature Biotechnology* **31**, 230-232 (2013). https://doi.org/10.1038/nbt.2507
155 Jinek, M. *et al.* RNA-programmed genome editing in human cells. *Elife* **2** (2013). https://doi.org/ARTN e00471 10.7554/eLife.00471
156 Chylinski, K., Makarova, K. S., Charpentier, E. & Koonin, E. V. Classification and evolution of type II CRISPR-Cas systems. *Nucleic Acids Res* **42**, 6091-6105 (2014). https://doi.org/10.1093/nar/gku241
157 Jiang, F. G. & Doudna, J. A. CRISPR-Cas9 Structures and Mechanisms. *Annual Review of Biophysics, Vol 46* **46**, 505-529 (2017). https://doi.org/10.1146/annurev-biophys-062215-010822
158 Ran, F. A. *et al.* genome editing using Cas9. *Nature* **520**, 186-U198 (2015). https://doi.org/10.1038/nature14299
159 Yamada, M. *et al.* Crystal Structure of the Minimal Cas9 from

Reveals the Molecular Diversity in the CRISPR-Cas9 Systems. *Mol Cell* **65**, 1109-+ (2017). https://doi.org/10.1016/j.molcel.2017.02.007

160 Kim, E. *et al.* In Vivo Genome Editing with a Small Cas9 Orthologue Derived from Campylobacter Jejuni. *Mol Ther* **25**, 79-79 (2017).

161 Hu, F. Y. *et al.* Novel variants of
in Han Chinese families with Stargardt disease. *Bmc Med Genet* **21** (2020). https://doi.org/ARTN 213
10.1186/s12881-020-01152-5

162 Hu, J. H. *et al.* Evolved Cas9 variants with broad PAM compatibility and high DNA specificity. *Nature* **556**, 57-+ (2018). https://doi.org/10.1038/nature26155

163 Ran, F. A. *et al.* Genome engineering using the CRISPR-Cas9 system. *Nat Protoc* **8**, 2281-2308 (2013). https://doi.org/10.1038/nprot.2013.143

164 Song, B., Yang, S., Hwang, G. H., Yu, J. & Bae, S. Analysis of NHEJ-Based DNA Repair after CRISPR-Mediated DNA Cleavage. *Int J Mol Sci* **22** (2021). https://doi.org/ARTN 6397
10.3390/ijms22126397

165 Chu, V. T. *et al.* Increasing the efficiency of homology-directed repair for CRISPR-Cas9-induced precise gene editing in mammalian cells. *Nature Biotechnology* **33**, 543-U160 (2015). https://doi.org/10.1038/nbt.3198

166 Ceccaldi, R., Rondinelli, B. & D'Andrea, A. D. Repair Pathway Choices and Consequences at the Double-Strand Break. *Trends Cell Biol* **26**, 52-64 (2016). https://doi.org/10.1016/j.tcb.2015.07.009

167 Pierce, E. A. *et al.* Safety and Efficacy of EDIT-101 for Treatment of CEP290-associated Retinal Degeneration. *Invest Ophth Vis Sci* **64** (2023).

168 Siles, L., Ruiz-Nogales, S., Navinés-Ferrer, A., Méndez-Vendrell, P. & Pomares, E. Efficient correction of ABCA4 variants by CRISPR-Cas9 in hiPSCs derived from Stargardt disease patients. *Mol Ther-Nucl Acids* **32**, 64-79 (2023). https://doi.org/10.1016/j.omtn.2023.02.032

169 Larson, M. H. *et al.* CRISPR interference (CRISPRi) for sequence-specific control of gene expression. *Nat Protoc* **8**, 2180-2196 (2013). https://doi.org/10.1038/nprot.2013.132

170 Kampmann, M. CRISPRi and CRISPRa Screens in Mammalian Cells for Precision Biology and Medicine. *Acs Chem Biol* **13**, 406-416 (2018). https://doi.org/10.1021/acschembio.7b00657

171 Nakamura, M., Gao, Y. C., Dominguez, A. A. & Qi, L. S. CRISPR technologies for precise epigenome editing. *Nat Cell Biol* **23**, 11-22 (2021). https://doi.org/10.1038/s41556-020-00620-7

172 Gilbert, L. A. *et al.* Genome-Scale CRISPR-Mediated Control of Gene Repression and Activation. *Cell* **159**, 647-661 (2014). https://doi.org/10.1016/j.cell.2014.09.029

173 Peddle, C. F., Fry, L. E., McClements, M. E. & MacLaren, R. E. CRISPR Interference-Potential Application in Retinal Disease. *Int J Mol Sci* **21** (2020). https://doi.org/ARTN 2329
10.3390/ijms21072329

174 McCutcheon, S. R., Rohm, D., Iglesias, N. & Gersbach, C. A. Epigenome editing technologies for discovery and medicine. *Nature Biotechnology* **42**, 1199-1217 (2024). https://doi.org/10.1038/s41587-024-02320-1

175 Suh, S. *et al.* Restoration of visual function in adult mice with an inherited retinal disease via adenine base editing. *Nat Biomed Eng* **5** (2021). https://doi.org/10.1038/s41551-020-00632-6

176 Gaudelli, N. M. *et al.* Programmable base editing of A.T to G.C in genomic DNA without DNA cleavage. *Nature* **551**, 464-+ (2017). https://doi.org/10.1038/nature24644

177 Kantor, A., McClements, M. E. & MacLaren, R. E. CRISPR-Cas9 DNA Base-Editing and Prime-Editing. *Int J Mol Sci* **21** (2020). https://doi.org/ARTN 6240 10.3390/ijms21176240

178 Gaudelli, N. M. *et al.* Directed evolution of adenine base editors with increased activity and therapeutic application. *Nature Biotechnology* **38**, 892-U899 (2020). https://doi.org/10.1038/s41587-020-0491-6

179 Richter, M. F. *et al.* Phage-assisted evolution of an adenine base editor with improved Cas domain compatibility and activity (vol 15, pg 891, 2020). *Nature Biotechnology* **38**, 901-901 (2020). https://doi.org/10.1038/s41587-020-0562-8

180 Davis, J. R. *et al.* Efficient in vivo base editing via single adeno-associated viruses with size-optimized genomes encoding compact adenine base editors. *Nat Biomed Eng* **6**, 1272-+ (2022). https://doi.org/10.1038/s41551-022-00911-4

181 Zhang, E. M. Y., Neugebauer, M. E., Krasnow, N. A. & Liu, D. R. Phage-assisted evolution of highly active cytosine base editors with enhanced selectivity and minimal sequence context preference. *Nat Commun* **15** (2024). https://doi.org/ARTN 1697 10.1038/s41467-024-45969-7

182 Lam, D. K. *et al.* Improved cytosine base editors generated from TadA variants. *Nature Biotechnology* **41**, 686-+ (2023). https://doi.org/10.1038/s41587-022-01611-9

183 Kleinstiver, B. P. *et al.* Broadening the targeting range of

CRISPR-Cas9 by modifying PAM recognition. *Nature Biotechnology* **33**, 1293-+ (2015). https://doi.org/10.1038/nbt.3404

184 Walton, R. T., Christie, K. A., Whittaker, M. N. & Kleinstiver, B. P. Unconstrained genome targeting with near-PAMless engineered CRISPR-Cas9 variants. *Science* **368**, 290-+ (2020). https://doi.org/10.1126/science.aba8853

185 Tu, T. X. *et al.* A precise and efficient adenine base editor. *Mol Ther* **30**, 2933-2941 (2022). https://doi.org/10.1016/j.ymthe.2022.07.010

186 Wu, Y. D. *et al.* AAV-mediated base-editing therapy ameliorates the disease phenotypes in a mouse model of retinitis pigmentosa. *Nat Commun* **14** (2023). https://doi.org/10.1038/s41467-023-40655-6

187 Choi, E. H. *et al.* base editing rescues cone photoreceptors in a mouse model of early-onset inherited retinal degeneration. *Invest Ophth Vis Sci* **63** (2022).

188 Chen, L. *et al.* Adenine transversion editors enable precise, efficient A•T-to-C•G base editing in mammalian cells and embryos. *Nature Biotechnology* **42** (2024). https://doi.org/10.1038/s41587-023-01821-9

189 Zhao, D. D. *et al.* Glycosylase base editors enable C-to-A and C-to-G base changes. *Nature Biotechnology* **39**, 35-40 (2021). https://doi.org/10.1038/s41587-020-0592-2

190 Anzalone, A. V. *et al.* Search-and-replace genome editing without double-strand breaks or donor DNA. *Nature* **576**, 149-+ (2019). https://doi.org/10.1038/s41586-019-1711-4

191 Anzalone, A. V. *et al.* Programmable deletion, replacement, integration and inversion of large DNA sequences with twin prime editing. *Nature Biotechnology* **40**, 731-+ (2022). https://doi.org/10.1038/s41587-021-01133-w

192 She, K. Q. *et al.* Dual-AAV split prime editor corrects the mutation and phenotype in mice with inherited retinal degeneration. *Signal Transduct Tar* **8** (2023). https://doi.org/ARTN 57
10.1038/s41392-022-01234-1

193 Liu, Z. Q. *et al.* Efficient Rescue of Retinal Degeneration in Mice by Engineered Base Editing and Prime Editing. *Adv Sci* **11** (2024). https://doi.org/10.1002/advs.202405628

194 Zhao, Z. H., Shang, P., Mohanraju, P. & Geijsen, N. Prime editing: advances and therapeutic applications. *Trends Biotechnol* **41** (2023). https://doi.org/10.1016/j.tibtech.2023.03.004

195 Durrant, M. G. *et al.* Bridge RNAs direct programmable recombination of target and donor DNA. *Nature* **630** (2024). https://doi.org/10.1038/s41586-024-07552-4

196 Nishikura, K. A-to-I editing of coding and non-coding RNAs by ADARs. *Nat Rev Mol Cell Bio* **17**, 83-96 (2016). https://doi.org/10.1038/nrm.2015.4

197 Karlström, V. *et al.* ADAR3 modulates neuronal differentiation and regulates mRNA stability and translation. *Nucleic Acids Res* **52**, 12021-12038 (2024). https://doi.org/10.1093/nar/gkae753

198 Bellingrath, J. S., McClements, M. E., Fischer, M. D. & MacLaren, R. E. Programmable RNA editing with endogenous ADAR enzymes - a feasible option for the treatment of inherited retinal disease? *Front Mol Neurosci* **16** (2023). https://doi.org/ARTN 1092913
10.3389/fnmol.2023.1092913

199 Cox, D. B. T. *et al.* RNA editing with CRISPR-Cas13. *Science* **358**, 1019-1027 (2017). https://doi.org/10.1126/science.aaq0180

200 Wang, A. L., Carroll, R. C. & Nawy, S. Down-Regulation of the RNA Editing Enzyme ADAR2 Contributes to RGC Death in a Mouse Model of Glaucoma. *Plos One* **9** (2014). https://doi.org/ARTN e91288
10.1371/journal.pone.0091288

201 East-Seletsky, A. *et al.* Two distinct RNase activities of CRISPR-C2c2 enable guide-RNA processing and RNA detection. *Nature* **538**, 270-+ (2016). https://doi.org/10.1038/nature19802

202 Abudayyeh, O. O. *et al.* C2c2 is a single-component programmable RNA-guided RNA-targeting CRISPR effector. *Science* **353** (2016). https://doi.org/ARTN aaf5573
10.1126/science.aaf5573

203 Smargon, A. A. *et al.* Cas13b Is a Type VI-B CRISPR-Associated RNA-Guided RNase Differentially Regulated by Accessory Proteins Csx27 and Csx28. *Mol Cell* **65**, 618-+ (2017). https://doi.org/10.1016/j.molcel.2016.12.023

204 Kannan, S. *et al.* Compact RNA editors with small Cas13 proteins. *Nature Biotechnology* **40**, 194-+ (2022). https://doi.org/10.1038/s41587-021-01030-2

205 Konermann, S. *et al.* Transcriptome Engineering with RNA-Targeting Type VI-D CRISPR Effectors. *Cell* **173**, 665-+ (2018). https://doi.org/10.1016/j.cell.2018.02.033

206 Xu, C. L. *et al.* Programmable RNA editing with compact CRISPR-Cas13 systems from uncultivated microbes. *Nat Methods* **18**, 499-+ (2021). https://doi.org/10.1038/s41592-021-01124-4

207 Kumar, S. *et al.* Characterization of RNA editing and gene therapy with a compact CRISPR-Cas13 in the retina. *P Natl Acad Sci USA* **121** (2024). https://doi.org/ARTN e2408345121
10.1073/pnas.2408345121
208 Wang, Y. R., Havel, J. & Beal, P. A. A Phenotypic Screen for Functional Mutants of Human Adenosine Deaminase Acting on RNA 1. *Acs Chem Biol* **10**, 2512-2519 (2015). https://doi.org/10.1021/acschembio.5b00711
209 Kuttan, A. & Bass, B. L. Mechanistic insights into editing-site specificity of ADARs. *P Natl Acad Sci USA* **109**, E3295-E3304 (2012). https://doi.org/10.1073/pnas.1212548109
210 Fry, L. E. *et al.* Comparison of CRISPR-Cas13b RNA base editing approaches for USH2A-associated inherited retinal degeneration. *Commun Biol* **8** (2025). https://doi.org/ARTN 200
10.1038/s42003-025-07557-3
211 Xiao, Q. Q. *et al.* Rescue of autosomal dominant hearing loss by in vivo delivery of mini dCas13X-derived RNA base editor. *Sci Transl Med* **14** (2022). https://doi.org/ARTN eabn0449
10.1126/scitranslmed.abn0449
212 Xue, Y. *et al.* RNA base editing therapy cures hearing loss induced by OTOF gene mutation. *Mol Ther* **31**, 3520-3530 (2023). https://doi.org/10.1016/j.ymthe.2023.10.019
213 Katrekar, D. *et al.* In vivo RNA editing of point mutations via RNA-guided adenosine deaminases. *Nat Methods* **16**, 239-+ (2019). https://doi.org/10.1038/s41592-019-0323-0
214 Wettengel, J., Reautschnig, P., Geisler, S., Kahle, P. J. & Stafforst, T. Harnessing human ADAR2 for RNA repair - Recoding a PINK1 mutation rescues mitophagy. *Nucleic Acids Res* **45**, 2797-2808 (2017). https://doi.org/10.1093/nar/gkw911
215 Katrekar, D. *et al.* Efficient in vitro and in vivo RNA editing via recruitment of endogenous ADARs using circular guide RNAs. *Nature Biotechnology* **40**, 938-+ (2022). https://doi.org/10.1038/s41587-021-01171-4
216 Yi, Z. Y. *et al.* Engineered circular ADAR-recruiting RNAs increase the efficiency and fidelity of RNA editing in vitro and in vivo. *Nature Biotechnology* **40**, 946-+ (2022). https://doi.org/10.1038/s41587-021-01180-3
217 Sheriff, A. *et al.* ABE8e adenine base editor precisely and efficiently corrects a recurrent nonsense mutation. *Sci Rep-Uk* **12** (2022). https://doi.org/ARTN 19643
10.1038/s41598-022-24184-8
218 Villiger, L. *et al.* Treatment of a metabolic liver disease by in vivo genome base editing in adult mice. *Nat Med* **24**, 1519-+ (2018). https://doi.org/10.1038/s41591-018-0209-1
219 Bao, X. R., Pan, Y. D., Lee, C. M., Davis, T. H. & Bao, G. Tools for experimental and computational analyses of off-target editing by programmable nucleases. *Nat Protoc* **16**, 10-26 (2021). https://doi.org/10.1038/s41596-020-00431-y
220 Tsai, S. Q. *et al.* CIRCLE-seq: a highly sensitive screen for genome-wide CRISPR-Cas9 nuclease off-targets (vol 14, pg 607, 2017). *Nat Methods* **15**, 394-394 (2018). https://doi.org/10.1038/nmeth0518-394c
221 Chen, L. *et al.* Engineering a precise adenine base editor with minimal bystander editing. *Nat Chem Biol* **19**, 101-+ (2023). https://doi.org/10.1038/s41589-022-01163-8
222 Mali, P. *et al.* CAS9 transcriptional activators for target specificity screening and paired nickases for cooperative genome engineering. *Nature Biotechnology* **31**, 833-+ (2013). https://doi.org/10.1038/nbt.2675

223 Sato, K., Akiyama, M. & Sakakibara, Y. RNA secondary structure prediction using deep learning with thermodynamic integration. *Nat Commun* **12** (2021). https://doi.org/ARTN 941
10.1038/s41467-021-21194-4
224 Hofacker, I. L. Vienna RNA secondary structure server. *Nucleic Acids Res* **31**, 3429-3431 (2003). https://doi.org/10.1093/nar/gkg599
225 Lorenz, R. *et al.* ViennaRNA Package 2.0. *Algorithm Mol Biol* **6** (2011). https://doi.org/Artn 26
10.1186/1748-7188-6-26
226 Zuker, M. Mfold web server for nucleic acid folding and hybridization prediction. *Nucleic Acids Res* **31**, 3406-3415 (2003). https://doi.org/10.1093/nar/gkg595
227 Grieger, J. C., Choi, V. W. & Samulski, R. J. Production and characterization of adeno-associated viral vectors. *Nat Protoc* **1**, 1412-1428 (2006). https://doi.org/10.1038/nprot.2006.207
228 Strobel, B., Miller, F. D., Rist, W. & Lamla, T. Comparative Analysis of Cesium Chloride- and Iodixanol-Based Purification of Recombinant Adeno-Associated Viral Vectors for Preclinical Applications. *Hum Gene Ther Method* **26**, 147-157 (2015). https://doi.org/10.1089/hgtb.2015.051
229 Zolotukhin, S. *et al.* Recombinant adeno-associated virus purification using novel methods improves infectious titer and yield. *Gene Ther* **6**, 973-985 (1999). https://doi.org/DOI 10.1038/sj.gt.3300938
230 Bainbridge, J. W. B. *et al.* Long-Term Effect of Gene Therapy on Leber's Congenital Amaurosis. *New Engl J Med* **372**, 1887-1897 (2015). https://doi.org/10.1056/NEJMoa1414221
231 Jacobson, S. G. *et al.* Improvement and Decline in Vision with Gene Therapy in Childhood Blindness. *New Engl J Med* **372**, 1920-1926 (2015). https://doi.org/10.1056/NEJMoa1412965
232 Cideciyan, A. V. *et al.* Human retinal gene therapy for Leber congenital amaurosis shows advancing retinal degeneration despite enduring visual improvement. *P Natl Acad Sci USA* **110**, E517-E525 (2013). https://doi.org/10.1073/pnas.1218933110
233 Gardiner, K. L. *et al.* Long-Term Structural Outcomes of Late-Stage Gene Therapy. *Mol Ther* **28**, 266-278 (2020). https://doi.org/10.1016/j.ymthe.2019.08.013
234 Fry, L. E., McClements, M. E. & MacLaren, R. E. Analysis of Pathogenic Variants Correctable With CRISPR Base Editing Among Patients With Recessive Inherited Retinal Degeneration. *Jama Ophthalmol* **139**, 319-328 (2021). https://doi.org/10.1001/jamaophthalmol.2020.6418
235 Dadush, A. *et al.* DNA and RNA base editors can correct the majority of pathogenic single nucleotide variants. *Npj Genom Med* **9** (2024). https://doi.org/ARTN 16
10.1038/s41525-024-00397-w
236 Stone, E. M. *et al.* Clinically Focused Molecular Investigation of 1000 Consecutive Families with Inherited Retinal Disease. *Ophthalmology* **124**, 1314-1331 (2017). https://doi.org/10.1016/j.ophtha.2017.04.008
237 Jiang, F. *et al.* Screening of Gene in a Chinese Cohort With Stargardt Disease or Cone-Rod Dystrophy With a Report on 85 Novel Mutations. *Invest Ophth Vis Sci* **57**, 145-152 (2016). https://doi.org/10.1167/iovs.15-18190

238 Rosenberg, T., Klie, F., Garred, P. & Schwartz, M. N965S is a common ABCA4 variant in Stargardt-related retinopathies in the Danish population. *Mol Vis* **13**, 1962-1969 (2007).
239 Birtel, J. *et al.* Clinical and genetic characteristics of 251 consecutive patients with macular and cone/cone-rod dystrophy. *Sci Rep-Uk* **8** (2018). https://doi.org/ARTN 4824
10.1038/s41598-018-22096-0
240 Hu, F. Y. *et al.* Gene Screening in a Chinese Cohort With Stargardt Disease: Identification of 37 Novel Variants. *Front Genet* **10** (2019). https://doi.org/ARTN 773
10.3389/fgene.2019.00773
241 Duno, M., Schwartz, M., Larsen, P. L. & Rosenberg, T. Phenotypic and genetic spectrum of Danish patients with
-related retinopathy. *Ophthalmic Genet* **33**, 225-231 (2012). https://doi.org/10.3109/13816810.2011.643441
242 Xu, L. *et al.* Efficient precise in vivo base editing in adult dystrophic mice. *Nat Commun* **12** (2021). https://doi.org/ARTN 3719
10.1038/s41467-021-23996-y
243 Levy, J. M. *et al.* Cytosine and adenine base editing of the brain, liver, retina, heart and skeletal muscle of mice via adeno-associated viruses. *Nat Biomed Eng* **4**, 97-110 (2020). https://doi.org/10.1038/s41551-019-0501-5
244 Koblan, L. W. *et al.* In vivo base editing rescues Hutchinson-Gilford progeria syndrome in mice. *Nature* **589**, 608-+ (2021). https://doi.org/10.1038/s41586-020-03086-7
245 Yeh, W. H. *et al.* In vivo base editing restores sensory transduction and transiently improves auditory function in a mouse model of recessive deafness. *Sci Transl Med* **12** (2020). https://doi.org/ARTN eaay9101
10.1126/scitranslmed.aay9101
246 Hung, S. S. C. *et al.* AAV-Mediated CRISPR/Cas Gene Editing of Retinal Cells In Vivo. *Invest Ophth Vis Sci* **57**, 3470-3476 (2016). https://doi.org/10.1167/iovs.16-19316
247 Wei, T., Cheng, Q., Min, Y. L., Olson, E. N. & Siegwart, D. J. Systemic nanoparticle delivery of CRISPR-Cas9 ribonucleoproteins for effective tissue specific genome editing. *Nat Commun* **11** (2020). https://doi.org/10.1038/s41467-020-17029-3
248 Zhang, L. M. *et al.* Lipid nanoparticle-mediated efficient delivery of CRISPR/Cas9 for tumor therapy. *Npg Asia Mater* **9** (2017). https://doi.org/ARTN e441
10.1038/am.2017.185
249 Zuris, J. A. *et al.* Cationic lipid-mediated delivery of proteins enables efficient protein-based genome editing
and. *Nature Biotechnology* **33**, 73-80 (2015). https://doi.org/10.1038/nbt.3081
250 Porto, E. M., Komor, A. C., Slaymaker, I. M. & Yeo, G. W. Base editing: advances and therapeutic opportunities. *Nature Reviews Drug Discovery* **19**, 839-859 (2020). https://doi.org/10.1038/s41573-020-0084-6
251 Fujinami, K. *et al.* Detailed genetic characteristics of an international large cohort of patients with Stargardt disease: ProgStar study report 8. *Brit J Ophthalmol* **103**, 390-397 (2019). https://doi.org/10.1136/bjophthalmol-2018-312064
252 Muller, A. *et al.* High-efficiency base editing for Stargardt disease in mice, non-human primates, and human retina tissue. *bioRxiv*, 2023.2004.2017.535579 (2023). https://doi.org/10.1101/2023.04.17.535579
253 Böck, D. *et al.* In vivo prime editing of a metabolic liver disease in mice. *Sci Transl Med* **14** (2022). https://doi.org/ARTN eabl9238

10.1126/scitranslmed.abl9238
254 Zhi, S. Y. *et al.* Dual-AAV delivering split prime editor system for genome editing. *Mol Ther* **30**, 283-294 (2022). https://doi.org/10.1016/j.ymthe.2021.07.011
255 Kurata, M. *et al.* Highly multiplexed genome engineering using CRISPR/Cas9 gRNA arrays. *Plos One* **13** (2018). https://doi.org/ARTN e0198714
10.1371/journal.pone.0198714
256 Urnov, F. D. Give Cas a Chance: An Actionable Path to a Platform for CRISPR Cures. *Crispr J* **7**, 212-219 (2024). https://doi.org/10.1089/crispr.2024.0082
257 Guo, C. T., Ma, X. T., Gao, F. & Guo, Y. X. Off-target effects in CRISPR/Cas9 gene editing. *Front Bioeng Biotech* **11** (2023). https://doi.org/ARTN 1143157
10.3389/fbioe.2023.1143157
258 Zhang, X. H., Tee, L. Y., Wang, X. G., Huang, Q. S. & Yang, S. H. Off-target Effects in CRISPR/Cas9-mediated Genome Engineering. *Mol Ther-Nucl Acids* **4** (2015). https://doi.org/ARTN e264
10.1038/mtna.2015.37
259 Reautschnig, P. *et al.* Precise in vivo RNA base editing with a wobble-enhanced circular CLUSTER guide RNA. *Nature Biotechnology* (2024). https://doi.org/10.1038/s41587-024-02313-0
260 Mullard, A. RNA-rewriting candidate moves into the clinic. *Nature Reviews Drug Discovery* **23**, 407-409 (2024). https://doi.org/10.1038/d41573-024-00086-4
261 Komor, A. C., Kim, Y. B., Packer, M. S., Zuris, J. A. & Liu, D. R. Programmable editing of a target base in genomic DNA without double-stranded DNA cleavage. *Nature* **533**, 420-+ (2016). https://doi.org/10.1038/nature17946
262 Fukuda, M. *et al.* Construction of a guide-RNA for site-directed RNA mutagenesis utilising intracellular A-to-I RNA editing. *Sci Rep-Uk* **7** (2017). https://doi.org/ARTN 41478
10.1038/srep41478
263 Hanswillemenke, A., Kuzdere, T., Vogel, P., Jékely, G. & Stafforst, T. Site-Directed RNA Editing in Vivo Can Be Triggered by the Light-Driven Assembly of an Artificial Riboprotein. *J Am Chem Soc* **137**, 15875-15881 (2015). https://doi.org/10.1021/jacs.5b10216
264 Rees, H. A. & Liu, D. R. Base editing: precision chemistry on the genome and transcriptome of living cells (vol 19, pg 770, 2018). *Nat Rev Genet* **19**, 801-801 (2018). https://doi.org/10.1038/s41576-018-0068-0
265 Vogel, P. *et al.* Efficient and precise editing of endogenous transcripts with SNAP-tagged ADARs. *Nat Methods* **15**, 535-+ (2018). https://doi.org/10.1038/s41592-018-0017-z
266 Miller, S. M., Wang, T. A. & Liu, D. R. Phage-assisted continuous and non-continuous evolution. *Nat Protoc* **15**, 4101-4127 (2020). https://doi.org/10.1038/s41596-020-00410-3
267 Abudayyeh, O. O. *et al.* A cytosine deaminase for programmable single-base RNA editing. *Science* **365**, 382-+ (2019). https://doi.org/10.1126/science.aax7063
268 Huang, X. X. *et al.* Programmable C-to-U RNA editing using the human APOBEC3A deaminase (vol 39, e104741, 2020). *Embo J* **40** (2021). https://doi.org/ARTN e108209
10.15252/embj.2021108209

269 Sun, H. & Nathans, J. Stargardt's ABCR is localized to the disc membrane of retinal rod outer segments. *Nat Genet* **17**, 15-16 (1997). https://doi.org/DOI 10.1038/ng0997-15

270 Kluesner, M. G. *et al.* EditR: A Method to Quantify Base Editing from Sanger Sequencing. *Crispr J* **1**, 239-250 (2018). https://doi.org/10.1089/crispr.2018.0014

271 Schwarz, J. M., Rödelsperger, C., Schuelke, M. & Seelow, D. MutationTaster evaluates disease-causing potential of sequence alterations. *Nat Methods* **7**, 575-576 (2010). https://doi.org/10.1038/nmeth0810-575

272 Xu, X. S. *et al.* Engineered miniature CRISPR-Cas system for mammalian genome regulation and editing. *Mol Cell* **81**, 4333-+ (2021). https://doi.org/10.1016/j.molcel.2021.08.008

273 Cevik, S., Biswas, S. B., Ghosh, A. & Biswas-Fiss, E. E. Virus-like particles as robust tools for functional assessment Deciphering the pathogenicity of ABCA4 genetic variants of uncertain significance fi cance. *J Biol Chem* **300** (2024). https://doi.org/ARTN 107739 10.1016/j.jbc.2024.107739

274 Piccolo, D. *et al.* A Proximity Complementation Assay to Identify Small Molecules That Enhance the Traffic of ABCA4 Misfolding Variants. *Int J Mol Sci* **25** (2024). https://doi.org/ARTN 4521 10.3390/ijms25084521

275 Dawson, T. R., Sansam, C. L. & Emeson, R. B. Structure and sequence determinants required for the RNA editing of ADAR2 substrates. *J Biol Chem* **279**, 4941-4951 (2004). https://doi.org/10.1074/jbc.M310068200

276 Zambrano-Mila, M. S. *et al.* Dissecting the basis for differential substrate specificity of ADAR1 and ADAR2. *Nat Commun* **14** (2023). https://doi.org/ARTN 8212 10.1038/s41467-023-43633-0

277 Corsi, G. I. *et al.* CRISPR/Cas9 gRNA activity depends on free energy changes and on the target PAM context. *Nat Commun* **13** (2022). https://doi.org/ARTN 3006 10.1038/s41467-022-30515-0

278 Grünewald, J. *et al.* Transcriptome-wide off-target RNA editing induced by CRISPR-guided DNA base editors. *Nature* **569**, 433-+ (2019). https://doi.org/10.1038/s41586-019-1161-z

279 Park, S. & Beal, P. A. Off-Target Editing by CRISPR-Guided DNA Base Editors. *Biochemistry-Us* **58**, 3727-3734 (2019). https://doi.org/10.1021/acs.biochem.9b00573

280 Jonnal, R. S. *et al.* Imaging Outer Segment Renewal in Living Human Cone Photoreceptors. *Invest Ophth Vis Sci* **51** (2010).

281 Han, W. J. *et al.* Programmable RNA base editing with a single gRNA-free enzyme. *Nucleic Acids Res* **50**, 9580-9595 (2022). https://doi.org/10.1093/nar/gkac713

282 Mekler, V., Minakhin, L., Semenova, E., Kuznedelov, K. & Severinov, K. Kinetics of the CRISPR-Cas9 effector complex assembly and the role of 3'-terminal segment of guide RNA. *Nucleic Acids Res* **44**, 2837-2845 (2016). https://doi.org/10.1093/nar/gkw138

283 Evanoff, M. & Komor, A. C. Base editors: modular tools for the introduction of point mutations in living cells. *Emerg Top Life Sci* **3**, 483-491 (2019). https://doi.org/10.1042/Etls20190088

284 Kaukonen, M. *et al.* SaCas9 base editing as a treatment strategy for -associated retinitis pigmentosa. *Invest Ophth Vis Sci* **63** (2022).

285 Anzalone, A. V., Koblan, L. W. & Liu, D. R. Genome editing with CRISPR-Cas nucleases, base editors, transposases and prime editors. *Nature Biotechnology* **38**, 824-844 (2020). https://doi.org/10.1038/s41587-020-0561-9

286 Marquart, K. F. *et al.* Predicting base editing outcomes with an attention-based deep learning algorithm trained on high-throughput target library screens. *Nat Commun* **12** (2021). https://doi.org/ARTN 5114
10.1038/s41467-021-25375-z

287 Wang, T., Wei, J. J., Sabatini, D. M. & Lander, E. S. Genetic Screens in Human Cells Using the CRISPR-Cas9 System. *Science* **343**, 80-84 (2014). https://doi.org/10.1126/science.1246981

288 Gerbracht, J. V., Boehm, V. & Gehring, N. H. Plasmid transfection influences the readout of nonsense-mediated mRNA decay reporter assays in human cells. *Sci Rep-Uk* **7** (2017). https://doi.org/ARTN 10616
10.1038/s41598-017-10847-4

289 Zetoune, A. B. *et al.* Comparison of nonsense-mediated mRNA decay efficiency in various murine tissues. *Bmc Genet* **9** (2008). https://doi.org/Artn 83
10.1186/1471-2156-9-83

290 Clark, D. P. & Pazdernik, N. J. *Molecular biology*. 2nd edn, (Academic Press, 2013).

291 Metze, S., Herzog, V. A., Ruepp, M. D. & Mühlemann, O. Comparison of EJC-enhanced and EJC-independent NMD in human cells reveals two partially redundant degradation pathways. *Rna* **19**, 1432-1448 (2013). https://doi.org/10.1261/rna.038893.113

292 Song, Y. L. *et al.* irCLASH reveals RNA substrates recognized by human ADARs. *Nat Struct Mol Biol* **27**, 351-+ (2020). https://doi.org/10.1038/s41594-020-0398-4

293 Cella, W. *et al.* G1961E mutant allele in the Stargardt disease gene causes bull's eye maculopathy. *Exp Eye Res* **89**, 16-24 (2009). https://doi.org/10.1016/j.exer.2009.02.001

294 Kikutake, C. & Suyama, M. Possible involvement of silent mutations in cancer pathogenesis and evolution. *Sci Rep-Uk* **13** (2023). https://doi.org/ARTN 7593
10.1038/s41598-023-34452-w

295 Sauna, Z. E. & Kimchi-Sarfaty, C. Understanding the contribution of synonymous mutations to human disease. *Nat Rev Genet* **12**, 683-691 (2011). https://doi.org/10.1038/nrg3051

296 Ishida, K., Gee, P. & Hotta, A. Minimizing off-Target Mutagenesis Risks Caused by Programmable Nucleases. *Int J Mol Sci* **16**, 24751-24771 (2015). https://doi.org/10.3390/ijms161024751

297 Taha, E. A., Lee, J. & Hotta, A. Delivery of CRISPR-Cas tools for genome editing therapy: Trends and challenges. *J Control Release* **342**, 345-361 (2022). https://doi.org/10.1016/j.jconrel.2022.01.013

298 Lin, Y. N., Cradick, T. J., Brown, M. T., Deshmukh, H. & Bao, G. CRISPR/Cas9 Systems Have Off-Target Activity With Insertions or Deletions Between Target DNA and Guide RNA Sequences. *Mol Ther* **22**, S94-S95 (2014).

299 Chen, Q. C. *et al.* Genome-wide CRISPR off-target prediction and optimization using RNA-DNA interaction fingerprints. *Nat Commun* **14** (2023). https://doi.org/ARTN 7521
10.1038/s41467-023-42695-4

300 Singh, M. S. *et al.* Retinal stem cell transplantation: Balancing safety and potential. *Prog Retin Eye Res* **75** (2020). https://doi.org/ARTN 100779
10.1016/j.preteyeres.2019.100779
301 Chichagova, V. *et al.* Human iPSC differentiation to retinal organoids in response to IGF1 and BMP4 activation is line- and method-dependent. *Stem Cells* **38**, 195-201 (2020). https://doi.org/10.1002/stem.3116
302 Eiraku, M. *et al.* Self-organizing optic-cup morphogenesis in three-dimensional culture. *Nature* **472**, 51-U73 (2011). https://doi.org/10.1038/nature09941
303 Fligor, C. M., Huang, K. C., Lavekar, S. S., VanderWall, K. B. & Meyer, J. S. Differentiation of retinal organoids from human pluripotent stem cells. *Method Cell Biol* **159**, 279-+ (2020). https://doi.org/10.1016/bs.mcb.2020.02.005
304 Zhong, X. F. *et al.* Generation of three-dimensional retinal tissue with functional photoreceptors from human iPSCs. *Nat Commun* **5** (2014). https://doi.org/ARTN 4047
10.1038/ncomms5047
305 Brinkman, E. K., Chen, T., Amendola, M. & van Steensel, B. Easy quantitative assessment of genome editing by sequence trace decomposition. *Nucleic Acids Res* **42** (2014). https://doi.org/ARTN e168
10.1093/nar/gku936
306 Garita-Hernandez, M. *et al.* AAV-Mediated Gene Delivery to 3D Retinal Organoids Derived from Human Induced Pluripotent Stem Cells. *Int J Mol Sci* **21** (2020). https://doi.org/ARTN 994
10.3390/ijms21030994
307 McClements, M. E. *et al.* Tropism of AAV Vectors in Photoreceptor-Like Cells of Human iPSC-Derived Retinal Organoids. *Transl Vis Sci Techn* **11** (2022). https://doi.org/ARTN 3
10.1167/tvst.11.4.3
308 Schindelin, J. *et al.* Fiji: an open-source platform for biological-image analysis. *Nat Methods* **9**, 676-682 (2012). https://doi.org/10.1038/Nmeth.2019
309 Lane, A. *et al.* Modeling and Rescue of RP2 Retinitis Pigmentosa Using iPSC-Derived Retinal Organoids. *Stem Cell Rep* **15**, 67-79 (2020). https://doi.org/10.1016/j.stemcr.2020.05.007
310 West, E. L. *et al.* Antioxidant and lipid supplementation improve the development of photoreceptor outer segments in pluripotent stem cell-derived retinal organoids. *Stem Cell Rep* **17**, 775-788 (2022). https://doi.org/10.1016/j.stemcr.2022.02.019
311 Arbab, M. *et al.* Determinants of Base Editing Outcomes from Target Library Analysis and Machine Learning. *Cell* **182**, 463-+ (2020). https://doi.org/10.1016/j.cell.2020.05.037
312 Konstantakos, V., Nentidis, A., Krithara, A. & Paliouras, G. CRISPR-Cas9 gRNA efficiency prediction: an overview of predictive tools and the role of deep learning. *Nucleic Acids Res* **50**, 3616-3637 (2022). https://doi.org/10.1093/nar/gkac192
313 Schärfen, L. & Neugebauer, K. M. Transcription Regulation Through Nascent RNA Folding. *J Mol Biol* **433** (2021). https://doi.org/ARTN 166975
10.1016/j.jmb.2021.166975
314 Zemora, G. & Waldsich, C. RNA folding in living cells. *Rna Biol* **7**, 634-641 (2010). https://doi.org/10.4161/rna.7.6.13554
315 Rice, G. M., Leonard, C. W. & Weeks, K. M. RNA secondary structure modeling at consistent high accuracy using differential SHAPE. *Rna* **20**, 846-854 (2014). https://doi.org/10.1261/rna.043323.113

316 Chaney, J. L. & Clark, P. L. Roles for Synonymous Codon Usage in Protein Biogenesis. *Annu Rev Biophys* **44**, 143-166 (2015). https://doi.org/10.1146/annurev-biophys-060414-034333

317 Zhao, F. Z. *et al.* Genome-wide role of codon usage on transcription and identification of potential regulators. *P Natl Acad Sci USA* **118** (2021). https://doi.org/ARTN e2022590118 10.1073/pnas.2022590118

318 Zhou, M. *et al.* Non-optimal codon usage affects expression, structure and function of clock protein FRQ. *Nature* **495**, 111-115 (2013). https://doi.org/10.1038/nature11833

319 Fiflis, D. N. *et al.* Repurposing CRISPR-Cas13 systems for robust mRNA trans-splicing. *Nat Commun* **15** (2024). https://doi.org/ARTN 2325 10.1038/s41467-024-46172-4

320 Xiang, X. *et al.* Enhancing CRISPR-Cas9 gRNA efficiency prediction by data integration and deep learning. *Nat Commun* **12** (2021). https://doi.org/ARTN 3238 10.1038/s41467-021-23576-0

321 Graf, R., Li, X., Chu, V. T. & Rajewsky, K. sgRNA Sequence Motifs Blocking Efficient CRISPR/Cas9-Mediated Gene Editing. *Cell Rep* **26**, 1098-+ (2019). https://doi.org/10.1016/j.celrep.2019.01.024

322 Thuronyi, B. W. *et al.* Continuous evolution of base editors with expanded target compatibility and improved activity (vol 37, pg 1070, 2019). *Nature Biotechnology* **37**, 1091-1091 (2019). https://doi.org/10.1038/s41587-019-0253-5

323 Malina, A. *et al.* PAM multiplicity marks genomic target sites as inhibitory to CRISPR-Cas9 editing. *Nat Commun* **6** (2015). https://doi.org/ARTN 10124 10.1038/ncomms10124

324 Qu, L. *et al.* Programmable RNA editing by recruiting endogenous ADAR using engineered RNAs (vol 37, pg 1059, 2019). *Nature Biotechnology* **37**, 1380-1380 (2019). https://doi.org/10.1038/s41587-019-0292-y

325 Deng, W. L. *et al.* Gene Correction Reverses Ciliopathy and Photoreceptor Loss in iPSC-Derived Retinal Organoids from Retinitis Pigmentosa Patients (vol 10, pg 1267, 2018). *Stem Cell Rep* **10**, 2005-2005 (2018). https://doi.org/10.1016/j.stemcr.2018.05.012

326 Giacalone, J. C. *et al.* Concise Review: Patient-Specific Stem Cells to Interrogate Inherited Eye Disease. *Stem Cell Transl Med* **5**, 132-140 (2016). https://doi.org/10.5966/sctm.2015-0206

327 Eggington, J. M., Greene, T. & Bass, B. L. Predicting sites of ADAR editing in double-stranded RNA. *Nat Commun* **2** (2011). https://doi.org/ARTN 319 10.1038/ncomms1324

328 Matthews, M. M. *et al.* Structures of human ADAR2 bound to dsRNA reveal base-flipping mechanism and basis for site selectivity. *Nat Struct Mol Biol* **23**, 426-433 (2016). https://doi.org/10.1038/nsmb.3203

329 Li, X. Y., Zhang, L., Tang, F. & Wei, X. Retinal Organoids: Cultivation, Differentiation, and Transplantation (vol 15, 638439, 2021). *Front Cell Neurosci* **15** (2021). https://doi.org/ARTN 810268 10.3389/fncel.2021.810268

330 Capowski, E. E. *et al.* Reproducibility and staging of 3D human retinal organoids across multiple pluripotent stem cell lines. *Development* **146** (2019). https://doi.org/ARTN dev171686 10.1242/dev.171686

331 Wahlin, K. J. *et al.* Photoreceptor Outer Segment-like Structures in Long-Term 3D Retinas from Human Pluripotent Stem Cells. *Sci Rep-Uk* **7** (2017). https://doi.org/ARTN 766
10.1038/s41598-017-00774-9
332 Ames, A., Li, Y. Y., Heher, E. C. & Kimble, C. R. Energy-Metabolism of Rabbit Retina as Related to Function - High Cost of Na+ Transport. *J Neurosci* **12**, 840-853 (1992). https://doi.org/DOI 10.1523/jneurosci.12-03-00840.1992
333 Anderson, B., Jr. Ocular effects of changes in oxygen and carbon dioxide tension. *Trans Am Ophthalmol Soc* **66**, 423-474 (1968).
334 Yu, D. Y. & Cringle, S. J. Oxygen distribution and consumption within the retina in vascularised and avascular retinas and in animal models of retinal disease. *Prog Retin Eye Res* **20**, 175-208 (2001). https://doi.org/Doi 10.1016/S1350-9462(00)00027-6
335 Chichagova, V. *et al.* Incorporating microglia-like cells in human induced pluripotent stem cell-derived retinal organoids. *J Cell Mol Med* **27**, 435-445 (2023). https://doi.org/10.1111/jcmm.17670
336 Wang, M. H., Ma, W. X., Zhao, L., Fariss, R. N. & Wong, W. T. Adaptive Muller cell responses to microglial activation mediate neuroprotection and coordinate inflammation in the retina. *J Neuroinflamm* **8** (2011). https://doi.org/Artn 173
10.1186/1742-2094-8-173
337 Wang, M. H. & Wong, W. T. Microglia-Muller Cell Interactions in the Retina. *Adv Exp Med Biol* **801**, 333-338 (2014). https://doi.org/10.1007/978-1-4614-3209-8_42
338 Jha, B. S. & Bharti, K. Regenerating Retinal Pigment Epithelial Cells to Cure Blindness: A Road Towards Personalized Artificial Tissue. *Curr Stem Cell Rep* **1**, 79-91 (2015). https://doi.org/10.1007/s40778-015-0014-4
339 Song, M. J. & Bharti, K. Looking into the future: Using induced pluripotent stem cells to build two and three dimensional ocular tissue for cell therapy and disease modeling. *Brain Res* **1638**, 2-14 (2016). https://doi.org/10.1016/j.brainres.2015.12.011
340 Flores-Bellver, M. & Canto-Soler, M. V. Generation of Induced-Primary Retinal Pigment Epithelium from Human Retinal Organoids. *Methods Mol Biol* **2848**, 197-214 (2025). https://doi.org/10.1007/978-1-0716-4087-6_13
341 Grebenyuk, S. & Ranga, A. Engineering Organoid Vascularization. *Front Bioeng Biotech* **7** (2019). https://doi.org/ARTN 39
10.3389/fbioe.2019.00039
342 Su, J. *et al.* base editing rescues photoreceptors in a mouse model of retinitis pigmentosa. *Mol Ther-Nucl Acids* **31**, 596-609 (2023). https://doi.org/10.1016/j.omtn.2023.02.011
343 Yu, J. *et al.* Programmable RNA base editing with photoactivatable CRISPR-Cas13. *Nat Commun* **15** (2024). https://doi.org/ARTN 673
10.1038/s41467-024-44867-2
344 Monian, P. *et al.* Endogenous ADAR-mediated RNA editing in non-human primates using stereopure chemically modified oligonucleotides. *Nature Biotechnology* **40**, 1093-+ (2022). https://doi.org/10.1038/s41587-022-01225-1
345 Gramatikov, B. I. Modern technologies for retinal scanning and imaging: an introduction for the biomedical engineer. *Biomed Eng Online* **13** (2014). https://doi.org/Artn 52
10.1186/1475-925x-13-52

346 Issa, P. C. *et al.* Optimization of In Vivo Confocal Autofluorescence Imaging of the Ocular Fundus in Mice and Its Application to Models of Human Retinal Degeneration. *Invest Ophth Vis Sci* **53**, 1066-1075 (2012). https://doi.org/10.1167/iovs.11-8767
347 Colognori, D., Trinidad, M. & Doudna, J. A. Precise transcript targeting by CRISPR-Csm complexes. *Nature Biotechnology* **41**, 1256-+ (2023). https://doi.org/10.1038/s41587-022-01649-9
348 Du, M. H., Jillette, N., Zhu, J. J., Li, S. & Cheng, A. W. CRISPR artificial splicing factors. *Nat Commun* **11** (2020). https://doi.org/10.1038/s41467-020-16806-4
349 Zhang, C. *et al.* Structural Basis for the RNA-Guided Ribonuclease Activity of CRISPR-Cas13d. *Cell* **175**, 212-+ (2018). https://doi.org/10.1016/j.cell.2018.09.001
350 Núñez-Alvarez, Y. *et al.* A CRISPR-dCas13 RNA-editing tool to study alternative splicing. *Nucleic Acids Res* **52**, 11926-11939 (2024). https://doi.org/10.1093/nar/gkae682
351 Briese, M. *et al.* A systems view of spliceosomal assembly and branchpoints with iCLIP (vol 26, pg 930, 2019). *Nat Struct Mol Biol* **28**, 455-455 (2021). https://doi.org/10.1038/s41594-021-00595-5
352 Hauer, C. *et al.* Exon Junction Complexes Show a Distributional Bias toward Alternatively Spliced mRNAs and against mRNAs Coding for Ribosomal Proteins. *Cell Rep* **16**, 1588-1603 (2016). https://doi.org/10.1016/j.celrep.2016.06.096
353 Wessels, H. H. *et al.* Massively parallel Cas13 screens reveal principles for guide RNA design. *Nature Biotechnology* **38**, 722-+ (2020). https://doi.org/10.1038/s41587-020-0456-9
354 Reautschnig, P. *et al.* CLUSTER guide RNAs enable precise and efficient RNA editing with endogenous ADAR enzymes in vivo. *Nature Biotechnology* **40**, 759-+ (2022). https://doi.org/10.1038/s41587-021-01105-0
355 Gumerson, J. D. *et al.* Restoration of RPGR expression in vivo using CRISPR/Cas9 gene editing. *Gene Ther* **29**, 81-93 (2022). https://doi.org/10.1038/s41434-021-00258-6
356 Xiong, W. J. *et al.* AAV
-regulatory sequences are correlated with ocular toxicity. *P Natl Acad Sci USA* **116**, 5785-5794 (2019). https://doi.org/10.1073/pnas.1821000116
357 Qin, H. *et al.* Vision rescue via unconstrained in vivo prime editing in degenerating neural retinas. *J Exp Med* **220** (2023). https://doi.org/ARTN e20220776
10.1084/jem.20220776
358 Musunuru, K. *et al.* Patient-Specific In Vivo Gene Editing to Treat a Rare Genetic Disease. *New Engl J Med* **392**, 2235-2243 (2025). https://doi.org/10.1056/NEJMoa2504747
359 Liu, Z. *et al.* Efficient generation of mouse models of human diseases via ABE- and BE-mediated base editing. *Nat Commun* **9** (2018). https://doi.org/ARTN 2338
10.1038/s41467-018-04768-7
360 Zhang, H. *et al.* Simultaneous zygotic inactivation of multiple genes in mouse through CRISPR/Cas9-mediated base editing. *Development* **145** (2018). https://doi.org/ARTN dev168906
10.1242/dev.168906
361 Wang, X. J. *et al.* Efficient Gene Silencing by Adenine Base Editor-Mediated Start Codon Mutation. *Mol Ther* **28**, 431-440 (2020). https://doi.org/10.1016/j.ymthe.2019.11.022
362 Cullot, G. *et al.* CRISPR-Cas9 genome editing induces megabase-scale chromosomal truncations. *Nat Commun* **10** (2019). https://doi.org/ARTN 1136

10.1038/s41467-019-09006-2
363 Haapaniemi, E., Botla, S., Persson, J., Schmierer, B. & Taipale, J. CRISPR-Cas9 genome editing induces a p53-mediated DNA damage response. *Nat Med* **24**, 927-+ (2018). https://doi.org/10.1038/s41591-018-0049-z
364 Ihry, R. J. *et al.* p53 inhibits CRISPR-Cas9 engineering in human pluripotent stem cells. *Nat Med* **24**, 939-+ (2018). https://doi.org/10.1038/s41591-018-0050-6
365 Slesarenko, Y. S., Lavrov, A. V. & Smirnikhina, S. A. Off-target effects of base editors: what we know and how we can reduce it. *Curr Genet* **68**, 39-48 (2022). https://doi.org/10.1007/s00294-021-01211-1
366 Uehara, H. *et al.* Start codon disruption with CRISPR/Cas9 prevents murine Fuchs' endothelia corneal dystrophy. *Elife* **10** (2021). https://doi.org/ARTN e55637
10.7554/eLife.55637
367 Kolesnikov, A. V. *et al.* Retinol dehydrogenase 8 and ATP-binding cassette transporter 4 modulate dark adaptation of M-cones in mammalian retina. *J Physiol-London* **593**, 4923-4941 (2015). https://doi.org/10.1113/Jp271285
368 Liu, Y. J. *et al.* REPAIRx, a specific yet highly efficient programmable A > I RNA base editor. *Embo J* **39** (2020). https://doi.org/ARTN e104748
10.15252/embj.2020104748
369 Kim, D., Kim, D. E., Lee, G., Cho, S. I. & Kim, J. S. Genome-wide target specificity of CRISPR RNA-guided adenine base editors. *Nature Biotechnology* **37**, 430-+ (2019). https://doi.org/10.1038/s41587-019-0050-1
370 Banskota, S. *et al.* Engineered virus-like particles for efficient

delivery of therapeutic proteins. *Cell* **185**, 250-+ (2022). https://doi.org/10.1016/j.cell.2021.12.021
371 Hsiao, S. L. *et al.* Library-Assisted Evolution in Eukaryotic Cells Yield Adenine Base Editors with Enhanced Editing Specificity. *Adv Sci* **11** (2024). https://doi.org/ARTN 2309004
10.1002/advs.202309004
372 Neugebauer, M. E. *et al.* Evolution of an adenine base editor into a small, efficient cytosine base editor with low off-target activity. *Nature Biotechnology* **41**, 673-+ (2023). https://doi.org/10.1038/s41587-022-01533-6
373 Chan, C. C. *et al.* Periocular Inflammation in Mice with Experimental Systemic Lupus-Erythematosus - a New Experimental Blepharitis and Its Modulation. *J Immunol* **154**, 4830-4835 (1995).
374 Simpson, E. M. *et al.* Genetic variation among 129 substrains and its importance for targeted mutagenesis in mice. *Nat Genet* **16**, 19-27 (1997). https://doi.org/DOI 10.1038/ng0597-19
375 Steppan, J. *et al.* Commonly used mouse strains have distinct vascular properties. *Hypertens Res* **43**, 1175-1181 (2020). https://doi.org/10.1038/s41440-020-0467-4
376 Fink, D. *et al.* Ubiquitous Expression of the Monomeric Red Fluorescent Protein mCherry in Transgenic Mice. *Genesis* **48**, 723-729 (2010). https://doi.org/10.1002/dvg.20677
377 Shemiakina, I. I. *et al.* A monomeric red fluorescent protein with low cytotoxicity. *Nat Commun* **3** (2012). https://doi.org/ARTN 1204

10.1038/ncomms2208
378 Roy, S. Immune responses to CRISPR-Cas protein. *Prog Mol Biol Transl* **178**, 213-229 (2021). https://doi.org/10.1016/bs.pmbts.2020.12.003
379 Chew, W. L. *et al.* A multifunctional AAV-CRISPR-Cas9 and its host response. *Nat Methods* **13**, 868-+ (2016). https://doi.org/10.1038/nmeth.3993
380 Crudele, J. M. & Chamberlain, J. S. Cas9 immunity creates challenges for CRISPR gene editing therapies. *Nat Commun* **9** (2018). https://doi.org/ARTN 3497
10.1038/s41467-018-05843-9
381 Stefanidakis, M. *et al.* Preclinical assessment of
gene editing efficiency, specificity, and tolerability of EDIT-101, an investigational CRISPR treatment for Leber congenital amaurosis 10 (LCA10). *Hum Gene Ther* **29**, A101-A101 (2018).
382 Rashnonejad, A. *et al.* AAV-CRISPR-Cas13 gene therapy for FSHD:
gene silencing efficacy and immune responses to Cas13b protein. *Neuromuscular Disord* **32**, S103-S104 (2022). https://doi.org/10.1016/j.nmd.2022.07.255
383 Fry, L. E. *et al.* Association of Messenger RNA Level With Phenotype in Patients With Choroideremia Potential Implications for Gene Therapy Dose. *Jama Ophthalmol* **138**, 128-135 (2020). https://doi.org/10.1001/jamaophthalmol.2019.5071
384 Kim, N. *et al.* Deep learning models to predict the editing efficiencies and outcomes of diverse base editors. *Nature Biotechnology* **42** (2024). https://doi.org/10.1038/s41587-023-01792-x
385 Auld, D. S. & Inglese, J. in *Assay Guidance Manual* (eds S. Markossian *et al.*) (2004).
386 Maquat, L. E. & Li, X. J. Mammalian heat shock p70 and histone H4 transcripts, which derive from naturally intronless genes, are immune to nonsense-mediated decay. *Rna* **7**, 445-456 (2001). https://doi.org/Doi 10.1017/S1355838201002229
387 Hug, N., Longman, D. & Cáceres, J. F. Mechanism and regulation of the nonsense-mediated decay pathway. *Nucleic Acids Res* **44**, 1483-1495 (2016). https://doi.org/10.1093/nar/gkw010
388 Kluesner, M. G. *et al.* MultiEditR: The first tool for the detection and quantification of RNA editing from Sanger sequencing demonstrates comparable fidelity to RNA-seq. *Mol Ther-Nucl Acids* **25**, 515-523 (2021). https://doi.org/10.1016/j.omtn.2021.07.008
389 Sun, H., Smallwood, P. M. & Nathans, J. Biochemical defects in ABCR protein variants associated with human retinopathies. *Nat Genet* **26**, 242-246 (2000). https://doi.org/Doi 10.1038/79994
390 Quazi, F., Lenevich, S. & Molday, R. S. ABCA4 is an
-retinylidene-phosphatidylethanolamine and phosphatidylethanolamine importer. *Nat Commun* **3** (2012). https://doi.org/ARTN 925
10.1038/ncomms1927
391 Sun, H., Molday, R. S. & Nathans, J. Retinal stimulates ATP hydrolysis by purified and reconstituted ABCR, the photoreceptor-specific ATP-binding cassette transporter responsible for Stargardt disease. *J Biol Chem* **274**, 8269-8281 (1999). https://doi.org/DOI 10.1074/jbc.274.12.8269
392 Zhang, W. W. *et al.* In-depth assessment of the PAM compatibility and editing activities of Cas9 variants. *Nucleic Acids Res* **49**, 8785-8795 (2021). https://doi.org/10.1093/nar/gkab507

393 Zhou, X. Y. *et al.* Comprehensive evaluation and prediction of editing outcomes for near-PAMless adenine and cytosine base editors. *Commun Biol* **7** (2024). https://doi.org/ARTN 1389
10.1038/s42003-024-07078-5
394 Doench, J. G. *et al.* Optimized sgRNA design to maximize activity and minimize off-target effects of CRISPR-Cas9. *Nature Biotechnology* **34**, 184-+ (2016). https://doi.org/10.1038/nbt.3437
395 Doench, J. G. *et al.* Rational design of highly active sgRNAs for CRISPR-Cas9-mediated gene inactivation. *Nature Biotechnology* **32**, 1262-U1130 (2014). https://doi.org/10.1038/nbt.3026
396 Tian, N. *et al.* A structural determinant required for RNA editing. *Nucleic Acids Res* **39**, 5669-5681 (2011). https://doi.org/10.1093/nar/gkr144
397 Bass, B. RNA editing and hypermutation by adenosine deamination (vol 22, pg 157, 1997). *Trends Biochem Sci* **22**, 279-279 (1997).
398 Lehmann, K. A. & Bass, B. L. Double-stranded RNA adenosine deaminases ADAR1 and ADAR2 have overlapping specificities. *Biochemistry-Us* **39**, 12875-12884 (2000). https://doi.org/DOI 10.1021/bi001383g
399 Stephens, O. M., Haudenschild, B. L. & Beal, P. A. The binding selectivity of ADAR2's dsRBMs contributes to RNA-editing selectivity. *Chem Biol* **11**, 1239-1250 (2004). https://doi.org/10.1016/j.chembiol.2004.06.009
400 Wong, S. K., Sato, S. & Lazinski, D. W. Substrate recognition by ADAR1 and ADAR2. *Rna* **7**, 846-858 (2001). https://doi.org/Doi 10.1017/S135583820101007x
401 Kim, D., Kim, S., Kim, S., Park, J. & Kim, J. S. Genome-wide target specificities of CRISPR-Cas9 nucleases revealed by multiplex Digenome-seq. *Genome Res* **26**, 406-415 (2016). https://doi.org/10.1101/gr.199588.115
402 Tsai, S. Q. *et al.* GUIDE-seq enables genome-wide profiling of off-target cleavage by CRISPR-Cas nucleases. *Nature Biotechnology* **33**, 187-197 (2015). https://doi.org/10.1038/nbt.3117
403 Cancellieri, S. *et al.* Human genetic diversity alters off-target outcomes of therapeutic gene editing. *Nat Genet* **55**, 34-+ (2023). https://doi.org/10.1038/s41588-022-01257-y
404 Jin, S. *et al.* Cytosine, but not adenine, base editors induce genome-wide off-target mutations in rice. *Science* **364**, 292-+ (2019). https://doi.org/10.1126/science.aaw7166
405 Sretenovic, S. *et al.* Genome- and transcriptome-wide off-target analyses of a high-efficiency adenine base editor in tomato. *Plant Physiol* **193**, 291-303 (2023). https://doi.org/10.1093/plphys/kiad347
406 Zhao, N. *et al.* Evolved cytidine and adenine base editors with high precision and minimized off-target activity by a continuous directed evolution system in mammalian cells. *Nat Commun* **15**, 8140 (2024). https://doi.org/10.1038/s41467-024-52483-3
407 Fu, Y. F., Sander, J. D., Reyon, D., Cascio, V. M. & Joung, J. K. Improving CRISPR-Cas nuclease specificity using truncated guide RNAs. *Nature Biotechnology* **32**, 279-284 (2014). https://doi.org/10.1038/nbt.2808
408 Kocak, D. D. *et al.* Increasing the specificity of CRISPR systems with engineered RNA secondary structures. *Nature Biotechnology* **37**, 657-+ (2019). https://doi.org/10.1038/s41587-019-0095-1
409 Lee, S. H. *et al.* Bystander base editing interferes with visual function restoration in Leber congenital amaurosis. *bioRxiv* (2024). https://doi.org/10.1101/2024.10.23.619839

410 Jumper, J. *et al.* Highly accurate protein structure prediction with AlphaFold. *Nature* **596**, 583-+ (2021). https://doi.org/10.1038/s41586-021-03819-2

411 Chen, G. H., Katrekar, D. & Mali, P. RNA-Guided Adenosine Deaminases: Advances and Challenges for Therapeutic RNA Editing. *Biochemistry-Us* **58**, 1947-1957 (2019). https://doi.org/10.1021/acs.biochem.9b00046

412 Kumar, K. D. K. *et al.* An improved SNAP-ADAR tool enables efficient RNA base editing to interfere with post-translational protein modification. *Nat Commun* **15** (2024). https://doi.org/ARTN 6615
10.1038/s41467-024-50395-w

413 Jacobsen, C. S. *et al.* Library Screening Reveals Sequence Motifs That Enable ADAR2 Editing at Recalcitrant Sites. *Acs Chem Biol* **18**, 2188-2199 (2023). https://doi.org/10.1021/acschembio.3c00107

414 Ai, X. L. *et al.* Enhancing RNA editing efficiency and specificity with engineered ADAR2 guide RNAs. *Mol Ther Nucl Acids* **36** (2025). https://doi.org/ARTN 102447
10.1016/j.omtn.2025.102447

415 Pierce, E. A. *et al.* Gene Editing for
-Associated Retinal Degeneration. *New Engl J Med* **390**, 1972-1984 (2024). https://doi.org/10.1056/NEJMoa2309915

416 Tang, X. Z. E., Tan, S. X., Hoon, S. & Yeo, G. W. Pre-existing adaptive immunity to the RNA-editing enzyme Cas13d in humans. *Nat Med* **28**, 1372-+ (2022). https://doi.org/10.1038/s41591-022-01848-6

417 Bainbridge, J. W. B. *et al.* Effect of gene therapy on visual function in Leber's congenital amaurosis. *New Engl J Med* **358**, 2231-2239 (2008). https://doi.org/10.1056/NEJMoa0802268

418 Fischer, M. D. *et al.* Changes in Retinal Sensitivity after Gene Therapy in Choroideremia. *Retina-J Ret Vit Dis* **40**, 160-168 (2020). https://doi.org/10.1097/Iae.0000000000002360

419 Le Meur, G. *et al.* Postsurgical assessment and long-term safety of recombinant adeno-associated virus-mediated gene transfer into the retinas of dogs and primates. *Arch Ophthalmol-Chic* **123**, 500-506 (2005). https://doi.org/DOI 10.1001/archopht.123.4.500

420 Stieger, K. *et al.* Detection of Intact rAAV Particles up to 6 Years After Successful Gene Transfer in the Retina of Dogs and Primates. *Mol Ther* **17**, 516-523 (2009). https://doi.org/10.1038/mt.2008.283

421 Dimopoulos, I. S. *et al.* Two-Year Results After AAV2-Mediated Gene Therapy for Choroideremia: The Alberta Experience. *Am J Ophthalmol* **193**, 130-142 (2018). https://doi.org/10.1016/j.ajo.2018.06.011

422 Khabou, H., Cordeau, C., Pacot, L., Fisson, S. & Dalkara, D. Dosage Thresholds and Influence of Transgene Cassette in Adeno-Associated Virus-Related Toxicity. *Hum Gene Ther* **29**, 1235-1241 (2018). https://doi.org/10.1089/hum.2018.144

423 Moriya, H. Quantitative nature of overexpression experiments. *Mol Biol Cell* **26**, 3932-3939 (2015). https://doi.org/10.1091/mbc.E15-07-0512

424 Boutin, S. *et al.* Prevalence of Serum IgG and Neutralizing Factors Against Adeno-Associated Virus (AAV) Types 1, 2, 5, 6, 8, and 9 in the Healthy Population: Implications for Gene Therapy Using AAV Vectors. *Hum Gene Ther* **21**, 704-712 (2010). https://doi.org/10.1089/hum.2009.182

425 Mingozzi, F. *et al.* Prevalence and pharmacological modulation of humoral immunity to AAV vectors in gene transfer to synovial tissue. *Gene Ther* **20**, 417-424 (2013). https://doi.org/10.1038/gt.2012.55

426 Mingozzi, F. & High, K. A. Immune responses to AAV vectors: overcoming barriers to successful gene therapy. *Blood* **122**, 23-36 (2013). https://doi.org/10.1182/blood-2013-01-306647

427 Herrera-Barrera, M. *et al.* Peptide-guided lipid nanoparticles deliver mRNA to the neural retina of rodents and nonhuman primates. *Sci Adv* **9** (2023). https://doi.org/ARTN eadd4623
10.1126/sciadv.add4623

428 Colella, P., Ronzitti, G. & Mingozzi, F. Emerging Issues in AAV-Mediated Gene Therapy. *Mol Ther-Meth Clin D* **8**, 87-104 (2018). https://doi.org/10.1016/j.omtm.2017.11.007

429 Kwon, I. & Schaffer, D. V. Designer gene delivery vectors: Molecular engineering and evolution of adeno-associated viral vectors for enhanced gene transfer. *Pharm Res* **25**, 489-499 (2008). https://doi.org/10.1007/s11095-007-9431-0

430 Patel, S., Ryals, R. C., Weller, K. K., Pennesi, M. E. & Sahay, G. Lipid nanoparticles for delivery of messenger RNA to the back of the eye. *J Control Release* **303**, 91-100 (2019). https://doi.org/10.1016/j.jconrel.2019.04.015

431 Yan, A. L., Du, S. W. & Palczewski, K. Genome editing, a superior therapy for inherited retinal diseases. *Vision Res* **206** (2023). https://doi.org/ARTN 108192
10.1016/j.visres.2023.108192

432 Haldrup, J. *et al.* Engineered lentivirus-derived nanoparticles (LVNPs) for delivery of CRISPR/Cas ribonucleoprotein complexes supporting base editing, prime editing and in vivo gene modification. *Nucleic Acids Res* **51**, 10059-10074 (2023). https://doi.org/10.1093/nar/gkad676

433 Rees, H. A. *et al.* Improving the DNA specificity and applicability of base editing through protein engineering and protein delivery. *Nat Commun* **8** (2017). https://doi.org/ARTN 15790
10.1038/ncomms15790

434 Pulman, J. *et al.* Direct delivery of Cas9 or base editor protein and guide RNA complex enables genome editing in the retina. *Mol Ther Nucl Acids* **35** (2024). https://doi.org/ARTN 102349
10.1016/j.omtn.2024.102349

435 Albert, A. D. & Boesze-Battaglia, K. The role of cholesterol in rod outer segment membranes. *Prog Lipid Res* **44**, 99-124 (2005). https://doi.org/10.1016/j.plipres.2005.02.001

436 Yeagle, P. L. Modulation of membrane function by cholesterol. *Biochimie* **73**, 1303-1310 (1991). https://doi.org/10.1016/0300-9084(91)90093-g

437 Gilbert, L. A. *et al.* CRISPR-Mediated Modular RNA-Guided Regulation of Transcription in Eukaryotes. *Cell* **154**, 442-451 (2013). https://doi.org/10.1016/j.cell.2013.06.044

438 Healey, N. Next-generation CRISPR-based gene-editing therapies tested in clinical trials. *Nat Med* **30**, 2380-2381 (2024). https://doi.org/10.1038/d41591-024-00056-8

439 Davis, J. R. *et al.* Efficient prime editing in mouse brain, liver and heart with dual AAVs. *Nature Biotechnology* **42** (2024). https://doi.org/10.1038/s41587-023-01758-z

440 Cirincione, A. *et al.* A benchmarked, high-efficiency prime editing platform for multiplexed dropout screening. *Nat Methods* (2024). https://doi.org/10.1038/s41592-024-02502-4

441 Guzman-Aranguez, A., Loma, P. & Pintor, J. Small-interfering RNAs (siRNAs) as a promising tool for ocular therapy. *Brit J Pharmacol* **170**, 730-747 (2013). https://doi.org/10.1111/bph.12330

442 Karagiannis, T. C. & El-Osta, A. RNA interference and potential therapeutic applications of short interfering RNAs. *Cancer Gene Ther* **12**, 787-795 (2005). https://doi.org/10.1038/sj.cgt.7700857

443 Xue, K. M. & MacLaren, R. E. Antisense oligonucleotide therapeutics in clinical trials for the treatment of inherited retinal diseases. *Expert Opin Inv Drug* **29**, 1163-1170 (2020). https://doi.org/10.1080/13543784.2020.1804853

444 Montagud-Martínez, R., Márquez-Costa, R., Heras-Hernández, M., Dolcemascolo, R. & Rodrigo, G. On the ever-growing functional versatility of the CRISPR-Cas13 system. *Microb Biotechnol* **17** (2024). https://doi.org/ARTN e14418
10.1111/1751-7915.14418

445 Özcan, A. *et al.* Programmable RNA targeting with the single-protein CRISPR effector Cas7-11 (Jul, 10.1038/s41586-021-03886-5, 2022). *Nature* **608**, E30-E30 (2022). https://doi.org/10.1038/s41586-022-05003-6

446 Karali, M. *et al.* Genetic epidemiology of inherited retinal diseases in a large patient cohort followed at a single center in Italy. *Sci Rep-Uk* **12** (2022). https://doi.org/ARTN 20815
10.1038/s41598-022-24636-1

447 Li, R. T. *et al.* Split AAV8 Mediated ABCA4 Expression for Gene Therapy of Mouse Stargardt Disease (STGD1). *Hum Gene Ther* **34**, 616-628 (2023). https://doi.org/10.1089/hum.2023.017

448 Tornabene, P. *et al.* Intein-mediated protein trans-splicing expands adeno-associated virus transfer capacity in the retina. *Sci Transl Med* **11** (2019). https://doi.org/ARTN eaav4523
10.1126/scitranslmed.aav4523

449 Russell, S., Bennet, J., Wellman, J. A. & Simonelli, F. Efficacy and safety of voretigene neparvovec (AAV2-hRPE65v2) in patients with RPE65-mediated inherited retinal dystrophy: a randomised, controlled, open-label, phase 3 trial (vol 390, pg 849, 2017). *Lancet* **390**, 848-848 (2017).

450 Erkut, E. & Yokota, T. CRISPR Therapeutics for Duchenne Muscular Dystrophy. *Int J Mol Sci* **23** (2022). https://doi.org/ARTN 1832
10.3390/ijms23031832

451 Major, L., McClements, M. E. & MacLaren, R. E. A Review of CRISPR Tools for Treating Usher Syndrome: Applicability, Safety, Efficiency, and In Vivo Delivery. *Int J Mol Sci* **24** (2023). https://doi.org/ARTN 7603
10.3390/ijms24087603

452 Chuai, G. H. *et al.*: optimized CRISPR guide RNA design by deep learning. *Genome Biol* **19** (2018). https://doi.org/ARTN 80
10.1186/s13059-018-1459-4

453 Liu, X. Q. *et al.* Usherin is required for maintenance of retinal photoreceptors and normal development of cochlear hair cells. *P Natl Acad Sci USA* **104**, 4413-4418 (2007). https://doi.org/10.1073/pnas.0610950104

454 Garcia-Delgado, A. B. *et al.* Dissecting the role of EYS in retinal degeneration: clinical and molecular aspects and its implications for future therapy. *Orphanet J Rare Dis* **16** (2021). https://doi.org/ARTN 222
10.1186/s13023-021-01843-z
455 Chung, S. H., Sin, T. N., Ngo, T. & Yiu, G. CRISPR Technology for Ocular Angiogenesis. *Front Genome Edit* **2** (2020). https://doi.org/ARTN 594984
10.3389/fgeed.2020.594984
456 Lu, Y. C. *et al.* Reprogramming to Recover Youthful Epigenetic Information and Restore Vision. *Mol Ther* **29**, 52-52 (2021).
457 Yamaguchi, S., Kaneko, M. & Narukawa, M. Approval success rates of drug candidates based on target, action, modality, application, and their combinations. *Cts-Clin Transl Sci* **14**, 1113-1122 (2021). https://doi.org/10.1111/cts.12980
458 Cheng, S. Z., Xing, C. Y., Chen, Z. J., Zhang, S. & Chen, W. H. Clinical trial landscape of gene therapy for retinal degenerative diseases: an analysis based on the Trialtrove database. *Stem Cell Res Ther* **16** (2025). https://doi.org/ARTN 257
10.1186/s13287-025-04387-2
459 Doudna, J. A. The promise and challenge of therapeutic genome editing. *Nature* **578**, 229-236 (2020). https://doi.org/10.1038/s41586-020-1978-5
460 Fox, T. *et al.* Access to gene therapy for rare diseases when commercialization is not fit for purpose. *Nat Med* **29**, 518-519 (2023). https://doi.org/10.1038/s41591-023-02208-8
461 Aiuti, A., Pasinelli, F. & Naldini, L. Ensuring a future for gene therapy for rare diseases. *Nat Med* **28**, 1985-1988 (2022). https://doi.org/10.1038/s41591-022-01934-9
462 Risse, J., Krzemien, M., Schnalke, J. & Heinemann, T. Towards ethical drug pricing: the European Orphan Genomic Therapies Fund. *Gene Ther* **31**, 353-357 (2024). https://doi.org/10.1038/s41434-024-00452-2
463 Cyranoski, D. The CRISPR-baby scandal: what's next for human gene-editing. *Nature* **566**, 440-442 (2019). https://doi.org/10.1038/d41586-019-00673-1

9 Appendix

A. Supplemental Data

Chapter 4

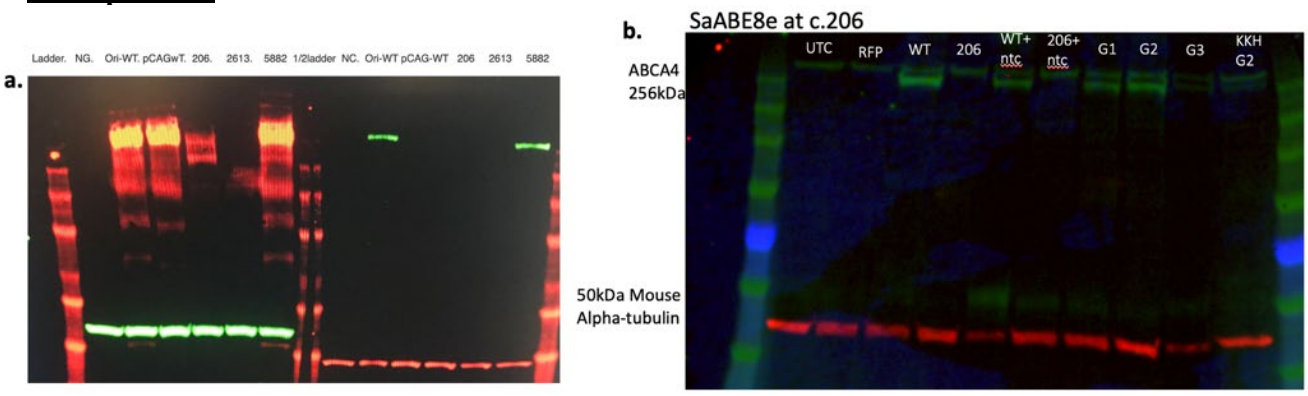

Figure 9-1: Supplementary western blots of mutant plasmid and SaABE8e base editor.
a. Two western blots testing for protein in the mutant plasmids using anti-ABCA4 (left) and anti-Myc (right). C. 206 G>A and c.2613 G>A result in premature stop codons so no protein was expected. C.5882 G>A resulted in wildtype levels of ABCA4 protein. C.206 G>A shows smeared bands when using the anti-ABCA4 antibody, however, this is likely overexposure given the general smearing in other lanes. C.2613 G>A was not targeted/used after this. NC= negative control, Ori-WT=CMV-ABCA4-myc tag, pCAGwt= CAG-ABCA4, 206 =CMV-ABCA4c.206G>A-myctag, 2613= CMV-ABCA4c.2613G>A-myctag, 5882 =CMV-ABCA4c.5882G>A-myctag. **b.** Western blot of targeting c.206 G>A using the SaABE8e with its corresponding PAM sites. Strong editing was observed using guide 1 (G1) and guide 2 (G2) relative to wildtype ABCA4 despite putting the target site at position 14. This was tested to compare SaABE8e and SaKKHABE8e at the same site. This was only tested once, though, so requires further investigation. UTC= untransfected control, RFP= red fluorescent protein, WT= wildtype, 206 = 206G>A mutant ABCA4, WT+NTC = non-targeting guide + wt ABCA4 + SaABE8e, 206 + NTC= non-targeting guide + 206 G>A ABCA4 + SaABE8e, G1/2/3= 206 G>A ABCA4 + SaABE8e + G1/2/3, KKH G2= 206 G>A + SaKKHABE8e + G2.

Chapter 5

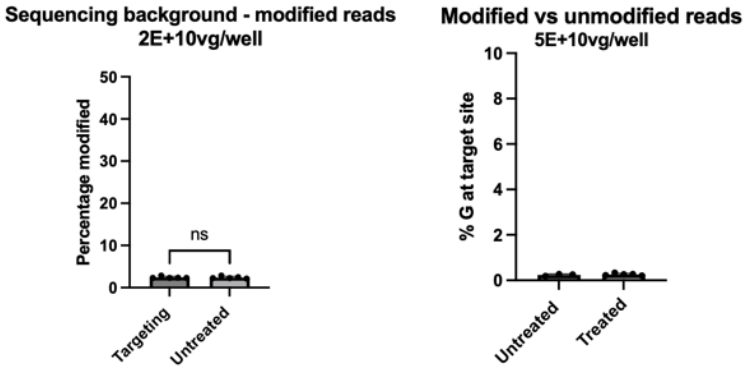

Figure 9-2: Deep sequencing retinal organoids, modified vs unmodified reads.
Observed background in the sequencing results. This is not site-specific and is across the whole amplicon.

Chapter 6

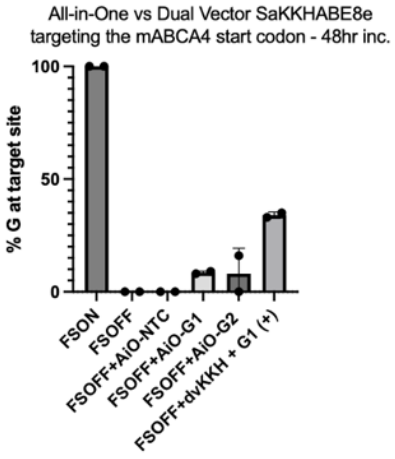

Figure 9-3: *In vitro* screen of all-in-one (EFS) SaKKHABE8e 48hr incubation.
The all-in-one (EFS) SaKKHABE8e was first tested using the 48hr incubation as previously undertaken and resulted in low-level editing compared to the dual vector approach. However, given the EFS promoter, a longer incubation of 72 hours was needed and resulted in a marked improved.

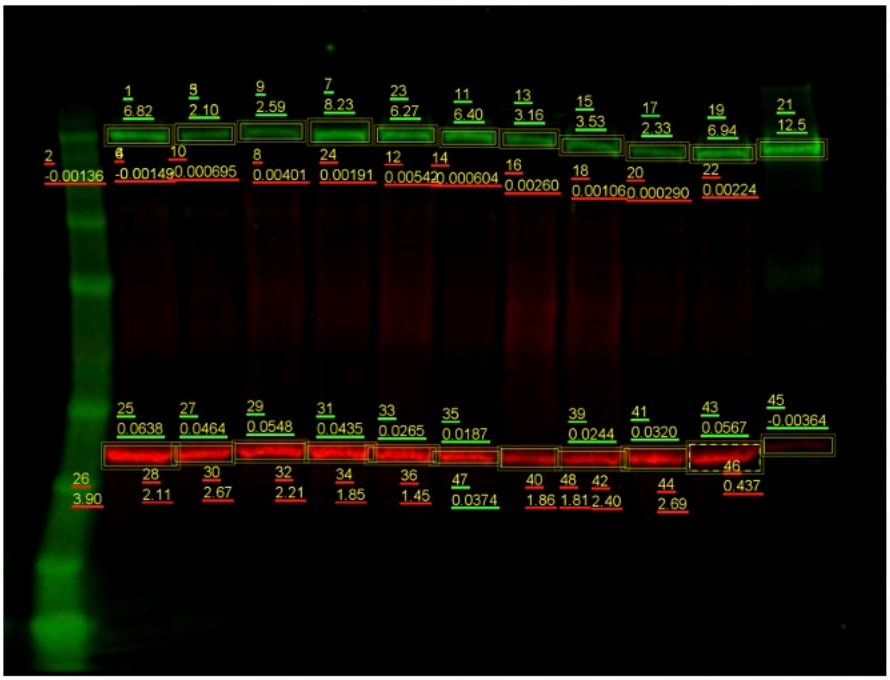

Figure 9-4: Representative example of blot quantitation.

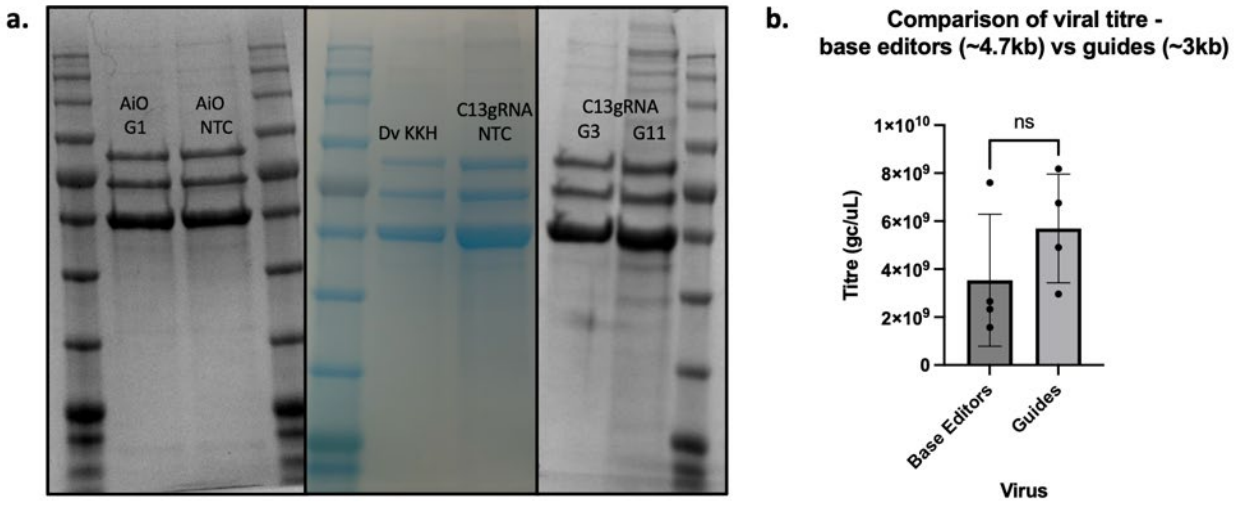

Figure 9-5:Virus titration SDS-PAGE and qPCR output.

a. SDS-PAGE of representative viruses. The gRNA samples tend to have thicker bands indicating a higher titre. C13gRNA G11 (far right) was discarded due to impurity. AiOG1/NTC= targeting (G1) and non-targeting (NTC) all-in-one SaKKH; DvKKH = SaKKH DNA base editor; C13gRNA= Cas13 gRNA virus, NTC= non-target control scrambled guide, G3/11= guide 3/11. **b.** Comparison of base editor and guide viral titres. Guide titres tended to be slightly higher, although this was not significant (p=0.76) by unpaired t-test. The all-in-one SaKKH was included with base editors given its size.

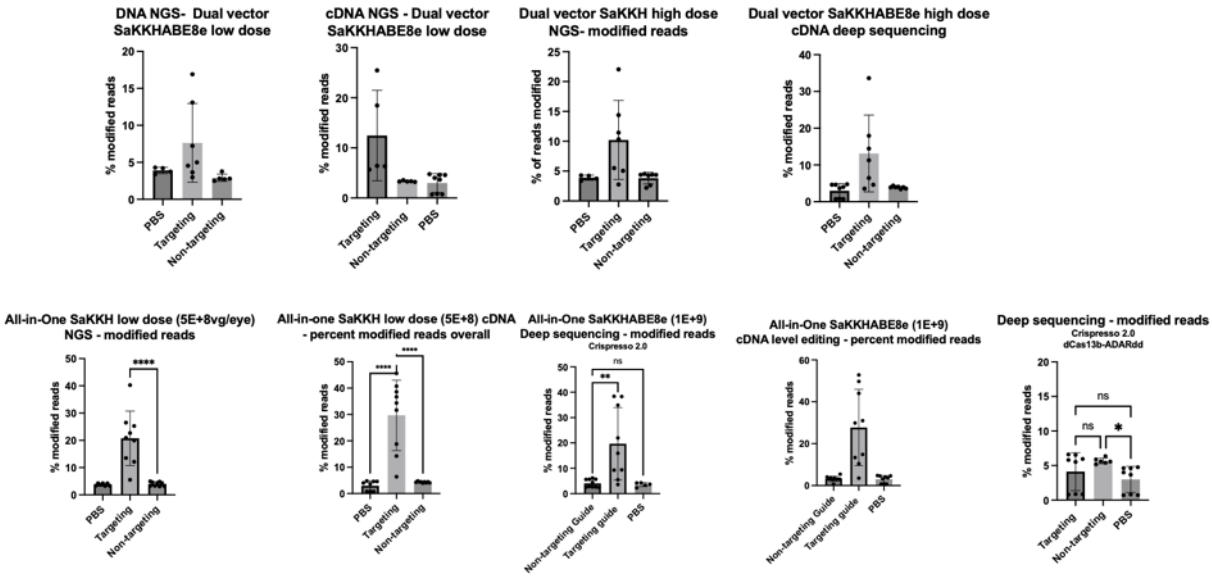

Figure 9-6: Deep sequencing background in *in vivo* cohorts, modified vs unmodified reads.
Observed background seen throughout the sequencing reads of modified vs unmodified reads. This is not site specific. Samples not denoted cDNA refer editing at the DNA-level.

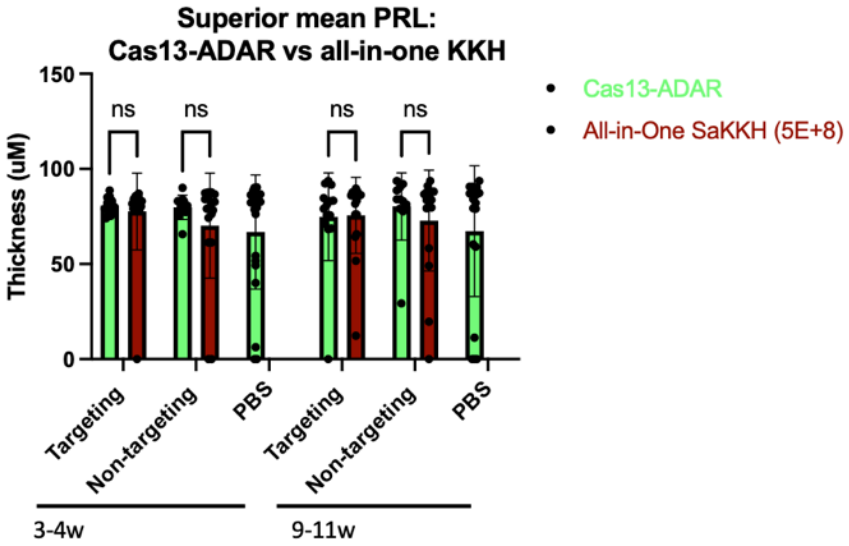

Figure 9-7: Comparison of superior mean PRL between All-in-one SaKKHABE8e low dose (5E+8vg/eye) and the Cas13-ADAR cohort.
The superior mean PRL at both timepoints was compared between the two least toxic cohorts. No significant difference was observed, both were well-tolerated relative to the PBS injected eyes.

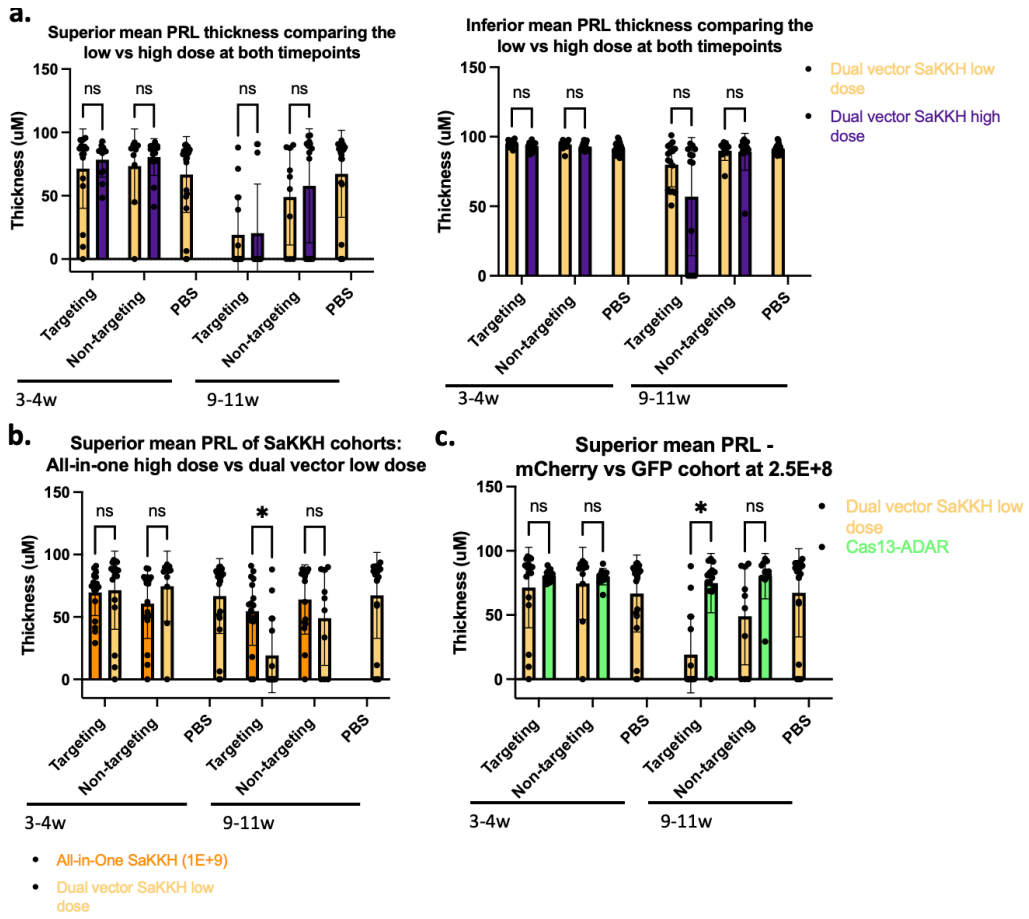

Figure 9-8: Comparison of retinal thinning across cohorts.
a. Comparison of the high and low dose dual vector SaKKH cohorts. Superior mean PRL measurements were compared at both timepoints and inferior mean PRL measurements were compared at both timepoints. There was no significant difference in thinning observed between the doses. **b.** Comparison of the dual vector SaKKH low dose superior mean PRL measurements to the all-in-one SaKKH high dose at both timepoints. The targeting guide at 9-11 weeks showed a significant difference in superior mean PRL ($p=0.0016$). **c.** Comparison of the superior mean PRL measurements between the dual vector SaKKH low dose and the Cas13-ADAR cohort to compare mCherry vs GFP toxicity at 2.5E+8vg.eye. While not an ideal comparison, the dual vector SaKKH targeting eye exhibited a significantly reduced mean PRL at 9-11 weeks ($p<0.0001$). Mann-Whitney tests.

B. Nucleotide Sequences and Key Plasmids

Plasmid	Source
pSGDlucV3.0	Kind gift of Lewis Fry; Addgene #119760
pSGDluc-206WT	Generated
pSGDluc-206G>A	Generated

pSGDluc-93WT	Generated
pSGDluc-93G>A_308	Generated
pSGDluc-93G>A_224	Generated
pSGDluc-93G>A_125	Generated
pC0043-PspCas13b gRNA	Kind gift of Lewis Fry; Addgene #103854
pC0043-PspCas13b gRNA-NTC (50nt)	Generate
AAV-U6-gRNA-CAG-GFP	Kind gift of Lewis Fry
pAK212 (ITR-U6-gRNA-CAG-mCherry)	Kind gift of Ariel Kantor
pAK212-NTC(20nt)	Generated
Human ABCA4	NM_00350; Origene RC213827
pC0053-CMV(or RK).IE-dPspCas13b-GS-ADAR2DD(E488Q)-delta-984-1090 [199]	Kind gift of Lewis Fry; Addgene 103869
pCMV-ecTadA(8e)-nSaCas9(KKH)[179]	Kind gift of Maria Kaukonnen; Addgene138502
pCMV-ecTadA(8e)-nSaCas9	Kind gift of Maria Kaukonnen; Addgene 138500
AAV-EFS-SaKKHABE8e-bGH-U6-sgRNA-BsmBI[180]	Kind gift of Ahmed Salman; Addgene 189923
CMV-SaCas9	Kind gift of Ahmed Salman
AAV-RK-SaCas9	Kind gift of Connie Han
psiCheck2™	Kind gift of Michelle McClements; promega
psiCheck2-mABCA4-FSON	Generated
psiCheck2-mABCA4-FSOFF	Generated
AAV-RK-ecTadA(8e)-nSaCas9(KKH)	Generated
AAV-RK-SaKKHABE8e-bGH-U6-sgRNA-BsmBI	Generated
pHelper	Kind gift of Michelle McClements Kind gift of Michelle McClements Plasmid Factory

Chapter 4

Name	Sequence 5'-3'
ABCA4-206GA *Luciferase assay target cassette*	**ACTCGAGC**GCTACAGCCATCATGAATGCCATTTCCCCAACAAGGCGATGCC CTCAGCAGGAATGCTGCCGT**[A/G]**GCTCCAGGGGATCTTCTGCAATGTGAAC AATCCCTGTTTTCAAAGCCCCA**AGATCT**
GFP-positive-control *Luciferase assay target cassette*	*CAACCCCGGGCCCTACTCGAGCAGA*AGGATCCATCCACCGGTCGCCACCATG GTGAGCAAGGGCT**[A/G]**GGAGCTGTTCACCGGGGTGGTACCCATCCTGGTC GAGCTGGACGGCGACGTAAACGGCCACAAGTTCAGCGTGTCCGGCGAGGG CGAGGGCGATGCCACCTACGGCAAGCTGACCCTGAAGTTCATCTGCACCAC

	CGGCAAGCTGCCCGTGCCCTGGCCCACCCTCGTGACCACCCTGACCTACGG CGTGCAGTGCTTCAGCCGCTACCCCGACCACATGAAGCAGCACGACTTCTT CAAGTCCGCCATGCCCGAAGGCAA*TAGATCTGAGGCACGGCATAAGCAAAA* *Bold and underlined -restriction sites PspXI and BglIII; Bold = target site. NEBuilder HiFi overhangs in italics.*

Guides – Cas13-ADAR	*Underlined portions are restriction overhangs*
ABCA4-206-G1	CACCGTCCCCTGGAGCCACGGCAGCATTCCTGCTGAGGGCATCGCCTTGTT GGGGCAAC
ABCA4-206-G2	CACCGGATCCCCTGGAGCCACGGTAACAGTCCTGCTGAAGGCATCGCCTTG TTGGCAAC
ABCA4-206-G3	CACCGAAGATCCCCTGGAGCCACGGCAGCATTCCTGCTGAGGGCATCGCCT TGTTCAAC
ABCA4-206-G4	CACCGGAAGATCCCCTGGAGCCACGGCAGCATTCCTGCTGAGGGCATCGCC TTGTCAAC
ABCA4-206-G5	CACCGAGAAGATCCCCTGGAGCCACGGCAGCATTCCTGCTGAGGGCATCGC CTTGCAAC
ABCA4-206-G6	CACCGCAGAAGATCCCCTGGAGCCACGGCAGCATTCCTGCTGAGGGCATCG CCTTCAAC
ABCA4-206-G7	CACCGGCAGAAGATCCCCTGGAGCCACGGCAGCATTCCTGCTGAGGGCATC GCCTCAAC
ABCA4-206-G8	CACCGTGCAGAAGATCCCCTGGAGCCACGGCAGCATTCCTGCTGAGGGCAT CGCCCAAC
ABCA4-206-G9	CACCGTTGCAGAAGATCCCCTGGAGCCACGGCAGCATTCCTGCTGAGGGCA TCGCCAAC
ABCA4-206-G10	CACCGCATTGCAGAAGATCCCCTGGAGCCACGGCAGCATTCCTGCTGAGGG CATCCAAC
ABCA4-206-G11	CACCGCACATTGCAGAAGATCCCCTGGAGCCACGGCAGCATTCCTGCTGAG GGCACAAC
ABCA4-206-G12	CACCGTTCACATTGCAGAAGATCCCCTGGAGCCACGGCAGCATTCCTGCTG AGGGCAAC
ABCA4-206-G13	CACCGTGTTCACATTGCAGAAGATCCCCTGGAGCCACGGCAGCATTCCTGC TGAGCAAC
ABCA4-206-G14	CACCGATTGTTCACATTGCAGAAGATCCCCTGGAGCCACGGCAGCATTCCT GCTGCAAC
ABCA4-206-G15	CACCGGGATTGTTCACATTGCAGAAGATCCCCTGGAGCCACGGCAGCATTC CTGCCAAC
ABCA4-5882-G5	CACCGACTCTCCAGGGCGAACTCCGACACACAGCCTGTCCACTGCTGGGCT GGAGCAAC
ABCA4-5882-G6	CACCGCACTCTCCAGGGCGAACTCCGACACACAGCCTGTCCACTGCTGGGC TGGACAAC
ABCA4-5882-G7	CACCGCACTCTCCAGGGCGAACTCCGACACACAGCCTGTCCACTGCTGGGC TGGCAAC

Guides – SaKKHABE8e	
206-SaKKH-G1	ACCGCGTAGCTCCAGGGGATCTTCAAC
206-SaKKH-G2	ACCGCCGTAGCTCCAGGGGATCTTCAAC
206-SaKKH-G3	ACCGGCCGTAGCTCCAGGGGATCTTCAAC
GFP-Sa-G1	ACCGACCGAAGGGCTAGGAGCTGTTCACAAC

Chapter 5

Name	Sequence 5'-3'
93pSGDlucV3.0 fragment 1 (308bp) *Luciferase assay target cassette*	*CAACCCCGGGCCCTACTCGAGCAGA*ATGGGCTTCGTGAGACAGATACAGCTTT TGCTCTGGAAGAACTGGACCCTGCGGAAAAGGCAAAAGATTCGCTTTGTGG TGGAACTCGTGTG**[A/G]**CCTTTATCTTTATTTCTGGTCTTGATCTGGTTAAGGA ATGCCAACCCGCTCTACAGCCATCATGAATGCCATTTCCCCAACAAGGCGATG CCCTCAGCAGGAATGCTGCCGTGGCTCCAGGGGATCTTCTGCAATGTGAACA ATCCCTGTTTTCAAAGCCCCACCCCAGGAGAATCTCCTGGAATTGTGTCAAA CTATAACAACTCCATCTTGGC*TAGATCTGAGGCACGGCATAAGCAAAA*
93pSGDlucV3.0 fragment 2 (224bp) *Luciferase assay target cassette*	*CAACCCCGGGCCCTACTCGAGCAGA*AACTGGACCCTGCGGAAAAGGCAAAAG ATTCGCTTTGTGGTGGAACTCGTGTG**[A/G]**CCTTTATCTTTATTTCTGGTCTTG ATCTGGTTAAGGAATGCCAACCCGCTCTACAGCCATCATGAATGCCATTTCCC CAACAAGGCGATGCCCTCAGCAGGAATGCTGCCGTGGCTCCAGGGGATCTTC TGCAATGTGAACAATCCCTGTTTTCAAAGCCCCACCCCAGG*TAGATCTGAGGC ACGGCATAAGCAAAA*
93pSGDlucV3.0 fragment 3 (125bp) *Luciferase assay target cassette*	*CAACCCCGGGCCCTACTCGAGCAGA*AACTGGACCCTGCGGAAAAGGCAAAAG ATTCGCTTTGTGGTGGAACTCGTGTG**[A/G]**CCTTTATCTTTATTTCTGGTCTTG ATCTGGTTAAGGAATGCCAACCCGCTCTACAGCCATCATGAATGCCA*TAGATC TGAGGCACGGCATAAGCAAAA*
	Bold is the target base, NEBuilder Hifi overhangs in italics.
	Primers to amplify inserts are listed in the Chapter 5 methods.

Name	Sequence 5'-3'
Guides – Cas13-ADAR	
ABCA4-93-G1	CACCGAAAGATAAAGGCCACACGAGTTCCACCACAAAGCGAATCTTTTGCC TTTTCAAC
ABCA4-93-G2	CACCGATAAAGATAAAGGCCACACGAGTTCCACCACAAAGCGAATCTTTTG CCTTCAAC
ABCA4-93-G3	CACCGAAATAAAGATAAAGGCCACACGAGTTCCACCACAAAGCGAATCTTT TGCCCAAC

ABCA4-93-G4	CACCGGAAATAAAGATAAAGGCCACACGAGTTCCACCACAAAGCGAATCTTTTGCCAAC
ABCA4-93-G5	CACCGAGAAATAAAGATAAAGGCCACACGAGTTCCACCACAAAGCGAATCTTTTGCAAC
ABCA4-93-G6	CACCGCAGAAATAAAGATAAAGGCCACACGAGTTCCACCACAAAGCGAATCTTTTCAAC
ABCA4-93-G7	CACCGCCAGAAATAAAGATAAAGGCCACACGAGTTCCACCACAAAGCGAATCTTTCAAC
ABCA4-93-G8	CACCGACCAGAAATAAAGATAAAGGcCACACGAGTTCCACCACAAAGCGAATCTTCAAC
ABCA4-93-G9	CACCGAGACCAGAAATAAAGATAAAGGcCACACGAGTTCCACCACAAAGCGAATCCAAC
ABCA4-93-G10	CACCGCAAGACCAGAAATAAAGATAAAGGcCACACGAGTTCCACCACAAAGCGAACAAC
ABCA4-93-G11	CACCGATCAAGACCAGAAATAAAGATAAAGGcCACACGAGTTCCACCACAAAGCGCAAC
ABCA4-93-G12	CACCGAGATCAAGACCAGAAATAAAGATAAAGGcCACACGAGTTCCACCACAAAGCAAC
ABCA4-93-G13	CACCGCCAGATCAAGACCAGAAATAAAGATAAAGGcCACACGAGTTCCACCACAACAAC
ABCA4-93-G14	CACCGAACCAGATCAAGACCAGAAATAAAGATAAAGGcCACACGAGTTCCACCACCAAC
ABCA4-93-G15	CACCGTTAACCAGATCAAGACCAGAAATAAAGATAAAGGcCACACGAGTTCCACCCAAC

Guides – SaKKHABE8e

93-KKH-gRNA1-F	ACCGGTGTGACCTTTATCTTTATTAAC
93-KKH-gRNA2-F	ACCGCGTGTGACCTTTATCTTTATTAAC
93-KKH-gRNA3-F	ACCGTCGTGTGACCTTTATCTTTATTAAC
93-KKH2	ACCGCCTTTATCTTTATTTCTGGTAAC
93-KKH	ACCGATCTTTATTTCTGGTCTTGAAAC
93-SaABE_SaCas9	ACCGTTCTGGTCTTGATCTGGTTAAAC

Chapter 6

Name	Sequence 5'-3'
mABCA4 luc. assay: 5'UTR-exon 1	*AGTACTTAATACGACTCACTATAGG*GCTGGACGTGGTCCTAGCGGCCTTTGTGTCCGGTGCTTGCCTGAGCCCCAGCTCGGGGTGATTCTCCCGGTGCTGGGGTGGTCCGGCGTGGGCTTCCTCAGACAGATACAGCTTTTGCTTTGGAAGAACTGGACTCTGAGGAAAAGGCAGAAG*CCACCATGGCTTCCAAGGTGTACGA* *Italics are NEBuilder HiFi overhangs.*

Rhodopsin kinase (-112/+87) -promoter	GGGCCCCAGAAGCCTGGTGGTTGTTTGTCCTTCTCAGGGGAAAAGTGAGGC GGCCCCTTGGAGGAAGGGGCCGGGCAGAATGATCTAATCGGATTCCAAGCA GCTCAGGGGATTGTCTTTTTCTAGCACCTTCTTGCCACTCCTAAGCGTCCTC CGTGACCCCGGCTGGGATTTAGCCTGGTGCTGTGTCAGCCCCG
EF-1 alpha short (EFS)-promoter	TAGGTCTTGAAAGGAGTGGGAATTGGCTCCGGTGCCCGTCAGTGGGCAGAG CGCACATCGCCCACAGTCCCCGAGAAGTTGGGGGGAGGGGTCGGCAATTG ATCCGGTGCCTAGAGAAGGTGGCGCGGGGTAAACTGGGAAAGTGATGTCGT GTACTGGCTCCGCCTTTTTCCCGAGGGTGGGGGAGAACCGTATATAAGTGCA GTAGTCGCCGTGAACGTTCTTTTTCGCAACGGGTTTGCCGCCAGAACACAG
AAV-GRK1-AiO fragment	*Fragment for cloning RK-promoter into All-in-One SaKKHABE8e* GGGCCCCAGAAGCCTGGTGGTTGTTTGTCCTTCTCAGGGGAAAAGTGAGGC GGCCCCTTGGAGGAAGGGGCCGGGCAGAATGATCTAATCGGATTCCAAGCA GCTCAGGGGATTGTCTTTTTCTAGCACCTTCTTGCCACTCCTAAGCGTCCTC CGTGACCCCGGCTGGGATTTAGCCTGGTGCTGTGTCAGCCCCGGACCGGTG CCACCATGAAACGGACAGCCGACGGAAGCGAGTTCGAGTCACCAAAGAAG AAGCGGAAAGTCTCTGAGGTGGAGTTTTCCCACGAGTACTGGATGAGACAT GCCCTGACCCTGGCCAAGAGGGCACGGGATGAGAGGGAGGTGCCTGTGGG AGCCGTGCTGGTGCTGAACAATAGAGTGATCGGCGAGGGCTGGAACAGAG CCATCGGCCTGCACGACCCAACAGCCCATGCCGAAATTATGGCCCTGAGAC AGGGCGGCCTGGTCATGCAGAACTACAGACTGATTGACGCCACCCTGTACG TGACATTCGAGCCTTGCGTGATGTGCGCCGGCGCCATGATCCACTCTAGGAT CGGCCGCGTGGTGTTTGGCGTGAGGAACTCAAAAAGAGGCGCCGCAGGCT CCCTGATGAACGTGCTGAACTACCCCGGCATGAATCACCGCGTCGAAATTAC CGAGGGAATCCTGGCAGATGAATGTGCCGCCCTGCTGTGCGATTTCTATCGG ATGCCTAGACAGGTGTTCAATGCTCAGAAGAAGGCCCAGAGCTCCATCAAC
	Fragments for cloning ITRs and RK-promoter into dual vector SaKKHABE8e. Primers bind first and last 25bp.
ITR-RK-DVKKH-F1	ATACGACTCACTATAGGGAGAGCCGCCACCATGAAACGGACAGCCGACGGA AGCGAGTTCGAGTCACCAAAGAAGAAGCGGAAAGTCTCTGAGGTGGAGTT TTCCCACGAGTACTGGATGAGACATGCCCTGACCCTGGCCAAGAGGGCACG GGATGAGAGGGAGGTGCCTGTGGGAGCCGTGCTGGTGCTGAACAATAGAG TGATCGGCGAGGGCTGGAACAGAGCCATCGGCCTGCACGACCCAACAGCC CATGCCGAAATTATGGCCCTGAGACAGGGCGGCCTGGTCATGCAGAACTAC AGACTGATTGACGCCACCCTGTACGTGACATTCGAGCCTTGCGTGATGTGC GCCGGCGCCATGATCCACTCTAGGATCGGCCGCGTGGTGTTTGGCGTGAGG AACTCAAAAAGAGGCGCCGCAGGCTCCCTGATGAACGTGCTGAACTACCC CGGCATGAATCACCGCGTCGAAATTACCGAGGGAATCCTGGCAGATGAATG TGCCGCCCTGCTGTGCGATTTCTATCGGATGCCTAGACAGGTGTTCAATGCT CAGAAGAAGGCCCAGAGCTCCATCAACTCCGGAGGATCTAGCGGAGGCTC CTCTGGCTCTGAGACACCTGGCACAAGCGAGAGCGCAACACCTGAAAGCA GCGGGGGCAGCAGCGGGGGGTCAGGGAAGCGAAATTACATTCTGGGGCTG

	GCCATTGGCATTACATCAGTGGGCTATGGCATCATTGACTACGAGACAAGGG ACGTGATCGACGCCGGCGTGAGACTGTTCAAGGAGGCCAACGTGGAGAAC AATGAGGGCCGGAGATCCAAGAGGGGAGCAAGGCGCCTGAAGCGGAGAA GGCGCCACAGAATCCAGAGAGTGAAGAAGCTGCTGTTCGATTACAACCTGC TGACCGACCACTCCGAGCTGTCTGGCATCAATCCTTATGAGGCCAGAGTGA AGGGCCTGTCCCAGAAGCTGTCTGAGGAGGAGTTTAGCGCCGCCCTGCTGC ACCTGGCAAAGAGGAGAGGCGTGCACAACGTGAATGAGGTGGAGGAGGA CACCGGCAACGAGCTGTCCACAAAGGAGCAGATCAGCCGCAATTCCAAGG CCCTGGAGGAGAAGTATGTGGCCGAGCTGCAGCTGGAGCGGCTGAAGAAG GATGGCGAGGTGAGGGGCTCCATCAATCGCTTC
ITR-RK-DVKKH-F2	AGACCTCTGACTACGTGAAGGAGGCCAAGCAGCTGCTGAAGGTGCAGAAG GCCTACCACCAGCTGGATCAGTCCTTTATCGATACATATATCGACCTGCTGGA GACAAGGCGCACATACTATGAGGGACCAGGAGAGGGCTCTCCCTTCGGCTG GAAGGACATCAAGGAGTGGTACGAGATGCTGATGGGCCACTGCACCTATTT TCCAGAGGAGCTGAGAAGCGTGAAGTACGCCTATAACGCCGATCTGTACAA CGCCCTGAATGACCTGAACAACCTGGTCATCACCAGGGATGAGAACGAGA AGCTGGAGTACTATGAGAAGTTCCAGATCATCGAGAACGTGTTCAAGCAGA AGAAGAAGCCTACACTGAAGCAGATCGCCAAGGAGATCCTGGTGAACGAG GAGGACATCAAGGGCTACCGCGTGACCTCCACAGGCAAGCCAGAGTTCAC CAATCTGAAGGTGTATCACGATATCAAGGACATCACAGCCCGGAAGGAGAT CATCGAGAACGCCGAGCTGCTGGATCAGATCGCCAAGATCCTGACCATCTAT CAGAGCTCCGAGGACATCCAGGAGGAGCTGACCAACCTGAATAGCGAGCT GACACAGGAGGAGATCGAGCAGATCAGCAATCTGAAGGGCTACACCGGCA CACACAACCTGAGCCTGAAGGCCATCAATCTGATCCTGGATGAGCTGTGGC ACACAAACGACAATCAGATCGCCATCTTTAACCGGCTGAAGCTGGTGCCAA AGAAGGTGGACCTGTCCCAGCAGAAGGAGATCCCAACCACACTGGTGGAC GATTTCATCCTGTCTCCCGTGGTGAAGCGGAGCTTCATCCAGAGCATCAAAG TGATCAACGCCATCATCAAGAAGTACGGCCTGCCCAATGATATCATCATCGA GCTGGCCAGGGAGAAGAACTCCAAGGACGCCCAGAAGATGATCAATGAGA TGCAGAAGAGGAACCGCCAGACCAATGAGCGGATCGAGGAGATCATCAGA ACCACAGGCAAGGAGAACGCCAAGTACCTGATCGAGAAGATCAAGCTGCA CGATATGCAGGAGGGCAAGTGTCTGTATTCTCTGGAGGCCATCCCTCTGGAG GACCTGCTGAACAATCCATTCAACTACGAGGTGGATCACATCATCCCCCGGA GCGTGAGCTTCGACAATTCTTTTAACAA
ITR-RK-DVKKH-F3	TAAGGTGCTGGTGAAGCAGGAGGAGAACAGCAAGAAGGGCAATAGGACCC CTTTCCAGTACCTGTCTAGCTCCGATTCTAAGATCAGCTACGAGACATTCAA GAAGCACATCCTGAATCTGGCCAAGGGCAAGGGCCGCATCAGCAAGACCA AGAAGGAGTACCTGCTGGAGGAGCGGGACATCAACAGATTCTCCGTGCAG AAGGACTTCATCAACCGGAATCTGGTGGACACCAGATACGCCACACGCGGC CTGATGAATCTGCTGCGGTCTTATTTCAGAGTGAACAATCTGGATGTGAAGG TGAAGAGCATCAACGGCGGCTTCACCTCCTTTCTGCGGAGAAAGTGGAAGT TTAAGAAGGAGCGCAACAAGGGCTATAAGCACCACGCCGAGGATGCCCTG ATCATCGCCAATGCCGACTTCATCTTTAAGGAGTGGAAGAAGCTGGACAAG GCCAAGAAAGTGATGGAGAACCAGATGTTCGAGGAGAAGCAGGCCGAGAG CATGCCCGAGATCGAGACAGAGCAGGAGTACAAGGAGATTTTCATCACACC TCACCAGATCAAGCACATCAAGGACTTCAAGGACTACAAGTATTCTCACAG

	GGTGGATAAGAAGCCCAACCGCAAGCTGATCAATGACACCCTGTATAGCAC ACGGAAGGACGATAAGGGCAATACCCTGATCGTGAACAATCTGAACGGCCT GTACGACAAGGATAATGACAAGCTGAAGAAGCTGATCAACAAGTCTCCCGA GAAGCTGCTGATGTACCACCACGATCCTCAGACATATCAGAAGCTGAAGCT GATCATGGAGCAGTACGGCGACGAGAAGAACCCACTGTATAAGTACTATGA GGAGACAGGCAACTACCTGACAAAGTATAGCAAGAAGGATAATGGCCCCGT GATCAAGAAGATCAAGTACTATGGCAACAAGCTGAATGCCCACCTGGACAT CACCGACGATTACCCTAACTCTCGCAATAAGGTGGTGAAGCTGAGCCTGAA GCCATACCGGTTCGACGTGTACCTGGACAACGGCGTGTATAAGTTTGTGACA GTGAAGAATCTGGATGTGATCAAGAAGGAGAACTACTATGAGGTGAACAGC AAGTGCTACGAGGAGGCCAAGAAGCTGAAGAAGATCAGCAACCAGGCCGA GTTCATCGCCTCTTTTTACAAGAATGAC
ITR-RK-DVKKH-F4	CTGATCAAGATCAATGGCGAGCTGTATAGAGTGATCGGCGTGAACAATGATC TGCTGAACAGAATCGAAGTGAATATGATCGACATCACCTACAGGGAGTATCT GGAGAACATGAATGATAAGAGGCCCCCTCATATCATCAAGACCATCGCCTCT AAGACACAGAGCATCAAGAAGTACAGCACAGACATCCTGGGGAACCTGTAT GAAGTCAAGAGCAAGAAACATCCTCAGATTATCAAGAAAGGCTCTGGCGG CTCAAAAAGAACCGCCGACGGCAGCGAATTCGAGCCCAAGAAGAAGAGG AAAGTCTAACCGGTCATCATCACCATCACCATTGAGTTTAAACCCGCTGATC AGCCTCGACTGTGCCTTCTAGTTGCCAGCCATCTGTTGTTTGCCCCTCCCCC GTGCCTTCCTTGACCCTGGAAGGTGCCACTCCCACTGTCCTTTCCTAATAAA ATGAGGAAATTGCATCGCATTGTCTGAGTAGGTGTCATTCTATTCTGGGGGG TGGGGTGGGGCAGGACAGCAAGGGGGAGGATTGGGAAGACAATAGCAGGC ATGCTGGGGATGCGGTGGGCTCTATGGCTTCTGAGGCGGAAAGAACCAGCT GGGGCTCGATACCGTCGACCTCTAGCTAGAGCTTGGCGTAATCATGGTCATA GCTGTTTCCTGTGTGAAATTGTTATCCGCTCACAATTCCACACAACATACGA GCCGGAAGCATAAAGTGTAAAGCCTAGGGTGCCTAATGAGTGAGCTAACTC ACATTAATTGC
ITR-RK-backbone	GGCCGCAGGAACCCCTAGTGATGGAGTTGGCCACTCCCTCTCTGCGCGCTC GCTCGCTCACTGAGGCCGGGCGACCAAAGGTCGCCCGACGCCCGGGCTTT GCCCGGGCGGCCTCAGTGAGCGAGCGAGCGCGCAGCTGCCTGCAGGGGCG CCTGATGCGGTATTTTCTCCTTACGCATCTGTGCGGTATTTCACACCGCATAC GTCAAAGCAACCATAGTACGCGCCCTGTAGCGGCGCATTAAGCGCGGCGGG TGTGGTGGTTACGCGCAGCGTGACCGCTACACTTGCCAGCGCCTTAGCGCC CGCTCCTTTCGCTTTCTTCCCTTCCTTTCTCGCCACGTTCGCCGGCTTTCCCC GTCAAGCTCTAAATCGGGGGCTCCCTTTAGGGTTCCGATTTAGTGCTTTACG GCACCTCGACCCCAAAAAACTTGATTTGGGTGATGGTTCACGTAGTGGGCC ATCGCCCTGATAGACGGTTTTTCGCCCTTTGACGTTGGAGTCCACGTTCTTT AATAGTGGACTCTTGTTCCAAACTGGAACAACACTCAACTCTATCTCGGGCT ATTCTTTTGATTTATAAGGGATTTTGCCGATTTCGGTCTATTGGTTAAAAAAT GAGCTGATTTAACAAAAATTTAACGCGAATTTTAACAAAATATTAACGTTTA CAATTTTATGGTGCACTCTCAGTACAATCTGCTCTGATGCCGCATAGTTAAGC CAGCCCCGACACCCGCCAACACCCGCTGACGCGCCCTGACGGGCTTGTCTG CTCCCGGCATCCGCTTACAGACAAGCTGTGACCGTCTCCGGGAGCTGCATG TGTCAGAGGTTTTCACCGTCATCACCGAAACGCGCGAGACGAAAGGGCCTC GTGATACGCCTATTTTTATAGGTTAATGTCATGATAATAATGGTTTCTTAGACG

TCAGGTGGCACTTTTCGGGGAAATGTGCGCGGAACCCCTATTTGTTTATTTT
TCTAAATACATTCAAATATGTATCCGCTCATGAGACAATAACCCTGATAAATG
CTTCAATAATATTGAAAAAGGAAGAGTATGAGTATTCAACATTTCCGTGTCG
CCCTTATTCCCTTTTTTGCGGCATTTTGCCTTCCTGTTTTTGCTCACCCAGAA
ACGCTGGTGAAAGTAAAAGATGCTGAAGATCAGTTGGGTGCACGAGTGGG
TTACATCGAACTGGATCTCAACAGCGGTAAGATCCTTGAGAGTTTTCGCCCC
GAAGAACGTTTTCCAATGATGAGCACTTTTAAAGTTCTGCTATGTGGCGCGG
TATTATCCCGTATTGACGCCGGGCAAGAGCAACTCGGTCGCCGCATACACTA
TTCTCAGAATGACTTGGTTGAGTACTCACCAGTCACAGAAAAGCATCTTAC
GGATGGCATGACAGTAAGAGAATTATGCAGTGCTGCCATAACCATGAGTGAT
AACACTGCGGCCAACTTACTTCTGACAACGATCGGAGGACCGAAGGAGCTA
ACCGCTTTTTTGCACAACATGGGGGATCATGTAACTCGCCTTGATCGTTGGG
AACCGGAGCTGAATGAAGCCATACCAAACGACGAGCGTGACACCACGATG
CCTGTAGCAATGGCAACAACGTTGCGCAAACTATTAACTGGCGAACTACTTA
CTCTAGCTTCCCGGCAACAATTAATAGACTGGATGGAGGCGGATAAAGTTGC
AGGACCACTTCTGCGCTCGGCCCTTCCGGCTGGCTGGTTTATTGCTGATAAA
TCTGGAGCCGGTGAGCGTGGAAGCCGCGGTATCATTGCAGCACTGGGGCCA
GATGGTAAGCCCTCCCGTATCGTAGTTATCTACACGACGGGGAGTCAGGCAA
CTATGGATGAACGAAATAGACAGATCGCTGAGATAGGTGCCTCACTGATTAA
GCATTGGTAACTGTCAGACCAAGTTTACTCATATATACTTTAGATTGATTTAA
AACTTCATTTTTAATTTAAAAGGATCTAGGTGAAGATCCTTTTTGATAATCTC
ATGACCAAAATCCCTTAACGTGAGTTTTCGTTCCACTGAGCGTCAGACCCC
GTAGAAAAGATCAAAGGATCTTCTTGAGATCCTTTTTTTCTGCGCGTAATCT
GCTGCTTGCAAACAAAAAAACCACCGCTACCAGCGGTGGTTTGTTTGCCGG
ATCAAGAGCTACCAACTCTTTTTCCGAAGGTAACTGGCTTCAGCAGAGCGC
AGATACCAAATACTGTTCTTCTAGTGTAGCCGTAGTTAGGCCACCACTTCAA
GAACTCTGTAGCACCGCCTACATACCTCGCTCTGCTAATCCTGTTACCAGTG
GCTGCTGCCAGTGGCGATAAGTCGTGTCTTACCGGGTTGGACTCAAGACGA
TAGTTACCGGATAAGGCGCAGCGGTCGGGCTGAACGGGGGGTTCGTGCACA
CAGCCCAGCTTGGAGCGAACGACCTACACCGAACTGAGATACCTACAGCGT
GAGCTATGAGAAAGCGCCACGCTTCCCGAAGGGAGAAAGGCGGACAGGTA
TCCGGTAAGCGGCAGGGTCGGAACAGGAGAGCGCACGAGGGAGCTTCCAG
GGGGAAACGCCTGGTATCTTTATAGTCCTGTCGGGTTTCGCCACCTCTGACT
TGAGCGTCGATTTTTGTGATGCTCGTCAGGGGGGCGGAGCCTATGGAAAAA
CGCCAGCAACGCGGCCTTTTTACGGTTCCTGGCCTTTTGCTGGCCTTTTGCT
CACATGTCCTGCAGGCAGCTGCGCGCTCGCTCGCTCACTGAGGCCGCCCGG
GCGTCGGGCGACCTTTGGTCGCCCGGCCTCAGTGAGCGAGCGAGCGCGCA
GAGAGGGAGTGGCCAACTCCATCACTAGGGGTTCCTGCGGCCTCTAGCTAG
GTCTTGAAAGGAGTGGGAATTGGCTCCGGTGCCCGTCAGTGGGCAGAGCG
CACATCGCCCACAGTCCCCGAGAAGTTGGGGGGAGGGGTCGGCAATTGGG
GCCCCAGAAGCCTGGTGGTTGTTTGTCCTTCTCAGGGGAAAAGTGAGGCGG
CCCCTTGGAGGAAGGGGCCGGGCAGAATGATCTAATCGGATTCCAAGCAGC
TCAGGGGATTGTCTTTTTCTAGCACCTTCTTGCCACTCCTAAGCGTCCTCCG
TGACCCCGGCTGGGATTTAGCCTGGTGCTGTGTCAGCCCCGGGACCGG

Primers to amplify mABCA4-UTR-exon1 cassette luciferase assay cassette. Underlined indicates cassette.

mABCA4-FS-Fw	AGTACTTAATACGACTCACTATAGGGCTGGACGTGGTCCTAGCGGCCTTT
mABCA4-FS-Rv	TCGTACACCTTGGAAGCCATGGTGGATGGAGTTGTTATAGTTTGAGACAG
	Primers to amplify fragments for NEBuilder HiFi assembly of ABEs for in vivo work. Overhangs are underlined
GRK1-KKH-aio-F	CCTGCGGCCTCTAGAATTCGGGGCCCCAGAAGCCTGGTGGTTGTT
GRK1-KKH-aio-R	AGGAGCCTCCGCTAGATCCTCCGGAGTTGATGGAGCTCTGGGCCTTCTTC
DvKKH-GRK1-ITR-F1	GCCTGGTGCTGTGTCAGCCCCGCTAATACGACTCACTATAGGGAGAG
DvKKH-GRK1-ITR-R1	GCCTCCTTCACGTAGTCAGAGGTCTTGAAGCGATTGATGGAGCCCCTCAC
DvKKH-GRK1-ITR-F2	GTGAGGGGCTCCATCAATCGCTTCAAGACCTCTGACTACGTGAAGGAGGC
DvKKH-GRK1-ITR-R2	CTCCTCCTGCTTCACCAGCACCTTATTGTTAAAAGAATTGTCGAAGCTCA
DvKKH-GRK1-ITR-F3	TGAGCTTCGACAATTCTTTTAACAATAAGGTGCTGGTGAAGCAGGAGGAG
DvKKH-GRK1-ITR-R3	ACAGCTCGCCATTGATCTTGATCAGGTCATTCTTGTAAAAAGAGGCGATG
DvKKH-GRK1-ITR-F4	CATCGCCTCTTTTTACAAGAATGACCTGATCAAGATCAATGGCGAGCTGT
DvKKH-GRK1-ITR-R4	CCATCACTAGGGGTTCCTGCAATTAATGTGAGTTAGCTCACTCAT

Guides – Cas13-ADAR

mABCA4-met-cas13-g1	CACCGGAGGAAGCCCAcGCCGGACCACCCCAGCACCGGGAGAATCACCCC GAGCTCAAC
mABCA4-met-cas13-r2	CACCGCTGAGGAAGCCCAcGCCGGACCACCCCAGCACCGGGAGAATCACC CCGAGCAAC
mABCA4-met-cas13-g3	CACCGGTCTGAGGAAGCCCAcGCCGGACCACCCCAGCACCGGGAGAATCA CCCCGCAAC
mABCA4-met-cas13-g4	CACCGTGTCTGAGGAAGCCCAcGCCGGACCACCCCAGCACCGGGAGAATC ACCCCCAAC
mABCA4-met-cas13-g5	CACCGCTGTCTGAGGAAGCCCAcGCCGGACCACCCCAGCACCGGGAGAATC ACCCCAAC
mABCA4-met-cas13-g6	CACCGTCTGTCTGAGGAAGCCCAcGCCGGACCACCCCAGCACCGGGAGAAT CACCCAAC
mABCA4-met-cas13-g7	CACCGATCTGTCTGAGGAAGCCCAcGCCGGACCACCCCAGCACCGGGAGA ATCACCAAC

mABCA4-met-cas13-g8	CACCGTATCTGTCTGAGGAAGCCCAcGCCGGACCACCCCAGCACCGGGAGAATCACAAC
mABCA4-met-cas13-g9	CACCGGTATCTGTCTGAGGAAGCCCAcGCCGGACCACCCCAGCACCGGGAGAATCCAAC
mABCA4-met-cas13-g10	CACCGCTGTATCTGTCTGAGGAAGCCCAcGCCGGACCACCCCAGCACCGGGAGAACAAC
mABCA4-met-cas13-g11	CACCGAGCTGTATCTGTCTGAGGAAGCCCAcGCCGGACCACCCCAGCACCGGGAGCAAC
mABCA4-met-cas13-g12	CACCGAAAGCTGTATCTGTCTGAGGAAGCCCAcGCCGGACCACCCCAGCACCGGGCAAC
mABCA4-met-cas13-g13	CACCGCAAAAGCTGTATCTGTCTGAGGAAGCCCAcGCCGGACCACCCCAGCACCGCAAC
mABCA4-met-cas13-g14	CACCGAGCAAAAGCTGTATCTGTCTGAGGAAGCCCAcGCCGGACCACCCCAGCACCAAC
mABCA4-met-cas13-g15	CACCGAAAGCAAAAGCTGTATCTGTCTGAGGAAGCCCAcGCCGGACCACCCCAGCCAAC

Guides – SaKKHABE8e

mABCA4-SaKKH-G1	ACCGTCCGGCATGGGCTTCCTCAGAAC
mABCA4-SaKKH-G2	ACCGGTCCGGCATGGGCTTCCTCAGAAC
mABCA4-SaKKH-G3	ACCGGGTCCGGCATGGGCTTCCTCAGAAC
mABCA4-SaKKH-G4	ACCGCCGGCATGGGCTTCCTCAGAAC
mABCA4-SaKKH-G5	ACCGTGGTCCGGCATGGGCTTCCTCAGAAC
Dv-non-targeting guide	ACCGAAGGGCTAGGAGCTGTTCACCAA
AiO-SaKKH-G1	AAACCTGAGGAAGCCCATGCCGGACCCAC
AiO-SaKKH-G2	AAACCTGAGGAAGCCCATGCCGGACCCCAC
AiO-non-targeting guide	AAACGTGAACAGCTCCTAGCCCTTCCCAC

Used throughout thesis

Name	Sequence
	ABCA4 sequencing primers
F1.5ABCA4ori	GAAGAACTGGACCCTGC
ABCA4-F2	ATGAATGCCATTTCCCCAACAAGG
ABCA4-F3	GCTTCATCATCTTCAGCC
ABCA4-F4	CAAAATCGCTTGGAGGGC
ABCA4-F5	CCTGACATGTATCCCTGG
ABCA4-F7	GGACGAATTCAGCTTCC
ABCA4-F8	GGAAGGGACATTGAAACC
ABCA4-F9	CGTCTAAGGGTTTCTCC
ABCA4-F10	GATTCCAACACACCATCCG
ABCA4-F11	CCAGAGAACACAGCG

ABCA4-F12	GGAATCACCGTCATTAGC
ABCA4-F13.5	GGGCATCTTCATCGGGTTTC
ABCA4-F15	GGAGCAGTTCTTCCAGG
ABCA4-R9	GAATGTGGTTGTTTTGCCGG
ABCA4-R5	CTGGACGGACTTGAGAGTTG
ABCA4-DDK-F25	GGAGTACTCAGTCACACAG
ABCA4-DDK-F26	GCACAATCTTGGCTCACTG
ABCA4-DDK-F27	GAAAGAACATGTGAGCAAAAGG
ABCA4-DDK-F28	CAGTATTTGGTATCTGCGC
ABCA4-DDK-F29	TTTTATTGCCGTCATAGCGC
ABCA4-DDK-F30	GCGTGCAATCCATCTTGTTC
ABCA4-DDK-F31	CTCATGAGCGGATACATATTTG
ABCA4-DDK-F32	CGCTTACAATTTCCATTCGC
ABCA4-DDK-F33	ACGTATGTTCCCATAGTAACGC
ABCA4-DDK-R4	CCAGGATATCATTTGCTGCC
ABCA4-DDK-R5	GATTAGGAGTTGGAGACCAGC
ABCA4-DDK-R12	GAGCGGGTTGGCATTCC
	SaKKH sequencing primers
CMV-F	CGCAAATGGGCGGTAGGCGTG
SaABE-F1	CGCCATGATCCACTCTAGG
SaABE-F2	CCAGAGAGTGAAGAAGCTGC
SaABE-F3	CAAGGAGTGGTACGAGATGC
SaABE-F4	GGCCATCAATCTGATCCTGG
SaABE-F5	CCAAGTACCTGATCGAGAAG
SaABE-F6	TTCGAGGAGAAGCAGGC
SaABE-F7	GACATCACCGACGATTACCC
SaABE-F8	TCGAGCCCAAGAAGAAGAGG
SaABE-F9	GATACCGTCGACCTCTAGC
SaABE-F10	AGGACTATAAAGATACCAGGCG
SaABE-F11	AAGCAGCAGATTACGCGC
SaABE-F12	CGCCAGTTAATAGTTTGCGC
SaABE-F13	AGCCCATATATTGAGTTCCGC
SaABE-R1	GCTTCTTCTTTGGTGACTCG
SaABE-R2	TCTGGGCCTTCTTCTGAGC
SaABE-R3	CTCCTCCACCTCATTCACG
SaABE-R4	CGATCTGCTTCAGTGTAGGC
SaABE-R5	CTTTGATGCTCTGGATGAAGC
SaABE-R6	TGTTGATGTCCCGCTCCTCC
SaABE-R7	ACAGGGTGTCATTGATCAGC

SaABE-R8	TCTTCTTCAGCTTCTTGGCC
SaABE-R9	CAGCGGGTTTAAACTCAATGG
	Luciferase sequencing primers
pSGDluc-F1	CGAGGATATCAGATCAGCGC
pSGDluc-F2	TTGACCTTCTTAAGCTGGCG
pSGDluc-F3	AGGACCTTTCGGATCTGCC
pSGDluc-F4	ACGACATCTACAACGAGCG
pSGDluc-F5	AGCAAGGAGGTAGGTGAGG
pSGDluc-F6	GATAAGGATCCGTCGACCG
pSGDluc-F7	TACCTGTCCGCCTTTCTCC
pSGDluc-F8	GGTCCTGCTACTTTGTCCG
pSGDluc-F9	GACTCAAGGATCTTGCCGC
pSGDluc-R1	CTTCGAGTGGGTAGAATGGC
PCseqF4	CTTCCAAGGTGTACGAC
PCseqF5	TTGGTTCGAGCTGCTG
PCseqF6	AGATCCCTCTCGTTAAGG
TdTomF25	GTTACAACCGCCAAGAAGC

Name	**Sequence 5'-3'**
(CMV) -Promoter	GTGATGCGGTTTTGGCAGTACATCAATGGGCGTGGATAGCGGTTTGACTCAC GGGGATTTCCAAGTCTCCACCCCATTGACGTCAATGGGAGTTTGTTTTGGCA CCAAAATCAACGGGACTTTCCAAAATGTCGTAACAACTCCGCCCCATTGAC GCAAATGGGCGGTAGGCGTGTACGGTGGGAGGTCTATATAAGCAGAGCT
hU6 promoter	GAGGGCCTATTTCCCATGATTCCTTCATATTTGCATATACGATACAAGGCTGT TAGAGAGATAATTGGAATTAATTTGACTGTAAACACAAAGATATTAGTACAA AATACGTGACGTAGAAAGTAATAATTTCTTGGGTAGTTTGCAGTTTTAAAATT ATGTTTTAAAATGGACTATCATATGCTTACCGTAACTTGAAAGTATTTCGATTT CTTGGCTTTATATATCTTGTGGAAAGGACGAAACACC
bGH PolyA	CGACTGTGCCTTCTAGTTGCCAGCCATCTGTTGTTTGCCCCTCCCCCGTGCC TTCCTTGACCCTGGAAGGTGCCACTCCCACTGTCCTTTCCTAATAAAATGAG GAAATTGCATCGCATTGTCTGAGTAGGTGTCATTCTATTCTGGGGGGTGGGG TGGGGCAGGACAGCAAGGGGGAGGATTGGGAAGACAATAGCAGGCATGCT GGGGA
SV-40 promoter	CTGAGGCGGAAAGAACCAGCTGTGGAATGTGTGTCAGTTAGGGTGTGGAA AGTCCCCAGGCTCCCCAGCAGGCAGAAGTATGCAAAGCATGCATCTCAATT AGTCAGCAACCAGGTGTGGAAAGTCCCCAGGCTCCCCAGCAGGCAGAAGT ATGCAAAGCATGCATCTCAATTAGTCAGCAACCATAGTCCCGCCCCTAACTC

	CGCCCATCCCGCCCCTAACTCCGCCCAGTTCCGCCCATTCTCCGCCCCATGG CTGACTAATTTTTTTTATTTATGCAGAGGCCGAGGCCGCCTCGGCCTCTGAG CTATTCCAGAAGTAGTGAGGAGGCTTTTTTGGAGGCCTAGGCTTTTGCAAA
HSV-TK Promoter	AAATGAGTCTTCGGACCTCGCGGGGGCCGCTTAAGCGGTGGTTAGGGTTTG TCTGACGCGGGGGGAGGGGGAAGGAACGAAACACTCTCATTCGGAGGCGG CTCGGGGTTTGGTCTTGGTGGCCACGGGCACGCAGAAGAGCGCCGCGATCC TCTTAAGCACCCCCCCGCCCTCCGTGGAGGCGGGGGTTTGGTCGGCGGGTG GTAACTGGCGGGCCGCTGACTCGGGCGGGTCGCGCGCCCCAGAGTGTGAC CTTTTCGGTCTGCTCGCAGACCCCCGGGCGGCGCCGCCGCGGCGGCGACGG GCTCGCTGGGTCCTAGGCTCCATGGGGACCGTATACGTGGACAGGCTCTGG AGCATCCGCACGACTGCGGTGATATTACCGGAGACGTTCTGCGGGACGAGC CGGGTCACGCGGCTGACGCGGAGCGTCCGTTGGGCGACAAACACCAGGAC GGGGCACAGGTACACTATCTTGTCACCCGGAGGCGCGAGGGACTGCAGGA GCTTCAGGGAGTGGCGCAGCTGCTTCATCCCCGTGGCCCGTTGCTCGCGTT TGCTGGCGGTGTCCCCGGAAGAAATATATTTGCATGTCTTTAGTTCTATGATG ACACAAACCCCGCCCAGCGTCTTGTCATTGGCGAATTCGAACACGCAGATG CAGTCGGGGCGGCGCGGTCCCAGGTCCACTTCGCATATTAAGGTGACGCGT GTGGCCTCGAACACCGAGCGACCCTGCAGCGACCCGCTTAA

C. Key Resource List

Resource	Source	Code
Bacterial strains		
XL-10 Gold ultracompetent cells	Agilent technologies	200315
NEB® 5-alpha *E. Coli*	NEB	C2987I
Kits		
Qiaquick PCR purification kit	Qiagen	28104
Gel Extraction kit	Various	
DNeasy blood and tissue	Qiagen	69504
QIAamp DNA mini kit	Qiagen	53104/53106
Zyppy plasmid miniprep kit	Zymo Research	D4020
Monarch RNA extraction kit	NEB	T2010S
Allprep DNA/RNA/protein kit	Qiagen	80004
EndoFree® Plasmid maxi kit	Qiagen	12362
NucleoBond™ Xtra EF midi kit	Macherey-Nagel	12773550
Quickchange II XL kit	Agilent	200521
KOD Hotstart master mix	Sigma Aldrich	71842-4
Pierce™ BCA protein assay kit	Thermo Scientific™	23225

NEBuilder™ HiFi DNA Assembly Kit	NEB	E5520S
iTaq™ Universal SYBR® Green Supermix	Bio-Rad	1725121
TaqMan™ Fast Universal PCR Master Mix (2X), no AmpErase™ UNG	Applied Biosystems/ Thermo Scientific™	4366072
Qubit™ dsDNA broad range assay kit	Invitrogen™	Q32850
Qubit™ RNA assay kit, high sensitivity	Invitrogen™	Q32852
Evoscript universal cDNA master/ Transcriptor universal cDNA master	Roche	5893151001
DualGlo® Luciferase assay kit	Promega	E2940

Cell culture and AAV production

Tissue culture plates (12-, 24- well)	Starstedt	Various
White-walled adherent tissue culture plates (96-well)	Corning®, Greiner, Thermo Scientific™	Various
Vented culture flasks (T75, T175)	Starstedt	Various
Corning® CellBIND® Surface HYPERFLASK®	Corning®	CLS10030-4EA
Dulbecco's Modified Eagle Medium (DMEM) with/without phenol red and pyruvate	Gibco™	11995073; 31053028; 11960044
L-glutamine	Gibco™	25030081
Heat-inactivated fetal bovine serum	Gibco™	16140071
OptiMEM reduced serum medium	Gibco™	31985062
Penicillin-streptomycin	Sigma Aldrich	P4333-100mL
Sodium pyruvate	Gibco™	11360070
TransIT-LT1 transfection reagent	Mirus Bio	MIR 2300
Phosphate Buffered Saline (PBS)	Gibco™	10010023
TrypleE Express Dissociation reagent	Gibco™	12604039
0.4% Trypan Blue	Gibco™	15250061
Trans-IT Virus-GEN® transfection reagent	Mirus Bio	MIR 6705
Benzonase	Merck Millipore	1016950001
MgCl2 1M	CalBiochem	5985
KCl 0.075M	Sigma Aldrich	P9327
NaCl 5M	Sigma Aldrich	59222C-500mL
Phenol red	Sigma Aldrich	P0290
Amicon® Ultra 100k filters	Sigma Aldrich	UFC810024

Optiseal™ ultracentrifuge tubes (26x77mm)	Beckman-Coulter	361625
OptiPrep™ Density Gradient Medium	Sigma-Aldrich	D1556-250ML
Organoid media (proprietary)	New Cells Biotech	

Chemicals and reagents

Quickload® 100bp/1kb DNA ladder	NEB	N0467S/N0550S
Gel loading dye 6x	NEB	B7025
BLUeye protein size ladder	Sigma Aldrich	94964-500UL
Protein loading dye 5x	National diagnostics	NAT1252
Skim Milk Powder	Various	Various
Restriction enzymes	NEB, ThermoFisher	Various
Normal Donkey Serum	Abcam	Ab7475
ProLong Diamond Antifade Mountant with DAPI		P36962
Shrimp Alkaline Phosphatase	NEB	M0371S
RIPA Lysis Buffer 10x	Sigma Aldrich	S3401
Tris/glycine/SDS 10x running buffer	National Diagnostics	B9-0032
SOC medium	Various	Various
T4 DNA ligase	NEB	M0202S
DNase I	NEB	M0303S
Beta-mercaptethanol	Sigma-Aldrich	M6250-100ML
LB broth with Agar EZmix™	Sigma-Aldrich	L7533-6X500ML
Agar	Various	Various
Agarose	GeneFlow	A4-0700
LB	Invitrogen™	12795084
cOmplete™ mini protease inhibitor	Roche	11836153001
Tween-20	Sigma Aldrich	P1379-25ML
Triton-X 100	Sigma Aldrich	ACRO327372500
PBS tablets	Gibco™	18912-014
OCT compound	VWR	361603E
TBS 10x	Bio-Rad	1706435
Trans-blot turbo transfer buffer 5x	Bio-Rad	10026938
Methanol	Fisher; Sigma Aldrich	10317360; 32213-2.5L
Ethanol	Fisher	E/06665DF/17; BP2818-500
Isopropanol	VWR	20842.33
TAE Buffer 50x	Severn Biotech Ltd	20-6001-50
T4 polynucleotide kinase	NEB	M0201S
Rely+On Virkon tablets/powder	SLS ltd	33012/CLE1552SP

Formaldehyde (PFA) 16% w/v	Thermo-Fisher	
Pierce™ Bovine Serum Albumin Standard Ampules, 2 mg/mL	Thermo Scientific™	23209
TaqMan® Probes	Thermo Scientific™	Various (listed in methods)
Nuclease Free water	Invitrogen™	AM9939; AM9916
RNAse ZAP™	Invitrogen™	AM9786
DNA ZAP™	Invitrogen™	AM9890
DNA fragments	IDT G Blocks, Twist Biosciences	
Western blot antibodies	Various	Various (listed in methods)
IHC antibodies	Various	Various (listed in methods)
Bovine serum albumin (IHC)	Fisher Scientific	BP8703-100
GelRed	Cambridge Bioscience	41003

Other

7.5% Criterion TGX Gel 18 well 30 µl	Bio Rad	5671024
10% Criterion™ TGX™ Precast Midi Protein Gel, 12+2 well, 45 µl	Bio Rad	5671033
PureLink™ HiPure Precipitator Module	Invitrogen™	K210022
Petri Dishes	Various	Various
Kimble pestles RNAse Free	VWR	SCERSP749521-1590
96-well PCR plate, segmented semi-skirted	Various	Various
96-well qPCR plate	Bio-Rad	HSP9655
qPCR microseal ‘B’ sealing film	Bio-Rad	MSB1001
35g needles	World Precision Instruments	NF35BV-2
SuperFrost® Plus microslides, 75x25mm	VWR	631-0108
X100 Coverslip no.1, 22x50mm	Fisher	15787582
ImmEdge Hydrophobic Barrier PAP Pen	Vector Laboratories Inc	H-4000
L-shaped spreaders	VWR	612-1561
Disposable scalpel	SLS ltd	INS4765

Software

Biorender.com
Prism 10

Geneious Prime	
ImageJ	Fiji
MXfold2	
TIDE	
EditR	
Crispresso2	
MutationTaster	
EndNote 21	
ImageStudio	LI-COR

D. Publications, Presentations, Grants

Publications

Piotter E, McClements ME, MacLaren RE. The Scope of Pathogenic ABCA4 Mutations Targetable by CRISPR DNA Base Editing Systems-A Systematic Review. Front Genet. 2022;12:814131. doi: 10.3389/fgene.2021.814131.

Piotter E, McClements ME, MacLaren RE. Therapy Approaches for Stargardt Disease. Biomolecules. 2021;11(8):1179. doi: 10.3390/biom11081179.

Stevanovic M, Piotter E, McClements M, MacLaren RE. CRISPR Systems Suitable for Single AAV Vector Delivery. Curr Gene Ther. 2022;22(1):1-14. doi: 10.2174/1566523221666211006120355.

McClements, M. E., Butt, A., Piotter, E., Peddle, C. F. & MacLaren, R. E. An analysis of the Kozak consensus in retinal genes and its relevance to gene therapy. *Mol Vis* 27, 233-242 (2021).

Presentations

Retina UK, Somerset Chapter – 'Gene Editing for Stargardt Disease', March 2021.
Retina UK, Webinar series – 'Gene Editing for Stargardt Disease', August 2021.
Macular Society, Webinar Series: Working Age and Young People – 'Gene Editing for Stargardt Disease', March 2022.
Poster presentation, UK Eye Genetics Group annual conference – 'The Scope of Pathogenic ABCA4 mutations targetable by CRISPR DNA base editing systems,' September 2021.
Poster presentation, The Association for Research in Vision and Ophthalmology annual conference – 'Cas13 RNA base editing targeting a stop mutation in ABCA4', May 2022.

Presentation, CRISPR Workshop Oxford – ‘DNA and RNA base editing two stop mutations c.206 G>A and c.93 G>A in ABCA4’, June 2023.
Poster presentation, Cold Spring Harbor Laboratory – Genome Engineering: CRISPR Frontiers – ‘Comparison of Cas13 RNA base editing and SaKKH DNA base editing targeting the c.206 G>A stop mutation in ABCA4’, August 2023.
Poster presentation, The Association for Research in Vision and Ophthalmology annual conference – ‘Comparison of Cas13 RNA base editing and two SaKKH DNA base editors targeting the start codon of ABCA4’, May 2024.

Grants

MRC Harwell Genome Mice for Medicine Programme 2023. Generation of ABCA4 W31X humanized exon 2 novel mouse model. Co-applicant.